

Title	Spatiotemporal control of siponimod delivery for the regeneration of critical bone defects
Authors	Sartawi, Ziad
Publication date	2021
Original Citation	Sartawi, Z. 2021. Spatiotemporal control of siponimod delivery for the regeneration of critical bone defects. PhD Thesis, University College Cork.
Type of publication	Doctoral thesis
Rights	© 2021, Ziad Sartawi. - <a href="https://creativecommons.org/licenses/by-nc-nd/4.0/">https://creativecommons.org/licenses/by-nc-nd/4.0/</a>
Download date	2024-05-15 12:43:03
Item downloaded from	<a href="https://hdl.handle.net/10468/11851">https://hdl.handle.net/10468/11851</a>



# UCC

**University College Cork, Ireland**  
Coláiste na hOllscoile Corcaigh

Ollscoil na hÉireann, Corcaigh  
**National University of Ireland, Cork**



**Spatiotemporal control of siponimod delivery for the  
regeneration of critical bone defects**

Thesis presented by

**Ziad Sartawi**

for the degree of

**Doctor of Philosophy**

**University College Cork**

**School of Pharmacy**

Head of School: Prof. Brendan Griffin

Supervisors: Dr. Katie Ryan and Prof. Christian Waeber

2021

# Table of Contents

Declaration .....	vi
List of abbreviations.....	vii
Publications and presentations .....	xi
Thesis abstract.....	xiii
<b>Chapter 1 .....</b>	<b>1</b>
1.1 Bone tissue.....	2
1.2 Current state of bone defect repair.....	4
1.3 Bone tissue engineering .....	6
1.4 Properties of an implantable scaffold .....	8
1.5 Types of materials in bone tissue engineering.....	10
1.5.1 Polymers.....	11
1.5.2 Ceramics.....	13
1.6 Fabrication techniques .....	15
1.6.1 Solvent casting and particulate leaching .....	15
1.6.2 Gas foaming .....	16
1.6.3 Freeze-drying .....	17
1.6.4 3-D printing.....	17
1.6.5 Electric-field assisted techniques .....	18
1.7 Clinical considerations.....	23
1.8 Cell-based therapies in BTE .....	24
1.9 Growth factors in BTE.....	26
1.10 Pharmacological options in BTE .....	29
1.11 Thesis aim and objectives .....	35
<b>Chapter 2 .....</b>	<b>37</b>
2.1 Abstract.....	38
2.2 Introduction.....	39
2.3 Bone repair.....	43
2.4 S1P effect on progenitor stem cells .....	46
2.5 S1P and stem cell migration .....	47
2.6 S1P and stem cell differentiation .....	49
2.7 S1P and osteoblasts.....	50
2.7.1 Proliferative effect.....	50
2.7.2 Osteoblast differentiation .....	51

2.7.3	Osteoblast precursor migration .....	53
2.8	Other effect of S1P signalling in osteoblasts .....	54
2.9	S1P and osteoclasts .....	55
2.10	S1P and osteoclast recruitment .....	57
2.11	Therapeutic manipulation of osteoclast trafficking .....	58
2.12	S1P in the vasculature and the role of angiogenesis .....	67
2.13	Current efforts in S1P delivery .....	70
2.14	Conclusion .....	74
<b>Chapter 3</b>	.....	<b>78</b>
3.1	Abstract.....	79
3.2	Introduction.....	80
3.3	Materials and methods .....	82
3.3.1	Materials.....	82
3.3.2	Cell culture .....	82
3.3.3	Siponimod solution .....	83
3.3.4	Viability and proliferation.....	83
3.3.5	Osteogenic differentiation .....	84
3.3.6	Migration.....	85
3.3.7	Cell attachment.....	87
3.3.8	Cyclic AMP assay .....	87
3.3.9	Statistical analysis .....	87
3.4	Results.....	89
3.4.1	Siponimod solution .....	89
3.4.2	Viability and proliferation.....	91
3.4.3	Osteogenic differentiation .....	93
3.4.4	Migration.....	96
3.4.5	Cell attachment.....	101
3.4.6	Cyclic AMP assay .....	102
3.5	Discussion.....	103
3.6	Conclusion .....	109
<b>Chapter 4</b>	.....	<b>110</b>
4.1	Abstract.....	112
4.2	Introduction.....	113
4.3	Materials and methods .....	117
4.3.1	Materials.....	117

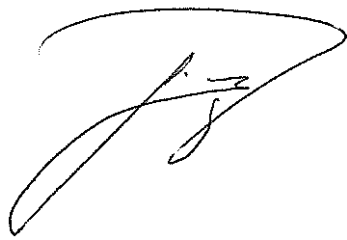
4.3.2	Electrospinning procedure .....	117
4.3.3	Scanning electron microscopy .....	118
4.3.4	HPLC methodology .....	119
4.3.5	Siponimod stability .....	119
4.3.6	Loading efficiency and drug release .....	120
4.3.7	Differential scanning calorimetry (DSC) .....	121
4.3.8	Fourier Transform Infra-red (FTIR) spectroscopy .....	121
4.3.9	Contact angle .....	121
4.3.10	Tensile strength .....	122
4.3.11	Biological characterisation and <i>in vitro</i> functional experiments .....	122
4.3.12	<i>In vivo</i> critical cranial defect .....	125
4.3.13	Statistical analysis .....	128
4.4	Results .....	129
4.4.1	Properties of electrospun fibres .....	129
4.4.2	Siponimod stability .....	131
4.4.3	Drug release .....	133
4.4.4	Physicochemical characterisation .....	136
4.4.5	Biological characterisation of electrospun material .....	140
4.4.6	<i>In vitro</i> functional experiments .....	144
4.4.7	<i>In vivo</i> critical cranial defect .....	147
4.5	Discussion .....	151
4.6	Conclusion .....	158
<b>Chapter 5</b>	.....	<b>160</b>
5.1	Abstract .....	161
5.2	Introduction .....	162
5.3	Materials & methods .....	165
5.3.1	Materials .....	165
5.3.2	Electrospray procedure .....	166
5.3.3	Scaffold preparation .....	167
5.3.4	Scanning electron microscopy .....	167
5.3.5	Pore volume .....	168
5.3.6	HPLC method for drug quantitation .....	168
5.3.7	Drug loading and release .....	169
5.3.8	Differential scanning calorimetry (DSC) .....	169
5.3.9	Young's modulus .....	170

5.3.10	Cell culture .....	170
5.3.11	Evaluation of metabolic activity .....	170
5.4	Results.....	173
5.4.1	Preparation of porous scaffolds.....	173
5.4.2	Loading efficiency and drug release .....	175
5.4.3	Physical characterisation – DSC & Young’s modulus .....	176
5.4.4	Evaluation of metabolic activity – Indirect & direct assessment.....	179
5.5	Discussion.....	181
5.6	Conclusion .....	186
<b>Chapter 6</b>	.....	<b>187</b>
6.1	Overview and Summary .....	189
6.2	Contribution to knowledge .....	192
6.3	Interpretation and implications of the thesis findings.....	193
6.3.1	Objective I.....	193
6.3.2	Objective II.....	194
6.3.3	Objective III .....	197
6.3.4	Objective IV .....	200
6.3.5	Objective V .....	201
6.4	Limitations.....	204
6.5	Recommendations for future work .....	205
6.6	Thesis conclusions .....	207
<b>References</b>	.....	<b>208</b>
<b>Appendices</b>	.....	<b>234</b>
Appendix A: Supplementary material to Chapter 3	.....	240
7.1	Introduction.....	241
7.2	Materials and methods .....	241
7.2.1	Materials.....	241
7.2.2	Cell culture materials .....	241
7.2.3	Viability and proliferation of MC3T3-E1 and Saos-2 .....	242
7.3	Results.....	242
7.4	Discussion.....	246
Appendix B: Supplementary material to Chapter 4	.....	247
8.1	Introduction.....	248
8.2	Materials and methods .....	250
8.2.1	Materials.....	250

8.2.2	Electrospun sample preparation .....	250
8.2.3	Cell culture .....	250
8.2.4	Procedure for H&E staining of cranial bone tissue.....	251
8.3	Results.....	252
8.3.1	Cell culture .....	252
8.3.2	Haematoxylin and Eosin staining .....	253
8.4	Discussion.....	257

## Declaration

This is to certify that the work I am submitting is my own and has not been submitted for another degree, either at University College Cork or elsewhere. All external references and sources are clearly acknowledged and identified within the contents. I have read and understood the regulations of University College Cork concerning plagiarism.



Signed: \_\_\_\_\_

Ziad Sartawi

## Author Contribution

All work was performed independently by the author, with the following exceptions:

Sectioning and histological staining of undecalcified cranial explants (**Chapter 4**) were performed by Ms. Carol Whiting, certified Histotechnician in the Department of Orthopaedic Surgery at the University of Michigan, MI, USA.



## List of abbreviations

% w/v Percentage weight per volume

% w/w: Percentage weight per weight

3-D: Three dimensional

ALP: Alkaline phosphatase

ANOVA: Analysis of variance

BG: Bioactive glass

BMP: Bone morphogenetic proteins

BMSC: Bone marrow derived mesenchymal stem cells

BrdU: Bromodeoxyuridine

BTE: Bone tissue engineering

CaP: Calcium phosphate

CLF: Chloroform

CO<sub>2</sub>: Carbon dioxide

C<sub>t</sub>: Cumulative drug release at time t

DMEM/F12: Dulbecco's Modified Eagle's Medium/Nutrient Mixture F-12 Ham

DMF: Dimethylformamide

DMSO: Dimethyl sulfoxide

DSC: Differential scanning calorimetry

ECGM: Endothelial cell growth medium

EO: Endochondral ossification

ERK: Extracellular signal-regulated kinases

ESC: Embryonic stem cell

FAK/PI3K/AKT (PKB): Focal adhesion kinase/ Phosphoinositide 3-kinase/ Protein kinase B

FBS: Foetal bovine serum

FTIR: Fourier transform infra-red

GPa: Giga Pascal

H&E: Haematoxylin and eosin

h: Height

HA: Hydroxyapatite

HFIP: Hexafluoroisopropanol

hFOB: Human foetal osteoblasts

HIF-1 $\alpha$ : Hypoxia-inducible factor 1-alpha

HPLC: High pressure liquid chromatography

HSC: Haematopoietic stem cells

HUVEC: Human umbilical vein endothelial cells

IL: Interleukin

IO: Intramembranous ossification

iPSC: Induced pluripotent stem cell

IQR: Interquartile range

JAK/STAT: Janus kinases/signal transducer and activator of transcription proteins

K: Release constant

K<sub>0</sub>: Zero-order release constant

kV: Kilovolts

MAPK: Mitogen-activated protein kinase

M-CSF: Macrophage colony-stimulating factor

MDSC: Modulated differential scanning calorimetry

MEK/MAPK: Mitogen-activated kinases

MG: Masson-Goldner trichrome

MicroCT: Micro computed tomography

MMP: Matrix metalloproteinase

MN: Meganewton

MPa: Mega Pascal

mRNA: Messenger ribonucleic acid

MSC: Mesenchymal stem cell

Mt/M $\infty$ : Fraction of drug released over time

MTT: Methyl thiazolyl tetrazolium (3-(4,5-dimethylthiazol-2-yl)-2,5-diphenyltetrazolium bromide)

*n*: Number of independently repeated experiments/Sample size

*n*: Release exponent

NBF: Neutral buffered formalin

NS: Not statistically significant

PBS: Phosphate buffered saline

PCL: Polycaprolactone

PDGF: Platelet derived growth factor

PGA: Poly (glycolic acid)

PGF2 $\alpha$ : Prostaglandin F2 alpha

PKC: Protein kinase C

PLA: Poly (lactic acid)

PLGA: Poly (lactide-co-glycolide)

pNPP: para-nitrophenylphosphate

PSI: Pound per square inch

*r*: Radius

RANK: Receptor activator of nuclear factor kappa-B

RANKL: Receptor activator of nuclear factor kappa-B ligand

rcf: Relative centrifugal force

rhBMP: Recombinant human bone morphogenetic protein

RNA: Ribonucleic acid

RPM: Revolutions per minute

S1P: Sphingosine 1-phosphate

SD: Standard deviation

SDF-1: Stromal cell-derived factor 1

SEM: Scanning electron microscopy

SiRNA: Small interfering ribonucleic acid

SK1: Sphingosine kinase 1

SKI-II: Sphingosine kinase inhibitor

t: Time

TCP: Tricalcium phosphates

Tg: Glass transition temperature

TGF: Transforming growth factor

TNF- $\alpha$ : Tumour necrosis factor alpha

Tris-HCl: tris(hydroxymethyl)aminomethane

V: Volume

VEGF: Vascular endothelial growth factor

VK: von Kossa

W<sub>dry</sub>: Scaffold dry mass

Wnt: Wingless-related integration site

W<sub>wet</sub>: Scaffold wet mass

## **Publications and presentations**

### ***Peer-reviewed publications***

**Sartawi, Z.,** Schipani, E., Ryan, K.B. and Waeber, C., 2017. Sphingosine 1-phosphate (S1P) signalling: Role in bone biology and potential therapeutic target for bone repair. *Pharmacological research*, 125, pp.232-245. DOI: 10.1016/j.phrs.2017.08.013

**Sartawi, Z.,** Ryan, K.B. and Waeber, C., 2020. Bone regenerative potential of the selective sphingosine 1-phosphate receptor modulator siponimod: *In vitro* characterisation using osteoblast and endothelial cells. *European Journal of Pharmacology*, p.173262. DOI: 10.1016/j.ejphar.2020.173262

**Sartawi, Z.,** Waeber, C., Schipani, E. and Ryan, K.B., 2020. Development of electrospun polymer scaffolds for the localized and controlled delivery of siponimod for the management of critical bone defects. *International Journal of Pharmaceutics*, p.119956. DOI: 10.1016/j.ijpharm.2020.119956

### ***Posters & Presentations***

**Sartawi, Z.,** Waeber, C., Ryan, K.B. Fingolimod and siponimod do not affect the proliferation of MC3T3-E1 cells. Poster presented at the 39th All Ireland schools of pharmacy (24-25/4/2017).

**Sartawi, Z.,** Waeber, C., Ryan, K.B. The effect of fingolimod and siponimod on osteoblastic cell lines. Oral presentation at the 2017 United Kingdom & Ireland Controlled Release Society symposium (30-31/5/2017).

**Sartawi, Z.,** Fullen, G., Waeber, C., Ryan, K.B. Electrospayed composite scaffolds for release of siponimod to augment bone regeneration. Poster presented at the 2018 United Kingdom & Ireland Controlled Release Society symposium (4-5/6/2018).

**Sartawi, Z.,** Waeber, C., Ryan, K.B. Developing an electrospun polymer fibre mat for the localized delivery of agents with bone regenerative potential. Oral presentation at the 2018 Controlled Release Society annual meeting & exposition (22-24/7/2018).

**Sartawi, Z.,** Waeber, C., Ryan, K.B. The potential of siponimod in bone regeneration & the development of an associated electrospun delivery device. Poster presented at the 2019 Keystone Symposium: Delivering Therapeutics Across Boundaries Conference (6-9/5/2019).

## Thesis abstract

Tissue engineering aims at regenerating damaged tissue by using synthetic or natural materials and has applications across the different tissue types, including bone. A major challenge in bone tissue engineering includes the availability of materials that possess desirable properties including osteogenic potential, as well as osteoconductive and osteoinductive features to support bone regeneration, this challenge is magnified in the case of critical bone defects. The gold-standard treatment for such defects is autologous bone grafting, which suffers from issues related to the availability of material and the morbidity associated with surgeries to harvest the tissue. Therefore, it is important to consider alternative materials and therapeutic options that may contribute to improving the outcomes of bone tissue engineering issues.

The overall aim of this thesis was to investigate the therapeutic potential of the small drug molecule, siponimod, to influence key cell process inherent in bone regeneration and to investigate the formulation design, functionality and regenerative potential of suitable scaffold constructs that exert spatiotemporal control over siponimod delivery both *in vitro* and in an *in vivo* critical defect model.

**Chapter 1** provided a general introduction of key concepts discussed throughout the thesis including a background on bone anatomy and biology. Thereafter, the chapter introduced tissue engineering in general with a focus on intrinsic aspects of bone tissue engineering namely scaffolds, cells, and signals. It described the key requirements in the design of scaffolds suitable for bone regeneration and provided an overview of the materials and techniques used in the fabrication of scaffolds for bone tissue engineering. In particular it highlighted, the materials used throughout this thesis, such

as the natural and synthetic polymers collagen and poly lactide-co-glycolide (PLGA) used in **Chapter 4 & 5**, and the bioactive ceramic hydroxyapatite (HA) used in **Chapter 5**. This first chapter also addressed the use of protein and small molecule signal therapeutics in bone tissue engineering, including a brief introduction of sphingosine 1-phosphate.

**Chapter 2** thus followed with an in-depth review of the role of sphingosine 1-phosphate (S1P) in bone biology and its potential therapeutic use in bone repair. The role of S1P in nervous, cardiovascular, and immune systems is well established, however, knowledge regarding its role in bone biology and the utility of specific S1P receptor modulation in bone repair was lacking. Therefore, **Chapter 2** not only aimed to add to the available literature on the role of S1P signalling in bone repair, but also to contribute to the identification of S1P mediated processes that could be targeted therapeutically. The culmination of the review in **Chapter 2** was the selection of S1P<sub>1</sub> receptor modulation as a target, and siponimod as a selective agonist for further investigation.

Thereafter, **Chapter 3** investigated the *in vitro* bone regenerative potential of the S1P receptor modulator, siponimod. Specifically, it aimed to identify the impact of siponimod on key cellular processes including cell viability, proliferation, differentiation and migration using human foetal osteoblasts (hFOB), as well as cell proliferation and migration using human umbilical vein endothelial cells (HUVEC). The hypothesis underpinning **Chapter 3** was that selective S1P<sub>1</sub> signalling using the S1P<sub>1/5</sub> agonist, siponimod would stimulate osteoblast proliferation, differentiation, and migration as well as endothelial cell proliferation and migration. The results of this



chapter showed for the first time that siponimod indeed promotes osteoblast differentiation while having no influence on viability and proliferation. Siponimod was also shown to promote the chemokinesis of endothelial cells, whereby it interfered with cell attachment and migration in the short-term (4 hrs) and caused a delayed (8 hrs) stimulation of endothelial migration. Taken together these results suggested that siponimod was worthy of further investigation in the context of bone regeneration. However, the balance of evidence in the bone repair literature supports the use of a localised delivery approach for sphingolipids, rather than systemic administration. This was the motivation supporting the research in **Chapter 4** and **Chapter 5**, which investigated suitable scaffold constructs for the localised delivery of siponimod.

Therefore, the hypothesis underpinning **Chapter 4** was that the design of a biocompatible and biodegradable polymeric scaffold would control the presentation of siponimod in a stable and functional manner at appropriate concentrations and over relevant timeframes to exploit its potential for enhanced bone regeneration. This chapter thus detailed the preparation, characterisation and *in vitro* assessment of PLGA-based electrospun material coupled with collagen and loaded with siponimod at different concentrations (0.5-2 % w/w). The physicochemical characteristics including drug stability in the solid and liquid state as well as drug loading and release properties were investigated. Additionally, *in vitro* cell-based investigations were carried out on the electrospun material to assess its compatibility with the cellular populations of interest, hFOB and HUVEC, and whether the released siponimod maintained the functional effects determined in **Chapter 3**. Results confirmed our hypothesis that siponimod could be successfully loaded with high efficiencies (80-94 %) and its release could be controlled in a stable manner (> 3 months), which was in

line with a planned 12-week *in vivo* cranial defect study. Furthermore, the released siponimod maintained its differentiation and migration effects on hFOB and HUVEC *in vitro*. The scaffolds were then implanted in rat critical cranial defects for 12-weeks to assess *in vivo* effectiveness of the siponimod loaded scaffold. Results showed that while there was some reduction in defect size, there was no statistically significant differences between the experimental groups regarding the histomorphometrically determined area of mineralisation within the defect space.

The scaffold described in **Chapter 5** was designed contemporaneously with the electrospun scaffold in **Chapter 4**, although only the latter design was progressed to the stage of *in vivo* analysis. Acknowledging this, **Chapter 5** provided a preliminary description of the design and characterisation of another scaffold design using electrospray-microparticles loaded with siponimod. As with the electrospun scaffold, this alternative design is based on a similar hypothesis that localised delivery of siponimod for bone regeneration was superior to systemic delivery. The microparticles were mould compressed with HA, the calcium phosphate mineral reminiscent of that found in native bone tissue, and a porogen, prior to high-pressure carbon dioxide (CO<sub>2</sub>) foaming and porogen leaching. The morphological properties of the microparticles and the completed scaffolds were assessed using scanning electron microscopy (SEM). Physicochemical properties investigated included porosity, mechanical properties, siponimod drug loading and release, and cell culture studies to assess the scaffold's effect on hFOB and HUVEC. Results of SEM showed that the diameters of microparticles was increased by the inclusion of siponimod, while scaffolds possessed a highly porous internal structure, with morphology affected by the inclusion of HA. Drug loading efficiency was lower than those seen in **Chapter 4**, which was expected

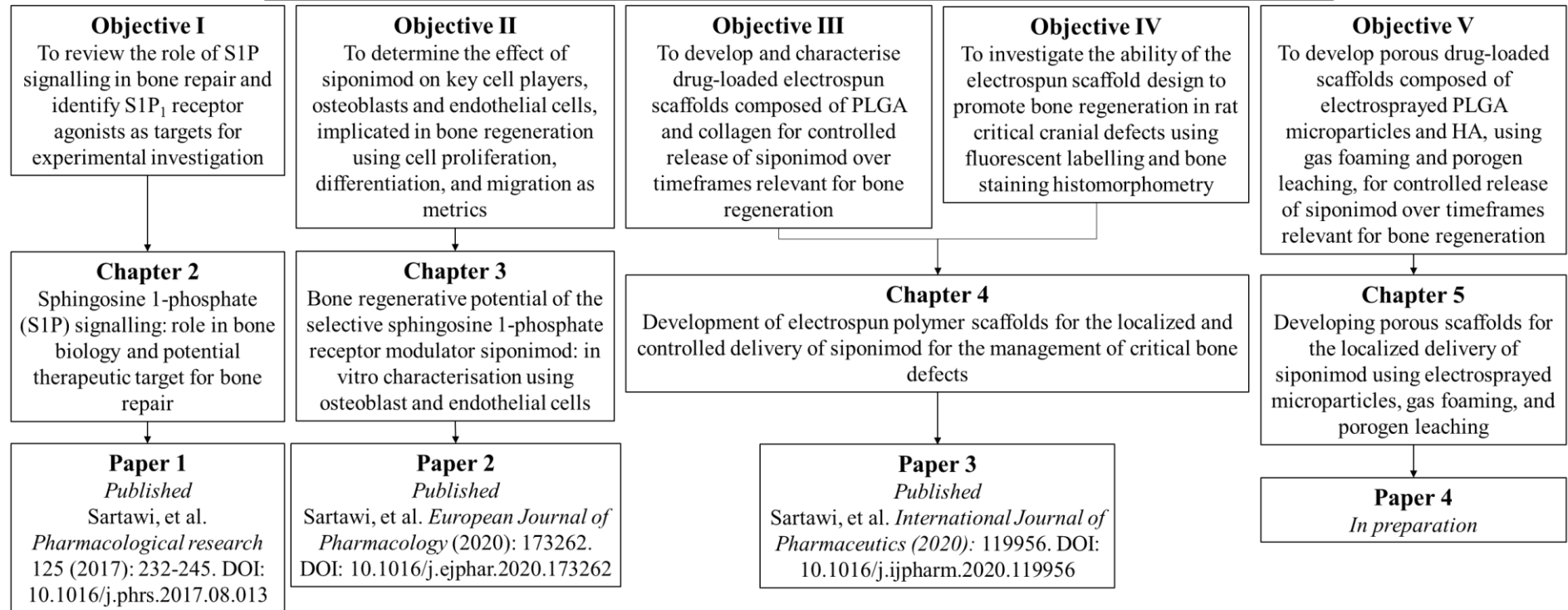
due to the method employed, although drug release was still sustained over 3 months. The scaffolds were found to be compatible with hFOB and HUVEC, whether seeded in direct or indirect contact with scaffolds and no significant changes to cell metabolic activity were observed.

In conclusion, this thesis showed that S1P receptors have a clear impact on the biology of bone repair, with novel findings contributing to our understanding of siponimod's *in vitro* effect on osteoblasts and endothelial cells, which could lead to siponimod-based therapeutic options for bone and other tissue regeneration applications. This thesis also detailed the first designs of controlled release scaffolds for siponimod, with the S1P<sub>1</sub> agonist successfully incorporated into two different scaffolds using both electrospinning and electrospraying production methods, which enabled constructs with different compositions and physical properties to be designed. Although *in vivo* results of cranial defect studies did not provide statistically significant evidence of improved bone regeneration, both scaffold designs demonstrated promising cell compatibility and drug release properties, that can be further optimised to fully utilise the bone regenerative potential of siponimod and other S1P agonists.

## Thesis Outline

**Thesis Title:** Spatiotemporal control of siponimod delivery for the regeneration of critical bone defects

**Thesis Aim:** To investigate the bone regenerative potential of siponimod, and the development of implantable delivery devices for the spatiotemporal control of siponimod delivery.



# Chapter 1

## Introduction

## 1.1 Bone tissue

Bone is a highly specialised connective tissue characterised by its mineralisation in its mature state. Bone fulfils several important functions, acting as a static protective frame supporting structural, and locomotor activities (Walsh, 2015). In addition, bone is a highly metabolically dynamic tissue that acts as a mineral reservoir (Copp and Shim, 1963), which is in a constant state of remodelling to repair damaged tissue and maintain mineral homeostasis (Raggatt and Partridge, 2010).

On an anatomical level, bone is divided into cortical (compact) and cancellous (spongy) bone. Cortical bone forms the hard exterior surface including the shafts of long bones (e.g. femur) and the exterior of flat bones (e.g. skull), while cancellous bone is present in the marrow cavities of long bone and the centres of flat bones (Kim et al., 2019a). The external surface of cortical bone is covered by the periosteum, which is made up of the outer fibrous layer and the inner cambium layer populated with progenitor and differentiated osteogenic cells (Dwek, 2010).

Looking more closely at composition, bone's dry weight composition consists of a 70/30 split between inorganic and organic materials. The inorganic fraction consists mainly of calcium phosphates, while the organic fraction is predominantly comprised of collagen ( $\approx 90\%$ ) as well other non-collagenous proteins and lipids (Shekaran and García, 2011, Mohamed, 2008).

Bone remodelling relies on the close coupling of bone formation and bone resorption, which is mediated by key cell populations, together termed the basic multicellular unit (Feng and McDonald, 2011). These include osteoblasts and osteocytes derived from local mesenchymal progenitors, and osteoclasts derived from haematopoietic

progenitors (Mohamed, 2008). Osteoblasts are responsible for the formation and deposition of new bone matrix and are subject to several fates, including becoming entrapped within the bone matrix as osteocytes, wherein they continue to regulate bone remodelling and repair through a process of mechanotransduction (Hinton et al., 2018). Osteoblasts can also develop into bone lining cells, which are quiescent cells that line the surfaces of bone that is not actively undergoing remodelling; their function is not fully understood but they appear to be involved in the supply of osteoblast cells (Matic et al., 2016). Osteoclasts are large multi-nucleated cells of haematopoietic origin that are responsible for the resorption of bone during remodelling (Teitelbaum, 2007). The bone remodelling process is an essential stage in bone repair, details of which are detailed in the following chapter (Section 2.3 Bone repair).

The structure of bone tissue is organised on a hierarchical scale from the molecular to macro-scales and is summarised in Figure 1.1. Primary collagen molecules are interstitially packed with HA and form oriented collagen fibrils, which are the basic component of collagen fibres. Concentric layers of collagen fibres arrange to form osteons (also known as Haversian systems), each of which is centred by a Haversian canal providing blood vessels and nerves (Nijsure and Kishore, 2017, Rho et al., 1998). At this level osteocytes are dispersed throughout the bone matrix along with the proteins that are essential for calcium binding and normal bone function such as osteocalcin, osteonectin, and bone sialoprotein (Clarke, 2008).

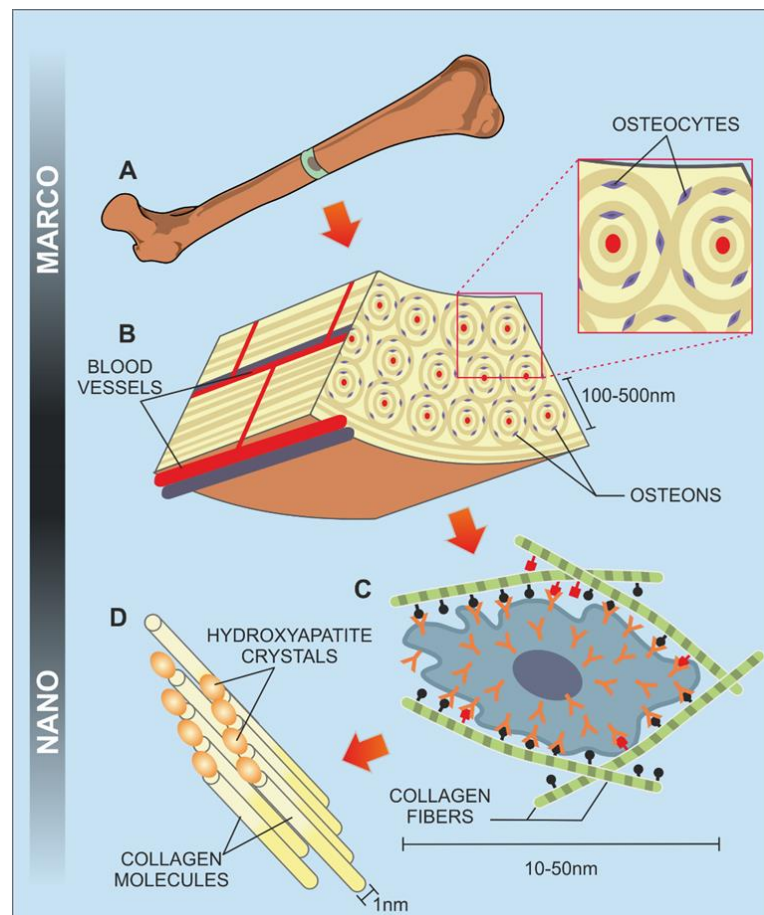


**Figure 1.1** Structural organisation of bone. (A) Bone (B) Osteons and haversian canals (C) Collagen fibres (D) Bone mineral crystals with molecular collagen. Adapted from (Ahern et al., 2013).

## 1.2 Current state of bone defect repair

Bone is a highly robust tissue capable of self-repair in most events of bone injury, and while only a small number (20 per 100 000 per annum) of injurious events are cases of non-union (Mills and Simpson, 2013), this type of injury can constitute a significant financial burden on health services, and severely impact on patients' quality of life (Kanakaris and Giannoudis, 2007), especially when it is considered that 49% of



patients who receive the gold standard therapy, autologous bone grafts, complain of significant side effects (Dahabreh et al., 2008). Furthermore, the frequency of bone-related medical conditions is on the rise, especially with ageing populations, this has led to a rise in the cost and impact that bone injuries and diseases have had on societies globally (Tatangelo et al., 2019). Conditions such as osteoporosis, bone loss after metastasis, and critical bone defects are notoriously challenging to manage.

In the case of critical bone defects, the current gold-standard for treatment includes the use of autologous bone grafts as well as allogenic bone grafts (Baldwin et al., 2019). Autologous bone grafts or autografts, involve the surgical excision of bone (typically from the iliac crest) to be used as an implantable material, with the main benefits being excellent biocompatibility and biological activity without the risk of immune rejection (Koons et al., 2020). Autografts are beneficial because they provide a matrix for bone growth (osteoconductive), they promote mesenchymal stem cell (MSC) differentiation along the osteoblast lineage (osteinduction) due to the presence of growth factors (e.g. Bone morphogenetic proteins (BMP), vascular endothelial growth factor (VEGF), and platelet derived growth factor (PDGF)) (Schmidmaier et al., 2006), cancellous autograft in particular also possesses excellent osteogenic potential arising from the abundance of transplanted osteogenic precursors with bone producing potential (Sun et al., 2019), and ultimately results in a high fusion rate at the transplant site. However, autografts are not without issue, as morbidity and logistical complications of procuring sufficient, easily accessible bone can arise (Goulet et al., 1997, Arrington et al., 1996). The morbidity risks include perioperative artery and nerve injuries and deep wound infections, as well as delayed complications such as hernia, nerve damage, and increased fracture risk (Banwart et al., 1995).

Allogenic bone grafts involve the receipt of donor or cadaver bone for use as a replacement material, this method alleviates some of the logistical concerns associated with the availability of autograft. However, the preference for freshly frozen allogenic bone may increase the risk of viral disease transmission (Wimmer et al., 1999).

### **1.3 Bone tissue engineering**

Tissue engineering is generally defined as the use of synthetic or natural materials to regenerate the form and function of damaged tissue (Vacanti and Vacanti, 2014). The field of bone tissue engineering (BTE) aims to apply the principles of engineering and biology to the development of functional tissue substitutes for damaged tissue, thereby overcoming the inherent limitations of autograft and allograft procedures, while attempting to replicate an equivalent level of biological activity in the designed replacement material (Montoro et al., 2014).

Tissue engineering has been applied across a range of tissue types including skin (Falanga et al., 2014), bone (Montoro et al., 2014), tendons and ligament (Goulet et al., 2014), and vascular tissue (Brewster et al., 2014), all of which have their own specific goals and challenges. Although significant progress has been made in the field as a whole, most notably the Dermal Regeneration Template, Integra® (Integra LifeSciences, USA) and the spinal fusion bone grafts, INFUSE® (Medtronic, USA) (Hoffman et al., 2019), it is clear that there is still much work required. For instance, INFUSE®, contains the osteoinductive growth factor, recombinant human BMP (rhBMP) -2 and has been associated with ectopic bone growth and increased likelihood of additional surgeries (Epstein, 2013).

Tissue engineering methods require a collaboration between the existing infrastructure of the damaged tissue and the three pillars of tissue engineering: cells, scaffolds, and signals (Nerem and Schutte, 2014) (Figure 1.2). ‘Cells’ represent the important cellular populations involved in the regeneration of a particular tissue, ‘scaffolds’ is a material that mimics the natural extracellular matrix of the regenerating tissue upon which cells can act, and finally ‘signals’ are natural or synthetic molecules that induce one or more biochemical activities in any or all of the cellular populations involved (Nerem and Schutte, 2014). A general overview of these three pillars will be presented in the following sections, beginning with the considerable research that has been dedicated to investigating different materials and techniques suitable for the preparation of ‘scaffolds’ for BTE (Turnbull et al., 2018, Roseti et al., 2017).

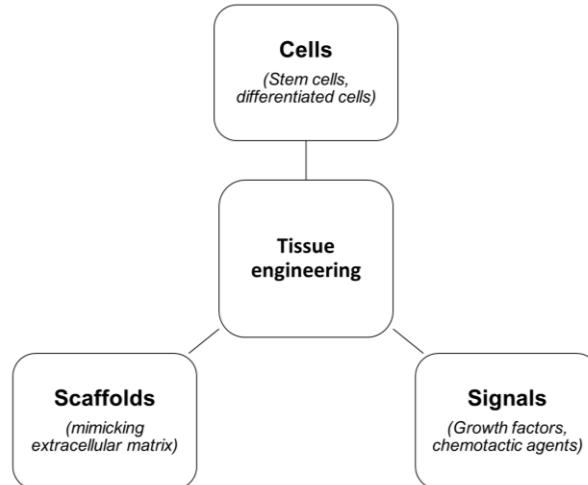


**Figure 1.2** Schematic of the key pillars of bone tissue engineering design (Hoffman et al., 2019).

## 1.4 Properties of an implantable scaffold

Any implantable scaffold designed to support the regeneration of critical bone defects will need to fulfil several criteria, all of which are inspired by the qualities of natural bone tissue (Figure 1.3).

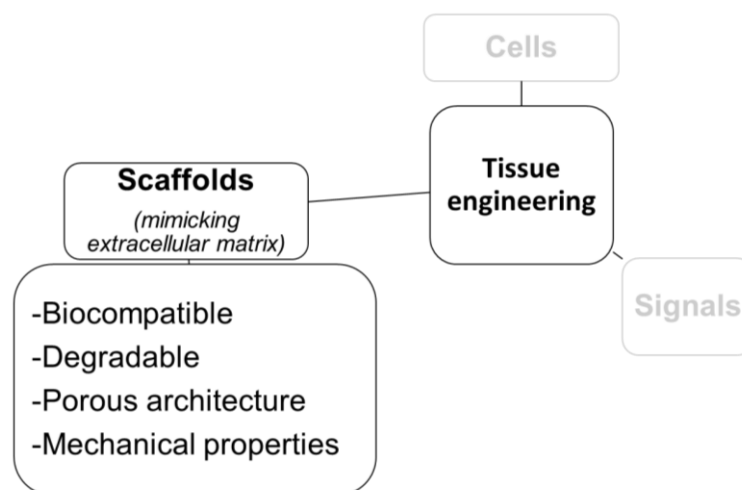


**Figure 1.3** Schematic highlighting the ‘Scaffolds’ pillar of tissue engineering design.

The scaffold should be non-toxic and biocompatible (Kohane and Langer, 2010), allowing the natural growth and behaviour of the native cell populations in the injured tissue. Stimulating a favourable interaction can be further manipulated by combining natural materials such as collagen or HA with inexpensive and abundant base materials such as biodegradable polymers, which should ideally not induce an immune response (Jin et al., 2019). The completed scaffold must also be compatible with an appropriate method of sterilisation, whether by heat (autoclave), irradiation (UV, Gamma), or chemical means (ethylene oxide, acetic acid) (Dai et al., 2016).

It is important that the architecture of the scaffold achieves a degree of biomimicry, approximating the architecture of natural bone. For example, the porosity of the material is essential for initial cell adhesion, preventing cell aggregation on the scaffold surface, and improving cell infiltration and should be in the range of hundreds of microns (Murphy et al., 2010). Micropores in the range of tens of microns are also important in increasing surface area for protein adsorption and influencing scaffold degradation (Zhang et al., 2018). Degradation is another design factor in BTE scaffolds (Rezwan et al., 2006), and therefore it is important to note that just as the process of bone regeneration develops over a period of several months (Loi et al., 2016), it must similarly be the case that an implanted scaffold closely match this timeframe in its degradation (Polo-Corrales et al., 2014). Additionally, much research has taken inspiration from the cues inherent in native bone tissue e.g. cortical or cancellous bone, and scaffolds have been designed to approximate bone in terms of its mechanical, and biological behaviour (Wang et al., 2016b) (Table 1.1). From an economic perspective, all materials and methods must eventually represent cost-effective and viable alternatives to autograft procedures while maintaining efficacy (Mehta et al., 2018).

**Table 1.1** Summary of mechanical properties of cortical and cancellous bone, adapted from (Hench, 2013). Compressive and tensile strength are the ability of a material to withstand the application of compressive and tensile stress without breakage or deformation. Strain to failure is the ratio between the change in sample length and the initial length, following breakage. Young's modulus measures a material's stiffness by quantifying the relationship between the force applied to a material (stress) and its deformation (strain) (Beer et al., 1999).

<b>Mechanical properties</b>	<b>Cortical (compact) bone</b>	<b>Cancellous (spongy) bone</b>
Compressive strength (MPa)	100 - 230	2 - 12
Tensile strength (MPa)	50 - 150	10 - 20
Strain to failure (%)	1 - 3	5 - 7
Young's (elastic) modulus (GPa)	7 - 30	0.05 - 0.5

## 1.5 Types of materials in bone tissue engineering

There are a number of materials that have been used to prepare scaffolds in BTE projects, but most can be placed into categories of polymers, ceramics and composites of the two (Roseti et al., 2017, Koons et al., 2020) (Table 1.2), these materials are the topics of the following sections. Metals (alloys of titanium and magnesium) (Malladi et al., 2018), and carbon-based nanomaterials (carbon nanotubes) (Eivazzadeh-Keihan et al., 2019) are interesting materials that should be mentioned, these materials possess exceptional mechanical strength and the potential to be chemically surface modified

to induce bioactivity (Cheng et al., 2016, Arnold et al., 2019). However, metal and carbon-based materials are somewhat outside the scope of this thesis, due to their specialised processing requirements and non-degradability.

**Table 1.2** Overview of polymer and ceramic materials, adapted from (Koons et al., 2020, De Witte et al., 2018).

Material	Example	Advantages	Disadvantages
Polymers	Natural: Collagen	Biomimetic (contains natural cell adhesion sites)	Potential immunogenicity
	Synthetic: PLGA	Biocompatible, biodegradable, with a wide range of modifiable compositions	Mechanical properties inconsistent with bone
Ceramics	Hydroxyapatite	High compressive modulus Osteoconductive	Brittle
	Bioactive glasses	High bonding with bone Osteoinductive Several are biodegradable	

### 1.5.1 Polymers

Polymers, long chains of covalently bonded repeating units, have a long history of use as biomaterials for the preparation of tissue engineering scaffolds (Dhandayuthapani et al., 2011). Polymers can be of synthetic or natural origin (Asghari et al., 2017). Natural polymers such as collagen (Dong and Lv, 2016), gelatin (derived from acid or alkaline hydrolysis of collagen) (Hoque et al., 2015) and hyaluronic acid (Collins and Birkinshaw, 2013) have been shown to have good biocompatibility, being generally hydrophilic and exhibiting low immunogenicity (Gasperini et al., 2014). Collagen, as the main organic constituent in bone, is a fundamental component of autograft and allograft, and is a critical carrier component in the spinal fusion bone graft, INFUSE®.

Furthermore, collagen is the component that adds flexural strength to bone and amino acid sequences within the protein structure act as sites for cellular attachment (Di Lullo et al., 2002). These properties have led to collagen being widely investigated in BTE (Stuckensen et al., 2018). Collagen despite its excellent biocompatibility and cell adhesion properties lacks rigidity and osteoinductivity and is often used in combination with other materials (Glowacki and Mizuno, 2008). Recent examples of collagen based scaffolds include a porous bioactive construct doped with strontium and silver that resulted in improved regeneration of a rat cranial defect (Liu et al., 2020). Another group prepared silica coated collagen scaffolds that successfully induced repair of a rabbit cranial defect without the addition of exogenous cells and growth factors (Wang et al., 2019).

Synthetic or semi-synthetic polymers are generally less hydrophilic and less biocompatible than natural polymers. However, their tuneable degradation and mechanical properties are key advantages (Roseti et al., 2017). Examples include polyanhydrides, and polyesters including polycaprolactone (PCL), poly (lactic acid) (PLA), and copolymers poly (lactide-co-glycolide) (PLGA) (Sabir et al., 2009). In particular PLGA has been extensively investigated for BTE applications, and has been prepared in a variety of forms, such as films, microspheres, and porous scaffolds (Gentile et al., 2014). PLGA has well documented biocompatibility, and its degradation products (lactic and glycolic acids) are ultimately excreted from the body as carbon dioxide (CO<sub>2</sub>) and water (Elmowafy et al., 2019). Degradation rate is affected by several factors related to the polymer including monomer ratio, molecular weight, stereochemistry and solid-state properties. For example, degradation rate is decreased as the ratio of lactide monomers increases, due to its increased



hydrophobicity (e.g. PLGA 85:15 degrades more slowly than PLGA 65:35) (Makadia and Siegel, 2011). Other properties that slow degradation include physical features of the construct e.g. reduced surface-area to volume by altering the size and shape of a scaffold matrix (Makadia and Siegel, 2011). The slowly degrading copolymer, PLGA 85:15 is already used in several maxillofacial bone fixation devices including RAPIDSORB<sup>®</sup> (DePuy Synthes Companies, USA), and LactoSorb<sup>®</sup> (Zimmer Biomet, USA), among others (Gilardino et al., 2009).

While PLGA is biocompatible it does not possess strong osteoconductive or any osteoinductive properties, therefore most recent applications of PLGA in cases of challenging bone defects are composite materials. An example being a PLGA porous scaffold coupled with magnesium powder and  $\beta$ -tricalcium phosphate resulting in enhanced osteogenic and angiogenic properties of the scaffold compared to PLGA controls (Lai et al., 2019). Another scaffold using similar materials,  $\beta$ -tricalcium phosphate and magnesium hydroxide, improved bone regeneration in a rat humoral defect through the added materials' respective impacts as osteoconductive and anti-inflammatory agents (Go et al., 2020). PLGA also has utility for controlled release of potent osteogenic agents in BTE scaffolds, for example the controlled release of BMP-2 from PLGA scaffolds which resulted in significant new bone formation in mouse cranial defects (Rahman et al., 2014).

### 1.5.2 Ceramics

The first generations of ceramic implants were based on zirconia and alumina, and while non-toxic, they did not interact with the surrounding tissue and so were termed bioinert and they are also non-bioresorbable (Vallet-Regí and Ruiz-Hernández, 2011).

Later generations consisted of implantable materials that react with the surrounding tissue in order to form new bone and degrade gradually as the natural tissue regenerated (bioresorbable), these are bioactive ceramics and include calcium phosphates (CaP) and bioactive glasses (Vallet-Regí and Ruiz-Hernández, 2011, Hench, 2013). Calcium phosphates including HA ( $\text{Ca}_{10}(\text{PO}_4)_6(\text{OH})_2$ ), and  $\alpha$ - and  $\beta$ -tricalcium phosphate (TCP) ( $\text{Ca}_3(\text{PO}_4)_2$ ) share a chemical similarity to the inorganic phase of bone, which has led to their extensive investigation in preparing BTE scaffolds (Ben-Nissan, 2003, Hoppe et al., 2011). Both HA and TCP are osteoconductive (Kokubo, 1998), and both support the adhesion (Annaz et al., 2004, Ergun et al., 2008) and differentiation of osteoblast progenitors (Shu et al., 2003, Chen et al., 2014). The degradation or resorption of CaP can be controlled by their Ca/P ratio with monocalcium phosphates (0.5 Ca/P ratio) being more resorbable than TCP (1.5 Ca/P ratio), which in turn resorbs quicker than HA (1.67 Ca/P ratio) (Dorozhkin, 2010). Bioactive glasses (BG), such as the prototypical 45S5 Bioglass<sup>®</sup> (Hench et al., 1971), are another bioactive ceramic based on compositions of sodium, calcium, phosphate, and silicate oxide glasses that form a strong adhesive bond to bone and to soft tissue (Hench et al., 2004). The BGs slowly bond with existing soft and hard tissue as they dissolve in biological fluids forming a carbonated HA layer, which adsorbs growth factors and supports cell growth, ultimately resulting in the formation of healthy and functional bone tissue (Rahaman et al., 2011).

Some recent applications of bioceramics in BTE included a study that described a composite ceramic scaffold design composed of HA/TCP, that was 3-D printed and implanted into canine mandibular defects for up to 8 weeks, and resulted in a significant increase in new bone formation (Kim et al., 2020). Another recent study

investigated a 3-D printed BG (AP40) seeded with bone marrow progenitor cells implanted in a rabbit mandibular defect for up to 9 months that resulted in near complete coverage of the defects by new bone and the formation of blood vessels within the pores of the implanted scaffold (Xu et al., 2020).

## **1.6 Fabrication techniques**

The choice of material is clearly an important aspect of designing a BTE scaffold. Equally important is the fabrication technique used to manipulate the material into the potential form with key structural features. Some conventional techniques include solvent casting/particulate leaching, freeze drying, and gas foaming (Roseti et al., 2017). Advances in fabrication techniques, particularly the advent of nanotechnology and additive manufacturing including 3-D printing and bioprinting (Masaeli et al., 2019), have enabled scaffolds with more precisely controlled and sophisticated features to be produced. Electric field-assisted techniques, such as electrospinning and electrospraying, although not considered an additive manufacturing technique, share more in common with additive manufacturing than the earlier conventional techniques (Dalton et al., 2013). Given their major role in the work conducted herein, electric field-assisted techniques are more thoroughly described alongside an overview of some of the other techniques in the following sections.

### **1.6.1 Solvent casting and particulate leaching**

This technique generally involves dissolving the polymer in an organic solvent, an insoluble salt (the porogen) is then admixed into the solution. Thereafter the organic solvent is evaporated leaving a solid polymer-salt construct, leaching out the salt leaves behind a 3-D porous polymeric scaffold (Sola et al., 2019). The benefits of this

method are tuneable porosity, by manipulating salt grain size, as well as the relative simplicity and low cost of the technique (Roseti et al., 2017). One example of this technique involved the preparation of a porous composite scaffold of poly (glycolic acid) (PGA) and  $\beta$ -TCP, which contributed a small but significant increase in bone volume in a rat femoral defect (Cao and Kuboyama, 2010). Another example involved the preparation of PCL/HA scaffolds, that stimulated the expression of markers of osteogenic differentiation *in vitro* and showed significant new bone formation in a murine cranial defect study (Chuenjitkuntaworn et al., 2010). The limitations of the solvent casting technique include production of scaffolds with simple architectures, as well as the possibility of residual solvent and porogen material in the final scaffold (Prasad et al., 2017).

#### 1.6.2 Gas foaming

Gas foaming is a process through which polymers are expanded to create foams (Costantini and Barbetta, 2018), either chemically by using additives (e.g. sulfamic acid and sodium nitrite) that react or decompose to release gas, or using physical blowing agents (e.g. CO<sub>2</sub>, pentane, argon, nitrogen) directly injected or pressurised into the polymer (Costantini and Barbetta, 2018).

For BTE, the main driving force behind using gas foaming is the preparation of scaffolds with a porous matrix while eliminating the risk of potentially dangerous residual solvents and porogens (Mooney et al., 1996). However, this method alone can lead to a non-interconnected pore structure, and a non-porous surface layer (Roseti et al., 2017, Prasad et al., 2017). To overcome these issues, foaming can be coupled with a porogen leaching step to improve pore interconnectivity (Harris et al., 1998). Gas

foaming has also been coupled with other techniques including freeze drying (the topic of the following section). In one case, gas foaming (in combination with freeze-drying) was used to prepare a chitosan/agarose/HA scaffold that supported the adhesion and growth of osteoblasts *in vitro* (Kazimierczak et al., 2020).

### 1.6.3 Freeze-drying

Freeze-drying or lyophilisation is a process by which a solution or slurry of a scaffold material is frozen, followed by sublimation of the solvent under vacuum resulting in a complex porous structure (Deville et al., 2006). The main advantages of freeze-drying are the avoidance of high temperatures that can reduce the activity of any incorporated biological factors, and the potential to manipulate pore size by controlling the rate of freezing (Roseti et al., 2017). As an example of a freeze-dried scaffold, a 58S-BG/collagen/phosphatidylserine composite scaffold was shown to support the formation of new bone in a rat femoral defect (Xu et al., 2011). A more recent example can be seen with a strontium doped HA/chitosan scaffold that improved the adhesion, spreading, and proliferation of bone marrow mesenchymal stem cells (Lei et al., 2017). The major limitation of freeze-drying remains the long timescales required for fabrication, with the previous two examples requiring 13 and 36 h of lyophilisation, respectively.

### 1.6.4 3-D printing

Following the original description of stereolithography in the latter half of the 1980s (Hull, 1984), 3-D printing and bioprinting have been categorised as types of additive manufacturing and are defined as the printing of structures using biomaterials, biomolecules, and cells in the case of bioprinting (Kačarević et al., 2018). 3-D printing

techniques are some of the fastest growing fabrication methods for BTE as accessibility to equipment and cost-effectiveness improve (Koons et al., 2020, Derakhshanfar et al., 2018, Haleem et al., 2020). There are several well-known printing techniques, including inkjet, extrusion, and laser-assisted methods (Kačarević et al., 2018). Some of the earliest and most common examples of 3-D printing were inkjet-based, and while they benefit from relatively low cost, high availability and high resolution, they are still limited by unreliable droplet directionality and inconsistent viability of live-cell encapsulation (Murphy and Atala, 2014). For comparison, Table 1.3 contrasts the different 3-D printing techniques.

**Table 1.3** General comparison of 3-D printer types, adapted from (Murphy and Atala, 2014).

	Inkjet	Extrusion	Laser-assisted
Preparation time	Low	Low-medium	Medium-high
Print speed	Fast	Slow	Medium-fast
Resolution	>50 $\mu\text{m}$	>5 $\mu\text{m}$	>100 $\mu\text{m}$
Cell viability	>85%	40–80%	>95%
Cost	Low	Medium	High

#### 1.6.5 Electric-field assisted techniques

Electric-field assisted techniques, also known as electrohydrodynamic processing, consisting of electrospinning and electrospraying, are two related techniques used in biomedical and tissue engineering applications (Haider et al., 2019). Electrospinning and electrospraying are increasingly investigated in preparing nano- and micro-sized

structures for BTE (Correia et al., 2014, Jeyhani et al., 2017, Jiang et al., 2015, Koons et al., 2020).

#### 1.6.5.1 Electrospraying

Electrospraying is a process by which a sufficiently high electric field applied to the surface of a liquid results in the emission of charged droplets (Cloupeau and Prunet-Foch, 1990). The most important parameters involved in the formation of droplet particles include the solution viscosity, applied voltage, solution flow rate, and working distance from collector plate (Cloupeau and Prunet-Foch, 1990, Haider et al., 2019). In general, once a polymer solution reaches a concentration that produces sufficient polymer entanglement, particles will be formed once the build-up of charge overcomes surface tension (Coulomb fission after exceeding Rayleigh limit). If polymer entanglement increases further (by increasing solution concentration), this can ultimately reach an upper limit whereby fibres rather than particles are formed after the surface tension is overcome (Almería et al., 2010).

Electrospraying is not extensively used in bone tissue engineering specifically, however, its utility as a highly efficient method of encapsulating therapeutic molecules gives weight to its potential use in biomedical and regenerative medicine as a whole (Bock et al., 2012). Aside from therapeutic molecules, electrospraying can also be used to encapsulate cellular cargoes for tissue engineering purposes (Xu et al., 2019). For example, electrosprayed alginate/gelatin microspheres have been embedded with bone marrow-derived stem cells (BMSC), these cell-laden microspheres were then incorporated into a 3-D printed PCL scaffold (Xu et al., 2019).

### 1.6.5.2 Electrospinning

Electrospinning is more commonly used than electrospray methods in tissue engineering applications (Soares et al., 2018). It involves extrusion of an electrically conductive solution from a hollow needle under the influence of an applied voltage, and deposition on a collector plate. Generally, solutions of polymeric materials dissolved in volatile solvents are used (Zhu and Chen, 2013). As the extruded solution travels towards the electrically grounded collector plate, the solution jet extends, rapidly increasing its surface area and rate of evaporation, leaving behind micro- and nano-sized fibres of solid polymer material (Agarwal et al., 2009, Agarwal et al., 2008). Figure 1.4 shows a graphical representation of the electrospinning process.

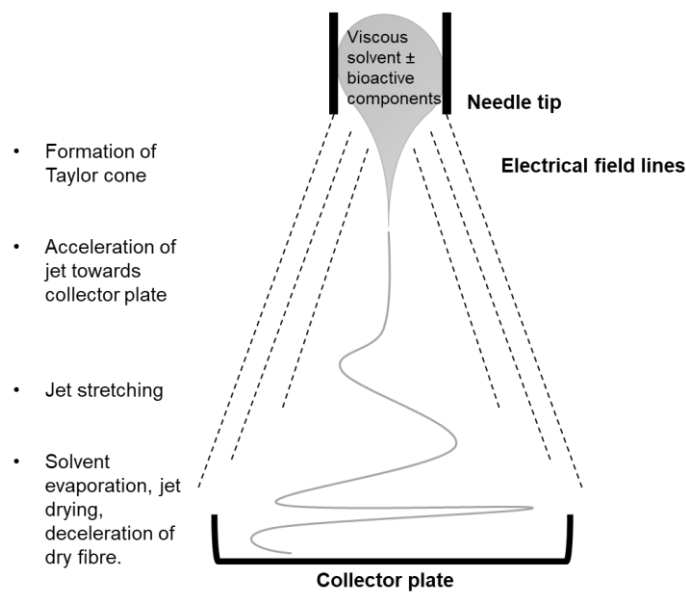


**Figure 1.4** Graphical illustration of the electrospinning process, listing the progression of the electrospinning solution from the needle tip until collection as dry fibres. Inspired by (Koons et al., 2020).



There are several variables in the electrospinning process (voltage, viscosity, flow rate) that may influence the physical characteristics of the electrospun material. Research has indicated that increasing voltage increased the density of “beading” defects in fibres, while increasing or decreasing solution viscosity directly influenced fibre diameter (Deitzel et al., 2001). A more recent study showed that fibre diameter is primarily controlled by voltage and that the relationship is inversely proportional. Solution viscosity was a secondary factor that influenced fibre diameter in a directly proportional manner, with flow rate considered as a minor contribution to fibre diameter (Korycka et al., 2018). Another study investigated the effects of voltage, flow rate, and needle-to-collector distance on fibre diameters, and showed that increasing voltage resulted in reduced fibre diameters, as did increasing flow rate, and increasing the tip-to collector distance (Akturk et al., 2020).

Different electrospinning methodologies exist in the preparation of electrospun membranes. Simple polymer blend electrospinning is the simplest technique, which can be used to produce fibres with a drug randomly distributed throughout (Hall Barrientos et al., 2017). A more organised drug distribution can be obtained from emulsion blends, whereby two immiscible solvents are used to compartmentalise a desired drug or additive (Wei et al., 2012). Increasing the structural complexity further has relied on co-axial electrospinning techniques, whereby a concentric needle system is used to extrude an electrospun material with a core-sheath morphology (Wang et al., 2014). This approach has the potential to produce a two or more phased fibre or indeed a hollow fibre morphology if necessary (Xue et al., 2019a).

There are a number of recent reviews detailing the application of the electrospinning technique in preparing biomaterial scaffolds in general (Ding et al., 2019), as well as in BTE specifically (Bhattarai et al., 2018). Some recent examples include a tri-component PLA/gelatin/RKKP-BG scaffold where the polymeric components were dissolved in hexafluoroisopropanol and the glass ceramic was added in suspension. The glass-ceramic was shown by dispersive X-ray spectrometry to be dispersed throughout the fibrous matrix and it led to a 15-30 % increase in fibre diameter, which was attributed to increasing the viscosity of the electrospinning preparation (Bochicchio et al., 2020). Results showed the fibre scaffold supported the growth and osteogenic differentiation of canine adipose derived MSC *in vitro* (Bochicchio et al., 2020). Another study describes the preparation of a PLGA electrospun structure coated with HA/collagen that improved cell spreading, differentiation, and osteogenic gene expression in MSC (Yang et al., 2018).

The main advantages of electrospinning are its versatility in processing different materials (Roseti et al., 2017), and its ability to mimic the fibrillar properties and dimensions of bone extracellular matrix (Hendrikson et al., 2017), thus simulating an hospitable environment for the spread, growth, and infiltration of cells during the repair process (Jang et al., 2009). Another advantage is the possibility of using electrospinning in combination with growth factors (Zhang et al., 2019b), or natural components of the extracellular matrix such as HA and collagen (Yang et al., 2018). The main disadvantage of electrospinning is its use of organic solvents and the difficulties in controlling the 3-D porosity of the completed material (Haider et al., 2018).

## 1.7 Clinical considerations

The choice or design of an implantable material is dependent on the defect site and the nature of the defect (Roseti et al., 2017, Koons et al., 2020). Indeed, the results seen with any particular scaffolds may differ depending on the anatomical site and the scaffold interaction with cortical or cancellous bone (Walsh et al., 2019). Similarly, when formulating a plan for the repair of a long bone defect, it is important to consider optimal vascularisation (Johnson et al., 2011), and the potential need of load bearing capacity (Bao et al., 2017). In contrast, when considering flat bones, a more critical issue than functional weight-bearing may be the complexity of the defect, with regard to its shape and the close interaction of numerous tissue types (nerves, muscle, blood vessels) (Kretlow et al., 2009).

In cases of osteoporotic defects, it may be preferable to target the limitation of bone resorption, as described by one study using a bisphosphonate/gelatin/45S5-BG injectable gel that supported the regeneration of osteoporotic femoral defects in rats while also enhancing bone density in the periphery of the defect (Diba et al., 2017). In cases of bone defects related to malignancy, where growth factors may need to be avoided, studies have described magnetically induced hyperthermic scaffolds that can be activated to damage malignant cells while simultaneously acting as thermally activated drug delivery devices (Wu et al., 2011, Bañobre-López et al., 2014). Similarly, scaffolds have been designed to specifically target defects secondary to conditions of infection (Pearson et al., 2020) or inflammation (Zhao et al., 2019). Finally, regulatory considerations must be taken into account, especially when utilising scaffold designs that span multiple regulatory categories, whether medical devices, drugs, and other biological products as the regulatory pathway can impact the

studies involved in their clinical translation and the associated costs (Hunter and Sherman, 2017).

## **1.8 Cell-based therapies in BTE**

The cellular populations involved in bone healing change over the course of the repair process (Section 2.3 Bone repair), from the initial inflammatory response of neutrophils and macrophages removing debris, setting the stage for an angiogenic response (Perez et al., 2018), to revascularisation and essential recruitment of MSC, the progenitors of bone forming osteoblasts (Marsell and Einhorn, 2011).

It is possible to incorporate primary osteoblasts into BTE scaffolds, as described in a study, which pre-loaded a silk fibroin scaffold with mature mineral forming osteoblasts and implanted them in mice. In this system, the cells acted as a driver of scaffold vascularisation alongside the host immune cells, ostensibly by osteoblast-derived pro-angiogenic growth factors (Ghanaati et al., 2011). However, directly seeding mature osteoblasts is uncommon due to difficulties associated with harvesting and maintaining meaningful cell numbers (Perez et al., 2018). Therefore, most cell-based therapies utilise a variety of stem cell-based options (Figure 1.5).

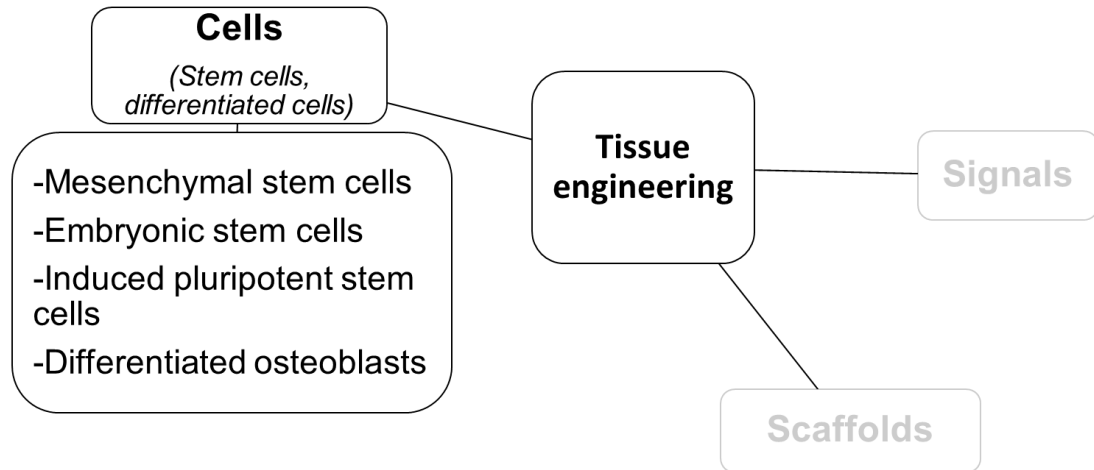


**Figure 1.5** Schematic highlighting the “Cells” pillar of bone tissue engineering design.

Well-established sources of MSC include adipose tissue- and bone marrow-derived stem cells (Secunda et al., 2015). A recent example described a gelatin/HA/45S5-BG scaffold pre-seeded with BMSC that significantly improved new bone formation in rat, 5 mm radial bone defects, with the cell-seeded scaffold producing new bone volume comparable to autograft controls (Oryan et al., 2018).

Other potential cell-based therapies utilise embryonic stem cells (ESC), whose differentiation pathways span all germ layers (Thomson et al., 1998), and have previously been seeded on PLGA/HA scaffolds and found to result in bone formation when subcutaneously implanted in mice (Kim et al., 2008). Induced pluripotent stem cells (iPSC), which have comparable differentiation potential to ESC (Takahashi and Yamanaka, 2006) have also been investigated. Some examples include the pre-seeding and differentiation of iPSC on commercial gelatin scaffolds prior to subcutaneous

implantation, resulting in mineralisation and the expression of osteocalcin and bone sialoprotein (Bilousova et al., 2011). Another study describes a more direct approach, whereby iPSC were seeded on PLGA/HA scaffolds and implanted in murine critical cranial defects, resulting in a 49% regeneration of the defect (as determined by microCT) (Levi et al., 2012). That result was further improved to 96%, when the scaffold surface was coated with rhBMP-2.

## 1.9 Growth factors in BTE

There are several protein growth factors stored and released from the bone extracellular matrix following injury and during the bone repair process including BMP, VEGF, and PDGF, among several others (Perez et al., 2018). This abundance of growth factors in bone material plays a major role in the efficacy of autograft in contributing to bone repair (Schmidmaier et al., 2006). The initial phases of inflammatory bone repair are dominated by interleukins, and prostaglandins (Hankenson et al., 2015), followed by revascularisation and significant increases in PDGF, VEGF, and angiopoietin. Thereafter, rising levels of BMP are the major contributor to the bone formation phase (Hankenson et al., 2015). A more detailed description of the bone repair process is shown in **Chapter 2** (Section 2.3, Bone repair).

First reported in 1965, BMP are osteogenic growth factors (Urist, 1965). There are more than 30 different BMP, several of which, including BMP-2, -4, -5, -6, -7, and -9 have well documented roles in bone processes (Dumic-Cule et al., 2018). BMP-2 has, since 2002, been approved for anterior lumbar interbody fusion (Burkus et al., 2002),

while BMP-7 is a component of the collagen/cellulose based OP-1<sup>®</sup> Putty (Stryker, USA) (Vaccaro et al., 2003).

Some recent studies utilising BMP include a HA/collagen/carbon-nanotube scaffold loaded with BMP-9 and seeded with BMSC that significantly promoted new bone formation in rat cranial defects (Zhang et al., 2019a). Another recent study describes a  $\beta$ -TCP/PLGA/CaCO<sub>3</sub> electrospun scaffold loaded with BMP-2, that promoted MSC proliferation and differentiation *in vitro* and increased bone volume in a rat posterolateral spinal fusion (Glaeser et al., 2020). The main concerns associated with the use of BMP include the need for large doses due to challenges related to stability and controlled release, heterotopic ossification and inconclusive evidence of post-operative cancer occurrence (Cahill et al., 2015).

Revascularisation is an essential phase of bone regeneration and VEGF is a fundamental factor involved during this phase (Hankenson et al., 2015). This can be seen in several studies utilising the growth factor in combination with implantable scaffolds. For example, one study described a gas-foamed, particulate leached PLGA/alginate scaffold loaded with VEGF that was implanted in rat cranial defects and produced significant increases in new blood vessel formation and new bone formation (Kaigler et al., 2006). Another study showed the design and *in vitro* evaluation of an electrospun PLGA/gelatin scaffold sequentially releasing both VEGF and BMP-2 that promoted the adhesion, proliferation and differentiation of BMSC (An et al., 2017). VEGF used alone is not sufficient to produce mature and stable vasculature, rather requiring a combinatorial approach with angiopoietin and PDGF (Jain et al., 2005). PDGF is a growth factor, which aids the structural stability of newly

formed blood vessels (Caplan and Correa, 2011). PDGF has for a long time been investigated as a component of implantable scaffolds for BTE, an early example described PDGF mixed with an injectable collagen implant having a stimulatory effect on rabbit tibial fracture healing (Nash et al., 1994). A more recent study utilised an electrospun PCL/collagen/HA scaffold that adsorbed and released PDGF over 8 weeks, with the released PDGF eliciting a significant chemotactic response from MSC *in vitro* (Phipps et al., 2012b). As with BMP, other growth factors are limited by their biologic stability, PDGF and VEGF have half-lives of 2 and 50 mins, respectively (Chen and Mooney, 2003). Furthermore, whether using a single growth factor or a combinatorial approach, several variables must be considered including: the concentration of the growth factors and formation of local gradients, local cell populations, the presence of other local growth factors, and the interaction between these variables (Mehta et al., 2012). Therefore, any attempt at using growth factors requires vehicles to ensure stable and spatiotemporal control over their delivery. A possible alternative to the use of protein and peptide growth factors is the use of more biochemically stable, small molecule pharmacological agents (Figure 1.6).



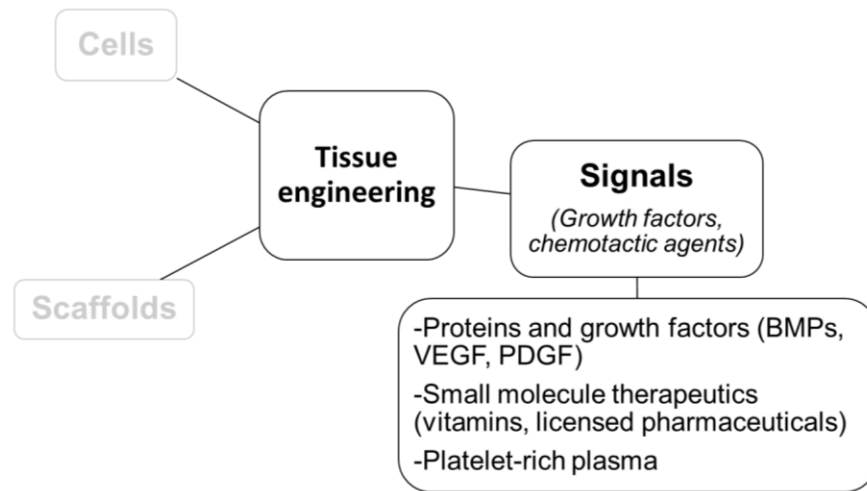


**Figure 1.6** Schematic highlighting the “Signals” pillar of bone tissue engineering design.

### 1.10 Pharmacological options in BTE

As discussed in the previous sections BMP are to date the only protein growth factors licensed for bone regenerative purposes. And although some of their drawbacks can be mitigated by alternative peptide techniques, such as BMP protein fragments (Kim et al., 2012, Kim et al., 2017), the focus of this section is on the option of using small molecule therapeutics with osteoinductive properties as an alternative to protein growth factors (Carbone et al., 2014, Laurencin et al., 2014). The pros and cons of protein-based vs small molecule therapeutics are summarised in Table 1.4.

**Table 1.4** Comparing the advantages and disadvantages of protein- and small molecules-based therapeutics, adapted from (Carbone et al., 2014).

Protein-based therapeutics	Small molecule therapeutics
<b>Advantages</b> Good specificity Good bioactivity  <b>Disadvantages</b> Instability High cost Risk of impurity and immunogenicity	<b>Advantages</b> Good stability Low cost Low impurity and immunogenicity <b>Disadvantages</b> Poor specificity

Small molecule therapeutics generally possess greater stability and longer biological half-life. Furthermore molecules smaller than 1000 Da are less likely to induce an immune response (Kadow et al., 2009). The major limiting factor for small molecule therapies is their lack of specificity and off-target side effects. Hence, the need to develop methods for their localised and controlled delivery. Several small molecule therapeutics, many marketed for other clinical indications, have shown potential in impacting key processes integral to bone regeneration.

Alendronate, a bisphosphonate indicated in osteoporosis that acts by reducing bone turnover, has been incorporated into collagen scaffolds and released in a sustained manner resulting in improved bone regeneration of a critical cranial defect in ovariectomised rats (Zeng et al., 2020). Another class of small molecule drugs includes the cholesterol lowering ‘statins’ simvastatin, rosuvastatin, and lovastatin that have shown an osteoinductive effect associated with inhibition of the mevalonate pathway intermediates (farnesyl and geranyl pyrophosphates), which produces an increased expression of BMP-2 mRNA (Ruan et al., 2012). A recent study described a chitosan

scaffold combined with simvastatin-loaded nanoparticles that stimulated BMSC differentiation *in vitro* and showed improved bone regeneration in a critical cranial defect *in vivo* (Xue et al., 2019b). Dexamethasone, a corticosteroid, is known to stimulate the differentiation of MSC and pre-osteoblastic cells (Mostafa et al., 2012, Igarashi et al., 2004), and is associated with increased expression of osteogenic proteins RUNX2, Osterix and bone matrix proteins (Igarashi et al., 2004). A recent article coupled dexamethasone with a gas foamed silk fibroin/PCL scaffold that promoted bone regeneration in a rat cranial defect (Goimil et al., 2019). The micronutrients vitamin D3 and ascorbic acid (vitamin C) possess osteoinductive properties, vitamin D3 stimulates the expression of osteogenic markers in MSC including alkaline phosphatase, osteopontin, and osteocalcin (Lou et al., 2017). Vitamin C has been shown to increase gene expression of BMP-2, RUNX2, osteocalcin, and type-1 collagen (Choi et al., 2019). A study using a solvent cast PLGA scaffold loaded with vitamin D3 and MSC, showed the formation of new osteoid and calcium deposition in a rabbit femoral defect (Yoon et al., 2007). Vitamin C is less common in the BTE literature and rarely used in isolation, for example one study investigated a polyurethane foam scaffold loaded with vitamin C, dexamethasone, and  $\beta$ -glycerophosphate. The scaffolds were implanted subcutaneously, and excised tissue showed histological and immunohistochemical evidence of mineralisation (Wang et al., 2017). There are several other small molecules that have shown interesting osteoinductive effects, including rolipram (Tokuhara et al., 2010), retinoic acid (Cowan et al., 2005), purmorphamine (Gellynck et al., 2013), tetracycline (Farzamfar et al., 2019), fingolimod (Das et al., 2014b), and S1P (Sefcik et al., 2008). All are

included in Table 1.5, which lists small molecule therapeutics that have been investigated using *in vivo* preclinical trials.

S1P and fingolimod, are of interest in this thesis due to evidence showing that their local administration via polymeric scaffolds can contribute to bone regeneration of critical defects *in vivo* (Das et al., 2014a, Petrie Aronin et al., 2010a, Petrie Aronin et al., 2010b, Sefcik et al., 2008). Both these molecules together with related analogues including siponimod motivated much of the work in the following chapters. **Chapter 2** is dedicated to the role of S1P and its associated receptors in bone biology and repair in more specific detail. A general summary of S1P receptor pharmacology and function in tissues outwith bone is shown in Table 1.6 and Figure 1.7.

**Table 1.5** Summary of small molecule agents investigated using *in vivo* preclinical studies.

	<b>Mechanism</b>	<b>References</b>
Alendronate	↓ Mevalonate pathway	(Zeng et al., 2020)
Simvastatin	↑ BMP mRNA	(Xue et al., 2019b)
Lovastatin	↓ Mevalonate signalling pathway	(Petit et al., 2020)
Rosuvastatin		(Türer et al., 2016)
Dexamethasone	↑ RUNX2, Osterix	(Goimil et al., 2019)
Vitamin D3	↑ ALP, osteopontin osteocalcin	(Yoon et al., 2007)
Vitamin C		(Wang et al., 2017)

Retinoic acid	↑ BMP-2, RUNX2, osteocalcin, and type-1 collagen ↑ activity of co-administered rhBMP-2	(Cowan et al., 2005)
Rolipram	↑ activity of co-administered rhBMP-2	(Tokuhara et al., 2010)
Purmorphamine	↑ Hedgehog signalling pathway	(Gellynck et al., 2013)
Tetracycline	↓ Matrix metalloproteinases	(Farzamfar et al., 2019)
Sphingosine 1-phosphate Fingolimod	↑ Sphingosine 1-phosphate pathway	(Sefcik et al., 2008) (Das et al., 2014b)

Table 1.6. S1P receptor subtype distribution, and examples of receptor-specific functions in different cell types and tissues, adapted from (Cannavo et al., 2017, Rosen et al., 2009, Patmanathan et al., 2017, Hla and Brinkmann, 2011, Takuwa et al., 2012).

Receptor	Distribution	Functions
S1P <sub>1</sub>	(Widespread), brain, heart, spleen, liver, lung, thymus, kidney, skeletal muscle, lymphoid tissue	Endothelial and pericyte cell development. Astrocyte and neural stem cell migration. B and T cell negative chemotaxis (blockage of egress).
S1P <sub>2</sub>	(Widespread), brain, heart, spleen, liver, lung, thymus, kidney, skeletal muscle	Cardiomyocyte protection in ischemia. Endothelial cell junction disruption. Epithelial cell development.

		Hepatocyte proliferation.
S1P <sub>3</sub>	(Widespread), brain, heart, spleen, liver, lung, thymus, kidney, testis, skeletal muscle	Endothelial cell development. Cardiomyocyte protection in ischemia.
S1P <sub>4</sub>	Lung, and lymphoid tissue	T cell migration
S1P <sub>5</sub>	Brain, skin, spleen	Lymphocyte trafficking. Oligodendrocyte survival. Oligodendrocyte progenitor negative chemotaxis.

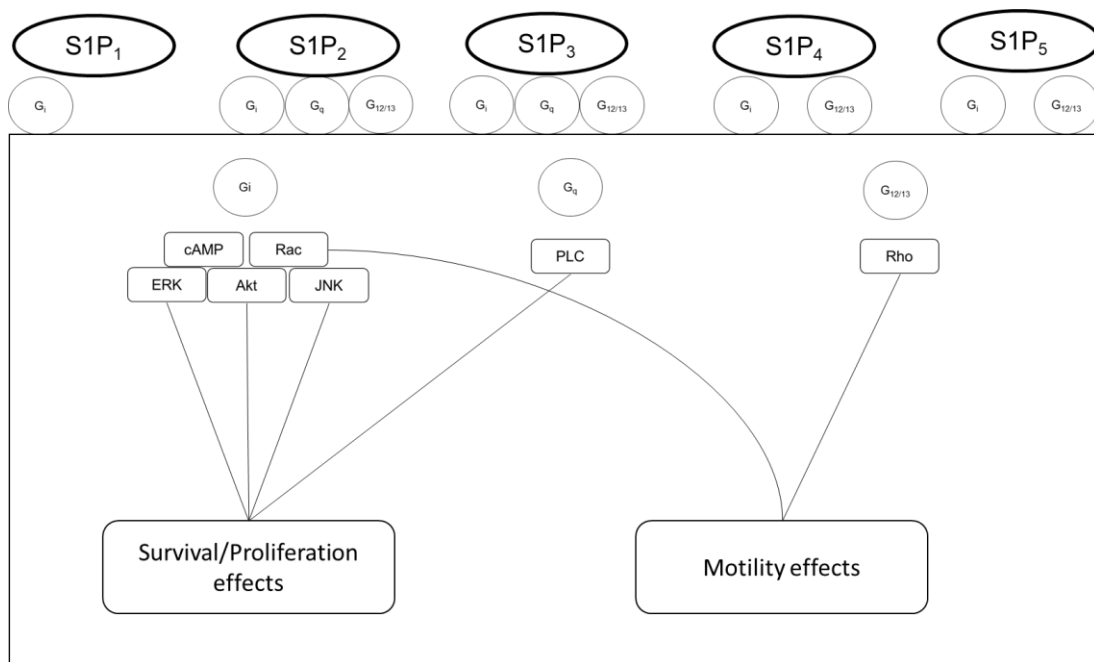


Figure 1.7. Schematic representation of S1P receptor signaling in relation to proliferation and motility effects, adapted from (Takuwa et al., 2012, Cannavo et al., 2017, Rosen et al., 2009).

### 1.11 Thesis aim and objectives

The aim of the research presented in this thesis can be condensed into two concepts. Firstly, the work aimed to improve our understanding of S1P signalling in bone biology, which duly led to a thorough investigation of the small molecule siponimod and its potential role in bone repair. And secondly, the development of implantable scaffolds for the spatiotemporal control of siponimod to augment bone regeneration.

Further to this a number of primary objectives were identified:

- I. To review the role of S1P signalling in bone repair and identify S1P<sub>1</sub> receptor agonists as targets for experimental investigation (**Chapter 2**).

- II. To determine the effect of siponimod on key cell players, osteoblasts and endothelial cells, implicated in bone regeneration using cell proliferation, differentiation, and migration as metrics (**Chapter 3**).
- III. To develop and characterise drug-loaded electrospun scaffolds composed of PLGA and collagen for controlled release of siponimod over timeframes relevant for bone regeneration (**Chapter 4**).
- IV. To investigate the ability of the electrospun scaffold design to promote bone regeneration in rat critical cranial defects using fluorescent labelling and bone staining histomorphometry (**Chapter 4**).
- V. To develop porous drug-loaded scaffolds composed of electrosprayed PLGA microparticles and HA, using gas foaming and porogen leaching, for controlled release of siponimod over timeframes relevant for bone regeneration (**Chapter 5**).



# Chapter 2

## Sphingosine 1-phosphate (S1P) signalling: role in bone biology and potential therapeutic target for bone repair

**Ziad Sartawi<sup>1</sup>, Ernestina Schipani<sup>2</sup>, Katie B. Ryan<sup>1</sup>, Christian Waeber<sup>1,3</sup>**

<sup>1</sup>School of Pharmacy, University College Cork, Cork, Ireland

<sup>2</sup>Departments of Medicine and Orthopaedic Surgery, University of Michigan, Ann  
Arbor, MI, USA.

<sup>3</sup>Department of Pharmacology and Therapeutics, University College Cork, Cork,  
Ireland

Revised from publication

Pharmacological research, November 2017

Volume 125, Part B, November 2017, Pages 232-245 DOI:

10.1016/j.phrs.2017.08.013

## 2.1 Abstract

The lipid mediator sphingosine 1-phosphate (S1P) affects cellular functions in most systems. Interest in its therapeutic potential has increased following the discovery of its G protein-coupled receptors and the recent availability of agents that can be safely administered in humans. Although the role of S1P in bone biology has been the focus of much less research than its role in the nervous, cardiovascular and immune systems, it is becoming clear that this lipid influences many of the functions, pathways and cell types that play a key role in bone maintenance and repair. Indeed, S1P is implicated in many osteogenesis-related processes including stem cell recruitment and subsequent differentiation, differentiation and survival of osteoblasts, and coupling of the latter cell type with osteoclasts. In addition, S1P's role in promoting angiogenesis is well-established. The pleiotropic effects of S1P on bone and blood vessels have significant potential therapeutic implications, as current therapeutic approaches for critical bone defects show significant limitations. Because of the complex effects of S1P on bone, the pharmacology of S1P-like agents and their physicochemical properties, it is likely that therapeutic delivery of S1P agents will offer significant advantages compared to larger molecular weight factors. Hence, it is important to explore novel methods of utilizing S1P agents therapeutically and improve our understanding of how S1P and its receptors modulate bone physiology and repair.

## 2.2 Introduction

The incidence of non-union fractures is relatively low (20 per 100000 cases) (Mills and Simpson, 2013). However, in severe fractures or in limb salvage following bone cancer, the incidence can be many fold higher (Gomez-Barrena et al., 2015). Current therapeutic options for non-union and other critical bone defects, mainly autologous grafts and allografts, suffer from drawbacks of both medical and logistical natures (Laurencin et al., 2006). There has been much hope that novel treatments based on the use of peptide or protein growth factors, mainly in combination with bone grafts or scaffolds, would show clinical benefit. Despite showing positive results, these strategies are limited by the need for high doses, as well as related ectopic growth (Kim and Tabata, 2015, Martino et al., 2015, Curry et al., 2016). A potential promising alternative is the manipulation of lower molecular weight, non peptidic mediators, such as the bioactive lipid S1P (Binder et al., 2015).

S1P is the product of sphingosine kinase (SK)-mediated phosphorylation of sphingosine, itself derived from cell membrane sphingolipids (Spiegel and Milstien, 2002, Spiegel and Milstien, 2003). S1P is an important player in cell death (Olivera and Spiegel, 1993) and proliferation (Zhang et al., 1991), with evidence that the balance between S1P and its pro-apoptotic precursors (sphingosine and ceramide) critically controls cell fate (Cuvillier et al., 1996). Furthermore, S1P signalling is involved in cell adhesion and motility, smooth muscle contraction, and platelet aggregation (Takuwa, 2002).

S1P and its 5 known receptors (S1P<sub>1-5</sub>) are expressed in several systems, including the vascular, immune, nervous, and reproductive systems (Hla, 2004). S1P<sub>1</sub> receptors

have been detected in blood vessels and mesenchymal cells around day 12 of embryonic development (Chae et al., 2004). Their genetic deletion leads to defective limb chondrocyte development, and embryonic lethality from defective vasculature. Limb defects occur both following non-specific deletion and in mice specifically lacking endothelial S1P<sub>1</sub> receptors, and there is evidence that S1P<sub>1</sub> receptors may play a role in chondrocyte organization. Indeed, by day 16 of murine embryogenesis, S1P<sub>1</sub> receptor mRNA expression is abundant in bones undergoing ossification (Liu and Hla, 1997). As will be seen throughout this chapter, S1P receptors have also been identified in the key cells involved in bone remodelling and repair, including S1P<sub>1-3</sub> receptors expressed in osteoblasts, and S1P<sub>1</sub> and S1P<sub>2</sub> receptors in osteoclast precursor cells.

The therapeutic potential of interfering with S1P signalling has mostly been explored in the immune (Hisano et al., 2012), nervous (Choi and Chun, 2013), and cardiovascular systems (Waeber and Walther, 2014). The function of S1P receptors in the immune system especially is increasingly better understood, with apparent roles in cell trafficking (Chi, 2011), allergic responses (Oskeritzian et al., 2010), and coagulation secondary to inflammatory conditions (Niessen et al., 2008). The role of S1P in maintaining vascular integrity is also linked to inflammatory cell trafficking (Camerer et al., 2009), suggesting that the effect of S1P on the immune and vascularization responses could contribute to bone repair, and could be exploited for therapeutic purposes in this context.

The focus herein will be on the role of S1P in bone regeneration, teasing out its interaction with the various cellular components of bone repair. It will evaluate whether the manipulation of S1P signalling has been effective in cases of critical bone

defects, bearing in mind the complexity of S1P signalling, and the uncertainty regarding the specificity of the pharmacological tools used in the studies in question (Salomone and Waeber, 2011). Table 2.1 lists the S1P receptor agonists and antagonists frequently mentioned in this chapter, with their presumed subtype selectivity/specificity.

Other agents activating or blocking S1P receptors or interfering with S1P metabolism have been described (Bigaud et al., 2014, Sanllehi et al., 2016). To the best of our knowledge, they have not yet been used to characterize the role of S1P signalling in bone biology and are therefore not listed here.

**Table 2.1** List of S1P associated agents mentioned in the chapter. Of note, many of these agents only show subtype selectivity with a narrow range of concentrations and have known non S1P receptor targets.

Agent	Selectivity/specificity	Notes
S1P	S1P <sub>1-5</sub> Agonist	Endogenous agonist
Fingolimod	Activates all S1P subtypes except S1P <sub>2</sub> , although recent evidence suggests S1P <sub>2</sub> might also be a target (Sobel et al., 2015).	Fingolimod is a prodrug (activated by sphingosine kinase 2). Phosphorylated fingolimod is likely to act as a functional antagonist of S1P <sub>1</sub> in its approved therapeutic role, as it rapidly downregulates S1P <sub>1</sub> receptors.  It is also a potent protein phosphatase 2A (PP2A)–activating drug. Effects of

		sphingosine kinases and S1P lyase have also been shown.
Sew2871	S1P <sub>1</sub> Agonist	First described S1P <sub>1</sub> -selective agonist. At variance with fingolimod, it demonstrates S1P <sub>1</sub> agonist activity without long-term decrease in surface receptor expression (Jo et al., 2005). It is 10 to 50 times less potent than CYM5442 and poorly water-soluble (Gonzalez-Cabrera et al., 2008).
JTE013	S1P <sub>2</sub> Antagonist	Most commonly used S1P <sub>2</sub> receptor antagonist, but its selectivity is questionable (Adada et al., 2013).
VPC23019	S1P <sub>1</sub> , S1P <sub>3</sub> Antagonist	pK <sub>B</sub> values of 7.5 and 6.0 for S1P <sub>1</sub> and S1P <sub>3</sub> receptors, respectively (Davis et al., 2005).
VPC01091	S1P <sub>1</sub> partial agonist, S1P <sub>3</sub> antagonist	The 1R,3S diastereomer is a conformationally constrained fingolimod analogue activated by sphingosine kinase 2 (Zhu et al., 2007).
W146	S1P <sub>1</sub> Antagonist	W146 is an antagonist, but it's <i>in vivo</i> effect often mimic those of S1P receptor agonists (Tarrason et al., 2011).
Cay10444	S1P <sub>3</sub> Antagonist	Also known as BML-241. Low potency and aqueous solubility agent. May also non-selectively inhibit increases in intracellular [Ca <sup>2+</sup> ] (Jongsma et al., 2006).

### 2.3 Bone repair

Bone is exceptionally proficient at self-repair, often able to avoid the formation of fibrous scar tissue in favour of complete regeneration (Petite et al., 2000). The cells responsible for bone development and repair are the same. Stem cells of mesenchymal origin are the source of bone forming osteoblasts and cartilage forming chondrocytes (Long, 2011) whereas haematopoietic stem cells are the source of the monocytes and macrophages that differentiate into multinucleated osteoclasts, responsible for bone resorption (Florencio-Silva et al., 2015). These cells collaborate in the formation of functional bone through intramembranous and endochondral ossification (Karaplis, 2002). The intramembranous pathway (IO) involves the direct differentiation of mesenchymal stem cells into osteoblasts and the deposition of bone, as occurs during the formation of bones of the skull. The endochondral pathway (EO), typical of long bone formation, involves an intermediary step, the formation of chondrocytes, and the deposition of cartilage, which acts as a template for osteoblasts as cartilage is systematically replaced by bone (Loi et al., 2016).

The process of bone repair echoes osteogenesis and resembles either EO or IO, depending on the size and location of the defect encountered. When the defect is sufficiently small and rigid, and adjacent bone cortices are in contact, deposition of bone may take place directly via IO, without intermediate cartilage formation. This direct, or primary, repair process requires the recruitment of osteoprogenitor cells, osteoclasts and undifferentiated mesenchymal stem cells to the fracture site. In contrast, indirect repair is similar to EO and involves the formation of a cartilaginous template (soft callus) that undergoes calcification into a hard callus and is eventually replaced by new woven bone (Loi et al., 2016). This process typically involves an

acute inflammatory phase, which includes haematoma formation at the defect site, an early response by platelets, and neutrophils, followed soon after by monocytes and macrophages, resulting in thrombus formation, debris removal and the eventual formation of granulation tissue. Inflammation is continuously supported by positive feedback from the release of interleukins (primarily IL-1, and -6, along with -11, and -18) and tumour necrosis factor  $\alpha$  (TNF- $\alpha$ ) mainly in the first 24 hrs after injury (Marsell and Einhorn, 2011). Other important factors include PDGF and macrophage colony-stimulating factor (M-CSF), which, together with stromal cell-derived factor 1 (SDF1, CXCL12) contribute to the recruitment of stem cells from the immediate bone environment and from the circulation (Loi et al., 2016, Marsell and Einhorn, 2011). These stem cells are essential for the next stage of regeneration, the formation of the soft callus. Hypoxic conditions in the haematoma may contribute to the promotion of chondrocyte differentiation from progenitor stem cells, and subsequent cartilage deposition (Amarilio et al., 2007, Mangiavini et al., 2015). Angiogenesis and blood vessel infiltration controlled by angiopoietin-1 and -2 and by VEGF increase until hypoxic conditions begin to resolve (Marsell and Einhorn, 2011). Improved circulation, as well as the activation of M-CSF, receptor activator of nuclear factor kappa B ligand (RANKL) and TNF- $\alpha$ , stimulate chondroclastogenesis and cartilage mineralization (Leijten et al., 2015). The resolution of hypoxic conditions is followed by osteoblast proliferation and differentiation, leading to the deposition of woven bone. Cytokines such as transforming growth factors (TGF)  $\beta$ 2 and 3 and BMP -2, -5, and -6 exert control over the healing process by supporting continued proliferation, differentiation, and activity of osteoblasts, as well as the long term remodelling and restoration of woven bone into lamellar, functional bone (Marsell and Einhorn, 2011,



Schindeler et al., 2008). The cell types and processes involved in bone repair are shown in Figure 2.1.

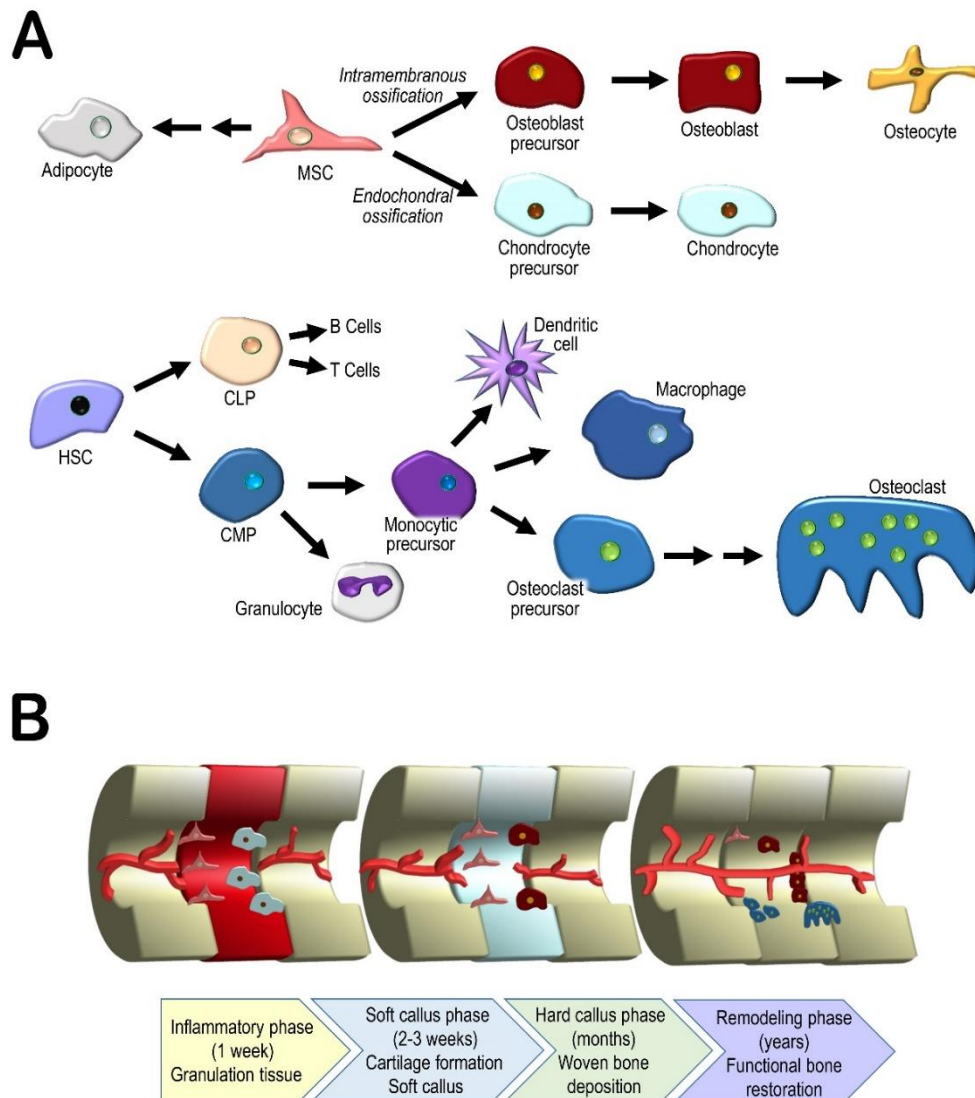


**Figure 2.1** (A) Simplified representation of the lineages of the cells involved in bone repair. Mesenchymal stem cells (MSC) differentiate into the major bone and cartilage forming cells, osteoblasts and chondrocytes (later replaced by osteoblasts), depending on whether ossification occurs through the intramembranous or endochondral pathways. Haematopoietic stem cells (HSC) differentiate into bone resorbing

osteoclasts through the myeloid pathway. (B) Process of bone repair divided into 4 phases: inflammatory, soft callus, hard callus, and remodelling. Briefly, an early inflammatory response results in the removal of debris and the eventual recruitment of mesenchymal stem cells, initiating the soft callus phase and cartilage deposition. Improving vascularization leads to cartilage mineralization and deposition of bone, which is then slowly remodelled, restoring function.

The role of several mediators and signalling pathways in bone repair (e.g., BMP, VEGF, Wnt and Notch pathways) and therapeutic attempts at harnessing them to improve bone repair have been the subject of various reviews (Kim and Tabata, 2015, Long, 2011, Chen et al., 2004, Chen and Alman, 2009, Secreto et al., 2009). Less attention has been paid to the role of S1P signalling in bone disorders and repair (Meshcheryakova et al., 2017). This chapter therefore summarises the key findings in this field, with emphasis on the effects of S1P on the migration, differentiation and survival of the cellular components of bone repair and their respective precursors. In addition to the well-known role of S1P in vascularization and immune cell trafficking, these effects are likely to underlie any observed improvement in repair of bone defects following pharmacological intervention targeting S1P signalling.

## **2.4 S1P effect on progenitor stem cells**

After injury, bone healing relies not only on differentiated bone cells but also on the recruitment of undifferentiated cells from bone and adjacent tissues. S1P regulates cell trafficking through surface receptors that respond to the S1P gradient between tissues

(where S1P is found in nanomolar concentrations) and the blood (where it is found at micromolar concentrations), a gradient which may arise due to high levels of S1P degrading enzymes in the tissue compared to the blood (Maceyka and Spiegel, 2014). In general S1P functions as a chemoattractant for quiescent stem cell populations (Liu et al., 2011), and also participates in their differentiation into specialist bone forming and bone resorbing cells, as will be explored in more detail in the forthcoming sections.

## **2.5 S1P and stem cell migration**

The balance between the major chemo-attractants CXCL12 (also known as SDF-1), predominantly found in bone marrow, and S1P, mainly found in the blood, dynamically regulates haematopoietic stem cell recruitment to the circulation versus their retention in the bone marrow. The principal chemoattractant retaining progenitor stem cells in a quiescent state in the bone marrow is CXCL12. Dissipating the S1P gradient between the blood and bone marrow by inhibiting S1P degradation in tissues or downregulating stem cell S1P<sub>1</sub> receptors using fingolimod both reduce the number of circulating progenitor stem cells (Bendall and Basnett, 2013). The S1P<sub>3</sub> receptor has been shown to have the reverse effect, whereby S1P<sub>3</sub> agonism stimulates CXCL12-based retention of haematopoietic stem cells within the bone marrow, and S1P<sub>3</sub> antagonism contributes to increased stem cell egress (Ogle et al., 2017). Stress, such as that occurring in a fractured bone, induces the downregulation of CXCL12 in the bone marrow and an increase in circulating S1P levels, leading to stem cell mobilization and migration into the blood stream (Golan et al., 2013). These

observations support a role for S1P in the exit of cells from the bone marrow, a finding reminiscent of S1P-mediated lymphocyte egress from lymph nodes (Hisano et al., 2012). Therefore, by manipulating S1P levels in the local environment of a tissue injury site, it may be possible to draw more of the local progenitor resources into the repair process.

S1P-treated stromal cells show increased expression of extracellular matrix protease (e.g., Matrix metalloproteinase (MMP) 1) (Annabi et al., 2003), which are important in breaking down collagen during the cell migration process (Ho et al., 2009). S1P also induces stromal cell migration and formation of capillary-like structures (Annabi et al., 2003) and Rho-dependent formation of stress fibres, followed by lamellipodia and filopodia, in bone marrow derived cells. MMP or MEK1-ERK1/2 inhibition reduces S1P-induced actin stress fibre formation, with no impact on lamellipodia or filopodia. MMP inhibition also interferes with S1P activation of RhoA and ERK, while Rho kinase blockage produces sustained S1P activation of ERK. This shows the intricate interplay downstream of S1P stimulation in the pathways involved in cell migration (Meriane et al., 2006).

Osteoclast-conditioned medium contains S1P that stimulates chemotaxis of MSC (Quint et al., 2013). Two parallel signalling pathways seem to be involved in this MSC migratory response: S1P<sub>1</sub> receptors activating the JAK/STAT pathway and S1P<sub>2</sub> receptors activating the FAK/PI3K/AKT pathway (Quint et al., 2013). Contrasting with these findings, a recent study showed that S1P<sub>2</sub> receptors played a critical role in the inhibition of MSC migration through ERK phosphorylation (Price et al., 2015), an effect more in line with the more commonly observed inhibition of migration by S1P<sub>2</sub>

receptors (Kong et al., 2014). Confirming the effects of S1P signalling on the recruitment of endogenous stem cells, exposure of bone marrow derived MSC to the S1P agonist fingolimod released from biodegradable polymer scaffolds enhanced MSC migration toward CXCL12 (Das et al., 2014a), but the pharmacological profile of this response was not assessed. In these experiments fingolimod also led to cellular mineralization, an indicator of differentiation into the osteoblast lineage, and promoted vascularization (Das et al., 2014a).

## **2.6 S1P and stem cell differentiation**

MSC can differentiate into osteoblasts and adipocytes; commitment to one lineage inhibits commitment to the other due to the existence of negative feedback loops. S1P reduced adipogenic differentiation in MSC (Hashimoto et al., 2015) and increased their differentiation into osteoblasts as shown by increases in alkaline phosphatase and osteocalcin mRNA, and the appearance of calcified deposits (Hashimoto et al., 2015). While the MSC cell line expressed both S1P<sub>1</sub> and S1P<sub>2</sub> receptors, the inhibition of C/EBP $\beta$  expression by S1P was sensitive to pertussis toxin (a specific Gi protein inhibitor), and W146 (a specific S1P<sub>1</sub> antagonist) suggesting that Gi-coupled S1P<sub>1</sub> receptors played a key role (Hashimoto et al., 2015). A recent study further defined the nature of the Wnt pathway involved in S1P-induced osteogenic differentiation of MSC, implicating the Wnt5a ligand and LRP5/6 receptor (Hashimoto et al., 2016). In another study, S1P-functionalized titanium oxide coated stainless steel used as a growth substrate for human adipose derived stem cells also fostered their osteogenic differentiation (Marycz et al., 2016). Both the S1P<sub>1/3</sub> receptor antagonist VPC23019

and blocking of BMP-6 with a neutralising antibody, polyclonal IgG reduced the mineralization response of human MSC to osteoclast-conditioned media, and similarly interferes with MSC migration. Indicating that osteoclasts and associated S1P release (among other osteoblast-osteoclast coupling factors) stimulate MSC differentiation and migration (Pederson et al., 2008).

## **2.7 S1P and osteoblasts**

### **2.7.1 Proliferative effect**

Short (10-45 min) but not protracted (24 hr) treatment with S1P induces ERK-dependent proliferation of both rat and human osteoblasts (Carpio et al., 1999, Lampasso et al., 2001). This time dependence has been tentatively explained by the possibility that S1P might first induce an early phase of cell growth, but, upon longer stimulation, lead to a phase of differentiation in which proliferation stops. Alternatively, the differential increase in the protein kinase C (PKC) alpha isoform following short- vs. long-term exposure to S1P might also have played a role (Lampasso et al., 2001). This possibility is supported by the observation that, in response to a 10 min S1P stimulation, PKC- $\alpha$  immunoreactivity was redistributed from the cytosol to the nucleus (Lampasso et al., 2002). Osteoblasts are known to express S1P<sub>1</sub>, S1P<sub>2</sub> and S1P<sub>3</sub> receptors (Grey et al., 2004, Ryu et al., 2006, Keller et al., 2014), but none of the studies mentioned above addressed the identity of the receptor involved in the proliferation response; while pertussis toxin sensitivity pointed to an S1P<sub>1</sub>-mediated effect (Lampasso et al., 2001), the S1P concentration used (10  $\mu$ M) was higher than usually needed to activate S1P receptors. A more recent

study reported increased DNA synthesis at S1P concentrations of 1  $\mu$ M (Grey et al., 2004); S1P induced activation of p42/44 MAP kinases, in a Gi- and calcium-dependent manner, but independently of PKC, and proliferation was observed in response to 24 hrs S1P treatment. When the effects of S1P were studied in human primary osteoblastic cells and the human osteosarcomal cell lines, G292 and MG-63, 10 min incubations with 10 nM S1P increased proliferation in a pertussis toxin-sensitive manner, while the effect of 24 hrs incubation were less consistent. In G292 cells, this longer exposure produced significant increases only with subnanomolar S1P, while higher doses had no effects; no proliferation was observed at any concentration in the other cell types (Dziak et al., 2003). Both proliferation and apoptosis control the number of osteoblasts, and Gi proteins are not only involved in S1P-induced osteoblast proliferation but also in their survival. However, the role of PI3K appears to be restricted to the latter effect, since PI3K inhibition does not prevent the proliferative actions of S1P in osteoblastic cells (Grey et al., 2002).

### 2.7.2 Osteoblast differentiation

Differentiation of osteoblast precursors into mature osteoblasts is accompanied by an increase in sphingosine kinase 1 (SK1) expression and enzyme activity, decreased levels of S1P<sub>1</sub> and S1P<sub>2</sub> receptor proteins, and increased levels of S1P<sub>3</sub> receptor proteins (Brizuela et al., 2014). Sphingosine kinase inhibitor (SKI-II), an anti-S1P antibody and the S1P<sub>1/3</sub> receptor antagonist VPC23019 all reduce alkaline phosphatase activity, while blocking S1P<sub>1</sub> receptors with W146, or S1P<sub>2</sub> receptors with JTE013, has no effect (Brizuela et al., 2014). A similar pharmacological profile was observed with RUNX2 expression (a key transcription factor associated with osteoblast

differentiation), suggesting the existence of an autocrine SK1/S1P/S1P<sub>3</sub> signalling pathway during osteoblastic differentiation (Brizuela et al., 2014).

Other S1P receptors and signalling pathways may also mediate osteoblastogenesis. Activation of S1P receptors in C2C12 myoblasts enhanced BMP-2-induced expression markers of osteoblast differentiation (Sato et al., 2012). The expression of RUNX2 was likewise increased in the presence of S1P or fingolimod, as were Smad transcription factors and ERK1/2 (Sato et al., 2012). S1P and fingolimod also enhanced BMP-2-stimulated Smad1/5/8 phosphorylation in C2C12 cells, and cell differentiation was sensitive to Pertussis toxin, to a MEK1/2 inhibitor, to the S1P<sub>1</sub> receptor antagonist W146, and, to a smaller extent, to the S1P<sub>2</sub> antagonist JTE013, whereas an S1P<sub>3</sub> antagonist (CAY10444) had no effect. A similar pharmacological profile was observed for the effects of S1P on other osteoblast-like cell lines (human Saos-2 and murine MC3T3-E1). In these cells, S1P activated PI3K/Akt signalling, inhibiting GSK-3 $\beta$ , promoting nuclear translocation of  $\beta$ -catenin and expression of osteoprotegerin (that inhibits osteoclastogenesis by acting as a soluble decoy receptor for RANKL), and enhancing ALP activity (Matsuzaki et al., 2013). In a more recent study by the same group, S1P stimulation of Smad1/5/8 phosphorylation was attributed to S1P<sub>2</sub>-G12/13-RhoA activity, leading to the nuclear translocation of the Smad complex, up-regulation of RUNX2 leading to increased ALP (Higashi et al., 2016). Of note, this (Matsuzaki et al., 2013) and another study (Ryu et al., 2006) found that S1P also increased RANKL mRNA in osteoblasts, but the OPG/RANKL ratio was higher after S1P treatment, which should lead to an overall inhibition of osteoclast maturation (Matsuzaki et al., 2013). Increased SK activity indeed reduces osteoclastogenesis in a monoculture of osteoclast precursors; however, in an



osteoblast/osteoclast co-culture system, which better reflects the reality of a healing bone, S1P stimulated osteoclastogenesis (Ryu et al., 2006).

As mentioned above, S1P is a key coupling factor between osteoclasts and osteoblasts, and is referred to as a clastokine (Teti, 2013). Osteoclasts lacking the bone degrading enzyme cathepsin K show increased SK 1 expression and culture media conditioned by these cells were shown to induce a larger increase in ALP and mineralized nodules in osteoblast cultures, due to their higher S1P content. This response was blocked by the S1P<sub>1/3</sub> antagonist VPC23019, in agreement with the studies described above (Lotinun et al., 2013).

### 2.7.3 Osteoblast precursor migration

Together with its activity on their proliferation and differentiation (Carpio et al., 1999, Lampasso et al., 2001, Lampasso et al., 2002, Grey et al., 2002, Grey et al., 2004, Dziak et al., 2003, Brizuela et al., 2014, Sato et al., 2012, Matsuzaki et al., 2013, Higashi et al., 2016, Lotinun et al., 2013), S1P also affects the migration of osteoblast precursors (Roelofsen et al., 2008). Treatment of mouse primary pre-osteoblasts with S1P drives cells toward the bone surface environment (Roelofsen et al., 2008). However, when precursors differentiate into mature osteoblasts, they become insensitive to S1P, although they retain their chemotaxis to PDGF (Roelofsen et al., 2008). The response to S1P is not sensitive to pertussis toxin, suggesting that a subtype other than S1P<sub>1</sub> is involved in the chemorepellent response to S1P. Indeed, expression studies and experiments with JTE-013 or with anti S1P<sub>2</sub> siRNA point to a developmental stage specific role of S1P<sub>2</sub> receptors. The chemorepellent effect of S1P<sub>2</sub> receptors is typical of this subtype in various cell types, whereas S1P<sub>1</sub> receptors are

associated with chemotaxis to S1P in other cells important for bone repair: MSC that give rise to cells of the osteoblast lineage (see (Quint et al., 2013) above), endothelial cells (Waeber et al., 2004) or osteoclasts (see below). The lack of S1P<sub>1</sub>-mediated positive chemotactic response in osteoblasts, despite high S1P<sub>1</sub> expression levels in these cells, is therefore unusual.

## **2.8 Other effect of S1P signalling in osteoblasts**

S1P has long been known to release calcium from intracellular stores in pre-osteoblasts (Lyons and Karin, 2001, Liu et al., 1995). Because of calcium's central role in cell signalling, it is therefore not surprising that S1P is implicated in many osteoblast functions. Indeed, S1P stimulates IL-6 synthesis in these cells in a p42/p44 MAPK dependent manner (Kozawa et al., 1997), induces the synthesis of heat-shock protein 27 (HSP27) via p38 activation (Kozawa et al., 1999), and enhances PGF2 $\alpha$ -induced phosphoinositide hydrolysis by phospholipase C through p38 MAPK (Kozawa et al., 2000, Di Paolo and De Camilli, 2006).

Administration of epidermal growth factor, a known mitogenic factor for osteoblasts, increased S1P levels which coincided with increased cell proliferation (Carpio et al., 2000). There is also evidence for the involvement of S1P signalling in calcitonin activity (Martin and Sims, 2015). Calcitonin is an anti-resorptive hormone previously indicated in osteoporosis, however it may also influence bone formation through its interactions in S1P signalling. By decreasing the expression of the S1P transporter Spns2 in osteoclasts (Keller et al., 2014), limiting the cross-talk between osteoclasts

and osteoblasts, and so also limiting S1P- or fingolimod-induced bone formation by osteoblasts which was found to be mediated by S1P<sub>3</sub> receptors (Keller et al., 2014).

S1P may also influence mature osteoblasts following their entombing as osteocytes in the bone matrix, whereby S1P signalling has been shown to play a role in osteocyte mechanotransduction via an S1P<sub>2</sub> receptor mediated mechanism (Zhang et al., 2015).

## **2.9 S1P and osteoclasts**

Osteoclasts are multinucleated, resorptive cells whose development is influenced by osteoblast lineage cells (Alford et al., 2015). Osteoclasts are responsible for the continuous remodelling of bone, working in tandem with bone forming osteoblasts (Walsh, 2015). The coupling between osteoclasts and osteoblasts in osteoclastogenesis is a clear example of the functional relationship between the two cell populations, and S1P plays an important role in the crosstalk between these two cell populations and their differentiation, as represented in Figure 2.2.

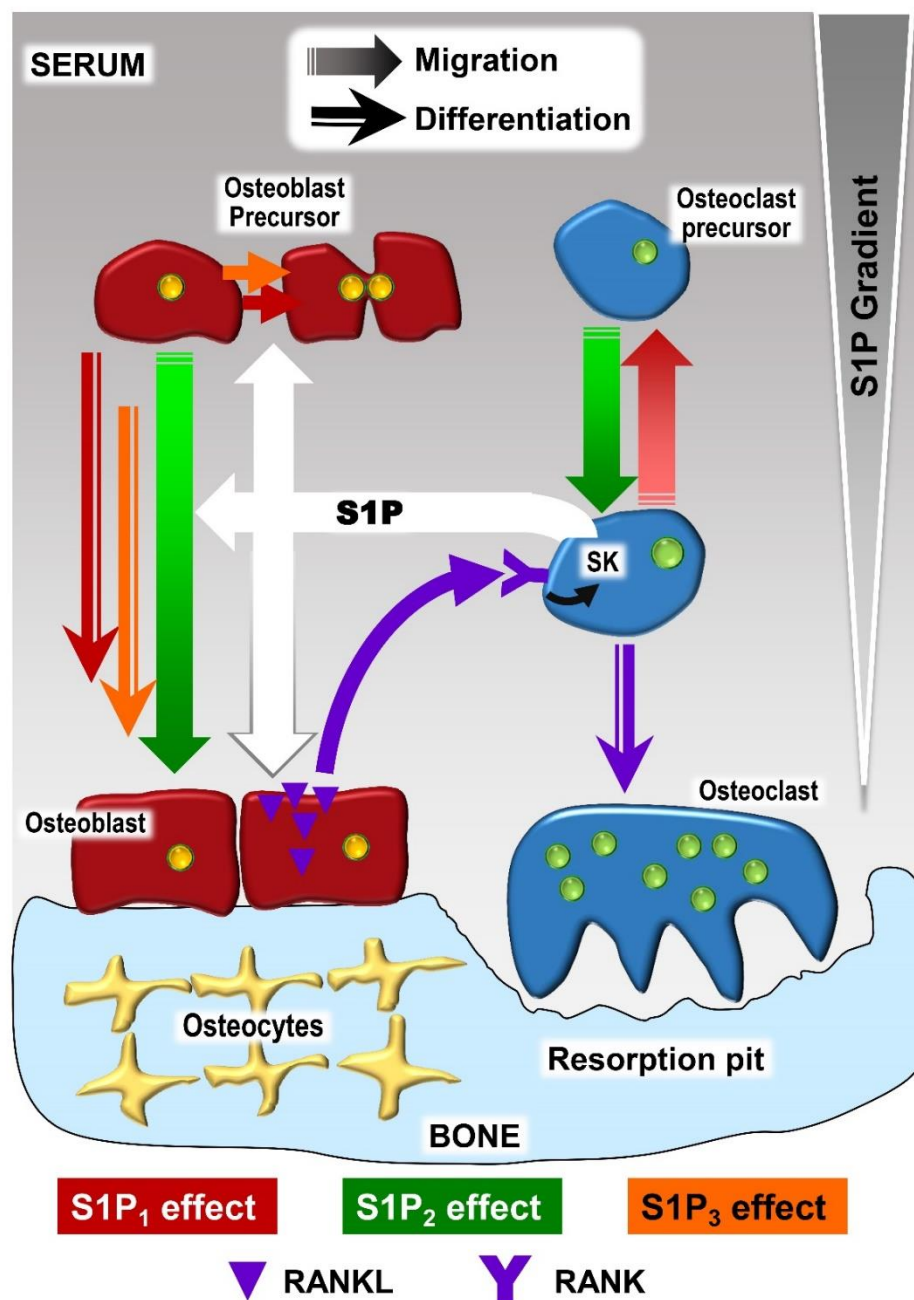


**Figure 2.2** Simplified illustration of the effects of S1P and its receptors on osteoblasts, osteoclasts, their respective precursors, and the role of S1P in osteoblast-osteoclast coupling. The involvement of the 3 major S1P receptor subtypes (red: S1P<sub>1</sub>, green: S1P<sub>2</sub>, orange: S1P<sub>3</sub>) in particular responses is indicated by different arrow shapes.

Briefly, osteoclast and osteoblast precursor migration is influenced by S1P<sub>1</sub>-mediated chemoattraction and S1P<sub>2</sub>-mediated chemorepulsion in response to the S1P concentration gradient (larger quantities of S1P are generated in serum mainly by red blood cells and endothelial cells, while lower S1P concentrations predominate in tissue compartments, such as bone). S1P, produced locally by osteoclasts or osteoclast precursors (Lotinun et al., 2013, Pederson et al., 2008, Keller et al., 2014), directly stimulates the proliferation of osteoblast precursors and their differentiation into mature osteoblasts, while increasing RANKL mRNA in osteoblasts, indirectly stimulating osteoclast precursor differentiation via RANK. The RANKL/RANK signalling pathway also upregulates SK in osteoclast precursors.

## **2.10 S1P and osteoclast recruitment**

S1P can regulate the migration of osteoclast precursors both *in vitro* and *in vivo*. Bone marrow derived monocytes (an *in vitro* model of osteoclast precursors) express both S1P<sub>1</sub> and S1P<sub>2</sub> receptors. Upon exposure to RANKL, these cells differentiate into osteoclast-like cells and show decreased S1P<sub>1</sub> expression, with concomitant loss of chemotactic response to S1P (Ishii et al., 2009). Knockout mice with specific S1P<sub>1</sub> deletion in the monocyte lineage are osteoporotic, a phenotype that has been attributed to the loss of S1P<sub>1</sub> control of osteoclast precursor migration and increased residency time at the bone surface (Ishii et al., 2009). The potential therapeutic significance of these findings was confirmed in an ovariectomy-induced osteoporosis model: fingolimod prevented bone loss in ovariectomized mice but had no effects in sham-operated mice. This effect was due to a reduction of osteoclast deposition onto bone

surfaces (Ishii et al., 2009). In a rat model of periodontitis, fingolimod was found to reduce the number of osteoclast precursors and mature osteoclasts at the defect site, and increase the number of precursors in blood, an effect attributed to S1P<sub>1</sub>-induced positive chemotaxis (Lee et al., 2017).

S1P<sub>2</sub> receptor deficient mice show higher bone density than control mice (Ishii et al., 2010), and S1P<sub>2</sub> receptors seem to antagonize the effect of S1P<sub>1</sub> receptors on osteoclast precursor migration. Positive and negative chemotaxis are attributed to S1P<sub>1</sub>-mediated activation of Rac via Gi, and S1P<sub>2</sub>-mediated activation of Rho via G<sub>12/13</sub>, respectively (Ishii et al., 2010). An *in vitro* migration assay of osteoclast precursors expressing both receptors subtypes showed that lower S1P concentrations stimulate positive chemotaxis, while higher concentrations stimulate negative chemotaxis, or chemorepulsion, suggesting that S1P<sub>2</sub> receptors may only be active at high S1P concentrations. S1P<sub>1</sub>-deficient osteoclast precursor cells show very little motility, while S1P<sub>2</sub>-deficient cells showed positive chemotaxis, even at high S1P concentration (Ishii et al., 2010). Intravital imaging confirmed the chemotactic effect of S1P<sub>2</sub> by showing that the antagonist JTE013 mobilised a small subset of monocytic lineage cells from the calvarium and led them to enter the blood circulation (Ishii et al., 2010).

## **2.11 Therapeutic manipulation of osteoclast trafficking**

While approved or investigational anti-resorptive agents (e.g., bisphosphonate or cathepsin K inhibitors) target mature osteoclasts, manipulating osteoclast precursors would provide a novel therapeutic modality for bone loss. Indeed, the opposing roles

of S1P<sub>1</sub> and S1P<sub>2</sub> receptors on precursor recruitment might underlie therapeutic interventions (i.e., activation of S1P<sub>1</sub> or blockade of S1P<sub>2</sub> receptors) that could prevent bone loss in conditions associated with inflammation and/or remodelling imbalance. This potential was ascertained using murine models of rheumatoid arthritis (in which fingolimod was as effective as prednisolone) and osteoporosis (fingolimod improved bone loss, but prednisolone had no effect) (Kikuta et al., 2011). In a model of periodontitis, a bacteria-driven inflammatory bone loss disease, fingolimod inhibited osteoclastogenesis and pro-inflammatory cytokines involved in osteoclast precursor recruitment (Yu et al., 2015).

Vitamin D analogues are used for the treatment of osteoporosis, but their mechanism of action is not completely clear. For instance, *in vitro* calcitriol increased RANKL expression in bone marrow stromal cells, thereby activating osteoclasts and bone resorption (Kikuta et al., 2013). A recent study showed that vitamin D's effect on osteoclast precursor migration might underlie its anti-resorptive activity. Indeed, calcitriol and its analogue eldecacitol were found to uniquely reduce S1P<sub>2</sub> receptor expression in monocytic osteoclast precursors (Kikuta et al., 2013), while circulating monocytes expressed fewer S1P<sub>2</sub> receptors in mice treated with calcitriol or eldecacitol, and monocyte mobility was observed to increase in eldecacitol-treated mice after treatment with JTE013 (Kikuta et al., 2013).

Whereas vitamin D analogues reduce S1P<sub>2</sub> receptor expression, a recent study showed that the inflammatory cytokine IL-6 induced S1P<sub>2</sub> mRNA, but not S1P<sub>1</sub> mRNA expression in osteoclast precursor cells (Tanaka et al., 2014). This effect was associated with a decrease in S1P-induced chemotaxis and an increased number of

precursors in tibial bone marrow. Systemic treatment with an anti-IL-6 receptor antibody prevented bone loss and decreased the number of precursors in tibial bone marrow via S1P<sub>2</sub> receptor down-regulation (Tanaka et al., 2014), further validating the potential therapeutic value of S1P<sub>2</sub> antagonists.

The following table summarises some of the effects of S1P receptors 1, 2, and 3 on the cellular components of bone repair. The roles of S1P<sub>4</sub> and S1P<sub>5</sub> in bone biology are not extensive in the literature, and their expression is limited in both mature osteoblasts and their precursors (Roelofsen et al., 2008).



**Table 2.2** Cell types involved in bone regeneration and some S1P receptor related effects.

Cell type	Agent	Receptor	Study	Effect	Ref.
Osteoblast cell models	S1P as part of osteoclast conditioned medium	S1P <sub>1/3</sub> involvement determined using VPC23019 (2 $\mu$ M and 10 $\mu$ M)	Murine long bone osteoblasts cultured in osteoclast conditioned medium	↑ALP ↑Mineralization	(Lotinun et al., 2013)
	S1P (1-30 $\mu$ M)	No S1P receptors were investigated	MC3T3-E1 cell line, treated with 1-30 $\mu$ M S1P, media contained 0.01% bovine serum albumin	↑IL-6	(Kozawa et al., 1997)
	S1P, various doses ranging from 1 nM to 10 $\mu$ M	S1P <sub>1</sub> as determined by pertussis toxin (Dziak et al., 2003). The remaining articles do not identify individual receptors.	Human osteoblast explant (Lampasso et al., 2001, Lampasso et al., 2002, Dziak et al., 2003), Foetal rat osteoblasts (Carpio et al., 1999, Grey et al., 2002, Grey et al., 2004), Saos-2 cell line (Grey et al., 2004), thymidine incorporation proliferation assays	↑Proliferation	(Carpio et al., 1999, Lampasso et al., 2001, Lampasso et al., 2002, Grey et al., 2002, Grey et al., 2004, Dziak et al., 2003)
	S1P (100 nM) added to top and/or bottom compartments of migration chamber	S1P <sub>2</sub> as determined using pertussis toxin (200 ng/mL), JTE013 (10 <sup>-8</sup> -10 <sup>-5</sup> M), and RNA interference	MC3T3-E1 cell line, migration assay for PDGF and S1P pre-and post-differentiation	Negative chemotaxis	(Roelofsen et al., 2008)

	Endogenous S1P	S1P <sub>3</sub> as determined using W146, JTE013, and VPC23019 (All 2 $\mu$ M)	MC3T3-E1 cell line cultured in osteoblast differentiation media, contained 10% serum	↑Maturation	(Brizuela et al., 2014)
	S1P (0.01-0.1 $\mu$ M) or fingolimod* (0.01-0.1 $\mu$ M)	S1P <sub>1</sub> as determined by the pertussis toxin (100 ng/mL), W146, JTE013, and CAY10444 (All 10 $\mu$ M)	C2C12 murine osteoblast precursor cultured in media containing 10% serum.  S1P and fingolimod used supplementary to BMP-2	↑ALP (↑↑*)  ↑Osteocalcin (↑↑*)  ↑RUNX2(↑*)	(Sato et al., 2012)
	S1P (0.1-2 $\mu$ M)	S1P <sub>1</sub> as determined using W146, JTE013, and CAY10444 (BML-241)	Human Saos-2 and murine MC3T3-E1 cell lines, cultured in media containing 10% serum	↑ALP  ↑Mineralization  ↑Osteoprotegerin  ↑RANKL mRNA  Nuclear localization of $\beta$ -catenin	(Matsuzaki et al., 2013)
	S1P (1 $\mu$ M for proliferation, 200 nM for differentiation)	S1P <sub>1/2</sub> as determined by western blot analysis and selective S1P <sub>1</sub> agonist SEW2871.	Human osteoblasts incubated with 24 hrs for proliferation and up to 3 weeks for differentiation.	↑Proliferation  ↑ALP activity	(Tantikanlayaporn et al., 2018)

	S1P (100 nM)	S1P <sub>3</sub> as determined by western blot.	Osteosarcoma cell lines MNNG-HOS and U-2OS incubated with S1P for up to 120 hrs.	↑Proliferation ↓Apoptosis	(Shen et al., 2019)
Osteoclast cell models	S1P (0.1 μM and 1 μM)	No receptors were investigated	Osteoclast from minced rabbit bones incubated on dentine slices. Treated for 16 hrs with S1P in media containing 10% serum	↓ Resorption	(Takeda et al., 1998)
	S1P (10 <sup>-10</sup> -10 <sup>-7</sup> M)	S1P <sub>1</sub> as determined by osteoclast lineage specific conditional S1P <sub>1</sub> knockout	Murine monocyte cell line migration assay  Cells cultured in media containing 10% serum	Positive chemotaxis	(Ishii et al., 2009, Ishii et al., 2010)
	fingolimod (3 mg/Kg) intraperitoneal injection	S1P <sub>1</sub> determined from S1P <sub>1</sub> knockout osteoclasts collected from transgenic mice	Murine model of osteoporosis	↓Bone density loss  Positive chemotaxis	(Ishii et al., 2009, Kikuta et al., 2011)
	S1P <sub>2</sub> receptor deficiency or blockade	S1P <sub>2</sub> as determined <i>in vitro</i> by targeting with RNA interference.  And <i>in vivo</i> by use of JTE013 3 mg/Kg	<i>In vitro</i> and <i>in vivo</i> investigation of the role of S1P <sub>2</sub> in the migration of osteoclast precursors	Osteopetrosis  ↑Bone density  ↓Negative chemotaxis (osteoclast precursors remain in circulation)	(Ishii et al., 2010)

	fingolimod (3 mg/Kg/Day) intraperitoneal injections	S1P <sub>1</sub> as determined using immunohistochemistry and an anti-S1P <sub>1</sub> receptor antibody	Rat model of periodontitis	Positive chemotaxis	(Lee et al., 2017)
	Calcitriol and eldecacitol ( <i>In vitro</i> : 10 <sup>-9</sup> -10 <sup>-8</sup> M  <i>In vivo</i> : 50 ng/Kg) effect on S1P (10 <sup>-6</sup> M) chemotaxis	S1P <sub>2</sub> receptor expression as determined by PCR	Monocytoid cell line migration assay  <i>In vivo</i> osteoporosis model	↓S1P <sub>2</sub> receptor expression  Positive chemotaxis  ↑Bone mineral density	(Kikuta et al., 2013)
	IL-6 (1-10 ng/mL) effect on S1P (10 <sup>-7</sup> M) chemotaxis	S1P <sub>2</sub> receptor expression as determined by PCR	Murine osteoclast precursors cultured in media containing fatty-acid free bovine serum albumin, migration assay.  <i>In vivo</i> arthritis model	↑S1P <sub>2</sub> Receptor expression  Negative chemotaxis  ↓Bone volume	(Tanaka et al., 2014)
	S1P <sub>2</sub> receptor antagonism	S1P <sub>2</sub> as determined by JTE013	Bone marrow cells exposed to osteoclastogenic agents.	↓Size and number of osteoclasts  ↓Resorption pits ( <i>In vitro</i> )	(Hsu et al., 2019)
Mesenchymal stem cells	S1P (1 μM)	No receptors were investigated	Murine bone marrow stromal cells cultured in 10% inactivated serum	↑Stress fibre formation  ↑Migration	(Meriane et al., 2006)

	S1P as part of murine osteoclast conditioned medium	S1P <sub>1</sub> as determined using VPC23019 (1 $\mu$ M), without any discussion of S1P <sub>3</sub> antagonism	Human mesenchymal stem cells cultured in media containing 10% serum and 10-fold concentrated conditioned media	<p>↑Mineralization</p> <p>↑Migration</p>	(Pederson et al., 2008)
	S1P as part of osteoclast conditioned medium, and S1P <sub>1</sub> agonist VPC24191 (5 $\mu$ M)	S1P <sub>1/2</sub> as determined using VPC23019 (100 nM), and JTE013 (20 nM), and S1P <sub>1</sub> antagonist W143 (1 $\mu$ M)	Human bone marrow derived MSC, cultured in media containing 10% serum	<p>↑Migration</p> <p>(Both S1P<sub>1/2</sub> led to increased migration although through different pathways)</p>	(Quint et al., 2013)
	S1P (1 $\mu$ M)	S1P <sub>1</sub> as determined by pertussis toxin (100 ng/mL), and W146 (10 $\mu$ M) receptor blockade	C3H10T1/2 murine MSC incubated with S1P for 15 mins to 24 hrs. Media contained 10% serum	<p>↑ALP</p> <p>↑Osteocalcin</p> <p>↑Mineralization</p> <p>↓Adipogenic differentiation</p> <p>No effect on proliferation</p>	(Hashimoto et al., 2015)
	S1P (40 mg/mL and 80 mg/mL)	S1P <sub>1/2</sub> as determined by changes in gene expression	Human adipose derived stem cells cultured on titanium oxide coated stainless steel doped in S1P, cells were exposed to S1P for 120 hrs	<p>↑Proliferation</p> <p>↑Mineralization</p> <p>↑Expression of S1P<sub>1</sub> and S1P<sub>2</sub> at 80 mg/mL</p>	(Marycz et al., 2016)

				↑Expression of S1P <sub>2</sub> only at 40 mg/mL	
	Antagonism of endogenous S1P	S1P <sub>1</sub> antagonist W146.	Bone marrow derived stromal cells incubated with S1P <sub>1</sub> agonists and antagonists.	↓F-actin structure assembly ↓MMP-2 expression and activity ↓Cell proliferation	(Sassoli et al., 2018)
Chondrocytes	S1P (0.1-3 µM)	S1P <sub>1-3</sub> receptors exhibit increased expression as determined by PCR	Bovine and human cartilage explants (monolayer culture), proliferation assay	↑Proliferation	(Stradner et al., 2008)
	S1P (0.1-10 µM)	Broad S1P receptor expression, though no specific receptor roles were identified, although Gi protein blockade with pertussis toxin reduced PGE2 induction by S1P	Human articular chondrocytes from osteoarthritis patients. Treated following serum starving (0.5% serum)	↑PGE2 release ↑Cartilage degradation No effect on proliferation and viability	(Masuko et al., 2007)
	S1P as part of murine osteoclast conditioned medium	S1P <sub>2</sub> as determined by JTE013.	Femoral head explants and primary murine chondrocytes cultured in osteoclast conditioned medium.	↓Extracellular matrix production ↑Osteoarthritis development in mice.	(Cherifi et al., 2016)
Osteocytes	Mechanical stimulation-S1P (100 nM)	S1P <sub>2</sub> as determined by pre-treatment with JTE013 (10 µM)	MLO-Y4 cell line, oscillatory fluid flow, JTE013	↑PGE2 release ↓RANKL/OPG	(Zhang et al., 2015)

## 2.12 S1P in the vasculature and the role of angiogenesis

The repair of cranial bone defects by scaffold-mediated delivery of S1P agents involves not only the recruitment of bone cell progenitors, but also production of new vessels in the defect space (Sefcik et al., 2008, Petrie Aronin et al., 2010a). Hence, while the previous sections focused on bone cells and their interactions, it is important to remember that bones are highly vascularized, perfused by up to 20 ml of blood/100 g of bone every minute (Tondevold and Eliassen, 1982). Blood vessels are not only an essential conduit for blood, providing minerals, nutrients, growth factors and osteoprogenitors, but the endothelium also acts as a paracrine and endocrine organ involved in growth factor production, coagulation, inflammation and the immune response (Inagami et al., 1995). Fracture disrupts the bone's vasculature, leading to hypoxia and necrosis of adjacent tissue. Re-establishment of the circulation and neovascularization in the tissue formed in response to injury are critical for successful fracture healing (Tomlinson and Silva, 2013). Unfortunately, bone repair strategies based on bone grafts or scaffolds have so far shown limited success due in part to the lack sufficient blood vessel supply during the early stages of the repair process (20, 21).

There are three main mechanisms for producing new vessels (Semenza, 2007). Vasculogenesis refers to the *de novo* generation of blood vessels that occurs for instance during embryogenesis. It differs from angiogenesis, which is the generation of new vessels *from pre-existing ones*. Angiogenesis occurs during physiological (e.g., wound healing or menstrual cycle) or pathological processes (e.g., neovascular disorders, rheumatoid arthritis and cancer). It can result from the formation of a new vessel branching off an existing vessel (sprouting angiogenesis) or from the splitting

of a blood vessel into two or more vessels (intussusceptive angiogenesis). Finally, arteriogenesis is the remodelling of an existing artery to increase its luminal diameter. While arteriogenesis, and possibly angiogenesis (Gaengel et al., 2012, Jung et al., 2012, Duran et al., 2017), occurs in response to physical forces such as increased blood flow, angiogenesis is initiated in poorly perfused tissues when low oxygen levels lead to increased levels of the transcription factor Hypoxia-Inducible Factor (HIF)-1 $\alpha$  in parenchymal cells.

VEGF is the main HIF-1 $\alpha$ -dependent pro-angiogenic factor, and inhibiting VEGF signalling impairs healing of femoral fractures and cortical bone defects in mice (Street et al., 2002). Although VEGF is the archetypical pro-angiogenic factor, it promotes by itself the formation of immature and leaky vessels (Yancopoulos et al., 2000). In contrast, angiopoietin-1 produces vessels that are resistant to leak (Thurston et al., 1999), suggesting that different vascular growth factors play complementary and coordinated roles in new vessel formation, and that therapeutic strategies aimed at promoting angiogenesis should target more than one mediator. Indeed, when surgically implanted in the ear of mice, chemically modified hyaluronan hydrogels pre-loaded with both VEGF and angiopoietin-1 promote a larger angiogenic response than delivery of single growth factors (Riley et al., 2006). More recently, sequential delivery of VEGF and S1P using a porous hollow fibre in a skin Matrigel plug assay was shown to lead to more endothelial cell recruitment and a higher maturation index than single factor delivery, reverse sequential delivery or even co-delivery (Tengood et al., 2010). The concept that temporal control of growth factor release produces more mature new vessels, able to integrate with the existing vasculature, was validated in



similar experiments using Basic Fibroblast Growth Factor and Platelet-Derived Growth Factor (Tengood et al., 2011).

These sequential release experiments were conducted over the course of a week, but the bone repair process takes months. Scaffold-mediated delivery of a low molecular weight, more lipophilic factor such as an S1P agent might be preferable to the delivery of recombinant proteins. The role of S1P in the vasculature and new vessel formation is well documented and has been the subject of numerous reviews (Waeber, 2013a, Takuwa et al., 2010, Lucke and Levkau, 2010). Endothelial cells express the same S1P receptor subtypes as intrinsic bone cells ( $S1P_1 > S1P_2 \approx S1P_3$ ); these receptors mediate generally similar cellular responses (proliferation, differentiation and migration), in addition to effects more specific to endothelial cells (modulation of cell adhesion and of the inflammatory/immune response).

S1P seems to play a key role in both vasculogenesis and angiogenesis. In a mouse hind limb ischemia model, S1P stimulates angiogenesis (Oyama et al., 2008), while postischemic blood flow recovery and angiogenesis are accelerated in transgenic mice overexpressing SK1 (Takuwa et al., 2008). At variance with the effects of VEGF however, the angiogenic response to S1P is not associated with increased vascular permeability in the ischemic limb, and many studies have shown that S1P actually enhances endothelial barrier integrity (Waeber, 2013a). In fact, in this model, S1P-containing PLGA microparticles not only stimulated post-ischemic angiogenesis at 28 days but also blocked oedema induced when VEGF was co-administered (Qi et al., 2010). The effects of  $S1P_1$  and  $S1P_3$  receptors on adherens junctions in endothelial cells were documented soon after the identification of these receptors (Lee et al., 1999a). While  $S1P_1$  and  $S1P_3$  receptors strengthen the formation of endothelial cell

junctions (Singleton et al., 2007, Singleton et al., 2005, Singleton et al., 2009, Camerer et al., 2009), S1P<sub>2</sub> receptors increase vascular permeability *in vitro* via disruption of adherens junctions (Sanchez et al., 2007, Lee et al., 2009). *In vivo*, S1P<sub>1</sub> receptor activation inhibit VEGF-induced vascular leakage in skin capillaries (Sanchez et al., 2003), whereas S1P<sub>1</sub> receptor antagonists have shown that they induce capillary leakage in the lung, kidney, skin, and intestine (Rosen et al., 2008, Sanna et al., 2006, Foss et al., 2007).

S1P<sub>1</sub> receptors promote vascular stabilization by regulating the interactions between endothelial and mural cells during the maturation process (Allende and Proia, 2002, Liu et al., 2000), and, in apparent contradiction with their pro-angiogenic effects mentioned above, S1P<sub>1</sub> receptors were recently shown to inhibit sprouting angiogenesis during vascular development (Ben Shoham et al., 2012), by stabilizing VE-cadherin at endothelial junctions and inhibiting VEGFR2 (Gaengel et al., 2012, Jung et al., 2012), suggesting the existence of an alternative mechanism that helps stabilize the newly formed vascular network and improves its barrier function.

These data showing that S1P plays a role both at the early stages of angiogenesis and at the stage of new vessel stabilization, taken together with the effects of this lipid on bone cells, suggest that scaffold-mediated delivery of S1P (most likely S1P<sub>1</sub>) agonists might promote bone repair via pleiotropic and possible synergistic mechanisms.

### **2.13 Current efforts in S1P delivery**

The importance of S1P as a chemoattractant, and in coupling the activity of osteoblasts and osteoclasts suggests it could be utilized systemically in bone repair, and in

disorders such as osteoporosis (Meshcheryakova et al., 2017). However, a study of daily subcutaneous fingolimod (6 mg/kg) did not lead to any improvement in fracture healing, either by influencing bone formation or erosion, of a murine femoral defect after 3 weeks (Heilmann et al., 2013). The authors highlighted that a failure to demonstrate if fingolimod could influence bone healing by impacting inflammatory cell recruitment may have been a cause of the lack of effect compared to studies that utilised a localised delivery of fingolimod (Petrie Aronin et al., 2010a, Petrie Aronin et al., 2010b, Sefcik et al., 2011). Indicating that a more localised approach of delivering S1P and related analogues, may lead to more promising results.

Local administration of S1P has typically involved the use of scaffolds, which often have the dual role of acting as drug delivery device and mimicking native tissue to elicit functional tissue development. Hence a range of biocompatible materials, including natural polymers (collagen, chitosan, silk), synthetic polymers (PLGA and PCL) and inorganic materials (ceramics and glasses) have been investigated to fabricate scaffolds that are conducive to tissue regeneration, and allow temporal control over the release of therapeutic cargoes (Ahern et al., 2013). Biodegradable PLGA is among the commonest copolymers investigated (Galvin et al., 2012) and has been used to control the release of S1P (Sefcik et al., 2008) and fingolimod (Das et al., 2014b), resulting in increased new bone formation post-implantation in a rat cranial defect model, an effect that was attributed to increased development of vasculature and the possible dose-dependent initiation of bone progenitor cell migration towards the defect site (Das et al., 2014b). The underlying mechanism was probed in a similar study investigating the delivery of S1P agonists and antagonists (S1P, fingolimod or VPC01091) from PLGA scaffold implants in a rat cranial defect model (Petrie Aronin

et al., 2010a). Although S1P is subject to much more rapid *in vivo* degradation than fingolimod, scaffolds loaded with either agonist were equally effective in generating new bone over 6 weeks, while VPC01091-loaded scaffolds did not differ from unloaded controls (Petrie Aronin et al., 2010a). This study suggests that sustained release from scaffolds may offset the challenges of employing therapeutic cargoes (e.g. S1P) with short half-lives, and that S1P<sub>3</sub> receptors synergize with S1P<sub>1</sub> receptors to influence the various processes underlying repair (i.e., vascular remodelling, cell proliferation and migration, inflammation), albeit to differing extents. fingolimod has been incorporated into electrospun nanofibers composed of PLGA and biodegradable PCL and showed significant improvement in defect healing and vascularization in a rat critical mandibular defect (Das et al., 2013). These fingolimod-loaded nanofibers increased neovascularization and enhanced the proportion of macrophages with an anti-inflammatory phenotype (M2) (Das et al., 2013), a cell population that is also known to play an important role in tissue repair (Ogle et al., 2016), and had been previously shown to be selectively attracted by fingolimod (Ogle et al., 2014). A similar result of anti-inflammatory macrophage stimulation was found in another study using a PLGA coated allograft (Das et al., 2015), and whilst SEW2871 was also observed to stimulate macrophage recruitment, details regarding phenotype were not reported (Murakami et al., 2014). An electrospun amphiphilic copolymer was developed to act as a carrier for S1P to promote vascularization in tissue repair applications, the amphiphilic nature of the copolymer was anticipated to mimic the binding of S1P to apolipoprotein M. S1P was first applied directly to endothelial cells (HUVEC) and showed pro-angiogenic effects in a tube formation assay. Tube length and uniformity were then improved when S1P was administered as part of the

amphiphilic scaffold, additional evidence of new vessel formation was shown in a 3 day chorioallantoic membrane assay (Zhang and Song, 2014).

Whether small molecule delivery alone will achieve sufficient and effective bone repair remains to be established, but it is worth noting that fingolimod PLGA microspheres in a chitosan gel improved bone regeneration in a rat cranial defect study, with no substantial improvement upon addition of BMP-2 to fingolimod-loaded microspheres (Das et al., 2014a), despite fingolimod being known to enhance BMP-2 mediated osteoblast differentiation *in vitro* (Sato et al., 2012). Conversely, SEW2871 alone failed to improve bone regeneration, but co-administration with platelet rich plasma improved the latter's performance, by enhancing macrophage recruitment and cell debris clearance (Kim et al., 2014). Combining SIP with low-cost, biocompatible, biodegradable polymers represents an enticing alternative prospect for current bone graft treatments. Unfortunately, results to date still show most polymeric biomaterials cannot match the efficacy of bone grafts, because they lack both the osteogenic and osteoinductive properties that make grafts so successful. Consequently, bioactive polymer-graft composites are a potential solution to recapitulate mechanical and biological properties of host tissue in an effort to repair critical-sized defects. In one case, fingolimod elution from a PLGA-coated devitalized-bone allograft in a critical rat tibial defect improved elastic modulus and ultimate compressive strength of the bone, outcomes attributed to evidence of enhanced active remodelling at the defect site (Petrie Aronin et al., 2010b). The same procedure was investigated further, and similarly attributed tissue regeneration to improved vascularization, while also presenting a more detailed discussion of the role of bone marrow derived cells in immune modulation (Das et al., 2015). Another PLGA coated allograft delivery

system for fingolimod showed a dose-dependent increase in bone volume in a cranial defect model at 2 and 4 weeks. Although differences in bone volumes were no longer significant at 8 weeks, fingolimod still enhanced host-graft integration at this time point (Huang et al., 2012). Notably, direct adsorption of fingolimod onto implanted allograft improved bone deposition and vascularisation (Wang et al., 2016a). Predictably, this method produced higher local concentrations of fingolimod, but lower increases in bone density compared to polymer-based delivery discussed above (Huang et al., 2012, Wang et al., 2016a).

## 2.14 Conclusion

Although the role of S1P in bone biology has been the focus of much less research than its role in the cardiovascular and immune systems, it is becoming clear that this lipid influences many of the functions, pathways and cell types that play a key role in bone repair. Indeed, S1P has a well-established role in promoting angiogenesis (Hla, 2004, Sefcik et al., 2008, Sefcik et al., 2011, Kono et al., 2004, Zhang and Song, 2014), but is also implicated in many other bone related processes including stem cell recruitment (Annabi et al., 2003, Quint et al., 2013, Ratajczak et al., 2014) and subsequent differentiation (Hashimoto et al., 2015). S1P stimulates the differentiation and survival of osteoblasts (Sato et al., 2012, Matsuzaki et al., 2013), and contributes to their intricate coupling with osteoclasts (Ryu et al., 2006). S1P is not only a key factor in its own right, it also seems to mediate the functions of critical bone growth factors, such as BMP (Pederson et al., 2008, Sato et al., 2012). Although the use of growth factors for bone repair has been widely explored, some issues remain, such as

those related to supra-physiologic doses (Tannoury and An, 2014), short half-lives (Yamamoto et al., 2003), an inability to maintain osteogenicity due to slow vascular integration of grafts (Gomez-Barrena et al., 2015), not to mention high costs (Garrison et al., 2007). As summarized in earlier sections, various groups have therefore begun to explore the use of non peptidic agents, such as S1P and analogues, to promote bone repair *in vivo*, with generally promising results. Remaining issues regarding pleiotropic activity (Maceyka et al., 2012), solubility (Murakami et al., 2014) and the need to maintain local concentrations over a number of weeks (Maceyka et al., 2012) may be addressed by using more specific agents and/or novel delivery options. A number of such delivery methods have been studied in the field of bone repair to enhance delivery of growth factors (Garrison et al., 2007, Dimitriou et al., 2005, Hankenson et al., 2015), small molecule drugs, and stem cell therapies (Leijten et al., 2015, Klontzas et al., 2016, Henkel et al., 2013). They have generally involved biomaterials for controlled release of drugs including biocompatible, biodegradable polymers, and bio-ceramics (Kim and Tabata, 2015, Henkel et al., 2013) and the use of high affinity delivery systems, which have led to reductions in required doses (Martino et al., 2015).

The use of S1P agents for bone repair is likely to be greatly accelerated by the much more active translational and clinical research of the role of S1P signalling in other fields, such as inflammation or cancer. The number of active clinical trials involving S1P receptor ligands in inflammatory conditions ranges from 2 and 3% of trials for inflammatory bowel disease and psoriasis, up to 32% of all trials for new multiple sclerosis therapies (Hanke et al., 2016). S1P<sub>1</sub> receptors have been the focus of most research in this field, as evidenced by the great emphasis placed on the development

of agents such as ponesimod, siponimod, and ozanimod, with improved specificity compared to fingolimod. Whilst other possible targets, such as S1P lyase inhibition have been less well investigated (Chew et al., 2016). In the field of bone repair, further basic and translational research will be needed to better define which S1P metabolic enzymes or receptors should be targeted, when and for what duration, and whether an agonist or an antagonist would be preferable. The latter issue is particularly critical considering that S1P<sub>1</sub> receptor agonists seem to exert their action as functional antagonists, with S1P<sub>1</sub> agonists and antagonists showing similar therapeutic effects (Quancard et al., 2012). Furthermore, some of the work quoted in this chapter has been based on qualitative or semi-quantitative data, and the pharmacological profile of the response was sometimes unclear, either due to incomplete dose response studies, or the use of agents with questionable specificity (Salomone and Waeber, 2011, Adada et al., 2013) .

To conclude, the manipulation of S1P signalling using systemic administration of therapeutic agents seems promising for the management of inflammatory or hormonally related bone loss, as S1P agents can be used to affect osteoblast/osteoclast coupling, the unbalancing of which manifests as conditions such as osteoporosis. In contrast, local administration of S1P agents has shown more compelling results in bone defect studies, and so improving local delivery of these agents will be key to optimising their regenerative potential. Critically, this may be achieved by not only increasing the recruitment of osteogenic cell precursors but also by inducing and supporting vascularization and modulating the immune response; S1P agents may be unique in that they are known to possess all three activities (Das et al., 2014b, Petrie



Aronin et al., 2010a, Das et al., 2013, Das et al., 2015, Kim et al., 2014, Petrie Aronin et al., 2010b, Huang et al., 2012, Wang et al., 2016a).

## Chapter 3

Bone regenerative potential of the selective sphingosine 1-phosphate receptor modulator siponimod: *in vitro* characterisation using osteoblast and endothelial cells

**Ziad Sartawi<sup>1</sup>, Katie B. Ryan<sup>1</sup>, Christian Waeber<sup>1,2</sup>**

<sup>1</sup> School of Pharmacy, University College Cork, Cork, Ireland

<sup>2</sup> Department of Pharmacology and Therapeutics, University College Cork, Cork,  
Ireland

Revised from publication

European Journal of Pharmacology, September 2020

Volume 882, 5 September 2020, 173262 DOI: 10.1016/j.ejphar.2020.173262

### 3.1 Abstract

The repair of critical bone defects remains a significant therapeutic challenge. While the implantation of drug-eluting scaffolds is an option, a drug with the optimal pharmacological properties has not yet been identified. Agents acting at sphingosine 1-phosphate (S1P) receptors have been considered, but those investigated so far do not discriminate between the five known S1P receptors. This work was undertaken to investigate the potential of the specific S1P<sub>1/5</sub> modulator siponimod as a bone regenerative agent, by testing *in vitro* its effect on cell types critical to the bone regeneration process.

hFOB and HUVEC were treated with siponimod and other S1P receptor modulators and investigated for changes in intracellular cyclic AMP content, viability, proliferation, differentiation, attachment and cellular motility.

Siponimod showed no effect on the viability and proliferation of osteoblasts and endothelial cells, but increased osteoblast differentiation (as shown by increased alkaline phosphatase activity). Furthermore, siponimod significantly increased endothelial cell motility in scratch and transwell migration assays.

These effects on osteoblast differentiation and endothelial cell migration suggest that siponimod may be a potential agent for the stimulation of localised differentiation of osteoblasts in critical bone defects.

### 3.2 Introduction

The restoration of tissue function after damage, involves complex interactions between various cell types, local tissue matrix, and chemical mediators, in various combinations.

The creation of new vasculature via angiogenesis is essential for the regeneration of any tissue, and in the case of bones, regeneration also involves the recruitment of osteoblast and osteoclast precursors to the defect area, their differentiation into their mature phenotypes as well as interaction between the two cell types, with bone-forming osteoblasts stimulating the maturation of bone resorbing osteoclasts, which in turn stimulate osteoblast recruitment and maturation (Chen et al., 2018).

S1P is a lipid mediator that modulates many biological processes, including calcium signalling, cell growth, differentiation, survival, motility and cytoskeleton organization (Spiegel and Milstien, 2000). It acts via 5 known G Protein-Coupled Receptors (S1P<sub>1-5</sub>), which are widely expressed throughout the body (Hla, 2004). The role of S1P in promoting angiogenesis is well-established (Waeber, 2013b). This, taken together with the pleiotropic effects of S1P on bone cells (Sartawi et al., 2017), suggests that modulating S1P signalling may promote bone repair. However, systemic administration of S1P agents did not improve fracture healing in a murine femoral defect (Heilmann et al., 2013), indicating that more localised approaches of delivering S1P and related analogues may be needed (Das et al., 2014b).

The pharmacological characterization of the various S1P-mediated responses, in bone and other tissues, has been hampered by the lack of well-characterized specific agents (Salomone and Waeber, 2011). S1P itself (with or without receptor antagonists), as

well as the S1P receptor modulator fingolimod (aka FTY720 or Gilenya®) have been investigated in *in vitro* and *in vivo* models of bone repair (Sartawi et al., 2017), but these agents do not discriminate between the 5 different receptor subtypes. Fingolimod, used clinically for the management of relapsing remitting multiple sclerosis, is a potent agonist at all S1P receptor subtypes except S1P<sub>2</sub> (Brinkmann et al., 2010). Its mechanism of action relies, at least in part, on the redistribution of lymphocytes to secondary lymphoid tissues following fingolimod-induced S1P<sub>1</sub> receptor internalization, resulting in their depletion from the peripheral blood and immunosuppression. Although fingolimod is relatively safe, activation of S1P<sub>3</sub> receptors by this agent may be associated with adverse effects (DiMarco et al., 2014, Cugati et al., 2014). Although the role of S1P<sub>3</sub> receptors in cardiac side effects may be unique to rodents (Gergely et al., 2012), these off-target effects led to the discovery and development of the S1P<sub>1/5</sub> selective agonist siponimod (aka BAF312, or Mayzent®) (Behrangi et al., 2019). In addition to its improved selectivity profile, siponimod is not a pro-drug (fingolimod must first be phosphorylated by sphingosine kinase 2) and has a shorter half-life that still allows once-daily oral dosing but enables rapid recovery of lymphocyte counts upon treatment cessation.

The effects of S1P and of fingolimod on cells relevant to bone repair have been extensively investigated (Sartawi et al., 2017), but far less is known on the effect of siponimod on these cells. The goal of these studies was therefore to test the effect of siponimod on the viability, proliferation, differentiation, and chemotactic behaviour of osteoblast and endothelial cells, with the aim of better understanding the potential of selective modulation of S1P<sub>1</sub> (or S1P<sub>5</sub>) receptors via localised delivery to repair critical bone defects.

### 3.3 Materials and methods

#### 3.3.1 Materials

Siponimod hemifumarate and fingolimod hydrochloride were kindly gifted from Novartis. D-erythro-Sphingosine 1-phosphate was acquired from Enzo Life Sciences. Dulbecco's Modified Eagle's Medium/Nutrient Mixture F-12 Ham, foetal bovine serum (FBS), L-Glutamine, penicillin-streptomycin, Thiazolyl Blue Tetrazolium Bromide (3-(4,5-dimethylthiazol-2-yl)-2,5-diphenyltetrazolium bromide) (MTT), dimethyl sulfoxide (DMSO), neutral buffered formalin (NBF), Fast Blue BB and Naphthol AS-MX phosphate, Roche Bromodeoxyuridine (BrdU) cell proliferation kit were acquired from Sigma-Aldrich. Endothelial cells (HUVEC) and endothelial cell growth medium (ECGM) with associated supplements were acquired from PromoCell. Pierce™ PNPP Substrate Kit was acquired from Thermo Fisher Scientific. cAMP-Glo™ Max Assay was acquired from Promega. Cell culture plasticware was acquired from Sarstedt Ltd. Human foetal osteoblasts (hFOB 1.19 (ATCC® CRL-11372™)) cell line was acquired from ATCC.

#### 3.3.2 Cell culture

hFOB were maintained in DMEM/F12 supplemented with FBS (10%), L-glutamine (1%), and penicillin-streptomycin (1%). Incubation was at 34 °C and 5% CO<sub>2</sub>. HUVEC were maintained in supplemented ECGM as per supplier's instruction at 37 °C and in 5% CO<sub>2</sub>. Although this medium contains only 2% serum, some HUVEC experiments were performed under reduced serum conditions (1/10<sup>th</sup> standard cell culture supplement) to rule out an effect of endogenous S1P (Hanel et al., 2007).

### 3.3.3 Siponimod solution

Siponimod was dissolved in DMSO and then diluted in PBS as required. DMSO concentration were limited to <0.5% v/v in cell culture experiments. The potential toxicity of exceeding this concentration of DMSO was explored using hFOB and HUVEC ( $2.5 \times 10^4$  cell/well in 24 well plates) incubated with increasing concentrations of DMSO (0.32 - 3.2% in cell culture medium) for two and three days respectively. Thereafter, resazurin 60  $\mu$ l of a 560  $\mu$ M stock solution was added to wells for 3.5 hrs before acquiring fluorescence at excitation 488 nm/emission 595 nm.

### 3.3.4 Viability and proliferation

To estimate the effect of siponimod on cellular viability, cells were seeded at a density of  $2.5 \times 10^4$  cells per well in 24-well plates, the following day test drugs (100 nM siponimod or PBS vehicle) were added to cell culture medium. Following two- and three-days incubation (HUVEC and hFOB, respectively), 60  $\mu$ l MTT solution (5 mg/ml stock) was added directly to wells and incubated for two hrs away from light. Wells were then rinsed with PBS. Formazan crystals were dissolved with DMSO and absorbance acquired at 570 nm using a Wallac Victor 2 plate reader (Perkin Elmer).

To determine the effect of siponimod on cellular proliferation, cells were seeded in 24-well plates at a density of  $2.5 \times 10^4$  cells per well. Siponimod (100 nM) or PBS vehicle were added to the cell culture medium for two- and three-days (HUVEC and hFOB, respectively). Thereafter, cells were detached using trypsin-EDTA 0.25%, diluted with cell culture medium, and individual well cell numbers manually counted using a haemocytometer. Additional cell counting experiments were conducted using hFOB maintained over 7 days (see section 2.4 for details)

As an additional measure of proliferation, a BrdU cell proliferation assay was conducted. BrdU is an analogue of pyrimidine and incorporated in its place into the DNA of proliferating cells and detected as part of a colorimetric enzyme-linked immunosorbent assay. In brief, cells were seeded in 96-well plates at densities of  $1 \times 10^4$  per well. Increased concentrations of siponimod, fingolimod, and S1P (all 1000 nM) and a PBS control were added the following day with fresh medium, and incubation continued for a further two days. Following treatment, BrdU was diluted in fresh medium and added to cells for 24 hrs. Thereafter cells were fixed for 30 mins, then incubated for 90 mins in a BrdU antibody solution, rinsed thoroughly with PBS followed by incubation with anti-BrdU substrate until sufficient colour development for plate reading at 405 nm.

### 3.3.5 Osteogenic differentiation

#### 3.3.5.1 Para-nitrophenylphosphate

Alkaline phosphatase (ALP) is an early marker of osteoblast differentiation. *In vitro* osteoblast differentiation was estimated using para-nitrophenylphosphate (pNPP) as a substrate of alkaline phosphatase that is dephosphorylated into a yellow product (p-nitrophenol), detectable by absorbance at 405 nm.

hFOB ( $5 \times 10^4$ ) were seeded in 24-well plates and treated on day 0, 2, 4, and 6 with 1000 nM of either siponimod, fingolimod or S1P, with PBS vehicle as a control. Test agents and controls were added directly to standard hFOB medium. As a positive differentiation control, cells were treated with osteogenic medium containing 50 µg/ml ascorbic acid and 7.5 mM β-Glycerophosphate. After 7 days, cells were detached with 100 µl trypsin-EDTA 0.25%, diluted with 200 µl fresh medium and counted using a



haemocytometer. The cells were then transferred to 1.5 ml tubes and centrifuged at 3000 relative centrifugal force (rcf) for 5 mins. Medium was aspirated from each tube and replaced with 100  $\mu$ l pNPP substrate solution, allowing 30 mins for yellow colour development. Absorbance was recorded at 405 nm using a Wallac Victor 2 plate reader (Perkin Elmer). The absorbance value of each sample was divided by its respective cell count, to normalize for differences due to cell numbers. Data are presented relative to the positive osteogenic medium control in each independent replicate.

#### 3.3.5.2 Fast blue staining

Because the pNPP-based assay above does not allow the determination of the fraction of differentiating cells, as a complimentary measure of ALP, staining was performed using Fast Blue BB and Naphthol AS-MX phosphate. hFOB ( $5 \times 10^4$ ) were seeded in 24-well plates and treated every other day with siponimod (10-1000 nM), PBS, or osteogenic medium for 7 days. Thereafter, cells were equilibrated in an alkaline buffer followed by incubation with fast blue dye for 60 mins. Using a BX51 microscope (OLYMPUS), three images were acquired per well (with a 4x objective). Using ImageJ analysis software, the number of stained cells and total cells was manually counted and expressed as a percentage of the total cell number.

#### 3.3.6 Migration

Cell migration assays were conducted for HUVEC and hFOB using the same techniques but using cell type specific media.

##### 3.3.6.1 Wound healing (scratch) assay

Cells were seeded at  $1 \times 10^5$  cells/well in 24-well plates and grown overnight to produce a nearly confluent monolayer. A linear scratch was created by hand using a 1 ml

pipette tip, wells were rinsed with PBS to remove debris and the cell culture medium was replaced as follows: for hFOB, DMEM/F12 supplemented with 0.1% FBS was used to reduce serum bioactive lipid effects. Likewise, for HUVEC, ECGM was supplemented with 1/10<sup>th</sup> the usual supplement. Siponimod and S1P (delivered in 20  $\mu$ l PBS), and PBS control were then added directly to cell culture medium. Brightfield images (4x objective) were acquired immediately and after 8 hrs using a BX51 microscope (OLYMPUS). Using the associated software, Stream (OLYMPUS), the distance between the edges of the scratch wound was measured and the change over time attributed to cellular migration into the empty space.

#### 3.3.6.2 Transwell migration

Transwell migration was conducted to assess chemotactic activity of S1P agents. Cells were seeded at  $5 \times 10^4$  cells in 100  $\mu$ l of medium in the upper chamber of 8  $\mu$ m pore polyethylene terephthalate transwell inserts. Siponimod, S1P, fingolimod (delivered in 20  $\mu$ l PBS), or PBS control were then added to the bottom chamber of the transwell system, which contained 600  $\mu$ l of medium. After 4, 8, or 24 hrs of incubation, culture medium was aspirated from the upper chamber, inserts were fixed with 10% NBF for 15 mins at room temperature, then stained with 0.5% crystal violet for 30 mins at room temperature. Thereafter inserts were rinsed with water to remove excess dye and the top side of the membrane was wiped with a cotton bud to remove non-migrated cells. Finally inserts were dried on the bench, before the membrane was visualized by light microscopy (BX43 microscope (OLYMPUS)). Five brightfield images per insert were acquired (10x objective), stained cells were manually counted using ImageJ analysis software.

### 3.3.7 Cell attachment

The influence of siponimod on HUVEC attachment was investigated by seeding  $5 \times 10^4$  cells in 24 well plates using ECGM that was supplemented with  $1/10^{\text{th}}$  standard supplement to reduce serum lipid effects. Siponimod and S1P (delivered in 20  $\mu\text{l}$  PBS), and PBS control were then added immediately to wells. After 4 hrs incubation, non-attached cells were removed by washing with PBS. Remaining cells were fixed with 10% NBF for 15 mins, followed by staining with crystal violet 0.5% w/v for 30 mins. Three brightfield images per well were acquired (10x objective), with stained cells manually counted using ImageJ analysis software.

### 3.3.8 Cyclic AMP assay

The effect of siponimod on intracellular cAMP levels was determined using the cAMP-Glo™ Max Assay (Promega). hFOB were seeded at  $2 \times 10^4$  cells per well in 96 well plates and cultured overnight. Cells were washed with PBS, then treated with forskolin, siponimod, forskolin & siponimod combined, and a control containing the DMSO vehicle (concentration 0.32 %) for 1 hr. All conditions included 500  $\mu\text{M}$  IBMX to inhibit phosphodiesterases. Luminescence was measured and cAMP concentrations calculated using a standard curve as per the manufacturer's protocol.

### 3.3.9 Statistical analysis

Results were expressed as mean  $\pm$  standard deviation (SD), unless otherwise stated. Determining statistical significance was performed using one-way analysis of variance (ANOVA) followed by Bonferroni post-test for multiple comparisons. Differences were considered significant at  $p < 0.05$ . We used extra-sum-of-squares F tests as previously described (Waeber and Moskowitz, 1995) to determine whether drug

responses were concentration-dependent (with the null hypothesis that data points were best fitted with a horizontal line, i.e. showed no concentration dependence).

### 3.4 Results

#### 3.4.1 Siponimod solution

Siponimod was applied to cells in *in vitro* experiments as an aqueous solution of PBS containing a small concentration of DMSO as a cosolvent (0.32 % v/v). In order to determine whether the use of DMSO as a cosolvent would negatively impact hFOB and HUVEC used throughout this work, increasing concentrations of DMSO were applied to cells and their viability determined by resazurin assay (Figure 3.1). For hFOB there was no statistically significant change in cell viability when using 0.32 % DMSO compared to PBS control ( $91.5 \pm 24.2$  % compared to  $100 \pm 26.7$  %). With increasing concentration of DMSO, cell viability trended downwards albeit without achieving statistical significance until a DMSO concentration of 3.22 % produced a significant fall in hFOB viability compared to PBS control and the 0.32 % condition ( $4.8 \pm 2.7$  % compared to  $100 \pm 26.7$  % and  $91.5 \pm 24.2$  %,  $p < 0.05$ ). For HUVEC incubated with a concentration of 0.32 % DMSO there was no statistically significant change in cell viability over the experimental duration compared PBS control ( $99.4 \pm 9.3$  % compared  $100 \pm 4.2$  %). As before DMSO showed a statistically significant reduction in cell viability at increased concentrations of 3.22 % compared to PBS and the 0.32 % condition ( $25.0 \pm 12.1$  % compared to  $100 \pm 4.2$  % and  $99.4 \pm 9.3$  %,  $p < 0.05$ ).

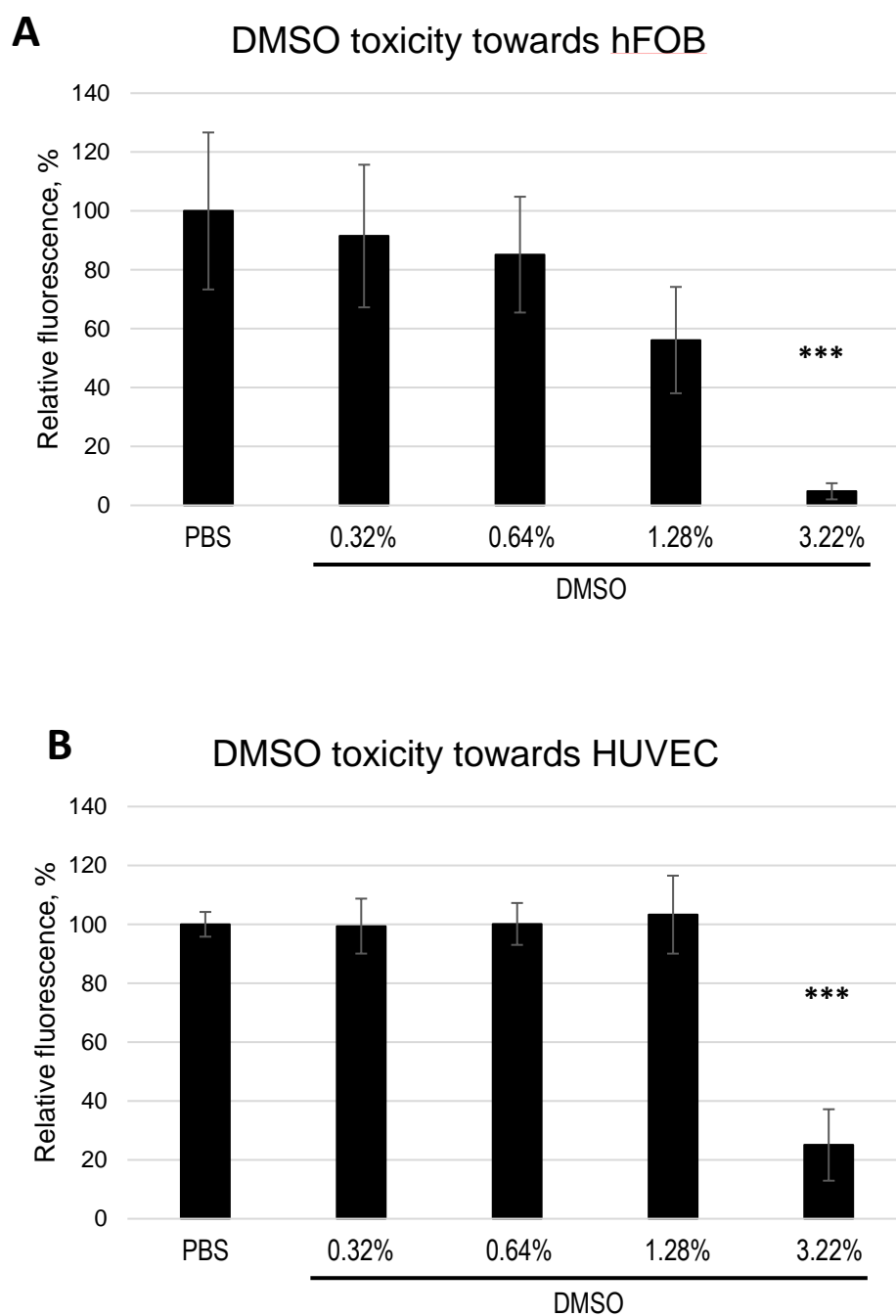


**Figure 3.1** Viability assay for hFOB and HUVEC incubated with increasing concentrations of DMSO. (A) hFOB resazurin assay after 72 hrs, (B) HUVEC resazurin assay after 48 hrs. Data is expressed as a percentage of PBS control and is presented as mean  $\pm$  SD from 3 independently repeated experiments (with 3 technical

replicates). For hFOB, increasing DMSO concentrations were added to cell culture medium containing 1/10<sup>th</sup> standard serum supplement. For HUVEC, DMSO concentrations were added to cell culture medium containing 1/3<sup>rd</sup> standard supplements. Statistical analysis was performed by one-way ANOVA. There was no statistically significant difference between any group except for 3.22% DMSO, which was statistically different from all other groups (\*\*\*:  $p < 0.001$ ).

#### 3.4.2 Viability and proliferation

Siponimod effect on cell viability and proliferation was investigated using hFOB and HUVEC. MTT assays were used to determine cell viability, with results presented as absorbance at 570 nm expressed as a percentage of positive control (for hFOB, fully supplemented DMEM/F12, for HUVEC, fully supplemented ECGM). Manual cell counting was used to determine cell proliferation, with data presented as average cell numbers expressed as a percentage of positive control. Viability of hFOB treated with 100 nM siponimod were not significantly different to those treated with PBS vehicle ( $42.1 \pm 7.6$  % compared to  $36.9 \pm 8.6$  %), this lack of effect was also seen in manual cell counting experiments comparing 100 nM siponimod and PBS vehicle ( $49.1 \pm 4.1$  % compared to  $44.9 \pm 0.8$  %) (Figure 3.2 A & B). For HUVEC 100 nM siponimod produced no significant difference in viability compared to PBS vehicle ( $80.9 \pm 8.8$  % compared to  $74.9 \pm 8.2$  %). There was similarly no statistically significant change in manual cell count results between 100 nM siponimod and PBS vehicle ( $68.1 \pm 12.7$  % compared to  $59.1 \pm 12.7$  %) (Figure 3.2 C & D). Additionally, BrdU assay confirmed the absence of a proliferative effect for 1000 nM siponimod on both the hFOB and HUVEC (Figure 3.2 E & F). The BrdU assays also showed that there was no discernible effect on proliferation for either S1P or fingolimod (1000 nM).

Over a 7 day experimental duration (Figure 3.2 G), none of siponimod, fingolimod or S1P (all 1000 nM) led to any statistically significant change in hFOB cell count compared to PBS control ( $87.9 \pm 16.5$  % for siponimod,  $88.7 \pm 10.3$  % for fingolimod, and  $72.5 \pm 18.7$  % for S1P compared to  $100 \pm 37.1$  % for PBS control). Likewise, increasing concentrations of siponimod (10-1000 nM (Figure 3.2 H)) did not show any statistically significant changes in cell number compared to PBS control ( $91.2 \pm 5.0$  % for 10 nM,  $95.8 \pm 15.5$  % for 100 nM, and  $82.2 \pm 24.2$  % for 1000 nM compared to  $100 \pm 14.7$  % for PBS control).

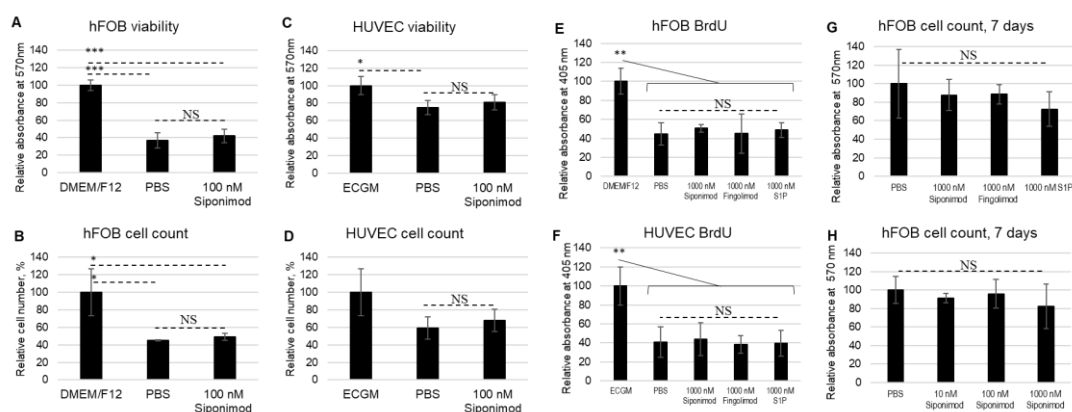


**Figure 3.2** Viability and proliferation assays for hFOB and HUVEC. (A & B) hFOB MTT assay and cell count after 72 hrs,  $n=3$  (4 technical replicates) (C & D) HUVEC MTT assay and cell count after 48 hrs,  $n=3$  (4 technical replicates) (E & F) hFOB and HUVEC BrdU assay,  $n=3$  (4 technical replicates) (G & H) hFOB cell count after 7 days incubation,  $n=4$  (3 technical replicates). For A-F, data is expressed as a percentage (positive control set to 100%), for G & H data is expressed as a percentage of PBS control. For hFOB (in A-F), factors were added to cell culture medium



containing 1/10th standard serum supplement, with standard growth medium (DMEM/F12) acting as positive control. For HUVEC (in A-F), factors were added to cell culture medium containing 1/3rd standard supplements, with standard growth medium (ECGM, containing 2% serum) acting as positive control. In G & H growth medium supplement was not altered. ‘‘n=’’ represents the number of independently repeated experiments. Data is presented as mean  $\pm$  SD, statistical analysis by one-way ANOVA. NS: No statistical significance. \*:  $p < 0.05$ . \*\*:  $p < 0.01$ . \*\*\*:  $p < 0.001$ .

### 3.4.3 Osteogenic differentiation

#### 3.4.3.1 Para-nitrophenylphosphate

hFOB were incubated in medium containing equal concentrations (1000 nM) of either siponimod, fingolimod, or S1P (Figure 3.3). Absorbance values for the ALP product p-nitrophenol were normalised according to manual cell counts. Data is expressed as a percentage of the osteogenic medium positive control across each replicate. Figure 3.3 A shows the results of the comparison between the three investigated drugs (siponimod, fingolimod, and S1P). Whereas 1000 nM fingolimod showed no significant difference compared to PBS vehicle ( $44.8 \pm 2.7$  % compared to  $39.8 \pm 9.5$  %), siponimod (1000 nM) increased absorbance/count compared to PBS vehicle ( $68.4 \pm 9.7$  % compared to  $39.8 \pm 9.5$  %,  $p < 0.05$ ). This increase was not significantly different from that induced by 1000nM S1P ( $78.1 \pm 10.3$  % compared to  $39.8 \pm 9.5$  % for PBS vehicle,  $p < 0.05$ ) and the response to siponimod ranging from 10-1000 nM was concentration dependent (F statistic = 11.46;  $p = 0.0069$ ) (Figure 3.3 B).

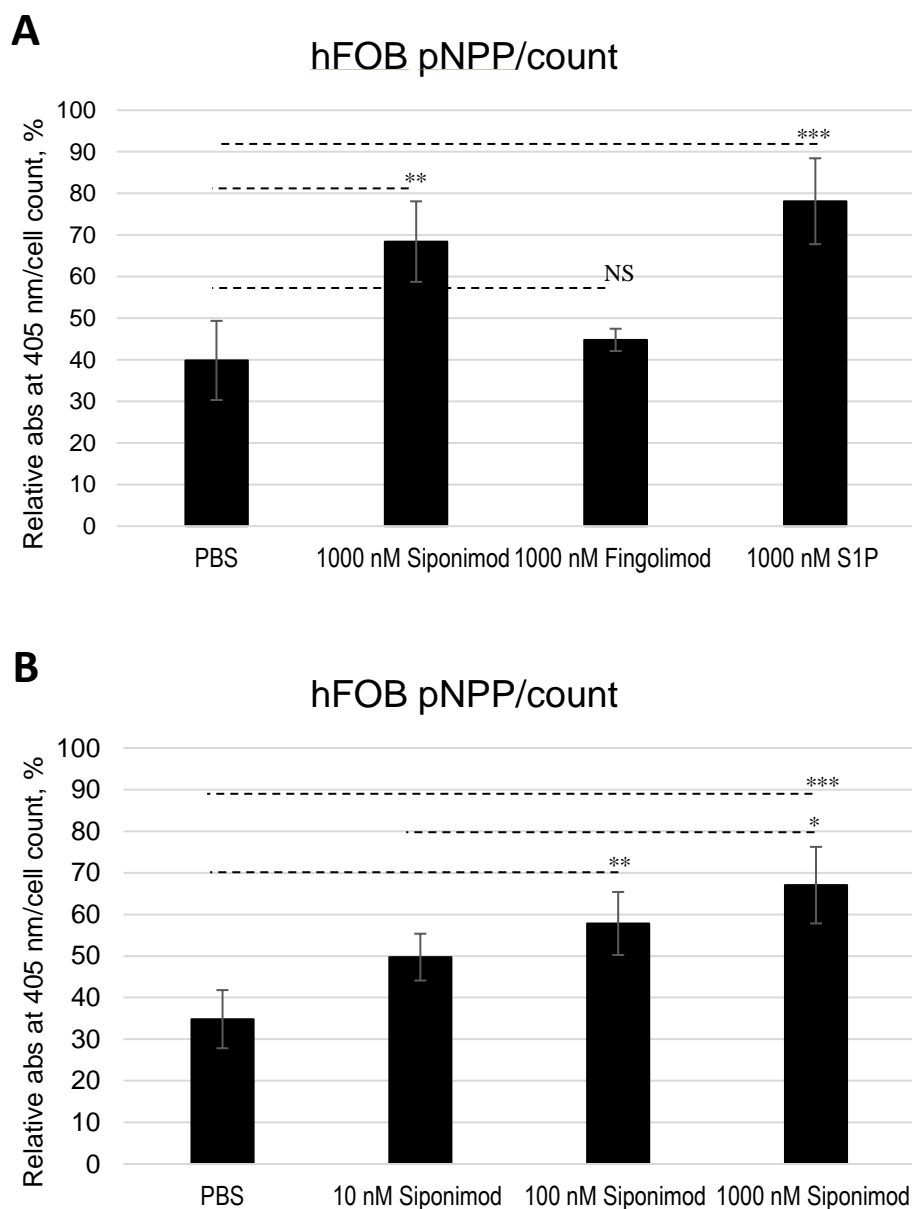


**Figure 3.3** Alkaline phosphatase activity as an early marker of differentiation in hFOB. (A) Effect of siponimod, fingolimod, and S1P (1000 nM) after 7 days,  $n=4$  (3 technical replicates) (B) Siponimod concentration response over 10-1000 nM after 7 days,  $n=4$  (3 technical replicates). For A & B, data represents pNPP absorbance at 405 nm divided by cell count, relative to the positive control (osteogenic medium containing 50  $\mu\text{g/ml}$  ascorbic acid & 7.5 mM  $\beta$ -glycerophosphate) in each independent

replicate. “ $n=$ ” represents the number of independently repeated experiments. Data is presented as mean  $\pm$  SD, statistical analysis by one-way ANOVA. NS: No statistical significance. \*:  $p < 0.05$ . \*\*:  $p < 0.01$ . \*\*\*:  $p < 0.001$ .

### 3.4.3.2 Fast blue staining

Alkaline phosphatase staining (Figure 3.4) was performed to complement the pNPP-based assessment above. Results represent the number of stained cells divided by the total number of cells, expressed as a percentage. hFOB were incubated with three concentrations of siponimod (10, 100, and 1000 nM). The concentrations 100 nM and 1000 nM resulted in an increased fraction of stained cells (100 nM siponimod  $3.7 \pm 0.6$  ( $p < 0.05$ ), and 1000 nM siponimod  $4.2 \pm 0.8$  % ( $p < 0.05$ ) compared to PBS vehicle  $1.9 \pm 0.6$  %) and the response was concentration dependent (F statistic = 6.53;  $p = 0.038$ ).

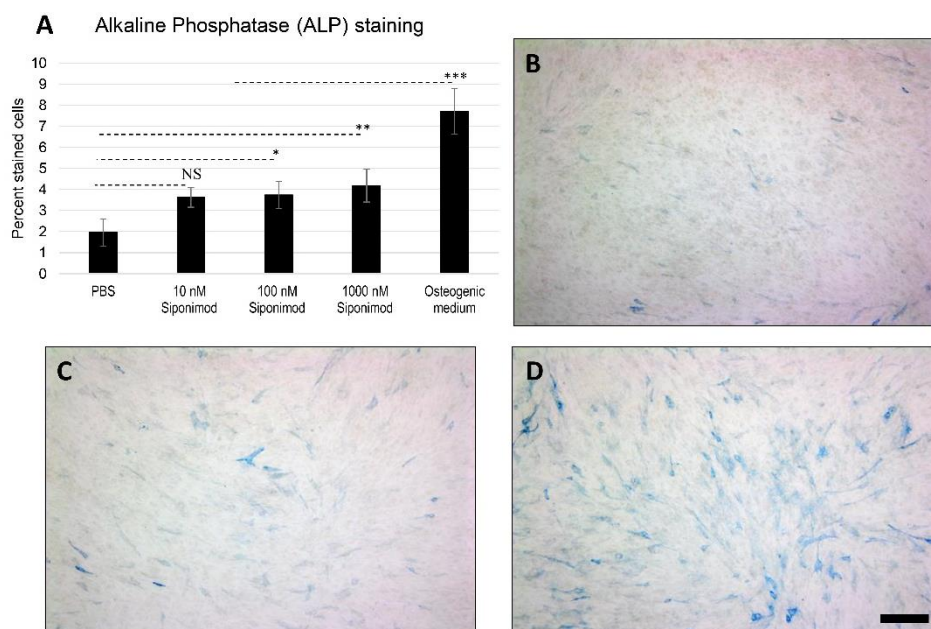


**Figure 3.4** Alkaline phosphatase (ALP) staining as an early marker of differentiation in hFOB. (A) Response to 10-1000 nM siponimod after 7 days,  $n=4$  (3 technical

replicates). Data represents the average number of manually counted Fast blue-stained cells divided by the total cell number. Osteogenic medium (containing 50 µg/ml ascorbic acid & 7.5 mM β-glycerophosphate) was used as a positive control. “*n*=” represents the number of independently repeated experiments. Data is presented as mean ± SD. Statistical analysis was done using one-way ANOVA. NS: No statistical significance. \*:  $p < 0.05$ . \*\*:  $p < 0.01$ . \*\*\*:  $p < 0.001$ . The percentage of ALP-stained cells in the presence of osteogenic medium was significantly different from the percentage of stained cells in all other conditions ( $p < 0.001$ ). B, C, and D are representative brightfield photomicrographs of hFOB exposed to PBS (B), 100 nM siponimod (C), and osteogenic medium (D); blue cells are cells with higher alkaline phosphatase activity, and hence a higher level of differentiation. Scale bar is 500 µm.

#### 3.4.4 Migration

##### 3.4.4.1 Wound healing (scratch) assay

Scratch assays were performed to investigate whether the migratory response of hFOB and HUVEC was increased by siponimod. While hFOB did not respond to 100 nM siponimod after 8 hrs (Figure 3.5 A), HUVEC scratch wound closure was doubled in the presence of 100 nM siponimod compared to PBS vehicle ( $45.8 \pm 4.0$  % compared to  $22.5 \pm 6.0$  %,  $p < 0.05$ ) (Figure 3.5 B). The concentration responsiveness of the effect was examined in a separate series of experiments; while all siponimod concentrations (1, 10, and 100 nM) produced a statistically significant increase in scratch wound closure compared to PBS vehicle ( $40.9 \pm 5.0$  %,  $42.3 \pm 3.5$  %, and  $45.9 \pm 2.9$  % compared to  $22.7 \pm 7.2$  %,  $p < 0.05$ ) (Figure 3.5 C), this response was found to not be concentration dependent (F statistic = 2.82;  $p = 0.14$ ). The migratory response of HUVEC to 100 nM S1P was qualitatively similar to the effect of siponimod (Figure

3.5 D);  $40.6 \pm 3.6$  % for S1P compared to  $18.1 \pm 3.5$  % for PBS,  $p < 0.05$ . However, these experiments were conducted independently, precluding a direct comparison.

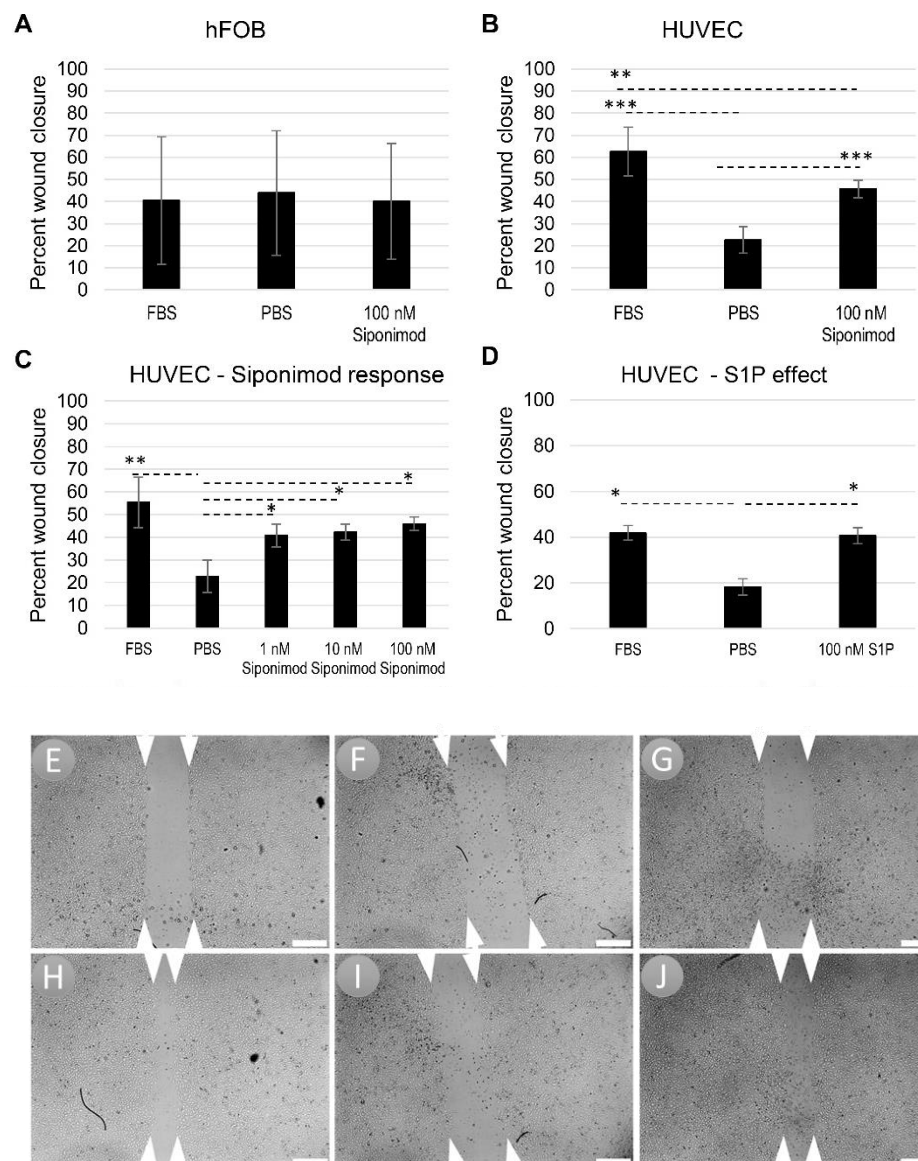


**Figure 3.5** Wound healing (scratch) assay for hFOB and HUVEC. (A) Effect of 100 nM siponimod on hFOB,  $n=4$  (3 technical replicates), (B) Effect of 100 nM siponimod on HUVEC,  $n=7$  (3 technical replicates), (C) Siponimod concentration response over 1-100 nM on HUVEC,  $n=3$  (3 technical replicates); (D) Effect of 100 nM S1P on HUVEC,  $n=2$  (3 technical replicates). Data represents the percentage closure of the

scratch wound after 8 hrs. ‘ $n=$ ’ represents the number of independently repeated experiments. Data is presented as mean  $\pm$  SD, statistical analysis by one-way ANOVA. \*:  $p < 0.05$ . \*\*:  $p < 0.01$ . \*\*\*:  $p < 0.001$ . E-J: Representative photomicrographs for the experiment shown in (B) are shown at 0 and 8 hrs: (E, H) positive control (FBS), (F, I) Vehicle (PBS) control, and (G, J) 100 nM siponimod. The white arrowheads at the top and bottom of each photomicrograph show the edge of the manually created scratch wound. Images were acquired using a 4x objective, scale bars are 500  $\mu$ m.

#### 3.4.4.2 Transwell migration

Following the data obtained from scratch wound assays, transwell migration assays were conducted to test the hypothesis that siponimod-enhanced migration of HUVEC was due to a chemotactic effect. Due to lack of scratch assay effect, hFOB were not investigated.

In transwell migration assays conducted under standard endothelial growth medium conditions (2 % v/v serum), 100 nM siponimod added to the bottom chamber of the transwell system resulted in a reduction in the number of migrated cells detected on the bottom side of the membrane compared to PBS vehicle ( $26.9 \pm 7.4$  % compared to  $71.6 \pm 10.3$  %,  $p < 0.05$ ) (Figure 3.6 A).

The concentration of S1P in serum is in the submicromolar range, i.e. sufficient to activate S1P receptors (Thuy et al., 2014). In contrast, much lower S1P concentrations are detected in tissues; this S1P gradient controls the trafficking of immune and hematopoietic stem progenitor cells (Liu et al., 2011). To test the hypothesis that the “repulsive” effect of siponimod added to the bottom chamber under high serum concentrations was due to siponimod-induced receptor internalization, thereby

blocking serum-induced cell migration, we tested the effects of S1P and siponimod added to the bottom chamber under reduced serum conditions (0.2% v/v serum). Under these conditions, 100 nM siponimod produced no statistically significant change in the number of migrated cells compared to PBS vehicle after 4 hrs ( $40.3 \pm 11.0$  % compared to  $33.8 \pm 10.1$  %) (Figure 3.6 B). S1P (100 nM) alone resulted in an increased number of migrated cells compared to PBS vehicle after 4 hrs ( $111.5 \pm 19.5$  % compared to  $36.2 \pm 16.7$  %,  $p < 0.05$ ) (Figure 3.6 C). When S1P was administered in combination with 100 nM siponimod, the number of migrated cells was significantly reduced ( $20.4 \pm 22.8$  % compared to  $111.5 \pm 19.5$  %,  $p < 0.05$ ) (Figure 3.6 C).

We then performed transwell migration assays over 8 hrs to more closely match scratch assay conditions. Here 100 nM siponimod produced a statistically significant increase in the number of migrated cells compared to PBS vehicle ( $34.7 \pm 7.9$  % compared to  $10.8 \pm 3.3$  %,  $p < 0.05$ ) (Figure 3.6 D). As in the 4 hr experiment, 100 nM S1P increased the number of migrated cells compared PBS vehicle ( $106.3 \pm 11.9$  % compared to  $10.8 \pm 3.3$  %,  $p < 0.05$ ), an effect that was antagonised by 100 nM siponimod ( $106.3 \pm 8.0$  % compared to  $16.8 \pm 7.3$  %,  $p < 0.05$ ) (Figure 3.6 D).

Migration over 24 hrs was investigated (Figure 3.6 E) and showed a substantial fall in the overall number of migrating cells compared to experiments conducted at 4 and 8 hrs.

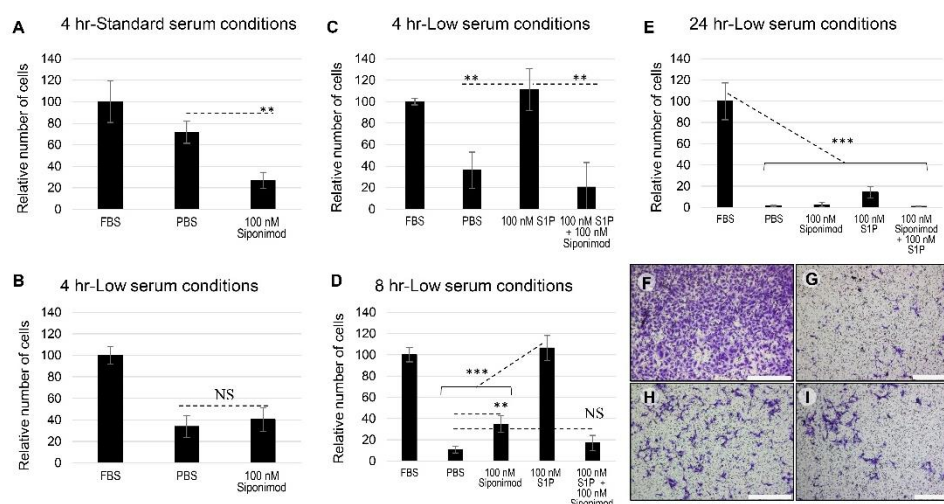


**Figure 3.6** Transwell migration assay for HUVEC. (A) Effect of 100 nM siponimod under standard growth medium conditions (2 % serum) over 4 hrs,  $n=4$  (3 technical replicates) (B) Effect of 100 nM siponimod under reduced serum conditions (1/10<sup>th</sup> standard cell culture supplement containing 0.2 % serum) over 4 hrs,  $n=5$  (3 technical replicates) (C) Effect of 100 nM S1P alone and combined with 100 nM siponimod under reduced serum conditions for 4 hrs,  $n=3$  (3 technical replicates) (D) Effect of 100 nM siponimod under reduced serum conditions over 8 hrs,  $n=5$  (2 technical replicates) (E) migration over 24 hrs,  $n=3$  (2 technical replicates. Data, presented as mean  $\pm$  SD, represents the number of cells counted on the bottom side of a transwell membrane, expressed as a percentage (positive control set to 100%). ‘ $n=$ ’ represents the number of independently repeated experiments. Statistical analysis by one-way ANOVA; ns: No statistical significance. \*\*:  $p < 0.01$ . \*\*\*:  $p < 0.001$ . (F-I) Representative photomicrographs for experimental conditions shown in (D): FBS (F), PBS (G), 100 nM siponimod (H) and 100 nM siponimod + 100 nM S1P (I). Scale bar: 500  $\mu$ m.



### 3.4.5 Cell attachment

To further rule out the possibility that the siponimod-induced reduction of HUVEC migration (Figure 3.6 A) was caused by an effect on cell attachment, we examined the effect of various test agents on this parameter (Figure 3.7). Alone, 100 nM siponimod resulted in no statistically significant change in cell attachment compared to PBS vehicle ( $67.0 \pm 0.6$  % compared to  $58.6 \pm 5.0$  %). S1P (100 nM) resulted in a statistically significant increase in cell attachment compared to PBS vehicle ( $88.4 \pm 6.4$  % compared to  $58.6 \pm 5.0$  %,  $p < 0.05$ ). This effect was antagonised when 100 nM siponimod was added with 100 nM S1P ( $88.4 \pm 6.4$  % attachment for S1P compared to  $51.3 \pm 2.7$  % for siponimod/S1P,  $p < 0.05$ ). Attachment in the presence of siponimod and S1P was not statistically different from attachment in the PBS vehicle condition ( $51.3 \pm 2.7$  % compared to  $58.6 \pm 5.0$  %).

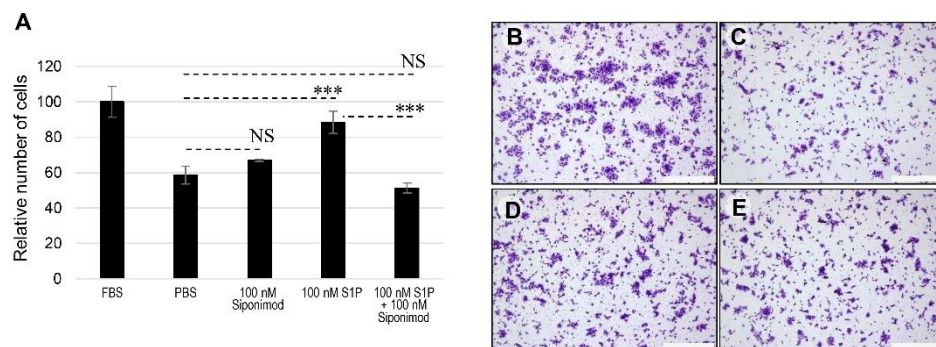


**Figure 3.7** Cell attachment assay for HUVEC. Effect of siponimod, S1P, and siponimod + S1P (all 100 nM) on cell attachment after 4 hrs incubation under reduced serum conditions,  $n=3$  (2 technical replicates. Data, presented as mean  $\pm$  SD, represents the number of cells attached to the well, expressed as a percentage (positive control set to 100%). ‘‘ $n=$ ’’ represents the number of independently repeated experiments. Statistical analysis by one-way ANOVA. NS: No statistical significance.

\*\*\*:  $p < 0.001$ ). (B-E) Representative images for experimental conditions shown in cell attachment assay: FBS (B), PBS (C), 100 nM siponimod (D) and 100 nM siponimod + 100 nM S1P (E). Scale bar: 500  $\mu\text{m}$ .

#### 3.4.6 Cyclic AMP assay

Intracellular cAMP was quantified in an attempt to confirm the identity of the S1P receptor involved and to examine potential signalling mechanisms involved in the response to siponimod. Results showed that after 1 hr, siponimod significantly inhibited forskolin-stimulated increases in intracellular cAMP ( $30.0\% \pm 22.9\%$  for 1  $\mu\text{M}$  forskolin + 100 nM siponimod compared to  $100\% \pm 11.5\%$  for 1  $\mu\text{M}$  forskolin,  $p < 0.05$ ) (Figure 3.8). Siponimod alone did not lead to any significant change in baseline cAMP ( $12.6 \pm 8.6\%$  for 100 nM siponimod compared to  $10.2 \pm 10.1\%$  for untreated control).

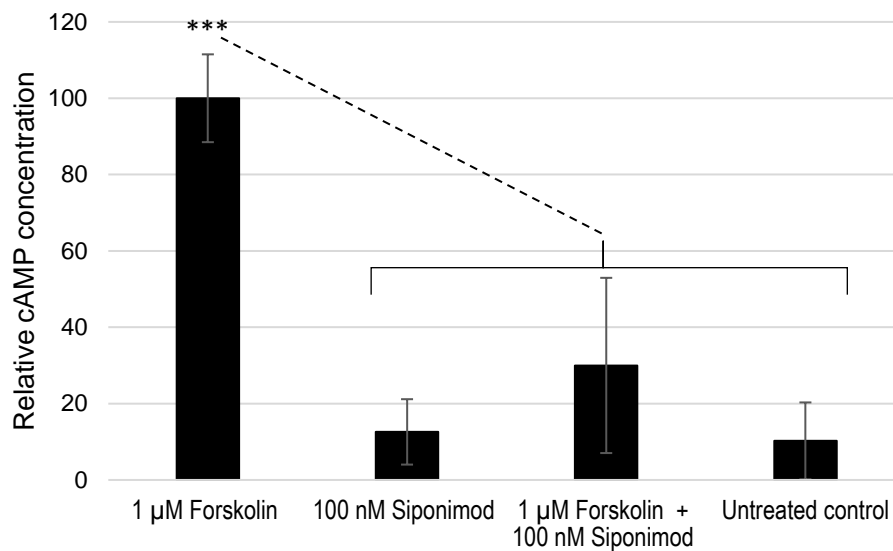


**Figure 3.8** Effects of siponimod on intracellular cAMP in hFOB. The effect of 100 nM siponimod alone and in combination with 1  $\mu\text{M}$  forskolin,  $n=4$  (3 technical replicates). Cells were incubated in the presence of the indicated drugs for 1 hr. Data,

presented as mean  $\pm$  SD, represents the concentration of intracellular cAMP, expressed relative to 1  $\mu$ M forskolin. ‘‘ $n=$ ’’ represents the number of independently repeated experiments. Statistical analysis by one-way ANOVA. \*\*\*:  $p < 0.001$ .

### 3.5 Discussion

The overall aim of these studies was to assess the suitability of siponimod as a potential bone regenerative agent, to be eluted by a localised delivery device to stimulate repair in critical bone defects. With this goal in mind, we investigated the effect of siponimod on osteoblast and endothelial cells proliferation, differentiation and migration. Primarily, it was necessary to show that solutions of siponimod, prepared using DMSO as a co-solvent, did not negatively impact cell viability. Therefore, experiments were conducted showing that the concentration of DMSO used (0.32 %) was non-toxic in both hFOB and HUVEC. This concurs with the literature, that a concentration less than 0.5 % should not impact cell viability (Shah et al., 2019). Shifting focus to the viability assays proper, S1P is well established in promoting endothelial cell proliferation, viability and survival, likely via the S1P<sub>1</sub> or S1P<sub>3</sub> receptors (Lee et al., 1999b, Wang et al., 1999, Lee et al., 2000, Rikitake et al., 2002, Kwon et al., 2001). Therefore, the lack of proliferative effect herein, as well as siponimod’s selectivity for receptors 1 and 5 may indicate that the S1P<sub>3</sub> receptor plays the more important role. Another possibility is that siponimod is behaving like fingolimod, which at concentrations below 250 nM has no effect on HUVEC viability but exhibits toxicity above 250 nM (Schmid et al., 2007). Siponimod also had no effect on osteoblast proliferation, perhaps explained by a possible role for siponimod in osteoblast

differentiation, pushing the cells towards a post-mitotic phase precluding extensive proliferation (Long, 2011).

ALP is commonly used as a marker of osteoblast differentiation. Here we show that exposure to siponimod (but not to fingolimod) increased ALP activity, an effect equivalent to that seen with the same concentration of S1P. Complementary ALP staining showed a corresponding siponimod-induced increase in the number of stained cells. S1P and fingolimod have previously been shown to increase markers of osteoblast differentiation as well as stimulating the osteogenic differentiation pathway of osteoblasts (Lotinun et al., 2013, Brizuela et al., 2014, Sato et al., 2012, Matsuzaki et al., 2013) and mesenchymal stems cells (Pederson et al., 2008, Hashimoto et al., 2016, Hashimoto et al., 2015, Marycz et al., 2016), but it is unclear whether S1P<sub>1</sub>, S1P<sub>3</sub> or both receptor subtypes mediate these effects. Studies of S1P on osteoblast differentiation with receptor antagonists have shown an exclusive role for S1P<sub>3</sub> in osteoblast maturation (Brizuela et al., 2014), whereas S1P<sub>1</sub> receptors were shown to mediate the effect of S1P and fingolimod on osteoblast differentiation, when used in conjunction with BMP-2 (Sato et al., 2012). There is conflicting evidence regarding the effect of fingolimod, which has recently been shown to reduce markers of bone formation (including ALP) in osteoblasts and chondrocytes (El Jamal et al., 2019). This study, which is more in line with our findings with fingolimod, taken together with the effects presented herein for the S1P<sub>1/5</sub> selective modulator siponimod, and the lack of detectable S1P<sub>5</sub> receptor mRNA expression in pre-osteoblasts and osteoblasts (Roelofsen et al., 2008), suggest that S1P<sub>1</sub> receptor stimulation plays a role in the induction of osteoblast differentiation.

S1P is known to stimulate the migration of osteoblast precursors, osteoclasts, and endothelial cells (Pederson et al., 2008, Roelofsen et al., 2008, Lee et al., 1999b, Lee et al., 2000, Ryu et al., 2002, Ohmori et al., 2001). Here we found that siponimod had no effect on the migration of hFOB. This lack of effect suggests that previously reported effects of S1P on osteoblast migration were mediated by a receptor other than S1P<sub>1</sub> or S1P<sub>5</sub>, or that this effect was dependent on the differentiation stage. While both S1P<sub>1</sub> and S1P<sub>2</sub> receptors have been shown to regulate the migration of cells of the osteoblast lineage, they only did so in MC3T3-E1 pre-osteoblasts (Roelofsen et al., 2008). Upon reaching cell confluence, cultures of hFOB express high levels of phenotypic markers associated with osteoblast differentiation (Harris et al., 1995). It is therefore possible that the cells used in our studies were more differentiated than the pre-osteoblasts known to migrate in response to S1P, although the relatively small fraction of cells expressing ALP in our studies, even after one-week exposure to osteogenic medium, would seem to argue against this explanation, leaving open the possibility that species differences may account for the discrepant migration response in hFOB (of human origin) and in murine MC3T3-E1 cells. Our studies did however show a significant effect on endothelial cell migration, doubling HUVEC cell motility in scratch assays. The effect of siponimod was found to be similar to that of S1P (Lee et al., 1999b, Lee et al., 2000, Ryu et al., 2002, Ohmori et al., 2001). However, the extent of this response did not seem to depend on siponimod's concentration (1-100 nM). It is possible that a concentration response relationship may have emerged with further independent experiments. Alternatively, the effect may already have been maximal at 1 nM siponimod, reaching a plateau thereafter. Indeed, siponimod is a potent and efficacious S1P<sub>1</sub> agonist, with subnanomolar EC<sub>50</sub> in [<sup>35</sup>S]GTPγS binding

assays (Lukas et al., 2014, Gergely et al., 2012). However, while siponimod is often tested at 100 nM in published functional cell culture experiments (Gentile et al., 2016, Lupino et al., 2019), we found only two reports showing a concentration response curve in such preparations, in which siponimod mediated a response with an EC<sub>50</sub> of 15.8 nM (Gergely et al., 2012) and only showed a non-significant trend at 1 nM (O'Sullivan et al., 2016).

In transwell assays designed to test whether the effect of siponimod in the scratch assay was due to increased chemokinesis or to chemotaxis, siponimod decreased the migration of endothelial cells under standard growth medium conditions (2% v/v serum). We hypothesized that siponimod may have internalized S1P receptors, blocking the effect of S1P present in the growth medium. Indeed, when transwell assays were conducted under low serum conditions (0.2% v/v serum), siponimod had no significant effect on cell migration, and S1P stimulated endothelial cell migration in a siponimod-sensitive manner and as effectively as serum.

To understand how siponimod interfered with S1P-mediated transwell migration, cell attachment studies performed under similar conditions to the transwell assays showed that siponimod interfered with S1P-mediated increases in cell attachment over 4 hrs. It is therefore possible that decreased cell attachment may have contributed to the reduced transwell migration observed after 4 hrs. Given that the effect of siponimod in scratch assays was determined over 8 hrs, additional 8 hrs transwell assays were conducted and showed that while siponimod still antagonised S1P mediated migration, it also induced a statistically significant increase in cell migration when added on its own, albeit with an effect 3-fold weaker than the effect of S1P. This may be due to

persistent signalling after internalisation of the S1P<sub>1</sub> receptor (Mullershausen et al., 2009), which may only lead to migration after long exposure (8 hrs) to siponimod, but not after 4 hrs, and may also indicate that siponimod behaves similarly to fingolimod, which has been shown to induce cellular motility in scratch assays (Mullershausen et al., 2009) but impede HUVEC migration across a membrane (Ho et al., 2005, LaMontagne et al., 2006, Tanaka et al., 2013). The same experiments were conducted over 24 hrs, however the substantial drop in the number of cells migrating indicated that the extended experimental duration under low serum conditions may have impacted HUVEC viability.

The role of intracellular cAMP in bone remodelling and bone cell differentiation has long been known (Rodan et al., 1975), but the relationship is complex. While some early studies have shown that parathyroid hormone stimulate the *in vitro* differentiation of osteoblasts via intracellular cAMP production (Nakatani et al., 1984), other reports show that the influence of cAMP on ALP expression changes depending on the stage of osteoblast differentiation, and parathyroid hormone may preferentially inhibit the differentiation of more mature osteoblasts (Isogai et al., 1996). Expanding on the complexity of the relation between cAMP and osteoblast differentiation markers, increasing levels of cAMP have been shown to result in decreased ALP but increased osteocalcin expression (Romanello et al., 2001). More recently, increasing cAMP levels have been shown to suppress osteoblast mineralisation (Nishihara et al., 2018). Forskolin-induced cAMP is known to be inhibited by both S1P and fingolimod after 1 hr incubation (Mullershausen et al., 2009), with results similar to those shown for siponimod. This effect is most likely associated with the inhibitory Gi protein coupled to the S1P<sub>1</sub> receptor, which is the

mechanism through which S1P and fingolimod produce the same inhibitory effect. Based on the somewhat contradictory existing literature, it is not straightforward to provide a mechanism linking the adenylate cyclase inhibiting effect of siponimod on our hFOB and the effects of this agent on hFOB cell differentiation. However, we hypothesize that siponimod may maintain a chronically low level of intracellular cAMP through its interaction with S1P<sub>1</sub> receptors, resulting in increased ALP activity, indicative of increased osteoblast differentiation.

Fingolimod, and now siponimod, both antagonise the chemotactic effect of S1P on endothelial cells. Fingolimod has shown proangiogenic effects *in vivo*, ultimately improving recovery of bone defects (Huang et al., 2012, Li et al., 2019b). Therefore, given siponimod's effect on osteoblast differentiation, it may be useful to incorporate siponimod into a localised delivery device to investigate the effects of siponimod *in vivo* towards the same end.

One of the limitations of the current study is that it does not consider osteoclasts, or the coupling between osteoblasts and osteoclasts (Pederson et al., 2008). This communication is known to involve S1P receptors and would likely impact significantly on healing outcomes in any potential *in vivo* studies. Also, our ALP staining studies showed that the total fraction of stained cells was relatively small, being less than 10% of the total number of cells. This may be due to the use of a relatively early time point for analysis (7 days). Conducting the experiment over a longer duration, more consistent with the effect of a drug eluting scaffold (Das et al., 2014a, Das et al., 2014b) may have led to a more meaningful effect on differentiation.



### 3.6 Conclusion

The aim of this work was to investigate the potential of siponimod in a bone regenerative context, ultimately towards its use in conditions of critical bone defects, as part of a localised delivery device, but improving on the specificity of the eluted drug (Das et al., 2014a, Das et al., 2014b, Huang et al., 2012, Li et al., 2019b). These studies add to the relatively small amount of literature on the functional effects of siponimod in cell culture models. In the context of bone repair, the differentiation effect of siponimod on osteoblasts, taken together with its effects on endothelial cells suggest that this selective S1P<sub>1</sub> modulator may be useful, particularly in conditions of critical defects that remain a significant therapeutic challenge. However, more robust *in vivo* experiments would be the next step before making any determinative conclusions.

## Chapter 4

### Development of electrospun polymer scaffolds for the localized and controlled delivery of siponimod for the management of critical bone defects

**Ziad Sartawi<sup>1</sup>, Christian Waeber<sup>1,2</sup>, Ernestina Schipani<sup>3</sup>, Katie B. Ryan<sup>1</sup>**

*<sup>1</sup>School of Pharmacy, University College Cork, Cork, Ireland*

*<sup>2</sup>Department of Pharmacology and Therapeutics, University College Cork, Cork,  
Ireland*

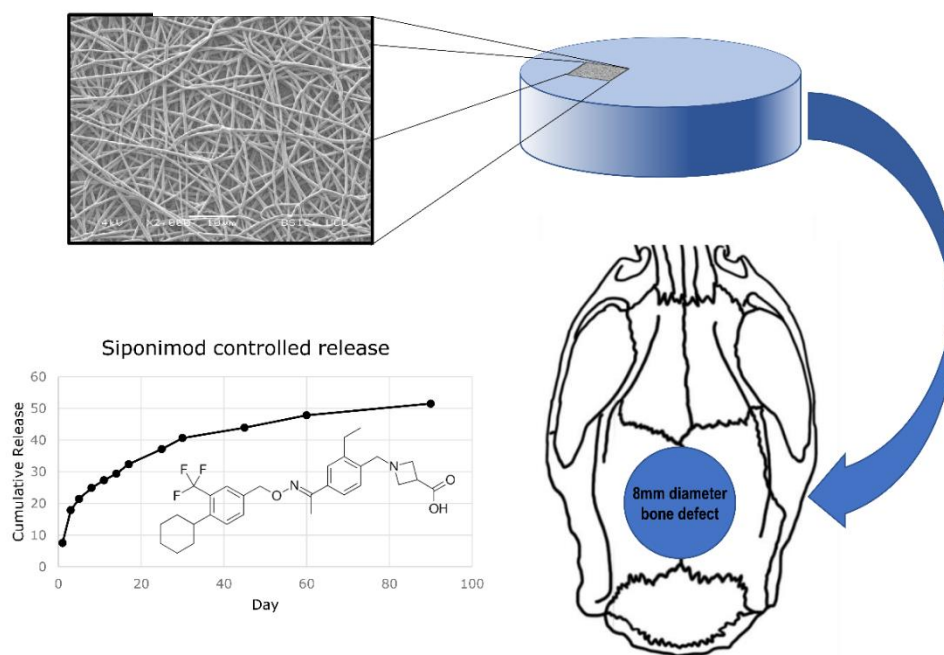
*<sup>3</sup>Department of Medicine and Orthopaedic Surgery, University of Michigan, Ann  
Arbor, MI, USA*

Revised from publication

International Journal of Pharmaceutics, October 2020

Volume 590, 30 November 2020, 119956 DOI: 10.1016/j.ijpharm.2020.119956

## Graphical Abstract



## 4.1 Abstract

Sphingosine 1-phosphate (S1P) receptor modulators can influence bone regeneration owing to their positive impact on osteoblast differentiation, and neovascularisation. While previous studies have utilised non-specific S1P and fingolimod, this study aims to design and characterise a controlled release vehicle to deliver the specific S1P<sub>1/5</sub> receptor modulator siponimod and test its effectiveness in rat critical cranial defects.

Electrospun scaffolds of PLGA were loaded with siponimod at drug:polymer mass ratios of 0.5:100 to 2:100. Where indicated, collagen was co-spun at collagen:polymer mass ratio of 2:100. Thereafter, scaffolds underwent *in vitro* physicochemical characterisation and *in vivo* assessment using a rat cranial defect model. Drug-loaded scaffolds showed controlled release of siponimod, biocompatibility with endothelial and osteoblast growth *in vitro*, and furthermore, showed that released siponimod stimulated osteoblast differentiation and endothelial cell migration. The *in vivo* cranial defect repair study showed regeneration was occurring in the defect, although there was no significant difference in the extent of mineralisation between scaffold experimental groups. To our knowledge, this is the first study investigating siponimod bone regeneration. *In vitro* studies confirm a positive impact on key cells involved in bone regeneration, however, the scaffolds did not result in significant repair of critical cranial defects.

## 4.2 Introduction

Autograft and allograft procedures are gold standard treatments for non-union defects, however they present a number of challenges including limited supply, donor site morbidity and the potential for disease transmission (Schlickewei et al., 2019). This has made the search for alternative replacement materials an active field of research (Laurencin et al., 2006). Ideally, a replacement material should not only provide a structural substrate for new bone cells to grow on, its degradation should be contemporaneous with new bone growth and it should provide appropriate cues to stimulate bone formation (Ahern et al., 2013).

Developing replacement materials that more closely mimic the natural bone environment and are thus more conducive to bone growth has focused on the addition of agents (chemical or biological) that induce or support bone regeneration. Potent, osteoinductive signalling molecules including the growth factor BMP-2 have attracted much attention in stimulating bone regeneration (Bal et al., 2020). Indeed BMP-2 has been used clinically to treat bone defects, although the use of supraphysiological doses and the rapid release from collagen scaffolds has resulted in abnormal bone formation (Krishnan et al., 2017). Strategies to address this problem have focused on better delivery modalities to enable control over the temporal presentation of BMP-2, thereby enabling lower doses to be administered (Kolambkar et al., 2011). More recently, alternative signalling molecules such as S1P, have been the object of increasing attention in the context of bone regeneration (Sartawi et al., 2017, Meshcheryakova et al., 2017). S1P is a lipid mediator that modulates calcium signalling, cell growth, differentiation, survival, motility and cytoskeleton

organization (Spiegel and Milstien, 2000), and acts via five known G Protein-Coupled Receptors (S1P<sub>1-5</sub>), which are widely expressed throughout the body (Hla, 2004).

In the context of bone regeneration, S1P receptor modulation has been shown to improve outcomes in murine studies of bone defects, ostensibly by supporting vascularization and chemotaxis of specific cellular contributors to bone repair (Huang et al., 2012, Das et al., 2013, Das et al., 2014b, Wang et al., 2016a, Das et al., 2015, Das et al., 2014a). However, S1P and the analogue fingolimod act at several of the known S1P receptor subtypes, and much medicinal chemistry effort has been dedicated to developing more selective modulators, in particular for the S1P<sub>1</sub> receptor (Marciniak et al., 2018). Although several S1P receptor subtypes are involved in bone physiology, there is evidence that S1P<sub>1</sub> receptor modulation, and the newly developed S1P<sub>1/5</sub> selective agent siponimod, may be advantageous in the context of bone repair (Sartawi et al., 2017). Siponimod (Mayzent®), was developed for secondary progressive multiple sclerosis (Behrangi et al., 2019), in response to side effects associated with the less selective agent fingolimod (DiMarco et al., 2014, Cugati et al., 2014, Gergely et al., 2012). Our own *in vitro* data has shown that siponimod increases endothelial cell chemokinesis and enhances pre-osteoblast differentiation (Sartawi et al., 2020a); these effects appear to be mediated through siponimod's interaction with the S1P<sub>1</sub> receptor.

Previous research investigating S1P mediators has shown the importance of the method of administration in achieving bone regeneration. Systemic administration of fingolimod does not improve fracture healing (Heilmann et al., 2013), whereas localised delivery of S1P and the S1P receptor modulator fingolimod using PLGA-

based scaffold methodologies (Sefcik et al., 2008, Das et al., 2014b, Petrie Aronin et al., 2010a) resulted in significant increases in bone volumes in a cranial defect model (Das et al., 2014b). Scaffolds are a fundamental pillar in tissue engineering, and the materials from which they are composed impact on the scaffold's degradation, controlled release of drug cargoes and interaction with the host tissue (Rezwan et al., 2006, Roseti et al., 2017). Biomaterials commonly investigated for bone tissue engineering include natural and synthetic polymers, inorganic ceramics including calcium phosphates and bioactive glass, as well as ceramic-polymer composites (Iaquinta et al., 2019, Henkel et al., 2013). From a materials perspective, polymer-based approaches are interesting due to their low cost and biodegradability over clinically relevant times frames. Synthetic polymers including PLGA are advantageous due to their solubility in common solvents, and their well-documented degradation properties (Gentile et al., 2014) and have been used to prepare controlled release protein therapies for bone regeneration (Fu et al., 2008, Lee et al., 2013) or implantable scaffolds pre-seeded with stem cells to stimulate regeneration (Zong et al., 2010). However, many synthetic materials are hydrophobic and do not readily promote cellular attachment. Efforts to overcome these limitations have included fabrication of scaffolds with components that more closely resemble the extracellular environment (structural proteins, glycosaminoglycans) and which act to enhance cell-matrix interactions (Alsberg et al., 2002, Silva et al., 2020). The organic component of bone is primarily composed of type I collagen and consequently this biomaterial has been used in bone regeneration applications (Cen et al., 2008). The utilisation of relatively small quantities of collagen can result in significant changes to osteoblast attachment, penetration (within a synthetic scaffold), and mineralisation (Chiu et al.,

2007). Furthermore, electrospun fibres of synthetic materials developed with the addition of collagen have been shown to stimulate gene expression associated with osteogenic differentiation of stem cells (Balaji Raghavendran et al., 2014).

This study focused on an implantable PLGA-based scaffold for the controlled delivery of siponimod to enhance bone regeneration. We investigated the design of a scaffold system using electrospinning technology to achieve temporal control over drug release, and whether the incorporation of collagen would help to address limitations associated with hydrophobic polymer materials, and thereby enhance cellular interactions at the scaffold interface. Scaffolds were physicochemically characterised to understand important changes to morphological, chemical, and physical attributes caused by the formulation process, and the addition of siponimod and collagen. *In vitro* studies were carried out using osteoblast and endothelial cells to determine the potential of the scaffold composites to influence key cell processes implicated in bone regeneration, in particular cell proliferation, differentiation and migration. Finally, we investigated the ability of selected siponimod, fingolimod, and drug-free scaffolds to regenerate bone in a rat model of a critical-sized cranial defect.



### 4.3 Materials and methods

#### 4.3.1 Materials

Electrospinning materials included: poly (D, L-lactide-co-glycolide) Resomer<sup>®</sup> RG 858 S (Evonik Industries, Germany), collagen type I (Elastin Products Company, USA), 1,1,1,3,3,3-Hexafluoro-isopropanol (Fluorochem, UK), chloroform and N, N-dimethylformamide (Sigma Aldrich, USA). Siponimod hemifumarate was kindly gifted from Novartis (Basel, Switzerland).

Dimethyl sulfoxide (DMSO), L-ascorbic acid,  $\beta$ -glycerophosphate, Dulbecco's phosphate buffer saline (PBS), foetal bovine serum (FBS), L-glutamine solution, Dulbecco's Modified Eagle's Medium/Nutrient Mixture F-12 Ham (DMEM/F12), Thiazolyl Blue Tetrazolium Bromide (MTT), neutral buffered formalin (NBF), Fast Blue BB, Naphthol AS-MX phosphate, magnesium chloride ( $\text{MgCl}_2$ ), sodium chloride ( $\text{NaCl}$ ), Tween<sup>®</sup> 20, and tris(hydroxymethyl)aminomethane (Tris-HCl) were acquired from Sigma Aldrich. Pierce<sup>™</sup> pNPP Substrate Kit was acquired from Thermo Fisher Scientific, USA. Human umbilical vein endothelial cells (HUVEC) and their growth medium (ECGM) with associated supplements were acquired from PromoCell, Germany. The human foetal osteoblast cell line hFOB 1.19 was acquired from ATCC (ATCC<sup>®</sup> CRL-11372<sup>™</sup>). Cell culture plasticware was acquired from Sarstedt Ltd, Germany. Buprenorphine, bupivacaine, and isoflurane were purchased from Abbeyville Veterinary Hospital, Cork, Ireland.

#### 4.3.2 Electrospinning procedure

Solutions of PLGA (85:15) were formulated as 8% w/w preparations in a mixture of chloroform (CLF) and dimethylformamide (DMF) at a 9:1 ratio, whilst

hexafluoroisopropanol (HFIP) was used as the solvent in the case of collagen-containing samples. Reagents were dissolved in glass vials overnight at 4 °C. Prior to starting the electrospinning process, solutions were equilibrated to room temperature to avoid viscosity changes. For siponimod loaded preparations, mass ratios of siponimod:PLGA 0.5:100, 1:100 and 2:100 (henceforth termed Si n:100, where 'n' indicates the ratio of siponimod in samples) were prepared in vials as before. The fingolimod loaded sample used exclusively *in vivo* was prepared in the same way, as fingolimod:PLGA 0.5:100 (henceforth termed Fi 0.5:100). Collagen was incorporated into samples of Si 0.5:100 at a mass ratio of 2:100 of the polymer resulting in samples termed SiCol 2:100. The electrospinning set-up consisted of a Spraybase<sup>®</sup> (Spraybase, Ireland) electrospray instrument kit (CAT000002), and an AL-2000 syringe pump (World Precision Instruments, USA). Sample solutions were decanted into a 10 mL glass syringe. The solutions were then primed in 1 mm diameter tubing connecting the syringe to the emitter nozzle (0.9 mm diameter). The syringe pump was set at a flow rate of 0.75 mL/h. A stainless-steel collection dish was covered in commercial aluminium foil and placed at a working distance of 15 cm from the emitter nozzle. A voltage of 16 kV was then applied, with samples processed continuously until a set volume of sample solution was dispensed. Collected samples were stored in the fume hood overnight to allow evaporation of any remaining solvent. Samples were then used immediately or stored at -20 °C.

#### 4.3.3 Scanning electron microscopy

Images were acquired using a JEOL JSM-5510 Scanning Electron Microscope (SEM). Samples were mounted on stubs with double sided carbon tape and sputter-coated with a 10 nm thick layer of gold-palladium (80:20). Standard working distance was 8 mm,

spot size 20-25, 3-5 kV accelerating voltage, and magnification 4000x were used. Images were analysed using the Olympus Stream software (Mason Technology Ltd, Ireland) to investigate fibre morphology and acquire fibre diameter data. 2-4 images were captured per sample with 25 individual fibre measurements per image.

#### 4.3.4 HPLC methodology

Liquid chromatography was used to detect and quantify the concentration of siponimod in the upcoming sections, the high pressure liquid chromatography (HPLC) method is detailed here. The protocol used an Agilent Technologies 1120 Compact LC instrument ( $\lambda_{\text{max}} = 278 \text{ nm}$ ), the stationary phase consisted of a Zorbax Eclipse Plus C18 column (4.6 x 150 mm, 5  $\mu\text{m}$ ). The mobile phase was composed of acetonitrile and water at a ratio of 65:35, supplemented with formic acid 0.5% v/v (pH  $\approx 3.0$ ), and operating conditions included a flow rate of  $1.2 \text{ ml min}^{-1}$  and an injection volume of 10  $\mu\text{l}$ . UV spectrometry of siponimod solutions was used to determine peak absorbance at 278 nm.

#### 4.3.5 Siponimod stability

The stability of solutions of siponimod was monitored over 12 weeks at 4 °C and at 37 °C. Solutions of siponimod were prepared in PBS (pH 7.4) and placed either in a refrigerator at 4 °C or a water bath set to 37 °C. At defined time-points over the 12-week experimental period, 50  $\mu\text{l}$  samples were taken and stored at -20 °C until HPLC analysis. The concentration of siponimod detected in solution over time was used as a measure of its stability in solution.

The stability of siponimod in the polymer formulations was ascertained at 4 and 12 weeks under several temperature storage conditions: -20 °C (freezer), 4 °C

(refrigerator), 20 °C (room temperature) and 37 °C (laboratory oven). The concentration of siponimod remaining in a scaffold sample was determined by disintegrating samples of known mass in HPLC mobile phase to release total siponimod content. The calculated drug content was divided by the drug loading values of freshly prepared samples, giving a percentage of the initial siponimod concentration.

#### 4.3.6 Loading efficiency and drug release

For *in vitro* siponimod release, electrospun samples of known initial mass (1.5-2.5 mg) were placed in 1.5 ml plastic sample tubes and incubated in 1 ml PBS at 37 °C under gentle shaking (40 revolutions per minute (RPM)) in a GLS aqua 12 plus water bath (Grant Instruments, UK), the volume was sufficient to achieve sink conditions. The samples investigated included three samples of increasing siponimod concentration (Si 0.5:100, Si 1:100, and Si 2:100, all of which were prepared using CLF/DMF). In addition, two samples prepared in HFIP were investigated in a similar manner (Si 0.5:100, and SiCol 0.5:100) in order to explore both the impact of collagen addition between Si 0.5:100 (HFIP) and SiCol 0.5:100, and the impact of using different solvents by comparing Si 0.5:100 (CLF/DMF) and Si 0.5:100 (HFIP). The complete release medium was collected at defined time-points over a 12-week period and stored at -20 °C prior to analysis. An equal volume of fresh PBS medium was replaced in the sample vial. Samples were vacuum-dried overnight, and the residue re-dissolved in mobile phase prior to analysing the unfiltered samples by HPLC analysis.

#### 4.3.7 Differential scanning calorimetry (DSC)

In order to investigate any changes in the thermal properties of the polymeric constituent of the scaffolds due to processing, residual solvent, or drug loading, electrospun samples underwent thermal analysis using a TA Q1000 differential scanning calorimeter (TA instruments, USA). All samples were run using modulated-DSC (MDSC) in aluminium pans (DSC Consumables, USA), using the following settings: modulation temperature amplitude  $\pm 1.0$  °C, modulation 60 seconds, ramp rate 3 °C/min and a temperature range of 0-150 °C.

#### 4.3.8 Fourier Transform Infra-red (FTIR) spectroscopy

To analyse the molecular spectra of electrospun scaffolds containing siponimod and collagen, solid samples and starting materials were subject to FTIR analysis using a PerkinElmer Spectrum Two spectrometer. Measurements were performed at 4 scans per spectrum between 4500  $\text{cm}^{-1}$ -400  $\text{cm}^{-1}$  at a resolution of 4  $\text{cm}^{-1}$ .

#### 4.3.9 Contact angle

Contact angle goniometry was conducted using an optical tensiometer (Biolin Scientific, Sweden). Samples of electrospun PLGA, Si 0.5:100, and SiCol 2:100 (8 mm diameter) were immobilised on a glass slide using double-sided carbon tape. MilliQ water (7-10  $\mu\text{l}$ ) was dropped onto the sample surfaces and images were acquired at 7.6 frames per second for 30 seconds. Using the associated Attension software (Biolin Scientific, Sweden), the average contact angle was acquired across  $\approx$  200 images per sample.

#### 4.3.10 Tensile strength

Electrospun samples (8 mm diameter and 0.5 mm thickness) were cut out with a commercial paper punch and loaded into miniature tensile grips. Prior to testing, the device was calibrated with a 100 g standard mass. Tensile strength of fibrous samples was acquired by pulling samples apart at a rate of 0.5 mm/sec until failure. The ultimate tensile strength was recorded for each sample ( $n=3$ ) using the Exponent software (Stable Micro Systems, UK).

#### 4.3.11 Biological characterisation and *in vitro* functional experiments

##### 4.3.11.1 Cell culture

hFOB were maintained in DMEM/F12 supplemented with FBS (10%), L-glutamine (1%), and penicillin-streptomycin (1%) at 34 °C and 5 % carbon dioxide (CO<sub>2</sub>). HUVEC were maintained in ECGM as per supplier's recommendations at 37 °C and 5 % CO<sub>2</sub>. All experiments were conducted within 10 passages for HUVEC and within 20 passages for hFOB.

##### 4.3.11.2 Evaluation of metabolic activity

###### 4.3.11.2.1 Indirect assessment

The metabolic activity of cells indirectly exposed to electrospun samples was evaluated in order to determine the impact of eluted compounds on cells in close proximity to the scaffold. PLGA, Si 0.5:100, and SiCol 0.5:100 samples were cut out using a commercial paper punch (8 mm diameter) and sterilised by UV irradiation for 2 hrs. Thereafter, samples were added to 24 well plates pre-seeded with  $5 \times 10^4$  cells/well of hFOB or HUVEC. The samples were incubated with the cells for 5 days, with culture medium changed every other day. To determine metabolic activity after

5 days, the scaffolds were removed and 60  $\mu$ l thiazolyl blue tetrazolium bromide (5 mg/ml solution) was added directly to 600  $\mu$ l of cell culture medium for 2 hrs. Resultant formazan crystals were solubilized with 600  $\mu$ l DMSO. 100  $\mu$ l of each well was transferred to a 96-well plate to measure absorbance at 570 nm using a Wallac Victor2 plate reader (Perkin Elmer, USA).

#### 4.3.11.2.2 Direct assessment

The metabolic activity of cells directly seeded on electrospun samples was evaluated in order to determine the impact of physical, chemical and mechanical properties of the composite scaffold on hFOB cell behaviour. As above, 8 mm diameter samples of PLGA, Si 0.5:100, and SiCol 0.5:100 were cut out and UV-sterilised. The scaffolds were fitted to the base of 96-well plates replacing the original growth surface and hFOB ( $5 \times 10^4$  cells in 70  $\mu$ l) were seeded directly onto the polymer surface for 10 mins before topping up with an additional 130  $\mu$ l of medium. Incubation continued for 5 days, with culture medium changed every other day. On days 1, 3, and 5 media was replaced with a combination of 100  $\mu$ l of medium and 10  $\mu$ l of resazurin (560  $\mu$ M stock solution). After 3.5 h, 90  $\mu$ l from each well was transferred to a new plate for fluorescent plate reading at excitation 488 nm/emission 595 nm.

#### 4.3.11.3 Haematoxylin and Eosin staining

Samples used in the resazurin assay described above were subsequently fixed in neutral buffered formalin, embedded in Shandon™ M-1 Embedding Matrix (Thermo Fisher Scientific, USA) and frozen. Sections (20  $\mu$ m) were cut using a Leica CM1900 cryostat microtome (Leica Biosystems, Germany). In brief, staining was performed using Mayer's haematoxylin for 8 mins followed by 1 min in Eosin Y. Using an

Olympus BX51 microscope and associated Olympus Stream software, images of stained sections were acquired using an extended depth of focus image and a 10x objective.

#### 4.3.11.4 Cell differentiation

Electrospun samples (8 mm diameter) of PLGA, Si 0.5:100, Si 2:100, and SiCol 0.5:100 were added to wells pre-seeded with hFOB at densities of  $5 \times 10^4$  cells/well. Cells were incubated with the electrospun scaffolds for 7 days and culture medium was changed every other day. Differentiation of hFOB incubated in osteogenic medium containing 50  $\mu\text{g/ml}$  ascorbic acid and 7.5 mM  $\beta$ -Glycerophosphate was used as a positive control (Bozycki et al., 2018). After 7 days, electrospun samples were removed and cells were detached using 100  $\mu\text{l}$  of 0.25 % trypsin and resuspended with an additional 200  $\mu\text{l}$  of cell culture medium. Cell numbers for each well were then determined using a haemocytometer. To determine alkaline phosphatase (ALP) activity, a solution of para-nitrophenylphosphate (pNPP) was added to the remaining cells, resultant paranitrophenyl formation was monitored at 405 nm with a Wallac Victor 2 plate reader (Perkin Elmer, USA). Absorbance values were then normalised against cell counts for each individual well.

Osteogenic differentiation of hFOB incubated with electrospun scaffolds was also confirmed by staining for ALP. In brief,  $5 \times 10^4$  hFOB were seeded in 24-well plates and incubated with electrospun scaffolds or osteogenic medium for 7 days. Thereafter, cells were equilibrated in 100 mM Tris-HCL pH 8.2, 100 mM NaCl, 0.1 % Tween<sup>®</sup> 20, and 50 mM  $\text{MgCl}_2$ , followed by incubation with a solution containing Fast blue dye and Naphthol phosphate for 60 mins. Using a BX51 microscope, three images



were acquired per well (with a 4x objective). Using ImageJ analysis software (Schneider et al., 2012), both the number of stained and unstained cells were manually counted, and the number of stained cells expressed as a percentage of the total cell number.

#### 4.3.11.5 HUVEC Cell migration

Siponimod has been found to influence the migration of endothelial cells (HUVEC) (Sartawi et al., 2020a). Therefore, in order to demonstrate the functionality of siponimod released from scaffolds, electrospun PLGA, Si 0.5:100, Si 2:100, and SiCol 0.5:100 were incubated in cell culture medium for 16 hrs to precondition medium. Thereafter, 8  $\mu$ m pore polyethylene terephthalate transwell migration inserts (Sarstedt, Germany) were set-up and seeded with  $5 \times 10^4$  HUVEC. Following 8 hrs incubation, cells were fixed with 10 % neutral buffered formalin for 15 mins, then stained with 0.5 % crystal violet for 30 mins. A cotton swab was used to remove non-migrated cells from the top side of the insert membrane. The bottom side of the membrane was visualised using a BX51 microscope and images (5 per insert) acquired using a 10x objective and associated Stream software. The images were used to manually count the number of cells on the bottom of the membrane, which were recognised as migrated cells.

#### 4.3.12 *In vivo* critical cranial defect

##### 4.3.12.1 Surgical procedure and scaffold implantation

The critical cranial defect was generated based on a previously published method (Spicer et al., 2012), and the procedure was approved by the Animal Experimentation Ethics Committee at University College Cork, and by the Health Products Regulatory

Authority of the Republic of Ireland (AE19130/P093). The investigators were first blinded to the nature of the experimental groups, and the different groups were then randomly allocated to the animals using Microsoft Excel random number generator. Blinding was maintained throughout the 12-week duration of the study and euthanasia, and subsequently during data collection and analysis.

In brief, 11-week old male Sprague-Dawley rats ( $n=30$ ) (Envigo RMS Ltd, UK) were anaesthetised by isoflurane gas inhalation and given subcutaneous injections of buprenorphine (0.05mg/kg) for perioperative pain, and bupivacaine 0.25 % w/v (0.1 ml) for local anaesthesia. A 1.5 cm incision was made exposing the coronal, sagittal, and lambdoidal sutures. The calvarium was scored using a 78001 microdrill (RWD Life Science, China) with an 8 mm diameter trephine. The microdrill headpiece was then replaced with a 1 mm burr attachment to thin the bone until a full thickness cut through the calvarium was achieved. Thereafter, the following electrospun samples of with masses of approximately 1.5 mg) were inserted into the defect and manually shaped and moulded to defect edges ( $n=6$  per condition): PLGA, Si 0.5:100, Si 2:100, SiCol 0.5:100, and Fi 0.5:100, with the fingolimod loaded sample acting as a positive control (Huang et al., 2012). All scaffolds had been sterilised by UV irradiation for 2 hrs and were only exposed to the surgical suite environment immediately prior to insertion.

The incision was then sutured and cleaned with iodine and saline. Thereafter, animals were moved to heating pads and monitored until alert. Animals were assessed daily for 7 days post-surgery using a scoresheet tracking animal weight, appearance,

behaviour, and wound healing. Animals whose score exceeded a predetermined acceptable level were euthanised, as were any animals exhibiting haemorrhage.

#### 4.3.12.2 Administering Fluorescent labels, euthanasia, and histology

One and three weeks after surgery, rats were given subcutaneous injections of alizarin 25 mg/kg and calcein green 25 mg/kg (both were dissolved in 1.26 % w/v sodium bicarbonate solution), respectively. It was anticipated that fluorescent micrographs of alizarin and calcein would be used to determine differences in the rate of calcium deposition in the defect area by measuring the area between the fluorescent mineralisation fronts at weeks 1 and 3. However, we failed to observe alizarin-stained tissue in experimental tissue. Alizarin staining is therefore no longer mentioned in this paper.

Twelve weeks after surgery, rats were euthanised by CO<sub>2</sub> asphyxiation and confirmed by cervical dislocation. The cranium was then extracted and immediately added to 25 mL neutral buffered formalin for 48 hrs fixation, followed by an additional 72 hrs in 70 % ethanol. Upon embedding in methyl methacrylate, samples were sectioned transversely to produce 5 µm thickness undecalcified bone samples. These were then stained using von Kossa (VK) and Masson-Goldner (MG) trichrome, to determine the extent of mineralisation, osteoid formation and entrapped osteocytes. Briefly, VK samples were submerged in 1 % silver nitrate for 45 mins under a 100-watt tungsten-halogen bulb at a distance of 20 cm, followed by 5 mins in 3 % sodium thiosulfate, and finally counterstained for 5 mins with van Gieson stain. Black/brown stained areas were representative of mineralised bone tissue. For MG trichrome, samples were stained for 25 mins in Wiegert's haematoxylin followed by 17 mins in a Ponceau-

Fuchsin solution, and 7 mins in phosphotungstic acid. The resulting green stained area represented mineralised tissue, while areas stained red were representative of osteoid. Fluorescent micrographs of unstained sections were used to detect calcein fluorescence, this was acquired with the application of a green fluorescent protein (GFP) optical filter.

Light microscope images were acquired using a BX51 microscope, the images were analysed using MCID Core 7.1 software (Interfocus Imaging, UK). The extent of mineralisation within the defect area was determined using the VK and MG stained sections by measuring the area of the black stained tissue for VK, and the area of green stained tissue for MG. Furthermore, MG stained sections were used to manually enumerate osteocytes within the defect area using 4 images per section. The images were acquired at a higher magnification (20x objective), and within each image an area of approximately 0.31 mm<sup>2</sup> was used to manually enumerate cells. As mentioned earlier it was anticipated that fluorescent labels would be used to determine differences in the rate of calcium deposition in the defect area by measuring the area between the fluorescent mineralisation fronts at 1 and 3 weeks. With the absence of alizarin, calcein labelling alone was used by measuring the area between the edge of the initial defect and the 3-week fluorescent calcein signal, and from that point to the 12-week position of the mineralisation front.

#### 4.3.13 Statistical analysis

Results are expressed as mean  $\pm$  standard deviation (SD), unless otherwise stated. Statistical analysis was performed using one-way analysis of variance (ANOVA) followed by Bonferroni post-test for multiple comparisons. When non-parametric

analysis was required, Kruskal-Wallis followed by Dunn's multiple comparisons tests were used to determine statistical significance. In all cases differences were considered significant at  $p < 0.05$ .

## **4.4 Results**

### **4.4.1 Properties of electrospun fibres**

Electrospinning was used to produce randomly aligned, fibrous constructs containing siponimod and collagen, as shown in Figure 4.1. The diameter of individual fibres of PLGA, Si 0.5:100, and SiCol 0.5:100 was measured using acquired SEM images. There was no statistically significant difference in fibre diameter distribution between unloaded PLGA samples (0.93  $\mu\text{m}$ ; 0.47  $\mu\text{m}$ ) and siponimod loaded Si 0.5:100 (0.92  $\mu\text{m}$ ; 0.53  $\mu\text{m}$ ), (diameters given as median diameter; interquartile range). However, the diameter of SiCol 0.5:100 fibres (0.56  $\mu\text{m}$ ; 0.32  $\mu\text{m}$ ) was significantly lower than both PLGA and Si 0.5:100 samples ( $p < 0.05$ ) and showed a narrower size distribution.

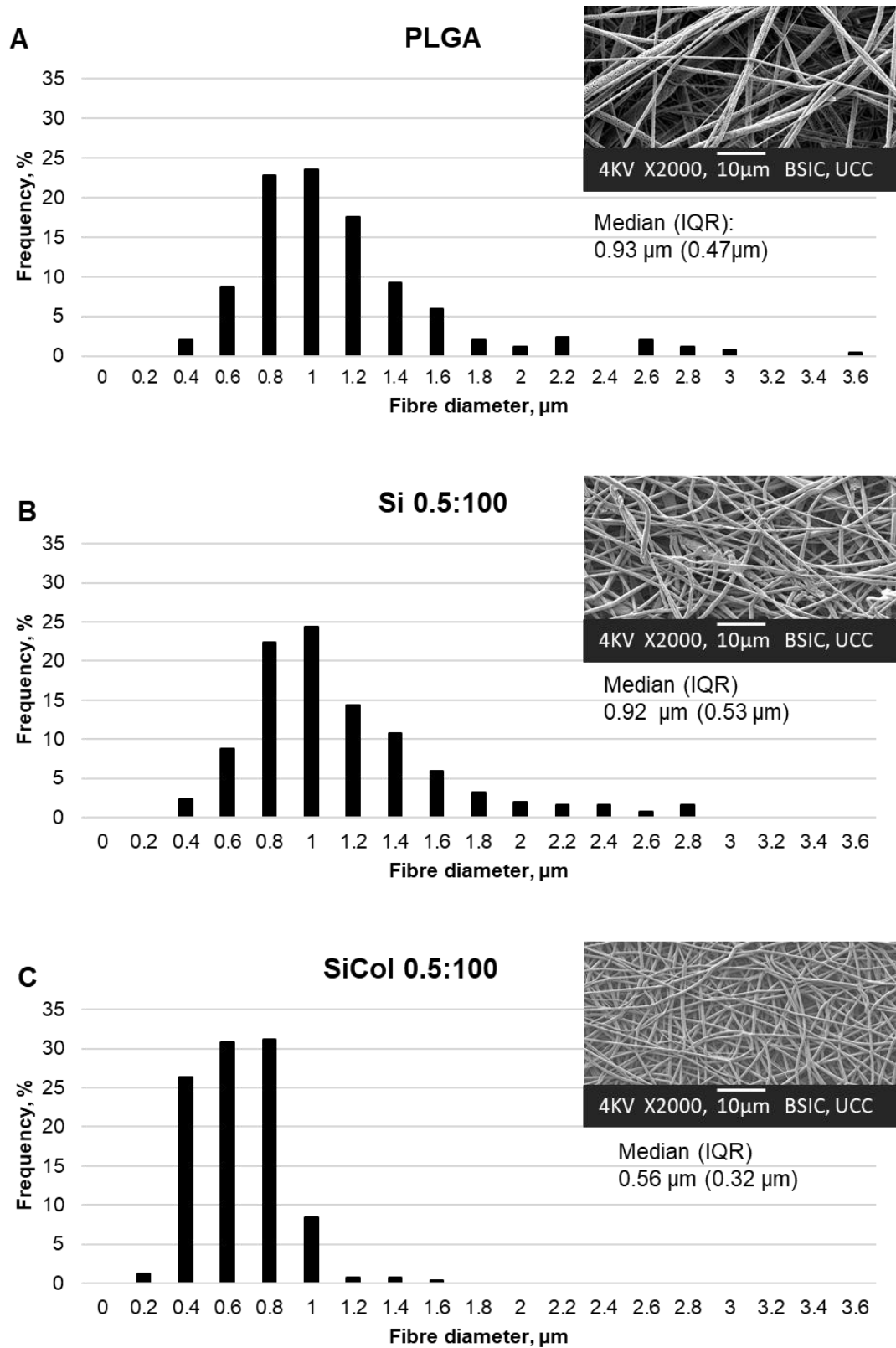


**Figure 4.1** Fibre size distribution (A) PLGA (B) Si 0.5:100(C) SiCol 0.5:100. Image magnification 2000x (10  $\mu\text{m}$  scale bar). Histograms represent the frequency distribution of fibre diameters as determined by manual measurements taken from SEM images (3 batches of electrospun material, 2-4 images per batch, 25 individual fibre measurements per image). Inset values represent the median and interquartile range. Statistical analysis of (A, B, and C) involved Kruskal-Wallis followed by Dunn's multiple comparisons tests to determine statistical significance.

#### 4.4.2 Siponimod stability

The concentration of siponimod solutions was monitored at defined intervals over a 90 day period. HPLC analysis showed that at physiological temperatures (37 °C), siponimod solution concentration was  $35.9 \pm 1.6$  % of initial concentration after 90 days (Figure 4.2A). At 4 °C, the siponimod solution concentration was  $81.0 \pm 2.0$  % of initial concentration after 90 days.

Loading efficiency was ascertained by HPLC (Table 4.1), with samples exhibiting drug loading efficiencies ranging from 80-94 % of theoretically ideal loading. In most cases there was no differences between the different scaffolds, however there was a statistically significant difference in loading efficiency between Si 0.5:100 (HFIP) ( $80.7 \pm 1.8$  %) and Si 2:100 ( $91.7 \pm 2.2$  %,  $p < 0.05$ ), as well as between Si 0.5:100 (HFIP) and SiCol 0.5:100 ( $93.9 \pm 6.1$  %,  $p < 0.01$ ). Freshly prepared Si 0.5:100 samples showed an average loading efficiency of  $88.0 \pm 4.7$  % and were used as a baseline to compare the solid-state stability of incorporated siponimod after storage for 4 and 12 weeks under varied temperature conditions.

**Table 4.1** Loading efficiency of electrospun samples as determined by HPLC. Data represents the concentration of solutions prepared by dissolving scaffolds of known mass and dividing the value by the theoretical concentration expected given the known mass,  $n=3$ .

Sample	Loading efficiency (%)	Standard deviation
Si 0.5:100 (HFIP)	80.7	1.8
Si 0.5:100 (CLF/DMF)	88.0	4.7
Si 1:100	89.4	0.5
Si 2:100	91.7	2.2
SiCol 0.5:100	93.9	6.1
SiCol 2:100	84.2	1.2

Change in siponimod concentration in the stored samples relative to the freshly prepared sample are shown in Figure 4.2B. After 4 weeks, drug concentration in polymer samples was  $93.2 \pm 4.7$  % at  $-20$  °C,  $91.4 \pm 4.9$  % at  $4$  °C,  $87.0 \pm 4.8$  % at  $20$  °C, and  $83.6 \pm 4.5$  % at  $37$  °C, none of which were significantly different from each other. After 12 weeks the drug concentrations in the samples were  $93.6 \pm 3.0$  % at  $-20$  °C,  $91.6 \pm 9.5$  % at  $4$  °C,  $85.5 \pm 0.2$  % at  $20$  °C, and  $73.2 \pm 4.6$  % at  $37$  °C, with the



drug concentration at 37 °C being statistically significantly lower than values at other storage temperatures ( $p < 0.05$ ).

#### 4.4.3 Drug release

Release studies showed electrospun samples controlled the release of siponimod over the experimental timeframe (Figure 4.2C and D). Figure 4.2C shows the results of siponimod release from formulations prepared with and without collagen and compares the release from formulations prepared using different solvents, HFIP and CLF/DMF. The correlation between cumulative drug release profiles and zero-order release was indicated by  $R^2$  value. The zero-order equation for fitting the data was  $C_t = k_0 \cdot t$  where  $C_t$  is cumulative drug release at time  $t$ , and  $k_0$  is the zero-order release constant.

The presence of collagen had no statistically significant effect on the drug release profile over the 90 day release period, and at day 90 drug release corresponded to  $41.0 \pm 0.6$  % for Si 0.5:100 (HFIP) ( $R^2 = 0.99$ ) and  $43.1 \pm 0.6$  % for SiCol 0.5:100 ( $R^2 = 0.99$ ) samples. There was a significant difference in siponimod release from samples prepared with HFIP compared to those prepared with CLF/DMF. Samples prepared using CLF/DMF produced biphasic release profiles and siponimod release was higher over the entire 90 day release period with  $57.7 \pm 0.25$  % release at day 90 (Si 0.5:100 (CLF/DMF)) ( $R^2 = 0.88$ ), compared to the result for Si 0.5:100 (HFIP) shown above.

The impact of increased drug loading on release behaviour was also assessed using samples Si 0.5:100, Si 1:100, and Si 2:100, all of which were prepared using CLF/DMF. Comparison of the profiles (Figure 4.2D) showed similar biphasic release patterns over the 90 day release period. At day 90, drug release corresponded to 57.7

$\pm 0.25$  % for Si 0.5:100 ( $R^2= 0.88$ ),  $48.3 \pm 0.5$  % for Si 1:100 ( $R^2= 0.75$ ), and  $51.5 \pm 0.1$  % for Si 2:100 ( $R^2= 0.79$ ). The apparent biphasic nature of the release profiles for CLF/DMF samples can be described by more rapid drug release up to day 30, which is then followed by a controlled, linear release profile thereafter.

Following the terminal sampling point in all release studies, samples were disintegrated, and the remaining drug was dissolved in HPLC mobile phase to measure the remaining entrapped drug to account for all the drug loaded in the samples.  $80.3 \pm 0.4$  % and  $87.8 \pm 6.7$  % of initial drug mass were accounted for in Si 0.5:100 (HFIP) and SiCol 0.5:100 samples, respectively (Figure 4.2C), while Si 0.5:100, Si 1:100, and Si 2:100 exhibited values of  $91.7 \pm 1.25$  %,  $87.3 \pm 4.0$  %, and  $84.5 \pm 2.6$  %, respectively (Figure 4.2D).

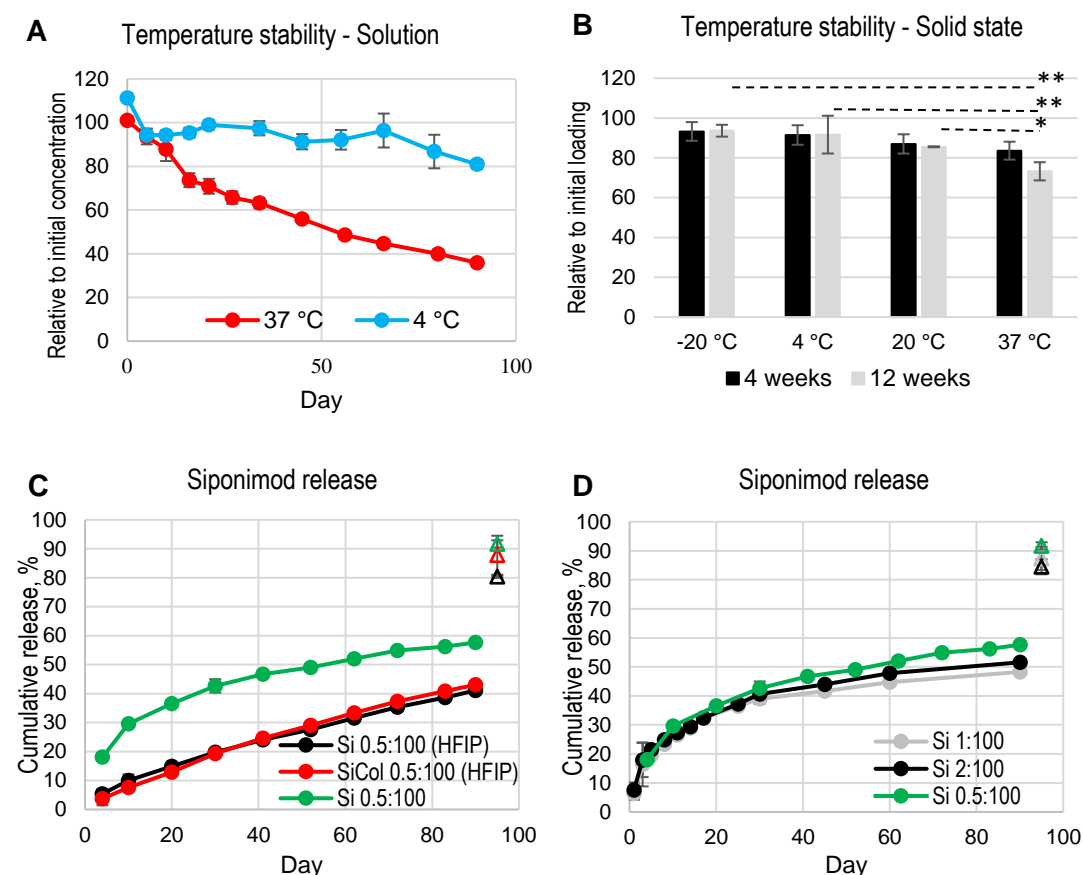


**Figure 4.2** Formulation design and its impact on siponimod stability and release. Temperature stability of (A) liquid- and (B) solid-state formulations of siponimod over time. Graphs show the change in concentration of siponimod within formulations over time relative to formulations at time zero. (C) Siponimod release from electrospun formulations prepared in HFIP (Si 0.5:100 and SiCol 0.5:100) compared to preparation using CLF/DMF (Si 0.5:100),  $n=2$  (3 technical replicates). (D) Siponimod release from electrospun formulations prepared in CLF/DMF: Si 0.5:100, Si 1:100 and Si 2:100,  $n=2$  (3 technical replicates). For figures C and D, data was multiplied by a correction factor taking into account each scaffold's loading efficiency (See Table 4.1). Additionally, in figures C and D, the hollow triangles represent the total amount of siponimod in the scaffold following the final time point (acquired by disintegrating

scaffolds in HPLC mobile phase). “ $n$ =” represents the number of independent experiments. Data is presented as mean  $\pm$  SD.

Finally, for Si 0.5:100 (HFIP) and SiCol 0.5:100, SEM images were acquired at the end of the 90 day release period. Although the gross integrity of the fibrous construct is intact, Figure 4.3A-C appear to show evidence of degradation of the fibre matrix over time, as suggested by the ubiquitous formation of pores on the surface of the fibre and some evidence of small fissures and weakening of the structure (arrows in Figure 4.3B). Figure 4.3C also shows a cross section of the SiCol 0.5:100 samples indicating that bulk degradation was occurring throughout the fibrous material.

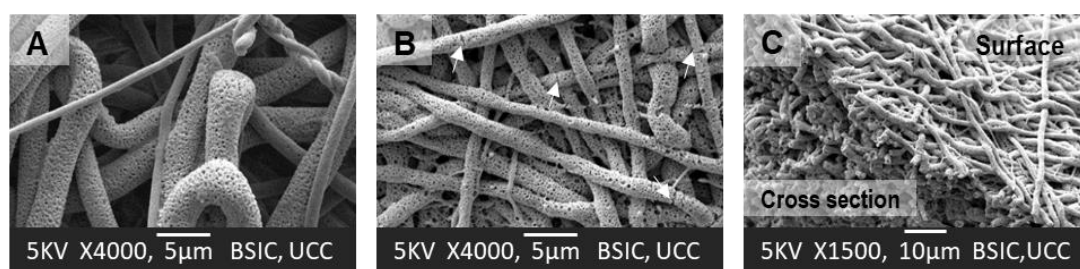


**Figure 4.3** SEM images following 90 day release study. (A) Si 0.5:100 (HFIP) (B) SiCol 0.5:100 (C) Surface and cross section of SiCol 0.5:100. For A and B magnification at x4000 (scale bar = 5  $\mu$ m), for C magnification at x1500 (scale bar = 10  $\mu$ m). White arrows indicate signs of general degradation.

#### 4.4.4 Physicochemical characterisation – DSC, FTIR, contact angle & tensile strength

As part of an overall physicochemical characterisation of the electrospun formulation, analysis was conducted to investigate any changes in the thermal behaviour of the

solid electrospun formulations due to processing (Figure 4.4A). The unprocessed PLGA starting material showed a glass transition temperature ( $T_g$ ) at 53.6 °C, and after processing using the solvent mixture CLF/DMF, exhibited a  $T_g$  at 52.2 °C. Samples prepared using the solvent HFIP showed a marked reduction in  $T_g$  (37.9 °C) compared to the unprocessed PLGA starting material. A reduction in  $T_g$  was observed for all samples prepared using HFIP including PLGA-Collagen (39.7 °C), and SiCol 0.5:100 (40.4 °C). Samples containing siponimod processed using CLF/DMF exhibited polymer  $T_g$  (Si 0.5:100 (52.23 °C), and Si 2:100 (52.15 °C)) similar to the  $T_g$  of the PLGA base material (53.60 °C)

FTIR spectroscopy was performed on electrospun samples to investigate any fundamental changes in chemical bond interactions between the constituent materials (PLGA, siponimod, and collagen) (Figure 4.4B-C). The electrospinning procedure did not produce any differences when compared to the spectrum of the PLGA starting material. Indeed, the addition of siponimod at 0.5:100 (Figure 4.4B-C), 1:100 and 2:100 (data not shown) did not show any sign of the O-H and C-H stretching bands between 2800-3300  $\text{cm}^{-1}$  associated with the siponimod spectrum shown in Figure 4.4B. The low concentrations of siponimod used in these formulations may have made detection of drug-polymer interactions challenging. Therefore, samples were also prepared with higher drug concentrations (3.3:100), which showed the first indications of siponimod O-H and C-H stretching between 2500-3300  $\text{cm}^{-1}$  (arrows in Figure 4.4B). Collagen containing samples (Figure 4.4C) did not show any traces of known collagen amide peaks (Figure 4.4B) between 2900-3200  $\text{cm}^{-1}$ .

Contact angle goniometry was used to determine whether the addition of siponimod and/or collagen had any effect on the hydrophobicity of the electrospun scaffolds. All samples exhibited hydrophobic behaviour and  $\theta > 90^\circ$ , irrespective of composition or processing solvent, PLGA ( $125.9 \pm 13.5^\circ$ ), Si 0.5:100 ( $135.2 \pm 5.5^\circ$ ), Si 2:100 ( $131.4 \pm 10.7^\circ$ ) and SiCol 0.5:100 ( $118.2 \pm 6.9^\circ$ ). There were no statistically significant differences in the sample wettability of electrospun samples ( $p = 0.32$ ).

Electrospun samples were investigated for tensile strength (Figure 4.4D). The ultimate tensile strength of samples Si 0.5:100 and Si 2:100 ( $0.169 \pm 0.042 \text{ MN/m}^2$  and  $0.173 \pm 0.014 \text{ MN/m}^2$ ) showed no significant difference compared to electrospun PLGA control ( $0.144 \pm 0.054 \text{ MN/m}^2$ ). However, there was a significant increase in the ultimate tensile strength of SiCol 0.5:100 compared to electrospun PLGA control ( $0.274 \pm 0.044 \text{ MN/m}^2$  compared to  $0.144 \pm 0.054 \text{ MN/m}^2$ ,  $p < 0.05$ ).

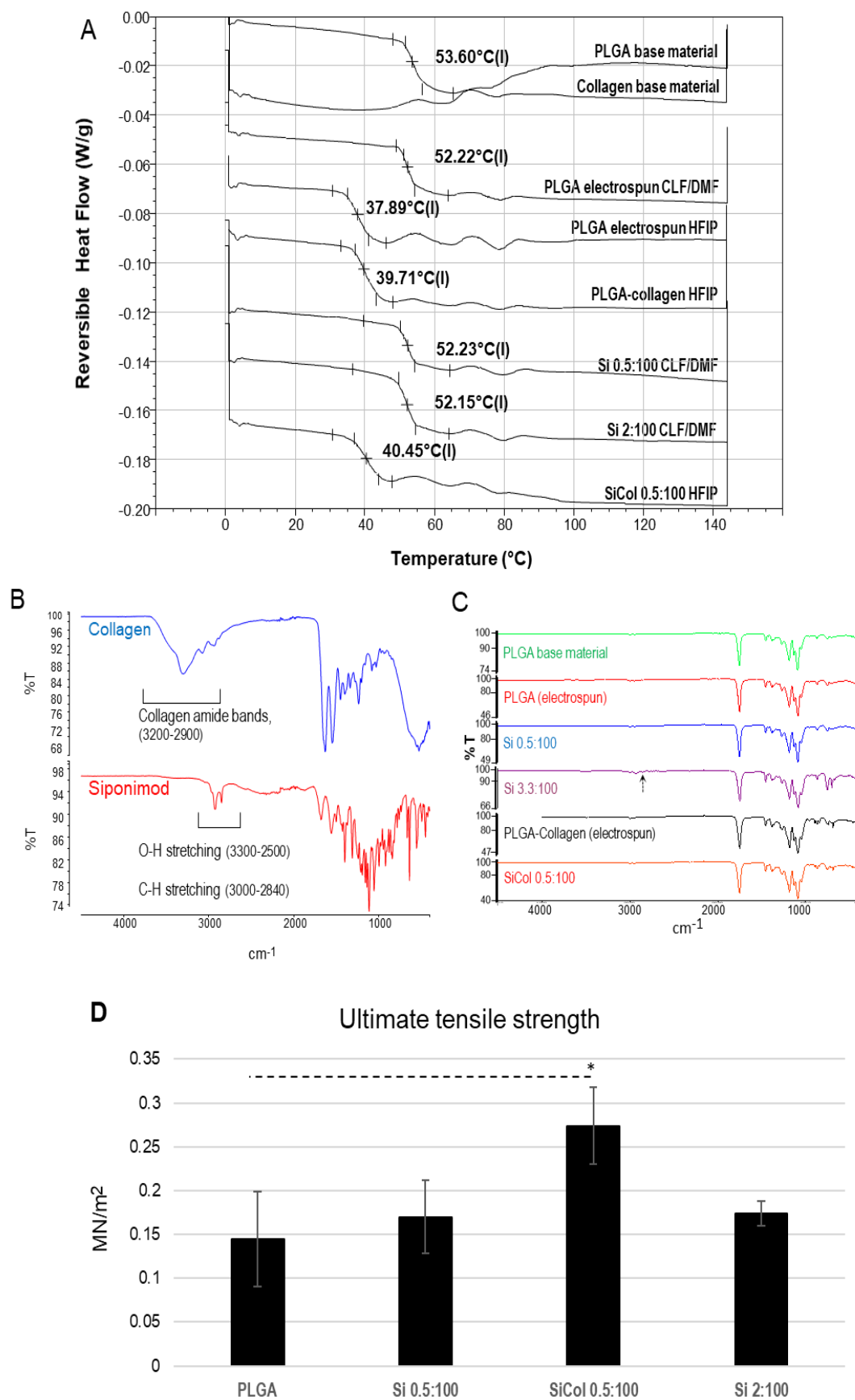


**Figure 4.4** Physicochemical properties of electrospun scaffolds. (A) Differential scanning calorimetry of electrospun scaffolds and base materials using MDSC. (B) FTIR spectra of collagen and siponimod (C) FTIR spectra of electrospun samples. (D) Ultimate tensile strength of electrospun scaffolds. Scaffolds were exposed to tensile force until failure,  $n=3$ . For D, data is presented as mean  $\pm$  SD, statistical analysis by one-way ANOVA. \*:  $p < 0.05$ .

#### 4.4.5 Biological characterisation of electrospun material

*In vitro* cell culture with hFOB and HUVEC was performed to determine the metabolic activity of cells incubated with electrospun scaffolds. Exposure was either indirect, by adding scaffolds to 24-well plates pre-seeded with cells, or direct, which involved seeding cells onto the surface of electrospun scaffolds inserted at the bottom of well plates. As shown in Figure 4.5A and B, indirect incubation of the electrospun scaffolds with both HUVEC and hFOB over the 5 day period did not significantly impact cell metabolism when compared to scaffold-free controls.

Figure 4.5C shows the metabolic activity of hFOB seeded directly on the scaffold surface and incubated for a period of 5 days. For each scaffold type there were statistically significant increases in metabolic activity over time (shown in fluorescent units). For the PLGA control scaffolds, values on day 3 ( $126.2 \pm 7.4$ ,  $p < 0.05$ ) and 5 ( $131.9 \pm 9.5$ ,  $p < 0.01$ ) were increased compared to day 1 ( $97.3 \pm 28.1$ ). The Si 0.5:100 sample showed a significant increase between day 3 ( $128.8 \pm 18.5$ ,  $p < 0.05$ ) and day 1 ( $102.7 \pm 16.0$ ), followed by a plateau by day 5 ( $127.1 \pm 10.0$ ). The sample SiCol 0.5:100 showed a similar stepwise increase in metabolic activity, with a significant increase between day 1 ( $68.1 \pm 6.8$ ) and day 5 ( $105.8 \pm 9.2$ ,  $p < 0.01$ ). Following the



direct incubation assay, scaffolds were fixed, sectioned and stained with haematoxylin and eosin. Qualitative light microscopy indicated that by day 5, cell growth occurred mainly on the surface of scaffolds, with some evidence of infiltration observed in Si 0.5:100 (Figure 4.5D-F, black arrows indicate infiltration).

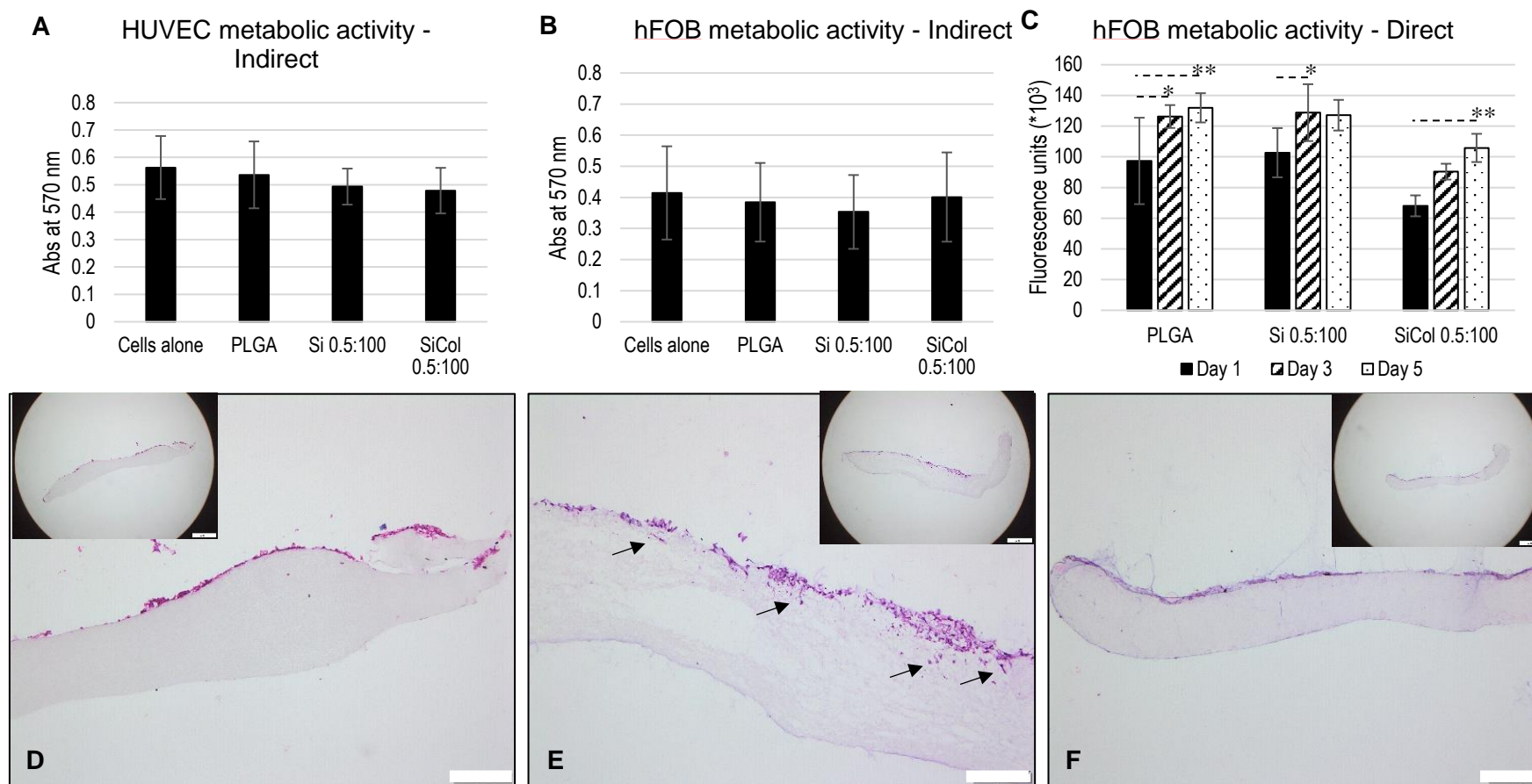


**Figure 4.5** Indirect and direct metabolic activity of cells incubated with electrospun scaffolds. (A) HUVEC metabolic activity and (B) hFOB metabolic activity was determined using MTT assay after 5 days indirect exposure between samples and cells, for both A & B  $n=3$

(3 technical replicates). Direct assessment (C) involved hFOB directly seeded on PLGA, Si 0.5:100, and SiCol 0.5:100 scaffolds for 5 days with assessments using the resazurin assay on days 1, 3, and 5,  $n=4$  (4 technical replicates). For graph A and B, data represents the average absorbance values at 570 nm. For graph C, data represents the average fluorescence at excitation 488 nm/emission 595 nm, expressed as fluorescence units. (D, E, F) Light microscopy images of H&E stained cells on PLGA, Si 0.5:100 and SiCol 0.5:100, respectively. Images were acquired at 10x magnification (scale bar = 200  $\mu\text{m}$ ) using extended focal image acquisition, inset within each image is the same sample acquired at lower magnification using 4x objective magnification. Stained cells (pink) can be seen growing on the surface of electrospun polymer scaffold (grey). “ $n=$ ” represents the number of independently repeated experiments. Data is presented as mean  $\pm$  SD. For (A & B) Statistical analysis was by one-way ANOVA. For (C) statistical analysis was by two-way ANOVA. \*:  $p < 0.05$ , \*\*:  $p < 0.01$ .

#### 4.4.6 *In vitro* functional experiments

In order to test the functional effect of the released drug, scaffolds were incubated with hFOB and their ALP activity was used as a marker for cell differentiation, while migration of HUVEC in response to released siponimod was assessed using transwell migration assays Figure 4.6. Based on release data and known masses of scaffolds, local concentrations of siponimod would likely fall in the nanomolar to low micromolar range. For example, from the release data it was estimated that 6.9 % of siponimod was released from the scaffolds after one day of incubation, which for the Si 0.5:100 sample would produce a local concentration of 1.5 $\mu$ M. By day 5 of incubation, a further 1.7 % of siponimod in scaffolds was released which would equate to 0.37 $\mu$ M. These concentrations would be expected to exert functional effects based on past research (Sartawi et al., 2020a).

Cells incubated with samples of Si 0.5:100 were found to exhibit significantly higher ALP activity compared to electrospun PLGA controls ( $92.2 \pm 6.1$  % compared to  $61.5 \pm 7.6$  %,  $p < 0.05$ ). While increasing drug concentration (Si 2:100) and the addition of collagen (SiCol 0.5:100) appeared to increase ALP activity compared to the electrospun PLGA control, differences were not statistically significant ( $78.0 \pm 10.3$  % for Si 2:100, and  $78.6 \pm 5.3$  % for SiCol 0.5:100 compared to  $61.5 \pm 7.6$  % for electrospun PLGA control) (Figure 4.6A). Additionally, hFOB were stained at day 7 using Fast Blue BB/Naphthol AS-MX phosphate to assess the number of cells with increased ALP activity (Figure 4.6B). Siponimod loaded scaffolds Si 0.5:100 and Si 2:100 showed an increase in the number of stained cells compared to scaffold-free controls ( $80.1 \pm 15.4$  % and  $77.6 \pm 15.1$  % compared to  $43.2 \pm 9.9$  %,  $p < 0.05$ ). However, neither the siponimod scaffold containing collagen (SiCol 0.5:100) nor

drug-free PLGA scaffolds ( $63.6 \pm 10.7$  % and  $51.5 \pm 8.6$  %, respectively) produced statistically significant increases in ALP activity compared to scaffold free controls ( $43.2 \pm 9.9$  %).

Transwell migration results are shown in Figure 4.6C as the number of migrated cells per field of view (FOV), with Si 0.5:100 and Si 2:100 producing statistically significant increases in the number of migrated HUVEC compared to the electrospun PLGA control ( $17.6 \pm 3.5$  cells/FOV and  $17.3 \pm 1.3$  cells/FOV compared  $5.7 \pm 0.5$  cells/FOV, respectively  $p < 0.05$ ). Samples containing both siponimod and collagen SiCol 0.5:100 did not stimulate significant increases in cell migration compared to the electrospun PLGA control ( $6.0 \pm 0.6$  cells/FOV compared to  $5.7 \pm 0.5$  cells/FOV).

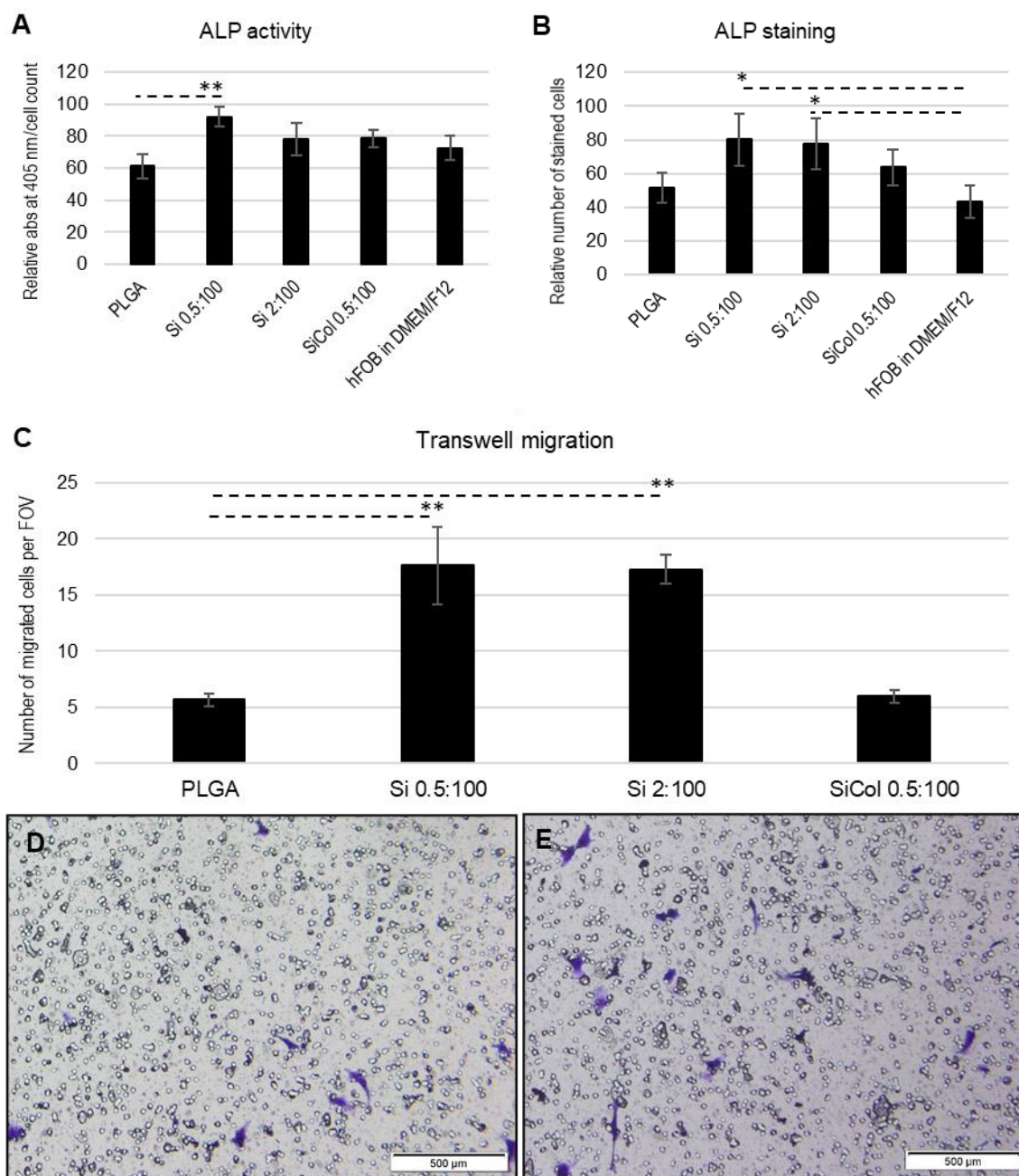


**Figure 4.6** *In vitro* functional experiments investigating differentiation and migration.

(A) ALP activity after 7 days,  $n=3$  (3 technical replicates). Data represents the average of pNPP absorbance at 405 nm divided by cell number, data is expressed relative to positive osteogenic control (hFOB incubated in cell culture medium containing 50  $\mu$ g/ml ascorbic acid & 7.5 mM  $\beta$ -glycerophosphate). (B) ALP Fast blue staining after

7 days,  $n=4$  (3 technical replicates), data is expressed relative to positive osteogenic control. (C) HUVEC transwell migration after 8 hrs,  $n=3$  (2 technical replicates). (D, E) Representative images of transwell migration data for samples PLGA and Si 0.5:100, respectively. Images were acquired at 4x magnification (scale bar = 500  $\mu\text{m}$ ). Data is presented as mean  $\pm$  SD, statistical analysis by one-way ANOVA. \*:  $p < 0.05$ , \*\*:  $p < 0.01$ , \*\*\*:  $p < 0.001$ .

#### 4.4.7 *In vivo* critical cranial defect

Following previous research demonstrating the effects of siponimod on osteoblast and endothelial cells (Sartawi et al., 2020a), and the *in vitro* research findings presented herein demonstrating the controlled release of siponimod from PLGA scaffolds on the same cell populations, the next step was to determine whether those cellular effects translated to *in vivo* efficacy in bone defect regeneration.

Labelling with calcein was used with the aim of estimating the temporal progression of mineralisation (Blum et al., 2003). The extent of mineralisation depicted in Figure 4.7 (fluorescent labelling (magnified)) represents the results of calcein administration at the 3 week time-point after surgery.



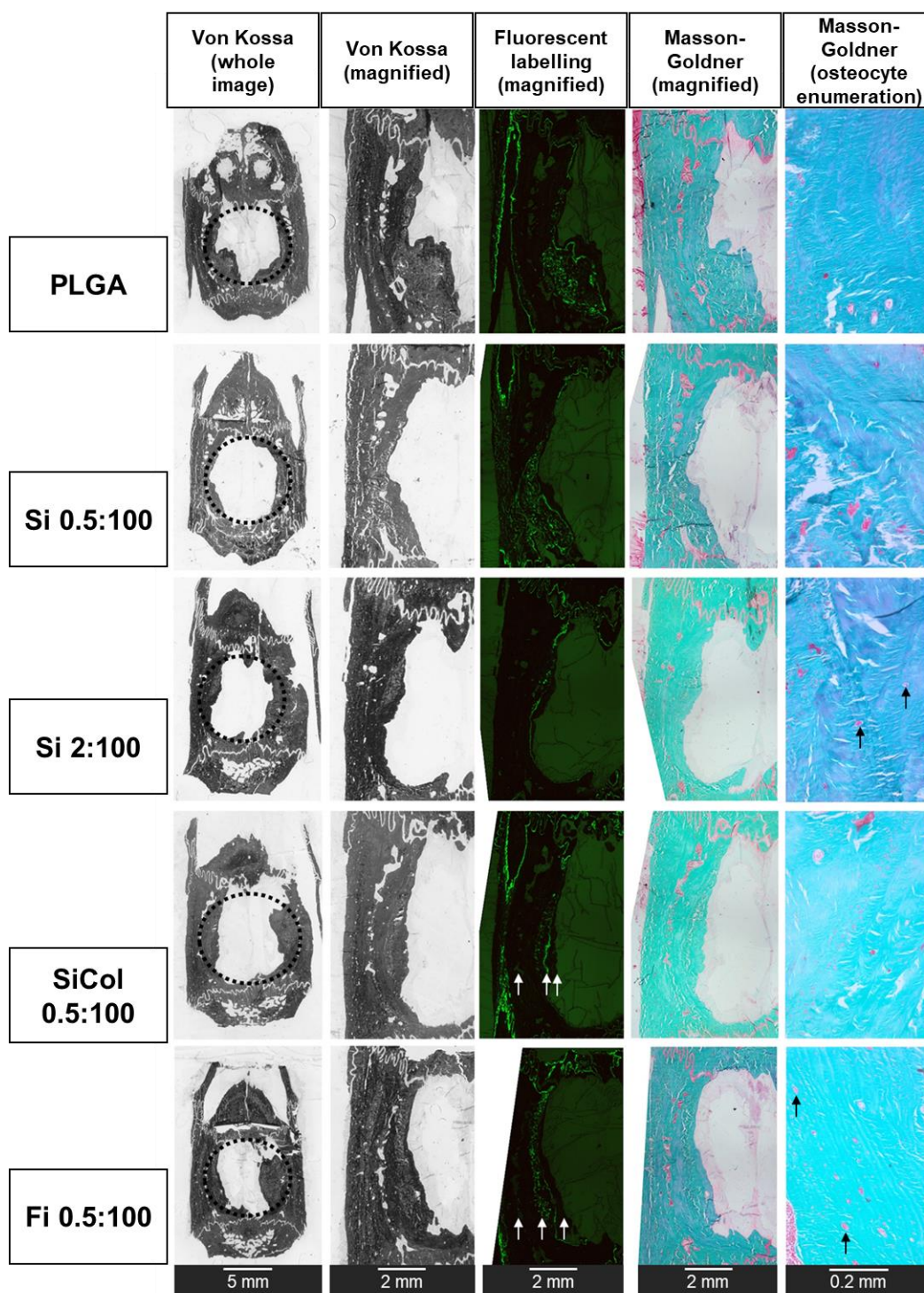


**Figure 4.7** Columns of images: representative images. Columns indicate VK staining (whole image), VK staining (magnified), Calcein fluorescent labelling (magnified), MG staining (magnified), and MG staining (osteocyte enumeration). Rows of images:



correspond to the different experimental groups used in critical cranial defect study PLGA, Si 0.5:100, Si 2:100, SiCol 0.5:100, and Fi 0.5:100. The black dashed lines in VK staining (whole image) give an approximation of the original defect area. The white arrows in the fluorescent micrographs indicate in progression from left-to-right, the original defect edge, the 3-week fluorescent signal, and the 12-week position of regenerating bone. The black arrows in the osteocyte enumeration micrographs indicate examples of counted osteocytes. Scale bars are indicated for each column of images.

The images in Figure 4.7 were used to acquire the quantitative data shown in Figure 4.8. For example Figure 4.8A shows the value for the area of early regeneration (0-3 weeks), and late regeneration (3-12 weeks) determined from fluorescent labelling images. Of the investigated scaffolds, the greatest extent of regeneration by 12 weeks appeared to be associated with Si 0.5:100 when compared to PLGA control, however neither Si 0.5:100 nor any of the other scaffolds resulted in statistically significant increases in area of regeneration ( $26.1 \pm 8.6 \text{ mm}^2$  for Si 0.5:100 compared to  $22.8 \pm 8.1 \text{ mm}^2$  for PLGA control). Furthermore, the extent of early regeneration appeared to be greater than that of late regeneration. In the case of most scaffolds this difference was not statistically different, with the exception of Si 0.5:100, which showed a significantly greater area of regeneration at earlier stages ( $17.5 \pm 6.0 \text{ mm}^2$  for 0-3 week period compared to  $8.6 \pm 5.5 \text{ mm}^2$  for the 3-12 week period,  $p < 0.5$ ).

In Figure 4.8B and C, both MG trichrome and VK staining demonstrated that there was no significant change in mineralisation between the different experimental

groups. Indeed, in MG trichrome, the best performing scaffold, Si 0.5:100, resulted in an equivalent area of mineralised tissue compared to PLGA control ( $22.18 \pm 6.0 \text{ mm}^2$  for Si 0.5:100 compared to  $22.5 \pm 7.6 \text{ mm}^2$  for PLGA control). A similar result was found with VK staining, where Si 0.5:100 appeared to result in an equivalent level of mineralisation compared to PLGA control ( $25.7 \pm 10.7 \text{ mm}^2$  for Si 0.5:100 compared to  $25.4 \pm 10.7 \text{ mm}^2$  for PLGA control).

The MG trichrome staining images in Figure 4.7 were used to enumerate osteocytes within selected fields of view (an area of  $0.31 \text{ mm}^2$ ), the quantitative values of which are shown in Figure 4.8D. There was no significant difference between the experimental groups examined, with the greatest number of enumerated osteocytes associated with the Si 2:100 scaffold not statistically different from PLGA control ( $29.3 \pm 5.8 \text{ cells}/0.31 \text{ mm}^2$  for Si 2:100 compared to  $25.7 \pm 5.3 \text{ cells}/0.31 \text{ mm}^2$  for PLGA control).

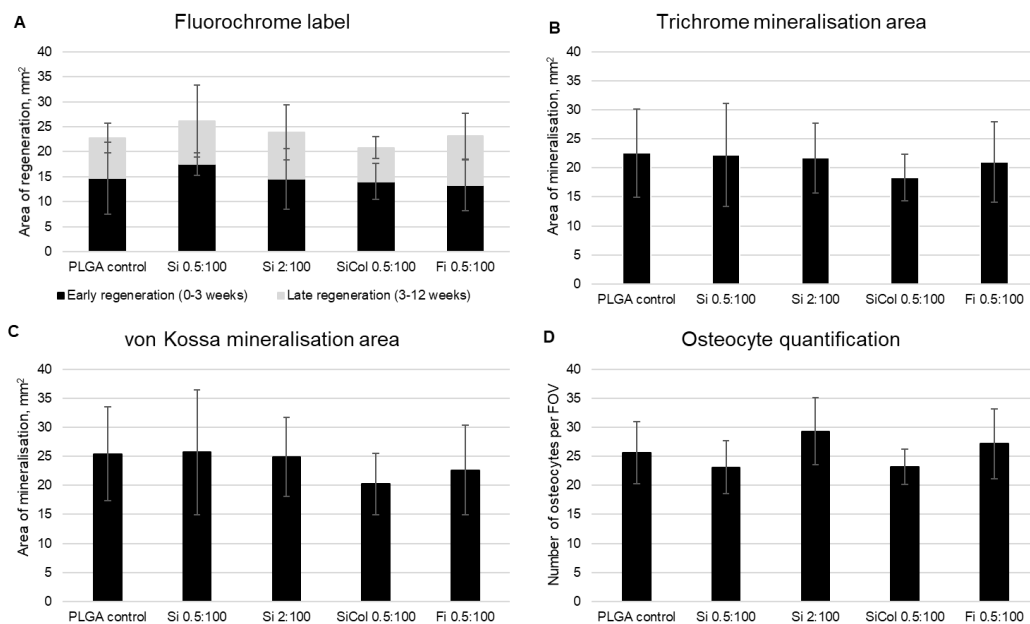


**Figure 4.8** Histomorphometric analysis of critical cranial defect sections. (A) Area of repair before and after calcein labelling at 3 weeks,  $n=6$  animals (2 measurements per animal). (B) Area of mineralisation determined using Masson-Goldner trichrome stain,  $n=6$  animals (2 measurements per animal). (C) Area of mineralisation determined using von Kossa stain,  $n=6$  animals (2 measurements per animal) (D) Manual quantification of osteocytes within regenerated defect using Masson-Goldner trichrome stained sections,  $n=6$  animals (4 fields of view per section each with an area of  $0.31 \text{ mm}^2$ ).

## 4.5 Discussion

The overall aim of this work was to develop and characterise a siponimod loaded implantable scaffold for the localised and controlled release of siponimod, to augment bone regeneration in cases of critical bone defects. With this in mind, we prepared an

electrospun scaffold loaded with siponimod and collagen. The aim of adding siponimod was to exploit its ability to attract endothelial cells and enhance pre-osteoblast differentiation (Sartawi et al., 2020a) within a bone defect, over a timeframe relevant to bone repair. The choice of siponimod was further based on a body of literature investigating the impact of another S1P modulator, fingolimod, on critical bone defects, which showed increases in bone area and vascularisation of defects (Das et al., 2013). Siponimod is more selective than fingolimod, does not require activation by phosphorylation, and has potentially fewer side effects (Behrangi et al., 2019). The concentration of siponimod was similarly chosen based on previous studies investigating the S1P analogue, fingolimod (Huang et al., 2012, Das et al., 2014b, Das et al., 2013). To the best of our knowledge, this is the first study examining siponimod for bone regeneration and the first to evaluate its delivery from a controlled release polymer system. Therefore, we initially determined the solid and liquid stability of siponimod preparations at different temperatures and showed that siponimod degradation was reduced when entrapped within the polymer matrix. This conservation of drug stability is essential given the extended timeframe required for research targeting bone regeneration. Other groups investigating S1P for bone regeneration have also investigated formulation design to tailor drug release. For instance, S1P has been prepared as part of silicon-PLGA-chitosan scaffolds for tissue engineering applications, providing a steady release of S1P and an adequate surface for cell proliferation (Pandolfi et al., 2016). Keeping in mind the grade of PLGA (50:50) used was of a variant with relatively more rapid degradation giving rise to release over a mere 11 days. In comparison, the formulation described herein releases its cargo over several months, a timeframe more suitable for bone regenerative

purposes. This is attributed to the grade of PLGA (85:15) used in this study, which degrades more slowly due to its more hydrophobic properties associated with the increased portion of lactic acid monomer (Makadia and Siegel, 2011). Indeed, SEM images of the fibrous constructs retrieved from the release study after 90 days demonstrated the scaffolds were still intact, albeit with evidence of ubiquitous pore formation.

Looking more closely at siponimod release, the release patterns depended on the solvent used in their preparation although the profiles were similar across respective samples processed in each of the different solvents. Siponimod release from samples prepared in CLF/DMF was biphasic showing an initial burst followed by a slow linear release, while samples prepared using HFIP showed little to no initial burst release, correlating more closely with zero-order release throughout. In reality, release from these electrospun scaffolds is likely complex and affected by several variables. Collagen samples processed with HFIP demonstrated reductions in polymer Tg close to physiological temperature, smaller and a narrower distribution of fibre diameter and lower % drug release. Previous research has demonstrated that thinner fibre meshes exhibited faster drug release (Okuda et al., 2010). It was expected that scaffolds processed with CLF/DMF, which had higher polymer Tg and larger fibre diameters (Si 0:5:100 (CLF/DMF)) would have smaller specific surface areas that could lead to lower drug release. However, these samples displayed a burst release component, and greater drug release over the analysis period compared to samples with significantly smaller fibre diameters (SiCol 0.5:100 - HFIP)). As contact angle goniometry confirmed both materials are hydrophobic, the smaller and denser fibre network may have acted to exclude the inner regions of the scaffolds from contact with the release

medium, resulting in linear release profile and a reduction in drug release. Another factor influencing drug release is distribution of drug in the polymer fibre during the formulation step. The processing solvents employed have different boiling points, and viscosities. HFIP has a higher density and viscosity (Costa et al., 1982) and is more volatile due to its lower boiling point 52 °C (Xia et al., 2014), whereas the co-solvent mix of CLF and DMF have boiling points of 61.6 and 153.1, respectively (Ye et al., 2009). It is possible that the increased viscosity and higher evaporation rate associated with HFIP resulted in more uniform drug distribution in the polymer, and the drug was entrapped throughout the polymer fibre rather than partitioning to the polymer surface as the fibre formed. Uniform distribution of drug throughout polymer fibres electrospun with HFIP has been shown in the literature (Wu et al., 2020, Hall Barrientos et al., 2017). In all cases, the cumulative drug release did not exceed 60 % of total encapsulated drug. It should be noted that as polymer degradation increases a phase of rapid drug release may occur, potentially resulting in an increased rate of release for the remaining 40-50 % of encapsulated siponimod (Wu et al., 2020). Following the final drug release sampling point, scaffolds were disintegrated to account for the remaining drug within the scaffold. Results indicated that between  $80.3 \pm 0.4$  % to  $91.7 \pm 1.25$  % of drug in total was accounted for. It is possible that the remaining (between 8.3-19.7 %) siponimod underwent degradation while in solution between sampling points. This theory is supported by the siponimod stability study data at 37 °C (Figure 4.2A), which demonstrated that the drug degraded when stored in PBS solution at 37 °C, over 90 days.

Thermal analysis indicated a marked reduction in the polymer T<sub>g</sub> of the scaffolds (range 37.89-40.45 °C) processed using HFIP as a solvent. This may lead to changes

in the texture and brittleness of implantable materials when used *in vivo* (Park and Jonnalagadda, 2006), and was attributed to the known plasticizing effect of HFIP (Jose et al., 2009b, Zong et al., 2002). Tensile strength data also indicates that the electrospun material containing collagen had significantly higher values, which may be attributed to a denser network of smaller fibres (Wong et al., 2008). The addition of collagen to formulations resulting in fibres with smaller diameters has been shown in other studies utilising a similar technique (Hall Barrientos et al., 2017). Additionally, it is possible that the plasticising effect of the solvent altered the ductile properties of the polymer (Lim and Hoag, 2013). The tensile strength of the electrospun materials is several orders of magnitude lower than human bone 80 MN/m<sup>2</sup> (Wall et al., 1979), and so could be used in tandem with a mechanically competent material, as a replacement in non-weight bearing defects (Turan et al., 2016, Davies et al., 2018) or indeed to augment fracture repair.

The grade of PLGA was chosen for its slow degradation behaviour. However, the increased hydrophobicity was expected to pose a challenge with respect to cellular interaction and adhesion. Despite this, biological characterisation of electrospun materials demonstrated that cells were growing on the surface of the scaffolds after 5 days and showed signs of infiltration within the fibrous matrix of the Si 0.5:100 scaffold. At these early time-points, this was not observed in collagen containing samples and is most likely associated with the density of the fibre network due to the smaller fibre diameter, which was more suited to cell spreading rather than promoting cell infiltration (Ko et al., 2016). Added to this, the Si 0.5:100 sample also demonstrated the clearest functional effects with respect to the impact of released siponimod on ALP activity and endothelial cell migration. This ratio was based on a

study using a similar ratio of fingolimod, which resulted in increased bone volume *in vivo* (Das et al., 2014b). The lack of an effect or indeed an additive effect with increasing ratios of siponimod was unexpected but not surprising given that siponimod (Sartawi et al., 2020a) has been shown to achieve its maximal effect at low nanomolar concentration with effects plateauing thereafter as receptors become desensitised. The effect of siponimod is likely similar to that of fingolimod (Mullershausen et al., 2009), which is known to exhibit delayed persistent signalling following receptor internalisation, while SIP has been observed to exhibit both time and dose dependant effects on cell proliferation (Dziak et al., 2003).

The addition of collagen was intended to improve the biocompatibility of the hydrophobic PLGA polymer as the addition of collagen even at low concentrations ( $\approx 1$  % w/w) has been shown to improve cellular adhesion to polymer scaffolds, by increasing sites for cellular attachment (Chiu et al., 2007). However, this was not found to be the case in our results with no clear added advantage in quantitative assays of metabolic activity or qualitative histology. HFIP has previously been shown to be a suitable solvent for electrospinning collagen without causing denaturation (Pham et al., 2006), and in this study no evidence that processing the polymer composite using HFIP adversely impacted the collagen stability was determined using DSC. In particular, an endotherm in the region of 80 °C, which has previously been shown to indicate denaturation (Jose et al., 2009a), was not evident here. Other studies have also indicated electrospinning collagen results in substantial loss of the triple helix structure (Zeugolis et al., 2008, Yang et al., 2008), which may have reduced the likelihood of observing positive results. It is also likely that higher concentrations are required to impart significant effects, and concentrations closer to parity (50 % w/w)



would result in more substantial results as reported elsewhere (Ngiam et al., 2009). Ultimately, a selection of scaffolds was chosen for evaluation *in vivo* in a critical cranial defect, with the aim of comparing several siponimod loaded scaffolds with a fingolimod loaded scaffold informed by the available literature (Das et al., 2013). At the end of the 12 weeks, there was a reduction in the measured area of the defect. However, there was no significant difference in mineralisation when comparing drug loaded and drug-free scaffolds. This was despite the positive differentiation and migration results observed *in vitro* for the Si 0.5:100 scaffold. It must be noted, that the fingolimod loaded sample, which was used for comparative purposes, did not result in a significant increase in histomorphometric measures of defect mineralisation. However, there were some differences between the fingolimod loaded samples used here (PLGA based implant, 8 mm cranial defect, mineralised area determined by histomorphometry) and that used in the study cited (PCL/PLGA polymer composite implant, 5 mm mandibular defect, mineralised area determined by 3-D microCT). Moreover, the methodologies used in the literature to determine drug release *in vitro* (Huang et al., 2012, Sefcik et al., 2011, Das et al., 2013, Das et al., 2014b, Petrie Aronin et al., 2010b) and *in vivo* (Ogle et al., 2014) differ from those used here. Finally, fingolimod's effect on bone regeneration in the literature has been attributed to its impact on vascular network formation (Petrie Aronin et al., 2010a, Sefcik et al., 2011), and the local recruitment of regenerative immune cells (Ogle et al., 2014) rather than direct activity on bone cells. However, these effects were not examined here and represents a limitation in our study as it complicates our ability to make like-for-like comparisons.

There were some other limitations to the work conducted here, in the case of the release study, the experiment was a single compartment *in vitro* experiment that did not involve enzymatic activity or biorelevant medium, therefore it is expected that *in vivo* concentrations will not closely correlate with *in vitro* data. Cell culture experiments present another drawback, insofar as cells grown in 2-D isolation are a relatively poor substitute for the living environment of regenerating tissue. All of which may go some way to explaining the disparity that still exists between the *in vitro* and *in vivo* effect of siponimod loaded scaffolds. Additionally, regarding the *in vivo* cranial defect, it was clear that initial estimates of variability across the regenerating defects led to an underestimation in the sample size required to adequately show statistically significant changes in histomorphometric measures of bone regeneration.

#### 4.6 Conclusion

This work aimed to deliver the selective S1P<sub>1</sub> receptor agonist siponimod in a controlled manner to a critical cranial defect. It involved the design of a polymer-based scaffolds loaded with siponimod and co-spun with collagen as a potential replacement material in cases of non-weight bearing critical bone defects and represents the first application of siponimod as part of a controlled release system. The electrospun samples developed showed efficient drug loading and controlled release over timeframes suitable for regeneration. *In vitro* the added components had mixed results, siponimod increased osteoblast differentiation (ALP activity) and endothelial cell migration, while collagen gave rise to scaffolds with greater tensile strength but did

not increase cell attachment or promote enhanced cell interaction over 5 days. Formative animal studies showed that the scaffolds support the regeneration of critical bone defects, however the addition of siponimod did not result in a significant regenerative effect. Ultimately, the validity of targeting S1P receptors in bone repair is questionable due to the contradictory findings between studies. However, it is possible that modifying drug release from scaffolds, increasing collagen concentration, and increasing *in vivo* sample size may yield positive results.

# Chapter 5

Developing porous scaffolds for the localized  
delivery of siponimod using electrosprayed  
microparticles, gas foaming, and porogen leaching

## 5.1 Abstract

Bone tissue engineering regularly necessitates the preparation of 3-D porous scaffolds that mimic the natural extracellular matrix of bone, ideally using simple and efficient techniques. The combination of electrospraying, gas-foaming and porogen leaching represents a relatively simple and cost-effective approach to prepare scaffolds that possess a porous architecture suitable for bone regenerative applications while also providing a vehicle for the delivery of the specific S1P<sub>1/5</sub> receptor modulator siponimod.

Scaffolds composed of electrosprayed PLGA microparticles and HA were produced using CO<sub>2</sub> gas-foaming and porogen (NaCl) leaching. The polymer microparticles were loaded with siponimod at a drug:polymer mass ratio of 0.5:100. Thereafter, scaffolds underwent *in vitro* physicochemical characterisation using FTIR, DSC and SEM, as well as indirect and direct cytocompatibility analysis with osteoblast and endothelial cells. The scaffolds demonstrated pore volumes in the range of 70.1-83.7 % and pore sizes in the range 200-300 µm. Drug-loaded scaffolds showed controlled release of siponimod over the 3 month experimental timeframe, and furthermore, scaffolds showed compatibility with osteoblast and endothelial cells. To our knowledge, this is the first scaffold design combining siponimod and HA in a 3-D porous construct. *In vitro* studies confirmed desirable porosity and drug release attributes, however, further optimisation of the scaffold design supported by more extensive *in vitro* functional studies is warranted.

## 5.2 Introduction

Three-dimensional (3-D) polymeric scaffolds for bone tissue engineering must fulfil some important criteria if they are to support the regeneration of bone tissue and achieve good integration between the implanted scaffold and native tissue. Desirable properties include the presence of a porous and interconnected architecture (Abbasi et al., 2020), fabrication from biocompatible, osteoconductive materials with sufficient mechanical integrity (Qu et al., 2019, Hutmacher, 2000), and degradation contemporaneous with the regeneration of new tissue (Alsberg et al., 2003).

A porous scaffold is important when attempting to replicate bone extracellular matrix by enabling cell infiltration, proliferation and differentiation, nutrient and waste exchange and the development of functional vasculature and tissue growth throughout the structure (Henkel et al., 2013), in addition to providing sufficient surface area for cell adhesion (Dhandayuthapani et al., 2011). Studies investigating the implications of pore size in bone tissue engineering indicate the optimal pore size is in the range 100-350  $\mu\text{m}$  (Yang et al., 2001). However, a balance must be struck as high porosity in the scaffold structure will negatively impact a scaffold's mechanical properties leading to collapse under high weight-bearing loads, conversely insufficient porosity will adversely impact drug release, cell infiltration through the construct, and ultimately the scaffold's osteoconductivity (Byrne et al., 2007). An osteoconductive scaffold material, is one that is capable of supporting the formation of new bone by supporting cell attachment, proliferation, survival, and the deposition of bone matrix (Blokhuys and Arts, 2011). Osteoinductive materials have the capacity to evoke biological responses, and can be used to introduce bioactivity to the most commonly used synthetic polymers (Haugen et al., 2019).

The ability of a scaffold material (such as biodegradable polymers) to degrade and to do so in a timeframe commensurate with bone regeneration, gives the newly regenerated bone sufficient time to develop mechanical competency and restore its functionality (Ge et al., 2008). Numerous degradable materials have been used to prepare scaffolds for bone tissue engineering purposes, including degradable polymers such as polyanhydrides, poly(ortho esters), polyesters and polycyanoacrylates (Rey-Vinolas et al., 2019). Degradable or bioresorbable ceramics include calcium phosphate ceramics (Tan et al., 2013) as well as the bioactive glass ceramics first developed by Hench et al. (Hench et al., 1971). Calcium phosphates (CaP) including hydroxyapatite (HA) ( $\text{Ca}_{10}(\text{OH})_2(\text{PO}_4)_6$  (Gradinaru et al., 2015)) and tricalcium phosphates (TCP) ( $\text{Ca}_3(\text{PO}_4)_2$  (Jeong et al., 2019)), have been investigated due to their structural and functional similarity to bone mineral (Ramesh et al., 2018). One of the most common approaches to recapitulate the native bone tissue is to produce composite scaffolds composed of polymers and mineral phases, which can help address the limitations of individual materials. The inclusion of HA can improve the osteoconductive behaviour of synthetic polymer scaffolds, as polymers lack the biological properties of bone extracellular matrix (Kretlow and Mikos, 2007, Ahern et al., 2013). One recent example shows this, whereby PLGA/HA microsphere-based scaffolds promoted the adhesion, proliferation, and alkaline phosphatase activity of BMSC seeded directly on the scaffolds (He et al., 2016). While HA can contribute to improving the overall osteoconductivity of a scaffold, polymers (e.g. PLGA) contribute flexibility (Schneider et al., 2011), degradability (Makadia and Siegel, 2011), and a platform to control drug release (Sartawi et al., 2020b).

The method of fabrication is an important factor that influences scaffold properties. Numerous techniques have been utilised to prepare 3-D scaffold constructs (Li et al., 2019a, Yan et al., 2019, Zhai et al., 2018) including solvent-leaching (Sola et al., 2019), gas-foaming (Costantini and Barbetta, 2018), freeze-drying (Deville et al., 2006), 3-D printing (Kačarević et al., 2018), and electric field assisted techniques such as electrospinning and electrospraying (Zhu and Chen, 2013).

Porogen leaching has been used to create macroporous scaffolds with an interconnected pore architecture (Costantini and Barbetta, 2018). Leaching is considered an easy and cost-effective method of preparing macroporous (300-500  $\mu\text{m}$ ) scaffolds, possessing a high pore volume (>90 % pore volume) (Costantini and Barbetta, 2018). High-pressure  $\text{CO}_2$  has been used to sinter pre-prepared PLGA microspheres in the preparation of 3-D porous constructs, which supported cellular growth and infiltration throughout the scaffold (Singh et al., 2010). Although without a porogen, the overall porosity was limited to < 50 %. Compared to scaffolds prepared using mould-compressed HA, PLGA, and porogen leaching (Kim et al., 2006), resulted in scaffolds with pore volumes of >85 % with larger macropores (100-200  $\mu\text{m}$ ) and smaller interconnected pores (10-45  $\mu\text{m}$ ). All of which promoted rat calvarial osteoblast proliferation and differentiation *in vitro* as well as bone formation in subcutaneous implants in mice (Kim et al., 2006). Another study combined polymer microparticles with gas foaming and porogen leaching to fabricate an interconnected porous scaffolds (94 % porosity) preloaded with plasmid DNA that were released in a controlled manner over 3 weeks (Nof and Shea, 2002).



There are several other potential therapeutic options that can be incorporated into implantable materials that were discussed earlier in **Chapter 1**. Briefly, these included growth factors (e.g. BMP, VEGF, PDGF) (Perez et al., 2018), and small molecule therapeutics (e.g. bisphosphonates, vitamin D3) (Carbone et al., 2014). Of particular interest in this thesis has been sphingosine 1-phosphate (S1P) receptor modulation which has been shown to positively influence outcomes in bone defect studies, by supporting vascularization and chemotaxis of specific cellular contributors to bone repair (Huang et al., 2012, Das et al., 2013, Das et al., 2014b, Wang et al., 2016a, Das et al., 2015, Das et al., 2014a). Siponimod (Mayzent<sup>®</sup>), which is approved for the management of secondary progressive multiple sclerosis (Behrangi et al., 2019), is a specific agonist of S1P receptors 1 and 5 and similarly shows evidence of osteoblast differentiation and endothelial cell chemokinesis (Sartawi et al., 2020a).

The overall aim of this body of work was to design a siponimod loaded, porous, osteoconductive scaffold composed of PLGA and HA, whereby the hypothesized improvement in osteoconductivity, and the controlled localised release of siponimod would result in the induction of osteoblastic differentiation of local progenitors, ultimately contributing to enhanced bone regeneration.

## **5.3 Materials & methods**

### **5.3.1 Materials**

Electrospray materials included: poly (D, L-lactide-co-glycolide) Resomer<sup>®</sup> RG 858 S (Evonik Industries, Germany), chloroform and N, N-dimethylformamide (Sigma

Aldrich, USA), and siponimod hemifumarate was kindly gifted from Novartis (Basel, Switzerland).

Hydroxyapatite ( $\text{Ca}_5(\text{OH})(\text{PO}_4)_3$ , nanopowder <200 nm particle size), dimethyl sulfoxide (DMSO), Dulbecco's phosphate buffer saline (PBS), foetal bovine serum (FBS), L-glutamine solution, Dulbecco's Modified Eagle's Medium/Nutrient Mixture F-12 Ham (DMEM/F12), Thiazolyl Blue Tetrazolium Bromide (MTT), were acquired from Sigma Aldrich. Human umbilical vein endothelial cells (HUVEC) and their growth medium (ECGM) with associated supplements were acquired from PromoCell, Germany. The human foetal osteoblast cell line hFOB 1.19 was acquired from ATCC (ATCC<sup>®</sup> CRL-11372<sup>™</sup>).

### 5.3.2 Electrospray procedure

Solutions of PLGA (85:15) were formulated as 3 % w/w preparations in a mixture of chloroform (CLF) and dimethylformamide (DMF) at a 9:1 ratio. Reagents were dissolved in glass vials overnight at 4 °C. Prior to starting the electrospray process, solutions were equilibrated to room temperature to avoid viscosity changes. For siponimod loaded preparations, siponimod were physically mixed at a mass ratio of siponimod:PLGA 0.5:100 (henceforth termed Si 0.5:100) before dissolving reagents as before. The electrospray set-up consisted of a Spraybase<sup>®</sup> (Spraybase, Ireland) electrospray instrument kit (CAT000002), and an AL-2000 syringe pump (World Precision Instruments, USA). Sample solutions were decanted into a 10 mL glass syringe. The solutions were then primed in 1 mm diameter tubing connecting the syringe to the emitter nozzle (0.9 mm diameter). The syringe pump was set at a flow rate of 1 ml/h. A stainless-steel collection dish was covered in commercial aluminium

foil and placed at a working distance of 10-15 cm from the emitter nozzle. A voltage of 12 kV was then applied, with samples processed continuously until solution volume was dispensed. Microparticles were stored in the fume hood overnight to allow evaporation of any remaining solvent. Microparticles were then gently removed and stored in sealed plastic vials at room temperature away from light until further use.

### 5.3.3 Scaffold preparation

Scaffold preparation involved mixing PLGA/drug microparticles (7-10 mg) with NaCl porogen (size range, 250-400  $\mu\text{m}$ ) at a mass ratio of PLGA microparticles:NaCl, 1:19. The mixture was compressed in a 6 mm diameter die at a pressure (1 Ton) for 2 min. For scaffolds containing HA, the powder was combined with PLGA at a 1:6 ratio (HA:PLGA), prior to mixing with the NaCl porogen (e.g. PLGA 6 mg, HA 1 mg, NaCl 133 mg). Resultant cylindrical compacts were then saturated in  $\text{CO}_2$  gas at 800 PSI for 16 hrs prior to depressurisation. Scaffolds were then leached in MilliQ water for 12 hrs to remove the NaCl porogen and dried at room temperature, followed by storage in sealed plastic vials at room temperature, away from light until further use.

### 5.3.4 Scanning electron microscopy

Images of electrosprayed microparticles and scaffolds were acquired using a JEOL JSM-5510 scanning electron microscope (SEM). Samples were mounted on stubs with double-sided carbon tape and sputter-coated with a 10 nm thick layer of gold-palladium (80:20). Standard working distance was 8 mm, spot size 20-25, and a 3-5 kV accelerating voltage. For microparticles, images were used to investigate the morphology of samples and measure particle diameters. Three images (magnification 2000x) were acquired for each batch, with 34 individual microparticle diameters per

image manually measured using Olympus Stream software (Mason Technology Ltd, Ireland). For scaffolds, 3 images (magnification 70x) of scaffold cross-sections were acquired and used as a qualitative assessment of scaffold pore morphology.

### 5.3.5 Pore volume

To determine the porosity of prepared scaffolds, PLGA control scaffolds and composite PLGA/HA scaffolds ( $n=4$  of each) of known dry mass ( $W_{\text{dry}}$ ) and theoretical cylindrical volumes ( $V = \pi r^2 h$ ,  $V$ :volume,  $r$ :radius,  $h$ :height) were submerged in deionised water for 30 min with gentle agitation. Thereafter, surface water was carefully removed, and scaffold wet mass ( $W_{\text{wet}}$ ) was acquired. The mass of water occupying the pore volume in the scaffolds was calculated by subtracting  $W_{\text{dry}}$  from  $W_{\text{wet}}$ , which is converted to a volume assuming a water density of 1 g/ml. The pore volume was then calculated using the following equation: pore volume = Volume of ( $W_{\text{wet}} - W_{\text{dry}}$ ) / Volume of cylinder (calculated using scaffold dimensions) x 100 %.

### 5.3.6 HPLC method for drug quantitation

Liquid chromatography was used to detect and quantify the concentration of siponimod using the method detailed below. The protocol used an Agilent Technologies 1120 Compact LC instrument ( $\lambda_{\text{max}} = 278$  nm), the stationary phase consisted of a Zorbax Eclipse Plus C18 column (4.6 x 150 mm, 5  $\mu\text{m}$ ). The mobile phase was composed of acetonitrile and water at a ratio of 65:35, supplemented with formic acid 0.5 % v/v (pH  $\approx$  3.0), and operating conditions included a flow rate of 1.2 ml min<sup>-1</sup> and an injection volume of 10  $\mu\text{l}$ . UV spectrometry of siponimod solutions was used to determine peak absorbance at 278 nm.

### 5.3.7 Drug loading and release

Drug loading was determined by disintegrating samples of known mass in HPLC mobile phase to release and dissolve total siponimod content. The resulting solution underwent HPLC analysis following the protocol described above. The acquired values were divided by the theoretical loading for each scaffold, assuming ideal loading, giving a % loading efficiency.

*In vitro* release of siponimod was investigated using Si 0.5:100 scaffolds. Samples of known initial mass (ranging from 9.2-11.7 mg) were incubated in 1.5 ml PBS at 37 °C in a water bath, a volume sufficient to achieve sink conditions. The complete release medium was collected at defined time-points over a 12-week period and stored at -20 °C prior to analysis. An equal volume of fresh PBS medium was replaced in the sample vial. Prior to HPLC analysis samples were vacuum-dried overnight, and the residue re-dissolved in mobile phase, with drug content quantified following the protocol described earlier.

### 5.3.8 Differential scanning calorimetry (DSC)

In order to investigate any changes in the solid-state properties of the polymeric constituent of the scaffolds due to processing, residual solvent, inclusion of siponimod or HA, scaffolds underwent thermal analysis using a TA Q1000 differential scanning calorimeter (TA instruments, USA). All samples were evaluated using modulated-DSC (MDSC) in aluminium pans (DSC Consumables, USA), using the following settings: modulation temperature amplitude  $\pm 1.0$  °C, modulation 60 s, ramp rate 3 °C/min and a temperature range of 0-220 °C.

### 5.3.9 Young's modulus

Given the cylindrical shape of the scaffolds, Young's modulus was measured by subjecting scaffold to uniaxial compression under limited strain (30 %) to avoid scaffold rupture. Tests used a p-35 probe attached to TA texture analyser (Stable Micro Systems, UK) with associated Exponent<sup>®</sup> software. Scaffold of known dimensions were compressed at 0.1mm/sec until 30 % strain. Stress/Strain curves were produced and used to calculate the modulus of the scaffolds.

### 5.3.10 Cell culture

hFOB were maintained in DMEM/F12 supplemented with FBS (10 %), L-glutamine (1 %), and penicillin-streptomycin (1 %) at 34 °C and 5 % CO<sub>2</sub>. HUVEC were maintained in ECGM as per supplier's recommendations at 37 °C and 5 % CO<sub>2</sub>. All experiments were conducted within 10 passages for HUVEC and within 20 passages for hFOB.

### 5.3.11 Evaluation of metabolic activity

#### 5.3.11.1 Indirect assessment

The metabolic activity of cells indirectly exposed to scaffolds was evaluated in order to determine the impact of eluted drug and polymer breakdown products on cells in close proximity to the scaffolds. PLGA controls, and Si 0.5:100 scaffolds were sterilised in 70 % ethanol for 5 min, then washed in PBS and dried overnight. Thereafter, scaffolds were added to 24 well plates pre-seeded with  $5 \times 10^4$  cells/well of hFOB or HUVEC in 600 µl of their respective cell culture medium. The scaffolds were incubated with the cells for 5 days, with culture medium changed every other day. To determine metabolic activity after 5 days, the scaffolds were removed and 60

$\mu$ l thiazolyl blue tetrazolium bromide (5 mg/ml solution) was added directly to 600  $\mu$ l of cell culture medium for 2 hrs. Resultant formazan crystals were solubilized with 600  $\mu$ l DMSO. 100  $\mu$ l of each well was transferred to a 96-well plate to measure absorbance at 570 nm using a Wallac Victor2 plate reader (Perkin Elmer, USA).

#### 5.3.11.1 Direct assessment

The metabolic activity of hFOB seeded directly on scaffolds was evaluated in order to determine the impact of physical and chemical properties of the scaffolds on osteoblast cell metabolic activity. Selected scaffolds of PLGA, PLGA/HA, Si 0.5:100, and Si/HA 0.5:100 were sterilised in 70 % ethanol for 5 mins, washed in PBS, then incubated in FBS for 5 mins, before being dried overnight.

On the day of the experiment, scaffolds were placed in 24 well plates, and hFOB ( $2 \times 10^5$  cells in 20  $\mu$ l) were added to both the top and bottom of the scaffold, allowing 10 min before the scaffold was flipped over. Thereafter, cell culture medium was made up to 600  $\mu$ l slowly to avoid disturbing scaffold seeding. After 24 hrs (and again on days 3 and 5), scaffolds were transferred to new wells, and resazurin (120  $\mu$ l of a 560  $\mu$ M stock) was added to 600  $\mu$ l of freshly added cell culture medium and incubated for 3.5 h. Subsequently, 100  $\mu$ l of medium from each sample was transferred to a 96 well plate for fluorescent plate reading at excitation 488 nm/emission 595 nm using a Wallac Victor2 plate reader (Perkin Elmer, USA).

#### 5.3.12 Statistical analysis

Results are expressed as mean  $\pm$  standard deviation (SD), unless otherwise stated. Statistical analysis was performed using one-way analysis of variance (ANOVA)

followed by Bonferroni post-test for multiple comparisons. In all cases differences were considered significant at  $p < 0.05$ .



## 5.4 Results

### 5.4.1 Preparation of porous scaffolds

Guided by the published literature, the electrospray parameters were optimised by varying voltage, working distance and spray rate. Finalised parameters produced microparticles that were generally concave, biconcave, or raisin shaped. The particle size distribution of PLGA control and drug loaded Si 0.5:100 microparticles are presented in Figure 5.1. There was a statistically significant difference in microparticle diameter distribution between the PLGA control (3.4  $\mu\text{m}$ ; 0.47  $\mu\text{m}$ ) compared to Si 0.5:100 (4.1  $\mu\text{m}$ ; 1.0  $\mu\text{m}$ ) ( $p < 0.05$ ). Furthermore, the PLGA control exhibited a narrow size distribution compared to the siponimod loaded microparticles.

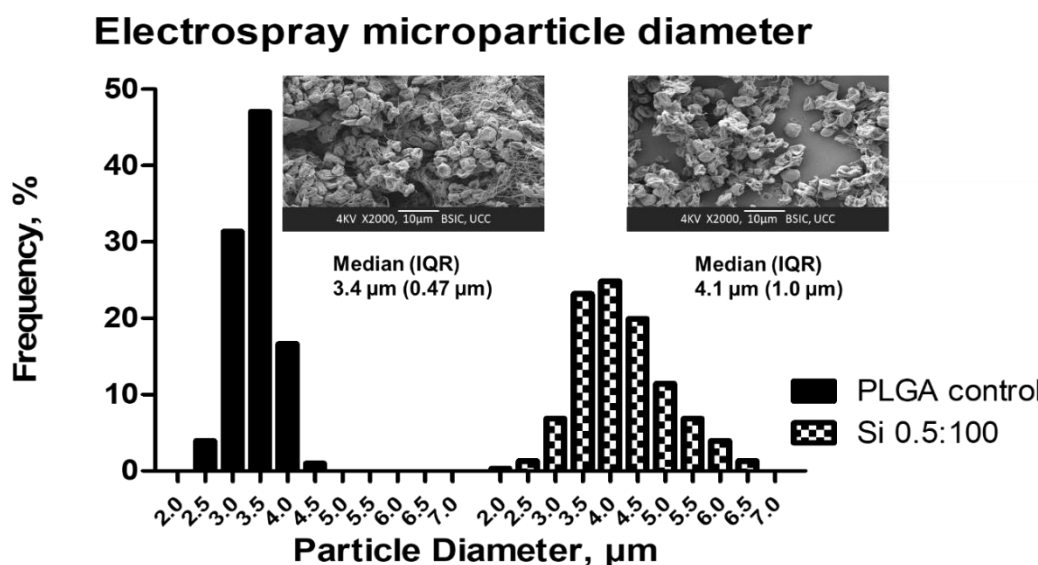


**Figure 5.1** Electrosprayed microparticle diameter determined from manual measurements of SEM images (Inset: representative image). (A) PLGA control microparticles ( $n=1$  batch, 3 images total) (B) Si 0.5:100 microparticles ( $n=3$  batches, 9 images total). Image magnification x2000 (10  $\mu\text{m}$  scale bar). Histograms represent

frequency of particle diameter distribution as determined by manual measurements taken from SEM images (3 images per batch, 34 individual particle measurements per image). Inset values represent the median and interquartile range. Statistical analysis of the two populations involved Mann-Whitney U test to determine statistical significance. Diameters are given as median diameter; interquartile range.

Scaffolds composed of electrosprayed particles together with NaCl were processed with CO<sub>2</sub> foaming and subsequent leaching of the NaCl produced a 3-D porous structure Figure 5.2. A qualitative assessment of cross-sectional images showed the outlines of pores with diameters ( $\approx 200\text{--}300\ \mu\text{m}$ ) corresponding to the porogen diameter (perimeter indicated in Figure 5.2). Additionally, Si/HA 0.5:100 appeared to possess smaller pores on the walls of the microporous structure (red arrows in Figure 5.2).

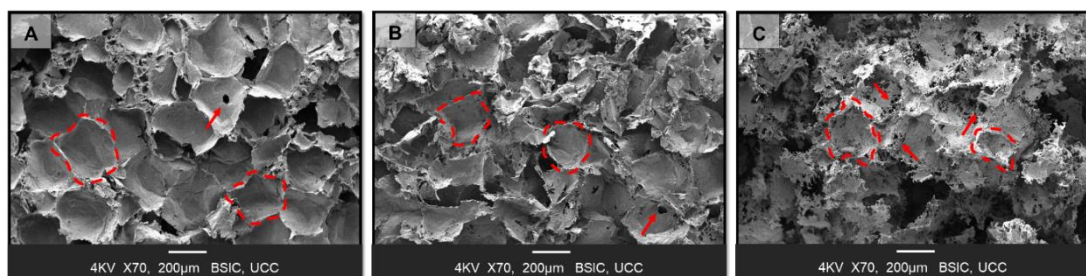


**Figure 5.2** SEM images of scaffold cross-sections. (A) PLGA control scaffold (B) Si 0.5:100 (C) Si/HA 0.5:100. Image magnification 70x (200  $\mu\text{m}$  scale bar). Red dashed lines indicate pore outlines, and red arrows indicate small interconnecting pores.

For a quantitative measure of porosity, pore volume was measured for PLGA control and PLGA/HA scaffolds. Results showed that PLGA control scaffolds had pore volume of  $70.1 \pm 3.3$  % while PLGA/HA scaffolds exhibited a porosity of  $83.7 \pm 9.5$  %, which was statistically significantly different ( $p < 0.05$ ).

#### 5.4.2 Loading efficiency and drug release

Drug loading efficiency corresponded to  $48.5 \pm 2.2$  % of theoretical mass of drug with actual drug loading ranging from 22.3-28.4  $\mu\text{g}$ . Figure 5.3 shows the results of cumulative siponimod release from porous scaffolds. By day 90, the cumulative drug release from Si 0.5:100 scaffolds was  $36.7 \pm 0.1$  % of actual drug loading. Following the terminal sampling point in the release study, scaffolds were disintegrated, and the remaining drug was dissolved in HPLC mobile phase to quantify the remaining entrapped drug. Results showed that  $64.5 \pm 3.2$  % of actual drug loaded mass was accounted for. Using the Korsmeyer-Peppas equation  $M_t/M_\infty = Kt^n$  where  $M_t/M_\infty$  is the fraction of drug released over time, K is the release rate constant, n is the release exponent the value of which characterises the release mechanism of the drug. The Si 0.5:100 had an 'n' value of 0.57, indicating siponimod release from these samples was consistent with Fickian diffusion (Peppas, 1983).

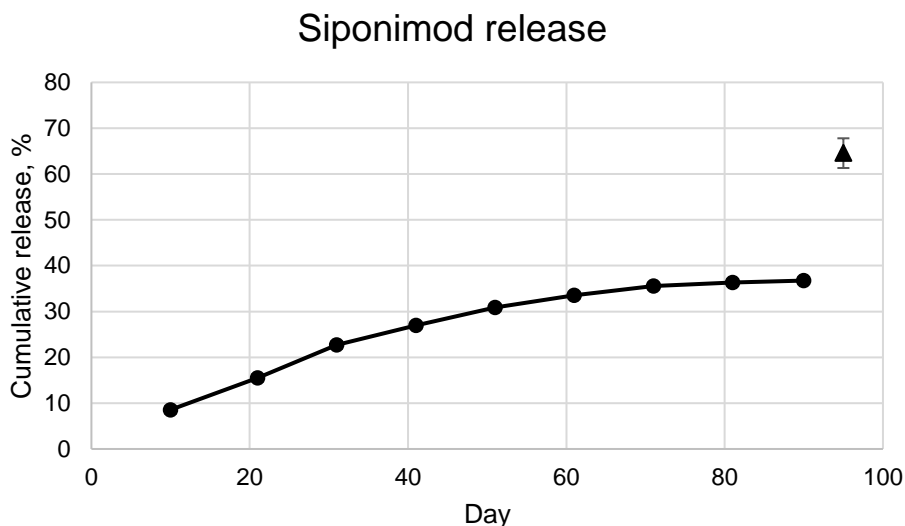


**Figure 5.3** Controlled release of siponimod from porous scaffolds over 90 days. Data represents samples of Si 0.5:100 ( $n=3$  batches, each with 3 technical replicates). Data was multiplied by a correction factor taking into account actual scaffold loading efficiency. The triangle represents the total amount of siponimod quantified including cumulative release at day 90 and drug remaining in the scaffold following the final time point (acquired by disintegrating scaffolds in HPLC mobile phase). Each data point is presented as mean  $\pm$  SD.

#### 5.4.3 Physical characterisation – DSC & Young's modulus

As part of the characterisation of a selection of scaffolds, PLGA control, PLGA/HA, Si 0.5:100, and Si/HA 0.5:100 were analysed alongside starting materials to investigate any changes in their solid-state behaviour due to processing (Figure 5.4A). The unprocessed PLGA starting material showed a glass transition temperature ( $T_g$ ) at 53.35 °C, HA base material showed no discernible thermal signals, while siponimod displayed a melting endotherm at 135.80 °C. The scaffolds showed no distinct changes with regard to the  $T_g$  of the polymeric constituent of scaffolds, with PLGA controls

(53.40 °C), PLGA/HA (52.28 °C), Si 0.5:100 (53.45 °C) and Si/HA 0.5:100 (54.57 °C) exhibiting similar values. The addition of HA and siponimod similarly did not result in any observable signals in their respective scaffolds.

Scaffolds were investigated for their Young's modulus (Figure 5.4B). The scaffolds' moduli are shown for PLGA control ( $0.22 \pm 0.09$  MPa), PLGA/HA ( $0.09 \pm 0.05$  MPa), Si 0.5:100 ( $0.22 \pm 0.14$  MPa), and Si/HA 0.5:100 ( $0.19 \pm 0.09$  MPa). There was no statistically significant difference between the experimental groups ( $p=0.28$ ), despite HA-containing samples appearing to show a reduction in Young's modulus. This is likely due to the inherent variability in the dataset.

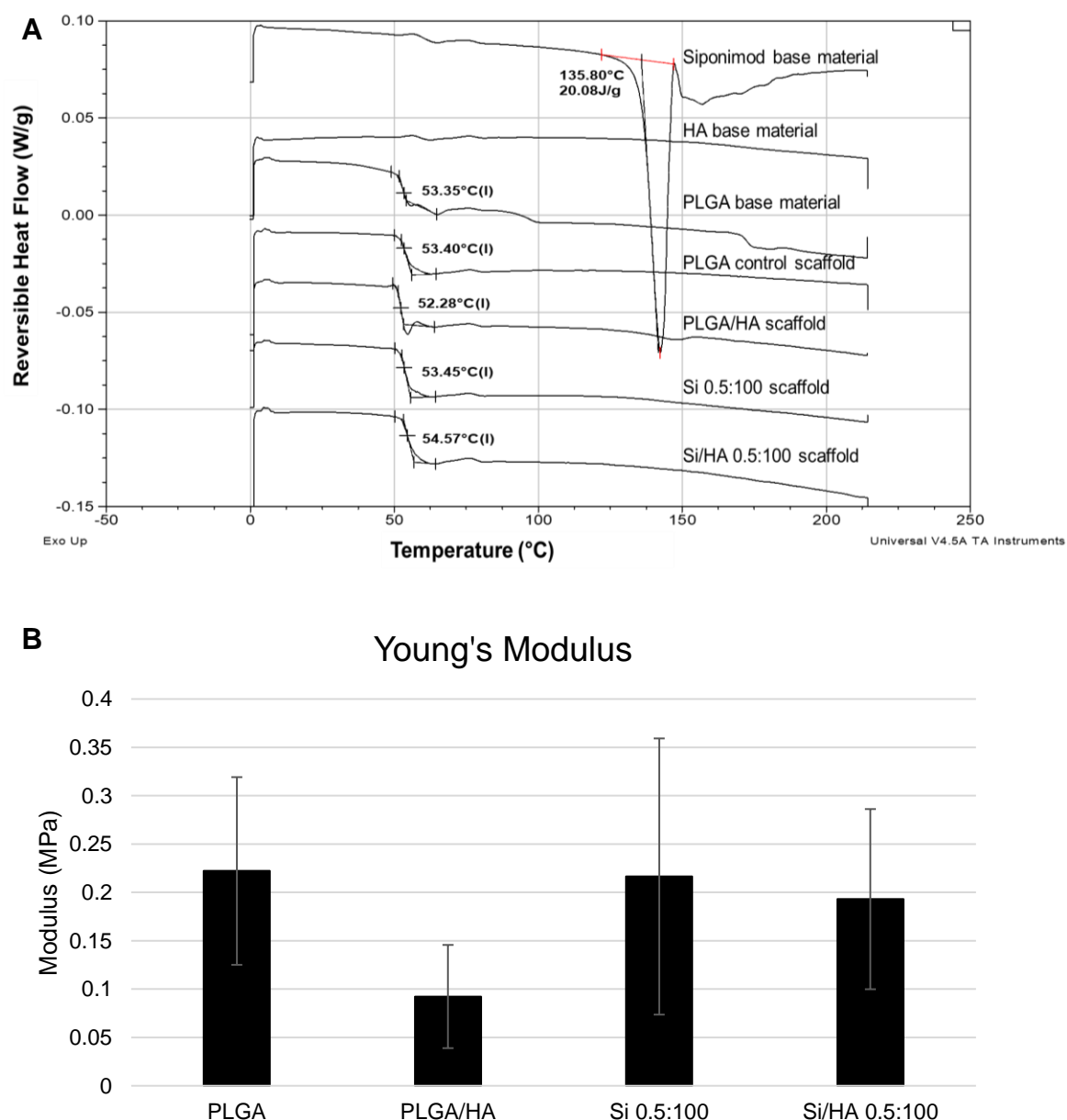


**Figure 5.4** Physical properties of scaffolds. (A) Differential scanning calorimetry of scaffolds and starting materials using MDSC. (B) Young's modulus of scaffolds (30 % strain), data represents scaffold samples of PLGA, PLGA/HA, Si 0.5:100, and Si/HA 0.5:100. In all cases  $n=1$  batch with 4 scaffolds per condition evaluated. Data is presented as mean  $\pm$  SD.

#### 5.4.4 Evaluation of metabolic activity – Indirect & direct assessment

In order to determine the indirect effect of scaffolds on the metabolic activity of hFOB and HUVEC, scaffolds were incubated with each of the two cell types for 5 days (Figure 5.5A&B). HUVEC incubated with PLGA control scaffolds exhibited absorbance values of  $0.81 \pm 0.11$ , which was similar to the scaffold free condition ( $0.86 \pm 0.13$ ). While HUVEC incubated with Si 0.5:100 scaffolds showed an absorbance of  $0.59 \pm 0.15$ , this difference was not statistically significant ( $p=0.10$ ). In the experiment using hFOB, PLGA control scaffolds exhibited absorbance values of  $0.73 \pm 0.12$ , which was comparable to the absorbance ( $0.73 \pm 0.15$ ) data for the scaffold free conditions. Again, the reduction in metabolic activity for cells incubated with Si 0.5:100 scaffolds was not statistically significant ( $p=0.35$ ).

The results of the direct assessment of the metabolic activity of hFOB incubated with scaffolds over 7 days are shown in Figure 5.5C. There were no statistically significant changes in the metabolic activity of hFOB directly seeded on scaffolds. However, a similar trend was observed across the experimental groups. Specifically, from day 1 to day 7 fluorescence values ( $\times 10^3$ ) for the PLGA control scaffold increased from  $45.3 \pm 11.7$  to  $57.7 \pm 2.9$ , PLGA/HA scaffolds showed values of  $53.0 \pm 12.6$  increasing to  $72.0 \pm 8.1$ , drug-loaded Si 0.5:100 scaffolds resulted in values of  $50.3 \pm 10.9$  increasing to  $57.3 \pm 2.8$ , and finally Si/HA 0.5:100 scaffolds which resulted in fluorescence values of  $47.9 \pm 11.2$  increasing to  $68.5 \pm 6.7$ .

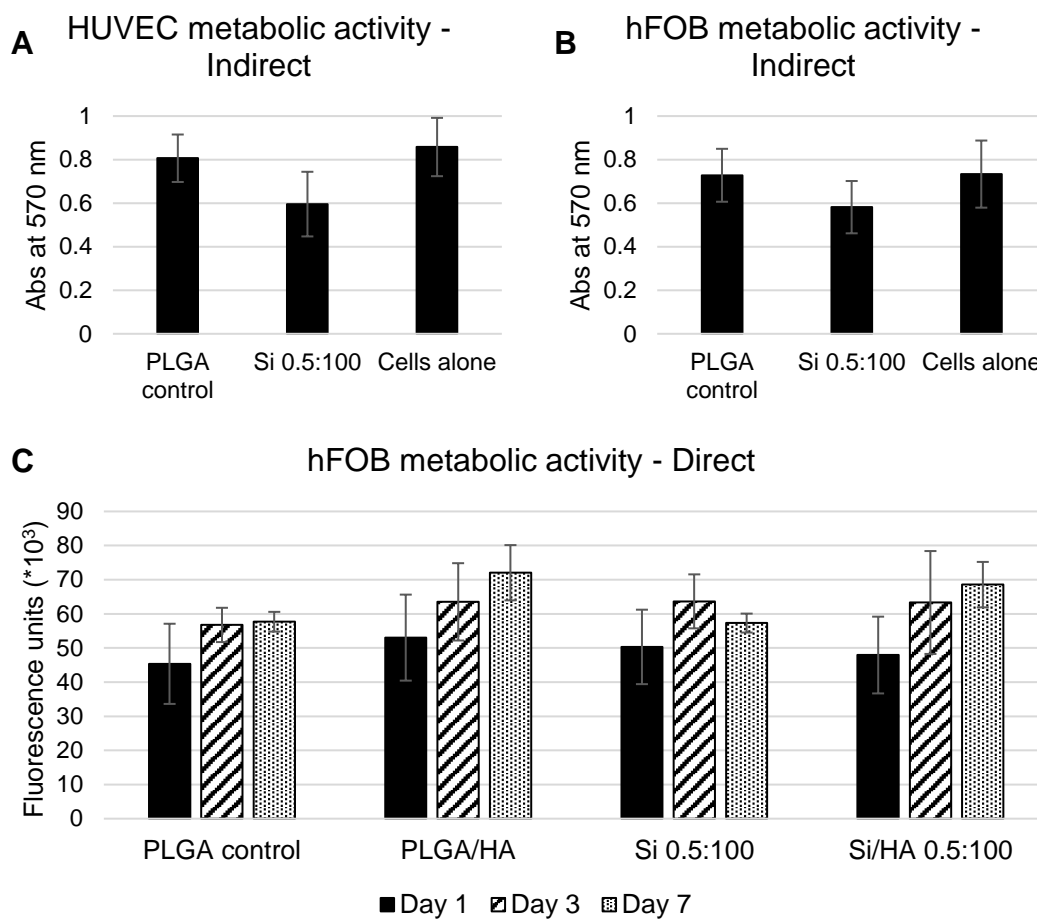


**Figure 5.5** Metabolic activity of cells incubated indirectly and directly with scaffolds over time. Indirect assessment using MTT after 5 days (A) HUVEC,  $n=3$  (3 technical replicates) (B) hFOB,  $n=3$  (3 technical replicates), data represents the mean  $\pm$  SD of absorbance at 570 nm. Direct assessment using resazurin assay over 7 days (C) hFOB,  $n=2$  (3 technical replicates), data represents the mean  $\pm$  SD of fluorescence units at excitation 488 nm/emission 595. ‘‘ $n$ ’’ represents the number of independently repeated experiments. Statistical analysis used one-way (for A & B) and two-way (for C) analysis of variance.



## 5.5 Discussion

The aim of this chapter was to develop and characterise a siponimod loaded, porous, osteoconductive scaffold composed of PLGA and HA. Siponimod loaded polymer microparticles were prepared using electrospraying, followed by high-pressure CO<sub>2</sub> foaming, and porogen leaching. These scaffolds underwent investigations to be followed by investigations into whether they can contribute to enhancing bone regeneration in tissue engineering applications.

Electrospraying is a highly efficient technique for the generation of particles, and which is of increasing interest in tissue engineering research (Correia et al., 2014, Jeyhani et al., 2017), due to flexibility in processing a wide array of materials, the capability to entrap a range of drug cargoes, and good production capacity (Deng et al., 2006, Parhizkar et al., 2017). The electrospray process resulted in microparticles with a collapsed morphology. The sphericity of electrosprayed particles has been associated with the concentration of added solutes and the concentration of the sprayed polymer (Bohr et al., 2012). Generally, sphericity is considered to increase with increasing concentrations of added solutes or of the base polymer, up to a point. However, after a defined concentration the jet of particles can deform and elongate into a jet of fibres (Jeyhani et al., 2017, Almería et al., 2010). Particle sizes can also be reduced by altering processing variables including decreasing the needle-collector distance, or the flow rate, or by increasing conductivity of the electrosprayed solution (Yao et al., 2008). The median particle sizes were 3.4 µm for PLGA control particles and were significantly smaller than Si 0.5:100 particles at 4.1 µm, this may be due to slight differences in the concentration of electrospray solution concentration, caused by the respective presence or absence of siponimod for each of the PLGA control and

Si 0.5:100 scaffolds, or indeed small changes to the conductivity of electrospray solutions containing siponimod might also have played a role. All told, perfectly spherical particles were not a prerequisite given the additional fabrication steps employed subsequently (compression, gas foaming, porogen leaching).

The purpose of combining gas foaming with porogen leaching was to produce a macroporous structure. In this work, scaffolds exhibited pores in the range of 200-300  $\mu\text{m}$  with smaller interconnected pores also evident. This range is known to be suitable to enabling cell infiltration (Yang et al., 2001).

High-pressure  $\text{CO}_2$  has been used for a number of scaffold materials, including ceramics (Kim et al., 2002), and polymers such as PLA, PCL, and PLGA (Matuana, 2008, Jang and Shea, 2003, Moghadam et al., 2017). One study illustrated the benefits of coupling gas foaming with porogen leaching, whereby polycaprolactone/HA scaffolds prepared using only supercritical  $\text{CO}_2$  gas foaming supported human mesenchymal stem cell growth. But the limited volume of pores (40-60 %) was said to impede more favourable cell adhesion and proliferation (Moghadam et al., 2017). In order to obtain scaffolds with high pore volumes, the polymer microparticles prepared herein were mould-compressed with a porogen and processed using high-pressure  $\text{CO}_2$ . This duly resulted in scaffolds with large pore volumes, with statistically significant differences in pore volume between PLGA control scaffolds ( $70.1 \pm 3.3$  %) and PLGA/HA scaffolds ( $83.7 \pm 9.5$  %), which may be due to the increased presence of in micropores and subsequently increased pore interconnectivity. However, there is the possibility that some of the smaller pores were due to leaching of HA.

Regarding drug loading, the electrospray process is known to result in good loading efficiencies upwards of 80 %, with high batch-to-batch reproducibility (Nguyen and Jeong, 2018). However, the scaffolds prepared in this study had a loading efficiency of  $48.5 \pm 2.2$  %, which was attributed to drug loss that occurred during the porogen leaching step. The loss suggests that siponimod was distributed both within and on the surface of the foamed polymer scaffolds. The loss of surface entrapped drug during the leaching step also explains the lack of burst effect in the early stages of the drug release study. The duration of the observed release pattern (months) was in line with timeframes associated with bone regeneration, and other similarly designed scaffolds for long-term applications (Zhang et al., 2017). The quantity of siponimod released,  $36.7 \pm 0.1$  % of the drug in the scaffold by day 90, suggests that local concentrations would be equivalent to  $\approx 500$  nM (assuming a volume of 1 ml and 0.5 % release per day), a concentration sufficient (Sartawi et al., 2020a) to elicit a response from *in vitro* cell targets (e.g. osteoblast differentiation). However, disintegration of scaffolds after the release tests to account for the remaining entrapped drug, highlighted that only  $64.5 \pm 3.2$  % of total drug loading was accounted for. This may have been due to the influence of experimental conditions i.e. experimental temperature of 37 °C on the stability of siponimod, which has been shown to have an adverse impact on the drug's stability (Sartawi et al., 2020b).

Considering physicochemical characterisation, DSC results did not show any indication of changes to thermal behaviour of the polymeric constituent of the scaffolds due the addition of HA, or indeed siponimod (a result similar to the scaffold design in **Chapter 4**). In particular, there were no changes in the T<sub>g</sub> of the polymeric constituent of the scaffolds throughout processing, while the HA component provided

no relevant signals. Siponimod showed a melting endotherm at 135.80 °C (122 – 147 °C), in comparison to a literature-based polymorphic form with a value of 110 °C (Liu et al., 2012). However, it is likely that the sensitivity of the calorimeter precluded detecting the small concentrations of siponimod within the scaffold samples. Regarding mechanical properties, synthetic polymers such as PLGA have generally provided poor structural properties when attempting to mimic the properties of bone (Koons et al., 2020). The addition of CaP is one method that has been used to enhance the Young's modulus of polymer composite scaffolds, as the mineral phase is thought to increase the low stiffness characteristic of polymers (Sui et al., 2007). Despite this there is evidence showing that the addition of HA often fails to improve mechanical strength of scaffolds (Wagoner Johnson and Herschler, 2011). Indeed, in our case the addition of HA to scaffolds did not result in a significant change in material stiffness, with Young's modulus values ranging from 0.09-0.22 MPa. Although the data was variable, and it is difficult to make a conclusive determination, the trend in the data suggested those scaffolds that contained HA appeared to have lower Young's modulus values (i.e. lower stiffness), this may have been due to the increased porosity of PLGA/HA compared to other scaffolds as increasing porosity can result in deterioration of a scaffold's resistance to compression potentially causing it to collapse (Byrne et al., 2007). Contrasting the values acquired for the scaffolds with the compressive Young's modulus of cancellous bone of 489 MPa (Røhl et al., 1991), and it remains clear that this type of design should only be considered in non-weight-bearing settings.

Experiments evaluating the impact of incubating scaffolds directly and indirectly with cells revealed there were no statistically significant increases in cell metabolic activity

compared to cell only controls. However, the data did indicate that the scaffolds were nonetheless compatible with the growth of osteoblasts and endothelial cells. This result is similar to that observed earlier in **Chapter 4** (Sartawi et al., 2020b).

With regard to limitations of this design and the study in general, the mechanical properties of the scaffolds were not shown to be consistent with natural bone. Additionally, the mechanical testing approach was limited by high variability, a more accurate measurements could be undertaken using nanoindentation (Chowdhury et al., 2005). Other more specific issues related to this work include the lack of uniform scaffold mass between some of the experimental procedure, which hindered making comparisons throughout the chapter. Another limitation was the lack of functional *in vitro* cell-based experiments to show the functionality of released siponimod. Another issue is the low drug-loading efficiency (<50 %), which although anticipated due to the porogen leaching step, indicated the need for additional modifications to the fabrication process to avoid excessive drug waste.

To the best of our knowledge siponimod has not previously been prepared as part of an electrosprayed, porous scaffold for bone regeneration applications. Siponimod has previously been incorporated into an electrospun scaffold that showed promising *in vitro* effects on osteoblasts and endothelial cells, however failed to significantly stimulate regeneration in a rat critical cranial defect (Sartawi et al., 2020b), possibly due to poor cellular infiltration within the dense fibre matrix limiting scaffold-bone interface. With further development the porous scaffold described herein may represent a better option in translating the *in vitro* effects of siponimod to an *in vivo* setting.

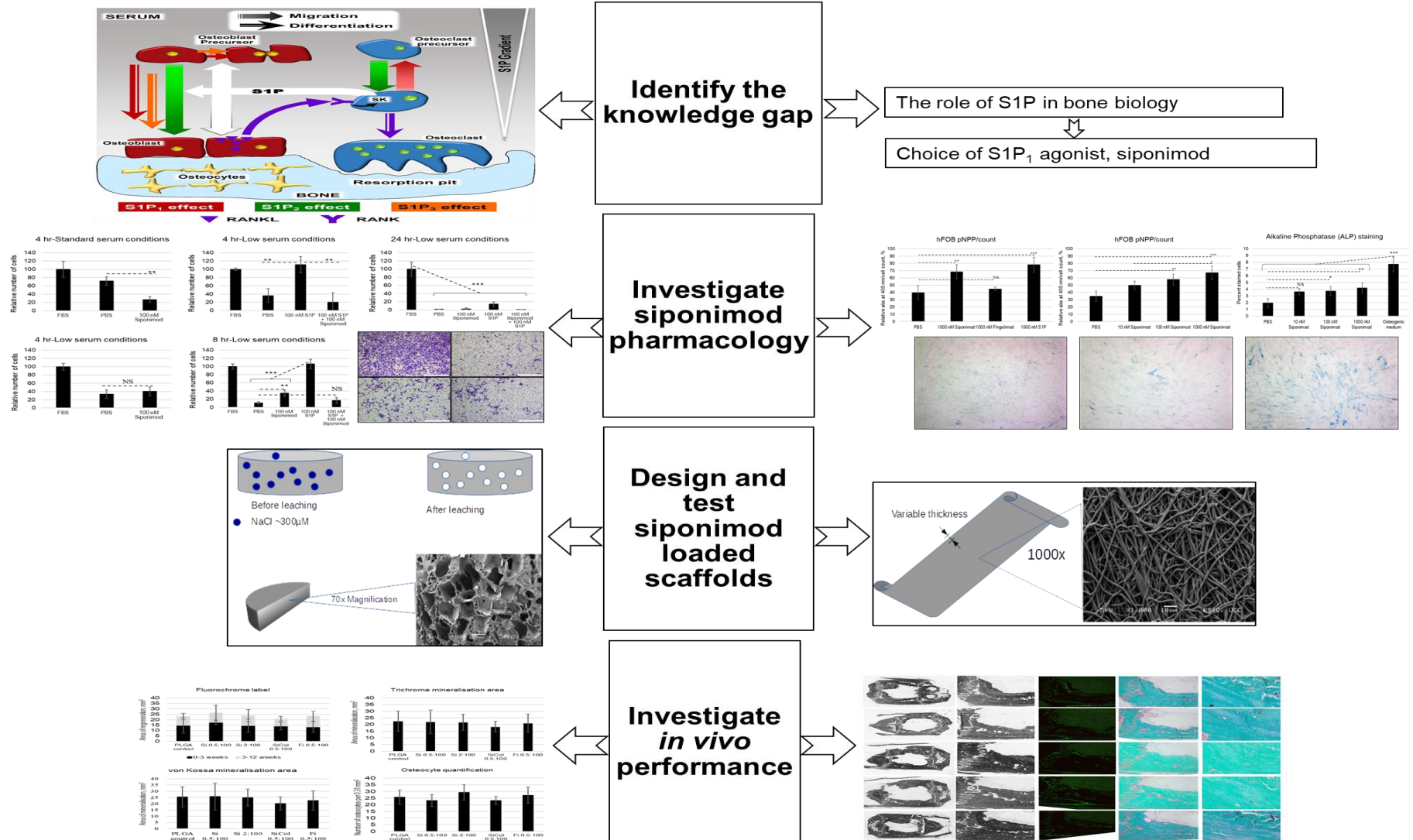
## 5.6 Conclusion

This preliminary work aimed to illustrate the design and *in vitro* characterisation of a porous scaffold fabricated using electrospraying, gas foaming, and porogen leaching. The scaffolds were comprised of a siponimod loaded microparticle polymer base, coupled with HA to improve osteoconductivity. The scaffold was designed as a potential replacement material in cases of non-weight bearing critical bone defects and marks a contribution to knowledge as it represents the first application of siponimod as part of an electrospray or gas foamed scaffold system. Scaffolds resulted in controlled drug release with a linear profile over a suitable timeframe for bone regeneration, however the use of porogen leaching likely adversely impacted loading efficiency. The scaffolds showed good porosity and were compatible with hFOB indicating stable metabolic activity over 7 days. The addition of HA did not result in any notable statistically significant results, rather it appeared to weaken the overall mechanical integrity of the scaffold, indicating further HA ratio optimisation is required. Changes to HA incorporation will most likely lead to positive improvements in scaffold osteoconductivity. However, the effects of siponimod in particular must be rigorously investigated both *in vitro* and *in vivo* using this scaffold design, before this design can be seen as a potential avenue of future research in bone tissue engineering applications.

# Chapter 6

## General discussion and conclusions

## Graphical Overview and Summary





## 6.1 Overview and Summary

Tissue engineering plays an important role in providing replacement materials to assist in the regeneration of the form and function of damaged tissue (Vacanti and Vacanti, 2014). There have been notable successes associated with the field, including the Dermal Regeneration Template, Integra<sup>®</sup>, and the spinal fusion bone graft, INFUSE<sup>®</sup> (Hoffman et al., 2019). However, despite the number of researchers and companies undertaking tissue engineering research, the exponential increase in research related publications (Hoffman et al., 2019) and even the progression of some products to clinical trials, the translation of new innovative products to the clinic has been poor (Kim et al., 2019b). It must also be noted that even relatively successful endeavours, such as INFUSE<sup>®</sup>, have limitations including ectopic bone growth and an increased likelihood of additional corrective surgeries (Epstein, 2013). Therefore, there remains a need to continue investigating and developing novel pharmaceutical and biomaterial strategies underpinning BTE research, namely scaffolds, cells and osteoinductive cues.

Research in BTE has taken its inspiration from the composition and structure of native bone tissue. Indeed, efforts have concentrated on scaffold constructs that attempt to recapture the hierarchical structure of bone (Nijsure and Kishore, 2017, Rho et al., 1998). This can be achieved by utilising materials that closely match the organic extracellular matrix components and inorganic mineral constituents of bone (Shekaran and García, 2011, Mohamed, 2008), in an effort to approximate the mechanical properties of bone (Wang et al., 2016b, Hench, 2013), and mimic the bioactive functionalities inherent in viable bone tissue (Walsh, 2015, Copp and Shim, 1963, Raggatt and Partridge, 2010). Clearly, approximating bone's mechanical, physical and

chemical properties is not a simple proposition, and no single material or biomaterial (outside of cortical autograft (Greenwald et al., 2001)) can realistically fulfil all of these requirements. Consequently, numerous materials have been investigated including natural and synthetic polymers, bioactive ceramics and glasses, and composites of the same (Stevens, 2008). Promising materials have also been coupled with active agents including biologicals such as growth factors (De Witte et al., 2018), small molecule therapeutics (Carbone et al., 2014) and platelet rich plasma (Cheng et al., 2018), to further impart beneficial regenerative potential to the BTE design. While often producing superior bioactivity, the use of growth factors is limited by side effects (Cahill et al., 2015) and biologic instability (Chen and Mooney, 2003). Small molecule therapeutics on the other hand, can avoid issues of biologic instability, but also possess limitations including weaker and less specific activity (Carbone et al., 2014).

Taking these factors into account, the general aim of this work has been to investigate the bone reparative potential of a novel, small molecule therapeutic agent, siponimod, and develop scaffold constructs appropriate for its spatiotemporal presentation for BTE applications. The design approach focused on utilising biomaterial orientated constructs consisting of the biodegradable and biocompatible polymer, PLGA as the base material coupled with additives to impart enhanced bioactivity.

This thesis began with a general introduction in **Chapter 1**, which provided context pertaining to the ideal and available scaffold materials, scaffold fabrication methods, and pharmacological additives. Furthermore, the chapter highlighted the benefits and limitations of current materials and scaffold fabrication techniques, providing recent examples for each. **Chapter 2** reviewed the available literature surrounding the

targeting of S1P signalling, and its role in bone biology. This analysis of the S1P literature informed our hypothesis that the S1P<sub>1/5</sub> receptor agonist siponimod would be a suitable small molecule bioactive agent in stimulating bone repair due to the balance of data supporting the role of the S1P<sub>1</sub> receptor in the proliferation, differentiation, and migration of osteoblasts and endothelial cells. The role of **Chapter 3** was then to test this hypothesis *in vitro* and investigate the bone regenerative potential of siponimod, by determining its impact on key cell players implicated in bone regeneration using relevant metrics - proliferation, differentiation, and migration effects on hFOB and HUVEC.

From the wider literature on bone repair, it was clear that the use of S1P agonists (and other small molecules or growth factors) benefit from a localised and controlled application rather than systemic delivery. Therefore, **Chapters 4 & 5** investigated formulation design aspects using electrospinning and electrospray/porogen leaching methods to prepare drug-loaded scaffold constructs that could fulfil the localised controlled release of siponimod. These techniques were used because electrospinning and electrospraying, as described in their respective chapters, are highly efficient methods of preparing drug-loaded microstructures that allow the formulation of a variety of potential materials and drug cargoes. The developed scaffolds were required to display several desirable features including biocompatibility, biodegradation, osteoconductivity and ideally appropriate mechanical properties. Only the electrospun formulation in **Chapter 4** was progressed to the stage of *in vivo* analysis, due to limitations of time and material. However, both **Chapter 4** and **Chapter 5** provided useful information, especially regarding scaffold performance and has provided a

good foundation for future design decisions both for bone regeneration and more broadly for other therapeutic applications.

## 6.2 Contribution to knowledge

All in all, despite the lack of *in vivo* bone regeneration seen with the developed electrospun scaffolds, this body of work contributes valuable new knowledge to the ever-growing fields of bone tissue engineering and S1P receptor research. The specific contributions to knowledge can be summarised as follows:

- **Chapter 2** – This survey of the literature informed our choice of a selective S1P<sub>1/5</sub> agonist, siponimod, as the small molecule of interest. As of writing, the published work associated with this chapter is one of only three available reviews contributing to our understanding of the involvement of S1P signalling, specifically the S1P<sub>1</sub> receptor, in bone regeneration.
- **Chapter 3** – This is the first published research utilising a selective S1P<sub>1/5</sub> agonist, siponimod, for its potential role in bone regeneration. It is one of the very few publications documenting an effect of siponimod in any biological system expressing endogenous S1P<sub>1</sub> receptors. The notable findings in this chapter were siponimod's stimulation of endothelial cell migration, and the stimulation of osteoblast differentiation with an effect equivalent to that of S1P.
- **Chapter 4** – This is the first published research describing the preparation of a siponimod loaded scaffold for bone regenerative applications. This work provided greater insights into factors impacting siponimod stability (e.g. solid

or liquid state, temperature, storage time), formulation design (e.g. the effect of solvent), and demonstrated that functionally active siponimod was released in a controlled and stable fashion across a range of concentrations. Despite ultimately showing no significant effect *in vivo*, this work provided useful insights for future experimentation and indeed for other investigators across other fields.

- **Chapter 5** – While early in development, this work provided the basis for an alternative formulation design with substantial porous architecture, effective cytocompatibility and controlled release of siponimod suitable for localised delivery. All of which warrants further development and investigation.

### 6.3 Interpretation and implications of the thesis findings

The following sections will provide a brief discussion of each of the thesis objectives, and their implications.

6.3.1 Objective I: To review the role of S1P signalling in bone repair and identify S1P<sub>1</sub> receptor agonists as targets for experimental investigation.

As a first step, the properties of S1P its receptor signalling and their involvement in bone biology and the process of bone repair were reviewed (**Chapter 2**). The chapter reviewed the effects of S1P in stimulating osteoblast precursor cell migration (Roelofsen et al., 2008) and differentiation (Brizuela et al., 2014), and discussed the mechanism of S1P signalling on osteoblast proliferation (Carpio et al., 1999, Lampasso et al., 2001, Grey et al., 2004), and differentiation (Grey et al., 2004, Sato et al., 2012) and the lack of migration response in mature osteoblasts. Thereafter, it

highlighted the influence of S1P signalling on osteoclast recruitment (Ishii et al., 2009, Lee et al., 2017) and osteoclast-osteoblast crosstalk (Meshcheryakova et al., 2017). The chapter concluded with some examples of efforts in S1P delivery, including the endogenous compound (Sefcik et al., 2008) as well as the synthetic analogue fingolimod (Das et al., 2014b).

This chapter indicated the knowledge gap that could be filled by investigating a specific S1P<sub>1</sub> receptor agonist and its potential in bone regeneration. Osteoblasts are known to express each of the S1P<sub>1</sub>, S1P<sub>2</sub> and S1P<sub>3</sub> receptors (Grey et al., 2004, Ryu et al., 2006, Keller et al., 2014), but the overall balance of the literature indicated that S1P<sub>1</sub> in particular and to a lesser extent S1P<sub>3</sub> receptors are promising targets for influencing the bone repair process. This narrowing of S1P receptor criteria eliminated the less selective agents, S1P and fingolimod. This resulted in a few potential therapeutic agents including siponimod (licensed as Mayzent® in January 2020), ozanimod (licensed as Zeposia® in March 2020), and ponesimod (in development) being considered for experimentation. From these siponimod was selected due to its availability and its position as the most advanced in clinical development at the time when these studies were initiated. Finally, after scrutinising the existing efforts in S1P delivery, it was clear that a localised controlled release approach was the most suitable.

6.3.2 Objective II: To determine the effect of siponimod on key cell players, osteoblasts and endothelial cells, implicated in bone regeneration using cell proliferation, differentiation, and migration as metrics.

The work in **Chapter 3**, aimed to advance the body of knowledge in the literature (described in **Chapter 2**), which indicated that S1P signalling was involved in several

cellular mechanisms fundamental to bone regeneration. Specifically, **Chapter 3** investigated the effects of the S1P<sub>1</sub> receptor agonist, siponimod, on osteoblasts and endothelial cells.

Beginning with siponimod's effect on osteoblasts, results showed that siponimod had no effect on osteoblast cell viability and proliferation, which was in contrast to the available literature, which had previously shown that stimulation with the endogenous and non-subtype selective S1P may support osteoblast viability (Carpio et al., 1999, Lampasso et al., 2001). This may indicate that S1P<sub>3</sub> plays the more substantial role with regards to cell viability, while S1P<sub>1</sub> receptor modulation influences differentiation rather than proliferation. The latter was confirmed by significant findings identifying siponimod's stimulation of osteoblast differentiation with an effect equivalent to that of S1P. Osteoblast differentiation via S1P signalling is known to be associated with the S1P<sub>1</sub> (Matsuzaki et al., 2013) and S1P<sub>3</sub> (Brizuela et al., 2014) receptors, however the literature is conflicted over which of the two is more relevant. Our results strongly suggest that it is indeed the S1P<sub>1</sub> receptor that produces the observed effects, this is supported by the high specificity of the siponimod molecule signified by its subnanomolar EC<sub>50</sub> (Lukas et al., 2014, Gergely et al., 2012).

With regard to siponimod's effect on endothelial cells, it is known that S1P receptors are implicated in vasculogenesis and angiogenesis (Oyama et al., 2008, Waeber, 2013a, Takuwa et al., 2010, Lucke and Levkau, 2010), and indeed S1P<sub>1</sub> is the predominant receptor subtype expressed in endothelial cells (Igarashi et al., 2003). Our results confirmed siponimod had no adverse effect on viability nor stimulation of cell proliferation, despite the known stimulatory effect of S1P on endothelial cells

(Kwon et al., 2001, Panetti, 2002). With regard to cell migration, siponimod showed a significant effect, whereby in scratch assays siponimod stimulated cell motility to an extent equivalent to that of S1P. In directional transwell migration assays siponimod had no inherent chemotactic effect in the short term (4 hrs), rather it blocked the chemotactic effect of FBS (containing high endogenous S1P levels) and exogenously added S1P, siponimod also blocked S1P mediated endothelial cell attachment. These results were similar to the known effects of fingolimod, which has been shown to induce motility in endothelial cells using scratch assays (Mullershausen et al., 2009) but to impede transwell HUVEC migration (Ho et al., 2005, LaMontagne et al., 2006, Tanaka et al., 2013). However, unlike fingolimod, siponimod produced a delayed increase in transwell migration when experimental durations were increased (8 hrs), possibly due to persistent signalling of internalised S1P<sub>1</sub> receptors (Mullershausen et al., 2009).

From a mechanistic point, it was posited that both the differentiation effect on osteoblasts and the migration effect on endothelial cells were associated with the S1P<sub>1</sub> receptor given the receptor affinities of siponimod. As an additional piece of evidence in relation to the differentiation effect, an analysis of cAMP was undertaken showing that forskolin-induced cAMP is inhibited by siponimod (Sartawi et al., 2020a), which is similar to results seen for both S1P and fingolimod (Mullershausen et al., 2009). Given that the literature has shown that increased levels of cAMP can decrease ALP (Romanello et al., 2001) and suppress osteoblast mineralisation (Nishihara et al., 2018), it is reasonable to propose that S1P<sub>1</sub> receptor-mediated decrease in cAMP levels is a possible mechanism through which siponimod may be producing its observed effect on cell differentiation.



Thus **Chapter 3** broadened our understanding of the signalling properties of siponimod and specifically highlighted the effects of siponimod on some of the cellular populations that contribute to bone regeneration. Furthermore, it identified the nature of siponimod's effect (or lack thereof) on osteoblast and endothelial cell behaviour in terms of proliferation, differentiation, and migration. Taken together this provided enough evidence to justify the inclusion of siponimod as the agent of choice for the development of a localised delivery device to augment bone regeneration. This was confirmed *in vitro* in **Chapter 4** where electrospun scaffolds loaded with siponimod produced similar differentiation and migration effects following release from the scaffold highlighting that the drug could be formulated into a delivery system that retained its stability and activity *in vitro*. Ultimately however, the effects did not translate into significant bone regeneration *in vivo*.

6.3.3 Objective III: To develop and characterise drug-loaded electrospun scaffolds composed of PLGA and collagen for controlled release of siponimod over timeframes relevant for bone regeneration.

Albeit limited, the literature has shown that the systemic delivery of molecules similar to siponimod, specifically fingolimod, did not produce positive results for bone regeneration (Heilmann et al., 2013), which was in contrast to the results reported for localised delivery (Das et al., 2014a, Petrie Aronin et al., 2010a, Petrie Aronin et al., 2010b, Sefcik et al., 2008). Therefore, in order to administer siponimod locally to support bone regeneration, it was necessary to develop a suitable delivery vehicle. The selection of electrospinning as the production method was influenced by previous experience in the literature that used electrospinning to prepare fingolimod loaded fibres (Das et al., 2013). Additional factors that supported the choice of

electrospinning were the versatility of electrospinning in the processing of materials with diverse properties, (e.g. growth factors (Zhang et al., 2019b) and natural extracellular matrix components (Yang et al., 2018)), as well as its ability to produce constructs that mimic the fibrillar properties and dimensions of bone extracellular matrix (Hendrikson et al., 2017). We therefore aimed to prepare electrospun scaffolds composed of PLGA and collagen, loaded with siponimod, with the goal of targeting the S1P<sub>1</sub> receptor effects identified in **Chapter 3**.

The electrospun formulations resulted in a flexible, fibrous polymer mat. Results from **Chapter 4** showed that electrospun scaffolds had high drug-loading efficiencies and controlled the release of siponimod over 90 days, which was in line with planned *in vivo* experiments (also described in **Chapter 4**). Importantly, siponimod released from electrospun formulations was shown *in vitro* to produce the same differentiation and migration effects demonstrated with free siponimod in **Chapter 3**, indicating the formulation could provide functionally active cargo and that the concentrations released were appropriate to elicit these effects. Furthermore, the controlled release profiles were similar as the concentration of siponimod in the scaffolds was increased, indicating the capability to control local concentrations by modifying initial drug loading concentrations within the formulation. The electrospun scaffolds supported increased osteoblast metabolic activity in the case of cells grown directly on the scaffold surface. However, over the short timeframe of the experiment, cellular in-growth throughout the fibre matrix was only observed for the Si 0.5:100 sample. The relatively poor cell infiltration overall may have been hampered by the packing density of hydrophobic fibres, especially in the case of the samples containing collagen, which may have resulted in a dense fibre mesh that hindered cell infiltration (Soliman et al.,

2011). It may be possible to reduce fibre density by altering the topology of the collection dish, by creating an abundance of irregular surfaces for fibre deposition rather than a single uniform flat surface (Phipps et al., 2012a). Another possibility is the addition of water-soluble sacrificial fibres to the formulation, which could then be subsequently leached out of the matrix to decrease overall fibre density (Phipps et al., 2012a, Wu and Hong, 2016).

In order to increase the osteoconductivity of the scaffold, the design included the addition of collagen, which is a primary component of bone (Shekaran and García, 2011, Mohamed, 2008). However, the addition of collagen had no discernible effect on the scaffold's cytocompatibility performance, despite evidence in the literature showing that similar concentrations can improve cellular adhesion to polymer scaffolds by increasing sites for cellular attachment (Chiu et al., 2007). Given collagen's importance in bone regeneration, the most likely path to maximise the impact of collagen is to investigate increased collagen concentrations (Ngiam et al., 2009). Reducing fibre packing may also be useful in this context by increasing the exposure of cells to the available collagen binding sites.

This chapter thus highlighted that siponimod can be incorporated at different concentrations into electrospun composite polymer formulations efficiently and easily. Additionally, controlled release of functionally active siponimod was successfully achieved, and the potential of the electrospun matrix to mimic bone extracellular matrix showed promising results when incubated directly with cells. However, longer-term studies supported by histology and immunohistochemistry are warranted to provide greater insights. Ultimately, investigating the scaffolds *in vivo* is

acknowledged to provide the clearest indication of the scaffolds' potential to promote regeneration of bone defects. Consequently, selected samples were progressed for *in vivo* experimentation.

6.3.4 Objective IV: To investigate the ability of the electrospun scaffold design to promote bone regeneration in rat critical cranial defects using fluorescent labelling and bone staining histomorphometry.

The results of **Chapter 4** showed that the prepared siponimod-loaded scaffolds released functionally active cargo in a controlled manner over 90 days, and that the scaffold constructs supported osteoblast growth. The next step involved the evaluation of the scaffolds in a critical cranial defect study to ascertain whether the *in vitro* differentiation effects translated into *in vivo* mineralisation and regeneration of bone tissue. The cranial defect model is commonly used in the literature as a model of critical bone defects (Spicer et al., 2012), and a similar study has been conducted for alternative designs of fingolimod loaded scaffolds (Petrie Aronin et al., 2010a).

Results from this *in vivo* study showed that the implanted scaffolds all produced a small reduction in defect size with signs of mineralisation. However, there was no significant difference in the histomorphometric results of drug-loaded and drug-free experimental groups, using fluorochrome analysis, von Kossa staining, or Masson's-Goldners trichrome staining. Supplementary H&E staining (**Appendix B**) data provided interesting, albeit qualitative data on defect morphology after the 12-week study, whereby most scaffolds exhibited degradation, and replacement by regenerating tissue. The SiCol 0.5:100 sample was a notable exception, the remains of which appeared more intact compared to other scaffolds, and with less native tissue

infiltration. Given that cell viability studies (direct and indirect) did not indicate adverse effects related to scaffolds (**Chapter 4**), it is postulated that this may be due to issues relating to fibre size and packing density. Another point of note, scaffolds containing fingolimod had been prepared to act as a positive control, however it failed to replicate the significant mineralisation that has been shown using similar electrospun designs (Das et al., 2013), and alternative microsphere-based moulded scaffolds (Das et al., 2014b). There were differences in the experimental conditions (i.e. defect size and type), methods and measures to assess regeneration (i.e. histomorphometry compared to microCT), and indeed the outcomes of those studies compared to the data presented herein, and so it is difficult to make like for like comparisons and conclude why fingolimod was unsuccessful as a positive control.

Thus, the cranial defect study described in **Chapter 4** highlighted that there remains a discrepancy between siponimod's stimulation of osteoblast differentiation *in vitro*, and the detection of significant mineralisation *in vivo*. And unless *in vivo* mineralisation or new bone formation can be detected, then the significance of siponimod's differentiation effects, and indeed the validity of using siponimod for bone regeneration will remain questionable.

6.3.5 Objective V: To develop porous drug-loaded scaffolds composed of electrospayed PLGA microparticles and HA, using gas foaming and porogen leaching, for controlled release of siponimod over timeframes relevant for bone regeneration.

An additional formulation design strategy, which again took inspiration from composition of native bone tissue was fabricated by combining electrospayed

microparticles of PLGA loaded with siponimod together with HA and a porogen prior to compression into a scaffold compact (**Chapter 5**), the compact was then exposed to high-pressure CO<sub>2</sub> foaming, followed by porogen leaching. The motivation underpinning this strategy was to design a scaffold with good porosity to facilitate enhanced cell infiltration, combined with the osteoconductive mineral, HA to enhance cell integration, and the S1P<sub>1/5</sub> agonist siponimod to stimulate osteoblast differentiation. This approach produced an interconnected, macroporous structure with pore volumes ranging from 70.1-83.7 %. Qualitative estimations of pore size were in the range of 200-300 µm, which is within the range (100-350 µm) deemed necessary to support the growth and survival of osteogenic cells (Yang et al., 2001). This method of preparing porous scaffolds was based on the literature (Harris et al., 1998, Mooney et al., 1996), and has been used to prepare scaffolds that support cell differentiation *in vitro* and bone formation in an *in vivo* subcutaneous model (Kim et al., 2006). The processing approach endowed samples with a porous architecture, which was hypothesised to be more amenable to cell infiltration representing an advantage over the more tightly packed electrospun samples, which appeared to present a highly dense microstructure that may have impeded cell infiltration (**Chapter 4**, *in vitro* and *in vivo* findings).

Siponimod loading was  $48.5 \pm 2.2$  % of theoretical drug mass and was substantially lower than the electrospun scaffolds developed in **Chapter 4**, which exhibited loading efficiencies of 80-94 % of theoretical drug mass. This difference was likely due to the inclusion of a 12 hrs porogen leaching step, which contributed to the loss of surface bound siponimod, an issue that may have been exacerbated by the high pore volume of this scaffold design. Linear controlled drug release was achieved over a 90 day

experimental duration, and by the 90 day time point, the porous scaffolds had released  $36.7 \pm 0.1$  % of actual drug loading, compared to  $57.7 \pm 0.25$  % for their electrospun counterpart. The difference in release patterns was attributed to the removal of the surface bound drug during leaching, which otherwise could have contributed to a burst release component.

Results of DSC and mechanical properties analysis did not highlight any significant consequences related to the addition of the different components of the scaffolds nor the fabrication process itself. However, the mechanical properties of HA-containing scaffolds showed a trend of impaired scaffold integrity, possibly due to higher porosity measured for HA-containing scaffolds which may have resulted from HA lost during leaching. Another possible explanation for the impaired integrity of HA samples may be due to inconsistent manual mixing of the HA and polymer microparticles. A possible modification that may remedy these potential issues (HA loss through leaching, inconsistent mixing), may be to incorporate HA prior to mould-compression, possibly as a PLGA/HA suspension electrosprayed as microparticles (Yuan et al., 2019).

Cell culture experiments conducted using osteoblasts and endothelial cells indicated that the scaffolds did not adversely affect the metabolic activity of these cells. The addition of siponimod and HA did not result in statistically significant changes in cell metabolic activity, a result similar to those seen in **Chapters 3 & 4** (Sartawi et al., 2020a, Sartawi et al., 2020b), although there were some differences between the experimental design of the respective studies due to the distinct dimensions and masses of the scaffold designs.

These data provide useful formative information although further work is warranted to again confirm siponimod functionality *in vitro*, and then to interrogate more deeply the exact impact of the scaffold on osteoblast and endothelial cell behaviour using longer-term cell culture and histology experiments. Only then could these porous scaffolds be considered as a candidate for further *in vivo* investigation.

## 6.4 Limitations

- In **Chapter 3**, the effects of siponimod were attributed to S1P<sub>1</sub> receptor signalling. Although this is a fair hypothesis given siponimod's known selectivity and its effect on cAMP levels, additional experiments showing detailed receptor expression (e.g. PCR followed by Western blot to document the presence of S1P<sub>1</sub> receptors and the lack of S1P<sub>5</sub> receptors, for which siponimod also shows a high affinity) would have provided stronger evidence.
- Regarding the cranial defect study described in **Chapter 4**, the high variability across the quantitative results clearly indicated that it was an error to divide the ex-plant samples in order to progress the samples using undecalcified and decalcified techniques. Instead all samples should have underwent undecalcified analysis according to initial estimates of sample size which were calculated based on the existing literature (Sikavitsas et al., 2003, Chesmel et al., 1998, van de Watering et al., 2012). However, it should be noted that the trend of the undecalcified results suggested that there was unlikely to be a significant difference even if the remaining samples had been included. Another issue pertained to the use the fluorescent labels, alizarin and calcein,



which were to be used to quantify the inter-label distance between the two calcium chelators (Sun et al., 1992). However, the unsuccessful detection of alizarin hampered the quantitation of this outcome measure.

- In **Chapter 5**, formative *in vitro* characterisation experiments have been conducted on the scaffolds prepared using electrospraying/porogen leaching which makes determinative statements on its efficacy currently difficult.

## 6.5 Recommendations for future work

The thesis provides new insights into the role and use of the selective agent, siponimod, in bone regeneration applications. It is the first work investigating siponimod for this application and provides a valuable starting point for the exploration of alternative small, molecule drug cargoes that may be used to direct cell activities and regenerative outcomes. Future work is recommended in the following areas.

- Further *in vitro* cell-culture studies investigating cell behaviour e.g. differentiation supported by qPCR and immunohistochemistry analysis to achieve a greater understanding concerning the impact of siponimod on bone forming cells. It would also be interesting to explore siponimod's effect on osteoclasts and indeed co-culture experiments of osteoclasts together with osteoblasts in order to investigate the impact of siponimod on the cross-talk between the two cell populations that control bone growth and remodelling, which might provide greater mechanistic insights. Furthermore, siponimod's effect on vascularisation should be clearly determined using blood vessel

formation studies. Additionally, a more thorough investigation of the mechanism of action is warranted, including a study of the signalling pathways involved, especially regarding persistent signalling of internalised S1P receptors.

- The electrospun formulations in **Chapter 4** resulted in a flexible, fibrous polymer mat, which could be promising to augment bone regeneration when used as a part of a combination approach with metallic bone fixation devices or alone as a bone void filler or flexible bone graft substitute. However, based on the results in the thesis, this design must yet be further optimised by enhancing the osteoconductivity by increasing the concentration of collagen to improve cell interaction. It was clear that samples incorporating collagen produced more densely packed compacts, hence strategies to increase the porosity and cell infiltration in these constructs should be investigated, e.g. by co-spinning water-soluble sacrificial fibres. Finally, and importantly, any bioactivity induced by the added sphingolipid must be confirmed *in vivo*.
- The research shown in **Chapter 5** highlighted formative data pertaining to another localised scaffold to control delivery of siponimod. Further optimisation of siponimod loading efficiency and HA incorporation can be achieved by optimising the electrospraying and porogen leaching steps. Additionally, this scaffold should undergo *in vitro* functional studies to confirm cellular infiltration, osteoblast differentiation and ideally vasculogenesis using key markers. If meritorious, this should be followed by more robust *in vivo* bone repair studies.

## 6.6 Thesis conclusions

- A detailed survey of the literature shows that S1P receptor modulators contribute to bone growth and by extension bone healing. The receptors most likely associated with bone biology are S1P<sub>1</sub>, S1P<sub>2</sub>, and S1P<sub>3</sub>, with compelling indications that the S1P<sub>1</sub> subtype is of particular significance.
- Siponimod, an S1P<sub>1/5</sub> receptor agonist, was for the first time shown to increase osteoblast differentiation and simulate endothelial cell migration both when formulated as a solution and in polymer scaffold presentations.
- Siponimod was readily incorporated into polymer constructs alone or as part of composite systems using electrospraying and electrospinning methods. These different composite scaffolds exhibited distinct properties in terms of morphology, presentation, and mechanical properties e.g. flexibility in electrospun mats compared to a more rigid conformation for the foamed/porogen-leached scaffolds. This offers the prospect to exploit their usage in bone applications with diverse requirements. Both systems showed acceptable drug loading and controlled drug release, with the electrospun scaffold also confirming functionally effective concentrations which persisted over prolonged timeframes relevant for bone regeneration.
- Under the experimental design set-up employed in this work, siponimod loaded electrospun scaffolds do not produce statistically significant improvements in bone regeneration in rat critical cranial defects compared to controls.

## References

- ABBASI, N., HAMLET, S., LOVE, R. M. & NGUYEN, N.-T. 2020. Porous scaffolds for bone regeneration. *Journal of Science: Advanced Materials and Devices*, 5, 1-9.
- ADADA, M., CANALS, D., HANNUN, Y. A. & OBEID, L. M. 2013. Sphingosine-1-phosphate receptor 2. *FEBS J*, 280, 6354-66.
- AGARWAL, S., WENDORFF, J. H. & GREINER, A. 2008. Use of electrospinning technique for biomedical applications. *Polymer*, 49, 5603-5621.
- AGARWAL, S., WENDORFF, J. H. & GREINER, A. 2009. Progress in the Field of Electrospinning for Tissue Engineering Applications. *Advanced Materials*, 21, 3343-3351.
- AHERN, E., DOODY, T. & RYAN, K. 2013. Bioinspired nanomaterials for bone tissue engineering. *Bioengineered nanomaterials. Boca Raton; London*, 369-412.
- AKTURK, A., EROL TAYGUN, M. & GOLLER, G. 2020. Optimization of the electrospinning process variables for gelatin/silver nanoparticles/bioactive glass nanocomposites for bone tissue engineering. *Polymer Composites*, 41, 2411-2425.
- ALFORD, A. I., KOZLOFF, K. M. & HANKENSON, K. D. 2015. Extracellular matrix networks in bone remodeling. *Int J Biochem Cell Biol*, 65, 20-31.
- ALLENDE, M. L. & PROIA, R. L. 2002. Sphingosine-1-phosphate receptors and the development of the vascular system. *Biochim Biophys Acta*, 1582, 222-7.
- ALMERÍA, B., DENG, W., FAHMY, T. M. & GOMEZ, A. 2010. Controlling the morphology of electrospray-generated PLGA microparticles for drug delivery. *Journal of Colloid and Interface Science*, 343, 125-133.
- ALSBERG, E., ANDERSON, K. W., ALBEIRUTI, A., ROWLEY, J. A. & MOONEY, D. J. 2002. Engineering growing tissues. *Proc Natl Acad Sci U S A*, 99, 12025-30.
- ALSBERG, E., KONG, H., HIRANO, Y., SMITH, M., ALBEIRUTI, A. & MOONEY, D. 2003. Regulating bone formation via controlled scaffold degradation. *Journal of dental research*, 82, 903-908.
- AMARILIO, R., VIUKOV, S. V., SHARIR, A., ESHKAR-OREN, I., JOHNSON, R. S. & ZELZER, E. 2007. HIF1 $\alpha$  regulation of Sox9 is necessary to maintain differentiation of hypoxic prechondrogenic cells during early skeletogenesis. *Development*, 134, 3917-28.
- AN, G., ZHANG, W., MA, D., LU, B., WEI, G., GUANG, Y., RU, C. & WANG, Y. 2017. Influence of VEGF/BMP-2 on the proliferation and osteogenetic differentiation of rat bone mesenchymal stem cells on PLGA/gelatin composite scaffold. *Eur Rev Med Pharmacol Sci*, 21, 2316-2328.
- ANNABI, B., THIBEAULT, S., LEE, Y. T., BOUSQUET-GAGNON, N., ELIOPOULOS, N., BARRETTE, S., GALIPEAU, J. & BELIVEAU, R. 2003. Matrix metalloproteinase regulation of sphingosine-1-phosphate-induced angiogenic properties of bone marrow stromal cells. *Exp Hematol*, 31, 640-9.
- ANNAZ, B., HING, K., KAYSER, M., BUCKLAND, T. & SILVIO, L. D. 2004. Porosity variation in hydroxyapatite and osteoblast morphology: a scanning electron microscopy study. *Journal of Microscopy*, 215, 100-110.
- ARNOLD, A. M., HOLT, B. D., DANESHMANDI, L., LAURENCIN, C. T. & SYDLIK, S. A. 2019. Phosphate graphene as an intrinsically osteoinductive scaffold for stem cell-driven bone regeneration. *Proceedings of the National Academy of Sciences*, 116, 4855-4860.
- ARRINGTON, E. D., SMITH, W. J., CHAMBERS, H. G., BUCKNELL, A. L. & DAVINO, N. A. 1996. Complications of iliac crest bone graft harvesting. *Clin Orthop Relat Res*, 300-9.

- ASGHARI, F., SAMIEI, M., ADIBKIA, K., AKBARZADEH, A. & DAVARAN, S. 2017. Biodegradable and biocompatible polymers for tissue engineering application: a review. *Artificial Cells, Nanomedicine, and Biotechnology*, 45, 185-192.
- BAL, Z., KUSHIOKA, J., KODAMA, J., KAITO, T., YOSHIKAWA, H., KORKUSUZ, P. & KORKUSUZ, F. 2020. BMP and TGF $\beta$ s Use and Release in Bone Regeneration. *Turk J Med Sci*.
- BALAJI RAGHAVENDRAN, H. R., PUVANESWARY, S., TALEBIAN, S., MURALI, M. R., NAVEEN, S. V., KRISHNAMURITHY, G., MCKEAN, R. & KAMARUL, T. 2014. A comparative study on in vitro osteogenic priming potential of electron spun scaffold PLLA/HA/Col, PLLA/HA, and PLLA/Col for tissue engineering application. *PLoS One*, 9, e104389.
- BALDWIN, P., LI, D. J., AUSTON, D. A., MIR, H. S., YOON, R. S. & KOVAL, K. J. 2019. Autograft, Allograft, and Bone Graft Substitutes: Clinical Evidence and Indications for Use in the Setting of Orthopaedic Trauma Surgery. *J Orthop Trauma*, 33, 203-213.
- BAÑOBRE-LÓPEZ, M., PIÑEIRO-REDONDO, Y., SANDRI, M., TAMPIERI, A., DE SANTIS, R., DEDIU, V. A. & RIVAS, J. 2014. Hyperthermia induced in magnetic scaffolds for bone tissue engineering. *IEEE Transactions on Magnetics*, 50, 1-7.
- BANWART, J. C., ASHER, M. A. & HASSANEIN, R. S. 1995. Iliac crest bone graft harvest donor site morbidity: a statistical evaluation. *Spine*, 20, 1055-1060.
- BAO, X., ZHU, L., HUANG, X., TANG, D., HE, D., SHI, J. & XU, G. 2017. 3D biomimetic artificial bone scaffolds with dual-cytokines spatiotemporal delivery for large weight-bearing bone defect repair. *Scientific Reports*, 7, 7814.
- BEER, F., JOHNSTON, E. & DEWOLF, J. 1999. Mechanics of materials, 5th SI Edition. *Stress*, 1, 1.12.
- BEHRANGI, N., FISCHBACH, F. & KIPP, M. 2019. Mechanism of Siponimod: Anti-Inflammatory and Neuroprotective Mode of Action. *Cells*, 8.
- BEN-NISSAN, B. 2003. Natural bioceramics: from coral to bone and beyond. *Current Opinion in Solid State and Materials Science*, 7, 283-288.
- BEN SHOHAM, A., MALKINSON, G., KRIEF, S., SHWARTZ, Y., ELY, Y., FERRARA, N., YANIV, K. & ZELZER, E. 2012. S1P1 inhibits sprouting angiogenesis during vascular development. *Development*, 139, 3859-69.
- BENDALL, L. J. & BASNETT, J. 2013. Role of sphingosine 1-phosphate in trafficking and mobilization of hematopoietic stem cells. *Curr Opin Hematol*, 20, 281-8.
- BHATTARAI, D. P., AGUILAR, L. E., PARK, C. H. & KIM, C. S. 2018. A Review on Properties of Natural and Synthetic Based Electrospun Fibrous Materials for Bone Tissue Engineering. *Membranes (Basel)*, 8.
- BIGAUD, M., GUERINI, D., BILLICH, A., BASSILANA, F. & BRINKMANN, V. 2014. Second generation S1P pathway modulators: research strategies and clinical developments. *Biochim Biophys Acta*, 1841, 745-58.
- BILOUSOVA, G., JUN, D. H., KING, K. B., DE LANGHE, S., CHICK, W. S., TORCHIA, E. C., CHOW, K. S., KLEMM, D. J., ROOP, D. R. & MAJKA, S. M. 2011. Osteoblasts Derived from Induced Pluripotent Stem Cells form Calcified Structures in Scaffolds Both In Vitro and In Vivo. *STEM CELLS*, 29, 206-216.
- BINDER, B. Y., WILLIAMS, P. A., SILVA, E. A. & LEACH, J. K. 2015. Lysophosphatidic Acid and Sphingosine-1-Phosphate: A Concise Review of Biological Function and Applications for Tissue Engineering. *Tissue Eng Part B Rev*, 21, 531-42.
- BLOKHUIS, T. J. & ARTS, J. J. C. 2011. Bioactive and osteoinductive bone graft substitutes: Definitions, facts and myths. *Injury*, 42, S26-S29.
- BLUM, J. S., BARRY, M. A., MIKOS, A. G. & JANSEN, J. A. 2003. In vivo evaluation of gene therapy vectors in ex vivo-derived marrow stromal cells for bone regeneration in a rat critical-size calvarial defect model. *Hum Gene Ther*, 14, 1689-701.

- BOCHICCHIO, B., BARBARO, K., DE BONIS, A., RAU, J. V. & PEPE, A. 2020. Electrospun poly(d,l-lactide)/gelatin/glass-ceramics tricomponent nanofibrous scaffold for bone tissue engineering. *Journal of Biomedical Materials Research Part A*, 108, 1064-1076.
- BOCK, N., DARGAVILLE, T. R. & WOODRUFF, M. A. 2012. Electro spraying of polymers with therapeutic molecules: State of the art. *Progress in Polymer Science*, 37, 1510-1551.
- BOHR, A., YANG, M., BALDURSDÓTTIR, S., KRISTENSEN, J., DYAS, M., STRIDE, E. & EDIRISINGHE, M. 2012. Particle formation and characteristics of Celecoxib-loaded poly(lactic-co-glycolic acid) microparticles prepared in different solvents using electro spraying. *Polymer*, 53, 3220-3229.
- BOZYCKI, L., KOMIAZYK, M., MEBAREK, S., BUCHET, R., PIKULA, S. & STRZELECKA-KILISZEK, A. 2018. Analysis of Minerals Produced by hFOB 1.19 and Saos-2 Cells Using Transmission Electron Microscopy with Energy Dispersive X-ray Microanalysis. *J Vis Exp*.
- BREWSTER, L., BREY, E. M. & GREISLER, H. P. 2014. Chapter 39 - Blood Vessels. In: LANZA, R., LANGER, R. & VACANTI, J. (eds.) *Principles of Tissue Engineering (Fourth Edition)*. Boston: Academic Press.
- BRINKMANN, V., BILLICH, A., BAUMRUKER, T., HEINING, P., SCHMOUDER, R., FRANCIS, G., ARADHYE, S. & BURTIN, P. 2010. Fingolimod (FTY720): discovery and development of an oral drug to treat multiple sclerosis. *Nat Rev Drug Discov*, 9, 883-97.
- BRIZUELA, L., MARTIN, C., JEANNOT, P., ADER, I., GSTALDER, C., ANDRIEU, G., BOCQUET, M., LAFFOSSE, J. M., GOMEZ-BROUCHET, A., MALAVALD, B., SABBADINI, R. A. & CUVILLIER, O. 2014. Osteoblast-derived sphingosine 1-phosphate to induce proliferation and confer resistance to therapeutics to bone metastasis-derived prostate cancer cells. *Molecular Oncology*, 8, 1181-1195.
- BURKUS, J. K., GORNET, M. F., DICKMAN, C. A. & ZDEBLICK, T. A. 2002. Anterior lumbar interbody fusion using rhBMP-2 with tapered interbody cages. *J Spinal Disord Tech*, 15, 337-49.
- BYRNE, D. P., LACROIX, D., PLANELL, J. A., KELLY, D. J. & PRENDERGAST, P. J. 2007. Simulation of tissue differentiation in a scaffold as a function of porosity, Young's modulus and dissolution rate: Application of mechanobiological models in tissue engineering. *Biomaterials*, 28, 5544-5554.
- CAHILL, K. S., MCCORMICK, P. C. & LEVI, A. D. 2015. A comprehensive assessment of the risk of bone morphogenetic protein use in spinal fusion surgery and postoperative cancer diagnosis. *J Neurosurg Spine*, 23, 86-93.
- CAMERER, E., REGARD, J. B., CORNELISSEN, I., SRINIVASAN, Y., DUONG, D. N., PALMER, D., PHAM, T. H., WONG, J. S., PAPPU, R. & COUGHLIN, S. R. 2009. Sphingosine-1-phosphate in the plasma compartment regulates basal and inflammation-induced vascular leak in mice. *J Clin Invest*, 119, 1871-9.
- CANNAVO, A., LICCARDO, D., KOMICI, K., CORBI, G., DE LUCIA, C., FEMMINELLA, G. D., ELIA, A., BENCIVENGA, L., FERRARA, N. & KOCH, W. J. 2017. Sphingosine kinases and sphingosine 1-phosphate receptors: signaling and actions in the cardiovascular system. *Frontiers in pharmacology*, 8, 556.
- CAO, H. & KUBOYAMA, N. 2010. A biodegradable porous composite scaffold of PGA/ $\beta$ -TCP for bone tissue engineering. *Bone*, 46, 386-395.
- CAPLAN, A. I. & CORREA, D. 2011. PDGF in bone formation and regeneration: new insights into a novel mechanism involving MSCs. *J Orthop Res*, 29, 1795-803.
- CARBONE, E. J., RAJPURA, K., JIANG, T., LAURENCIN, C. T. & LO, K. W. H. 2014. Regulation of bone regeneration with approved small molecule compounds. *Advances in Regenerative Biology*, 1, 25276.

- CARPIO, L. C., SHIAU, H. & DZIAK, R. 2000. Changes in sphingolipid levels induced by epidermal growth factor in osteoblastic cells. Effects of these metabolites on cytosolic calcium levels. *Prostaglandins Leukot Essent Fatty Acids*, 62, 225-32.
- CARPIO, L. C., STEPHAN, E., KAMER, A. & DZIAK, R. 1999. Sphingolipids stimulate cell growth via MAP kinase activation in osteoblastic cells. *Prostaglandins Leukotrienes and Essential Fatty Acids*, 61, 267-273.
- CEN, L., LIU, W., CUI, L., ZHANG, W. & CAO, Y. 2008. Collagen tissue engineering: development of novel biomaterials and applications. *Pediatr Res*, 63, 492-6.
- CHAE, S. S., PAIK, J. H., ALLENDE, M. L., PROIA, R. L. & HLA, T. 2004. Regulation of limb development by the sphingosine 1-phosphate receptor S1p1/EDG-1 occurs via the hypoxia/VEGF axis. *Dev Biol*, 268, 441-7.
- CHEN, D., ZHAO, M. & MUNDY, G. R. 2004. Bone morphogenetic proteins. *Growth Factors*, 22, 233-241.
- CHEN, R. R. & MOONEY, D. J. 2003. Polymeric growth factor delivery strategies for tissue engineering. *Pharmaceutical research*, 20, 1103-1112.
- CHEN, X., WANG, Z., DUAN, N., ZHU, G., SCHWARZ, E. M. & XIE, C. 2018. Osteoblast–osteoclast interactions. *Connective Tissue Research*, 59, 99-107.
- CHEN, Y. & ALMAN, B. A. 2009. Wnt pathway, an essential role in bone regeneration. *J Cell Biochem*, 106, 353-62.
- CHEN, Z., WU, C., GU, W., KLEIN, T., CRAWFORD, R. & XIAO, Y. 2014. Osteogenic differentiation of bone marrow MSCs by  $\beta$ -tricalcium phosphate stimulating macrophages via BMP2 signalling pathway. *Biomaterials*, 35, 1507-1518.
- CHENG, G., MA, X., LI, J., CHENG, Y., CAO, Y., WANG, Z., SHI, X., DU, Y., DENG, H. & LI, Z. 2018. Incorporating platelet-rich plasma into coaxial electrospun nanofibers for bone tissue engineering. *Int J Pharm*, 547, 656-666.
- CHENG, P., HAN, P., ZHAO, C., ZHANG, S., WU, H., NI, J., HOU, P., ZHANG, Y., LIU, J., XU, H., LIU, S., ZHANG, X., ZHENG, Y. & CHAI, Y. 2016. High-purity magnesium interference screws promote fibrocartilaginous entheses regeneration in the anterior cruciate ligament reconstruction rabbit model via accumulation of BMP-2 and VEGF. *Biomaterials*, 81, 14-26.
- CHERIFI, C., HAFSIA, N., LATOURTE, A., RICHETTE, P., HAY, E. & COHEN-SOLAL, M. 2016. Sphingosine 1 Phosphate Produced by Osteoclasts Promotes Chondrocyte Catabolism. *Osteoarthritis and Cartilage*, 24, S391-S392.
- CHESMEL, K. D., BRANGER, J., WERTHEIM, H. & SCARBOROUGH, N. 1998. Healing response to various forms of human demineralized bone matrix in athymic rat cranial defects. *Journal of Oral and Maxillofacial Surgery*, 56, 857-863.
- CHEW, W. S., WANG, W. & HERR, D. R. 2016. To fingolimod and beyond: The rich pipeline of drug candidates that target S1P signaling. *Pharmacological Research*, 113, 521-532.
- CHI, H. 2011. Sphingosine-1-phosphate and immune regulation: trafficking and beyond. *Trends Pharmacol Sci*, 32, 16-24.
- CHIU, J. B., LIU, C., HSIAO, B. S., CHU, B. & HADJIARGYROU, M. 2007. Functionalization of poly(L-lactide) nanofibrous scaffolds with bioactive collagen molecules. *J Biomed Mater Res A*, 83, 1117-27.
- CHOI, H. K., KIM, G.-J., YOO, H.-S., SONG, D. H., CHUNG, K.-H., LEE, K.-J., KOO, Y. T. & AN, J. H. 2019. Vitamin C Activates Osteoblastogenesis and Inhibits Osteoclastogenesis via Wnt/ $\beta$ -Catenin/ATF4 Signaling Pathways. *Nutrients*, 11, 506.
- CHOI, J. W. & CHUN, J. 2013. Lysophospholipids and their receptors in the central nervous system. *Biochim Biophys Acta*, 1831, 20-32.

- CHOWDHURY, S., THOMAS, V., DEAN, D., CATLEDGE, S. A. & VOHRA, Y. K. 2005. Nanoindentation on porous bioceramic scaffolds for bone tissue engineering. *Journal of nanoscience and nanotechnology*, 5, 1816-1820.
- CHUENJITKUNTAWORN, B., INRUNG, W., DAMRONGSRI, D., MEKAAPIRUK, K., SUPAPHOL, P. & PAVASANT, P. 2010. Polycaprolactone/hydroxyapatite composite scaffolds: Preparation, characterization, and in vitro and in vivo biological responses of human primary bone cells. *Journal of Biomedical Materials Research Part A*, 94A, 241-251.
- CLARKE, B. 2008. Normal bone anatomy and physiology. *Clinical journal of the American Society of Nephrology : CJASN*, 3 Suppl 3, S131-S139.
- CLOUPEAU, M. & PRUNET-FOCH, B. 1990. Electrostatic spraying of liquids: Main functioning modes. *Journal of Electrostatics*, 25, 165-184.
- COLLINS, M. N. & BIRKINSHAW, C. 2013. Hyaluronic acid based scaffolds for tissue engineering—A review. *Carbohydrate Polymers*, 92, 1262-1279.
- COPP, D. H. & SHIM, S. 1963. The homeostatic function of bone as a mineral reservoir. *Oral Surgery, Oral Medicine, Oral Pathology*, 16, 738-744.
- CORREIA, D. M., GONCALVES, R., RIBEIRO, C., SENCADAS, V., BOTELHO, G., RIBELLES, J. L. G. & LANCEROS-MENDEZ, S. 2014. Electrospayed poly(vinylidene fluoride) microparticles for tissue engineering applications. *Rsc Advances*, 4, 33013-33021.
- COSTA, G., RUSSO, S., BONARDELLI, P. & MOGGI, G. 1982. A Comparative Study on Some Fluoroalcohols as Potential Solvents for Aliphatic Polyamides. *Journal of Macromolecular Science: Part A - Chemistry*, 18, 299-312.
- COSTANTINI, M. & BARBETTA, A. 2018. 6 - Gas foaming technologies for 3D scaffold engineering. In: DENG, Y. & KUIPER, J. (eds.) *Functional 3D Tissue Engineering Scaffolds*. Woodhead Publishing.
- COWAN, C. M., AALAMI, O. O., SHI, Y.-Y., CHOU, Y.-F., MARI, C., THOMAS, R., QUARTO, N., NACAMULI, R. P., CONTAG, C. H. & WU, B. 2005. Bone morphogenetic protein 2 and retinoic acid accelerate in vivo bone formation, osteoclast recruitment, and bone turnover. *Tissue engineering*, 11, 645-658.
- CUGATI, S., CHEN, C. S., LAKE, S. & LEE, A. W. 2014. Fingolimod and macular edema: Pathophysiology, diagnosis, and management. *Neurol Clin Pract*, 4, 402-409.
- CURRY, A. S., PENSA, N. W., BARLOW, A. M. & BELLIS, S. L. 2016. Taking cues from the extracellular matrix to design bone-mimetic regenerative scaffolds. *Matrix Biol*, 52-54, 397-412.
- CUVILLIER, O., PIRIANOV, G., KLEUSER, B., VANEK, P. G., COSO, O. A., GUTKIND, S. & SPIEGEL, S. 1996. Suppression of ceramide-mediated programmed cell death by sphingosine-1-phosphate. *Nature*, 381, 800-3.
- DAHABREH, Z., CALORI, G. M., KANAKARIS, N. K., NIKOLAOU, V. S. & GIANNOUDIS, P. V. 2008. A cost analysis of treatment of tibial fracture nonunion by bone grafting or bone morphogenetic protein-7. *International Orthopaedics*, 33, 1407.
- DAI, Z., RONHOLM, J., TIAN, Y., SETHI, B. & CAO, X. 2016. Sterilization techniques for biodegradable scaffolds in tissue engineering applications. *Journal of tissue engineering*, 7, 2041731416648810-2041731416648810.
- DALTON, P. D., VAQUETTE, C., FARRUGIA, B. L., DARGAVILLE, T. R., BROWN, T. D. & HUTMACHER, D. W. 2013. Electrospinning and additive manufacturing: converging technologies. *Biomaterials Science*, 1, 171-185.
- DAS, A., BARKER, D. A., WANG, T., LAU, C. M., LIN, Y. & BOTCHWEY, E. A. 2014a. Delivery of bioactive lipids from composite microgel-microsphere injectable scaffolds enhances stem cell recruitment and skeletal repair. *PLoS One*, 9, e101276.



- DAS, A., SEGAR, C. E., CHU, Y., WANG, T. W., LIN, Y., YANG, C., DU, X., OGLE, R. C., CUI, Q. & BOTCHWEY, E. A. 2015. Bioactive lipid coating of bone allografts directs engraftment and fate determination of bone marrow-derived cells in rat GFP chimeras. *Biomaterials*, 64, 98-107.
- DAS, A., SEGAR, C. E., HUGHLEY, B. B., BOWERS, D. T. & BOTCHWEY, E. A. 2013. The promotion of mandibular defect healing by the targeting of S1P receptors and the recruitment of alternatively activated macrophages. *Biomaterials*, 34, 9853-62.
- DAS, A., TANNER, S., BARKER, D. A., GREEN, D. & BOTCHWEY, E. A. 2014b. Delivery of S1P receptor-targeted drugs via biodegradable polymer scaffolds enhances bone regeneration in a critical size cranial defect. *J Biomed Mater Res A*, 102, 1210-8.
- DAVIES, J. C., CHAN, H. H. L., BERNSTEIN, J. M., GOLDSTEIN, D. P., IRISH, J. C. & GILBERT, R. W. 2018. Orbital Floor Reconstruction: 3-Dimensional Analysis Shows Comparable Morphology of Scapular and Iliac Crest Bone Grafts. *J Oral Maxillofac Surg*, 76, 2011-2018.
- DAVIS, M. D., CLEMENS, J. J., MACDONALD, T. L. & LYNCH, K. R. 2005. Sphingosine 1-phosphate analogs as receptor antagonists. *J Biol Chem*, 280, 9833-41.
- DE WITTE, T.-M., FRATILA-APACHITEI, L. E., ZADPOOR, A. A. & PEPPAS, N. A. 2018. Bone tissue engineering via growth factor delivery: from scaffolds to complex matrices. *Regenerative biomaterials*, 5, 197-211.
- DEITZEL, J. M., KLEINMEYER, J., HARRIS, D. & TAN, N. B. 2001. The effect of processing variables on the morphology of electrospun nanofibers and textiles. *Polymer*, 42, 261-272.
- DENG, W. W., KLEMIC, J. F., LI, X. H., REED, M. A. & GOMEZ, A. 2006. Increase of electrospray throughput using multiplexed microfabricated sources for the scalable generation of monodisperse droplets. *Journal of Aerosol Science*, 37, 696-714.
- DERAKHSHANFAR, S., MBELECK, R., XU, K., ZHANG, X., ZHONG, W. & XING, M. 2018. 3D bioprinting for biomedical devices and tissue engineering: A review of recent trends and advances. *Bioact Mater*, 3, 144-156.
- DEVILLE, S., SAIZ, E. & TOMSIA, A. P. 2006. Freeze casting of hydroxyapatite scaffolds for bone tissue engineering. *Biomaterials*, 27, 5480-5489.
- DHANDAYUTHAPANI, B., YOSHIDA, Y., MAEKAWA, T. & KUMAR, D. S. 2011. Polymeric scaffolds in tissue engineering application: a review. *International journal of polymer science*, 2011.
- DI LULLO, G. A., SWEENEY, S. M., KÖRKKÖ, J., ALA-KOKKO, L. & SAN ANTONIO, J. D. 2002. Mapping the ligand-binding sites and disease-associated mutations on the most abundant protein in the human, type I collagen. *Journal of Biological Chemistry*, 277, 4223-4231.
- DI PAOLO, G. & DE CAMILLI, P. 2006. Phosphoinositides in cell regulation and membrane dynamics. *Nature*, 443, 651-7.
- DIBA, M., CAMARGO, W. A., BRINDISI, M., FARBOD, K., KLYMOV, A., SCHMIDT, S., HARRINGTON, M. J., DRAGHI, L., BOCCACCINI, A. R., JANSEN, J. A., VAN DEN BEUCKEN, J. J. J. P. & LEEUWENBURGH, S. C. G. 2017. Composite Colloidal Gels Made of Bisphosphonate-Functionalized Gelatin and Bioactive Glass Particles for Regeneration of Osteoporotic Bone Defects. *Advanced Functional Materials*, 27, 1703438.
- DIMARCO, J. P., O'CONNOR, P., COHEN, J. A., REDER, A. T., ZHANG-AUBERSON, L., TANG, D., COLLINS, W. & KAPPOS, L. 2014. First-dose effects of fingolimod: Pooled safety data from three phase 3 studies. *Mult Scler Relat Disord*, 3, 629-38.

- DIMITRIOU, R., TSIRIDIS, E. & GIANNOUDIS, P. V. 2005. Current concepts of molecular aspects of bone healing. *Injury*, 36, 1392-404.
- DING, J. X., ZHANG, J., LI, J. N., LI, D., XIAO, C. S., XIAO, H. H., YANG, H. H., ZHUANG, X. L. & CHEN, X. S. 2019. Electrospun polymer biomaterials. *Progress in Polymer Science*, 90, 1-34.
- DONG, C. & LV, Y. 2016. Application of collagen scaffold in tissue engineering: recent advances and new perspectives. *Polymers*, 8, 42.
- DOROZHUKIN, S. V. 2010. Bioceramics of calcium orthophosphates. *Biomaterials*, 31, 1465-1485.
- DUMIC-CULE, I., PERIC, M., KUCKO, L., GRGUREVIC, L., PECINA, M. & VUKICEVIC, S. 2018. Bone morphogenetic proteins in fracture repair. *International Orthopaedics*, 42, 2619-2626.
- DURAN, C. L., KAUNAS, R. & BAYLESS, K. J. 2017. S1P Synergizes with Wall Shear Stress and Other Angiogenic Factors to Induce Endothelial Cell Sprouting Responses. *Methods Mol Biol*.
- DWEK, J. R. 2010. The periosteum: what is it, where is it, and what mimics it in its absence? *Skeletal Radiol*, 39, 319-23.
- DZIAK, R., YANG, B. M., LEUNG, B. W., LI, S., MARZEC, N., MARGARONE, J. & BOBEK, L. 2003. Effects of sphingosine-1-phosphate and lysophosphatidic acid on human osteoblastic cells. *Prostaglandins Leukotrienes and Essential Fatty Acids*, 68, 239-249.
- EIVAZZADEH-KEIHAN, R., MALEKI, A., DE LA GUARDIA, M., BANI, M. S., CHENAB, K. K., PASHAZADEH-PANAHI, P., BARADARAN, B., MOKHTARZADEH, A. & HAMBLIN, M. R. 2019. Carbon based nanomaterials for tissue engineering of bone: Building new bone on small black scaffolds: A review. *Journal of Advanced Research*, 18, 185-201.
- EL JAMAL, A., BRIOLAY, A., MEBAREK, S., LE GOFF, B., BLANCHARD, F., MAGNE, D., BRIZUELA, L. & BOUGAULT, C. 2019. Cytokine- and stretch-induced sphingosine1-phosphate production by enthesis cells could favor abnormal ossification in spondyloarthritis. *J Bone Miner Res*.
- ELMOWAFY, E. M., TIBONI, M. & SOLIMAN, M. E. 2019. Biocompatibility, biodegradation and biomedical applications of poly(lactic acid)/poly(lactic-co-glycolic acid) micro and nanoparticles. *Journal of Pharmaceutical Investigation*, 49, 347-380.
- EPSTEIN, N. E. 2013. Complications due to the use of BMP/INFUSE in spine surgery: The evidence continues to mount. *Surgical neurology international*, 4, S343-S352.
- ERGUN, C., LIU, H., WEBSTER, T. J., OLCAY, E., YILMAZ, Ş. & SAHIN, F. C. 2008. Increased osteoblast adhesion on nanoparticulate calcium phosphates with higher Ca/P ratios. *Journal of Biomedical Materials Research Part A*, 85A, 236-241.
- FALANGA, V., FARIA, K. & BOLLENBACH, T. 2014. Chapter 77 - Bioengineered Skin Constructs. In: LANZA, R., LANGER, R. & VACANTI, J. (eds.) *Principles of Tissue Engineering (Fourth Edition)*. Boston: Academic Press.
- FARZAMFAR, S., NASERI-NOSAR, M., SAHRAPEYMA, H., EHTERAMI, A., GOODARZI, A., RAHMATI, M., AHMADI LAKALAYEH, G., GHORBANI, S., VAEZ, A. & SALEHI, M. 2019. Tetracycline hydrochloride-containing poly (ε-caprolactone)/poly lactic acid scaffold for bone tissue engineering application: in vitro and in vivo study. *International Journal of Polymeric Materials and Polymeric Biomaterials*, 68, 472-479.
- FENG, X. & MCDONALD, J. M. 2011. Disorders of bone remodeling. *Annual Review of Pathology: Mechanisms of Disease*, 6, 121-145.

- FLORENCIO-SILVA, R., SASSO, G. R., SASSO-CERRI, E., SIMOES, M. J. & CERRI, P. S. 2015. Biology of Bone Tissue: Structure, Function, and Factors That Influence Bone Cells. *Biomed Res Int*, 2015, 421746.
- FOSS, F. W., JR., SNYDER, A. H., DAVIS, M. D., ROUSE, M., OKUSA, M. D., LYNCH, K. R. & MACDONALD, T. L. 2007. Synthesis and biological evaluation of gamma-aminophosphonates as potent, subtype-selective sphingosine 1-phosphate receptor agonists and antagonists. *Bioorg Med Chem*, 15, 663-77.
- FU, Y. C., NIE, H., HO, M. L., WANG, C. K. & WANG, C. H. 2008. Optimized bone regeneration based on sustained release from three-dimensional fibrous PLGA/HAp composite scaffolds loaded with BMP-2. *Biotechnol Bioeng*, 99, 996-1006.
- GAENGEL, K., NIAUDET, C., HAGIKURA, K., LAVINA, B., MUHL, L., HOFMANN, J. J., EBARASI, L., NYSTROM, S., RYMO, S., CHEN, L. L., PANG, M. F., JIN, Y., RASCHPERGER, E., ROSWALL, P., SCHULTE, D., BENEDITO, R., LARSSON, J., HELLSTROM, M., FUXE, J., UHLEN, P., ADAMS, R., JAKOBSSON, L., MAJUMDAR, A., VESTWEBER, D., UV, A. & BETSHOLTZ, C. 2012. The sphingosine-1-phosphate receptor S1PR1 restricts sprouting angiogenesis by regulating the interplay between VE-cadherin and VEGFR2. *Dev Cell*, 23, 587-99.
- GALVIN, P., THOMPSON, D., RYAN, K. B., MCCARTHY, A., MOORE, A. C., BURKE, C. S., DYSON, M., MACCRAITH, B. D., GUN'KO, Y. K., BYRNE, M. T., VOLKOV, Y., KEELY, C., KEEHAN, E., HOWE, M., DUFFY, C. & MACLOUGHLIN, R. 2012. Nanoparticle-based drug delivery: case studies for cancer and cardiovascular applications. *Cell Mol Life Sci*, 69, 389-404.
- GARRISON, K. R., DONELL, S., RYDER, J., SHEMILT, I., MUGFORD, M., HARVEY, I. & SONG, F. 2007. Clinical effectiveness and cost-effectiveness of bone morphogenetic proteins in the non-healing of fractures and spinal fusion: a systematic review. *Health Technol Assess*, 11, 1-150, iii-iv.
- GASPERINI, L., MANO, J. F. & REIS, R. L. 2014. Natural polymers for the microencapsulation of cells. *Journal of the Royal Society Interface*, 11, 20140817.
- GE, Z., JIN, Z. & CAO, T. 2008. Manufacture of degradable polymeric scaffolds for bone regeneration. *Biomedical Materials*, 3, 022001.
- GELLYNCK, K., SHAH, R., PARKAR, M., YOUNG, A., BUXTON, P. & BRETT, P. 2013. Small molecule stimulation enhances bone regeneration but not titanium implant osseointegration. *Bone*, 57, 405-412.
- GENTILE, A., MUSELLA, A., BULLITTA, S., FRESEGNA, D., DE VITO, F., FANTOZZI, R., PIRAS, E., GARGANO, F., BORSELLINO, G., BATTISTINI, L., SCHUBART, A., MANDOLESI, G. & CENTONZE, D. 2016. Siponimod (BAF312) prevents synaptic neurodegeneration in experimental multiple sclerosis. *J Neuroinflammation*, 13, 207.
- GENTILE, P., CHIONO, V., CARMAGNOLA, I. & HATTON, P. V. 2014. An overview of poly(lactic-co-glycolic) acid (PLGA)-based biomaterials for bone tissue engineering. *Int J Mol Sci*, 15, 3640-59.
- GERGELY, P., NUESSEIN-HILDESHEIM, B., GUERINI, D., BRINKMANN, V., TRAEBERT, M., BRUNS, C., PAN, S., GRAY, N. S., HINTERDING, K., COOKE, N. G., GROENEWEGEN, A., VITALITI, A., SING, T., LUTTRINGER, O., YANG, J., GARDIN, A., WANG, N., CRUMB, W. J., SALTZMAN, M., ROSENBERG, M. & WALLSTROM, E. 2012. The selective sphingosine 1-phosphate receptor modulator BAF312 redirects lymphocyte distribution and has species-specific effects on heart rate. *British Journal of Pharmacology*, 167, 1035-1047.
- GHANAATI, S., UNGER, R. E., WEBBER, M. J., BARBECK, M., ORTH, C., KIRKPATRICK, J. A., BOOMS, P., MOTTA, A., MIGLIARESI, C. & SADER, R. A. 2011. Scaffold vascularization

- in vivo driven by primary human osteoblasts in concert with host inflammatory cells. *Biomaterials*, 32, 8150-8160.
- GILARDINO, M. S., CHEN, E. & BARTLETT, S. P. 2009. Choice of internal rigid fixation materials in the treatment of facial fractures. *Craniomaxillofacial trauma & reconstruction*, 2, 49-60.
- GLAESER, J. D., SALEHI, K., KANIM, L. E., JU, D. G., HYUK YANG, J., BEHRENS, P. H., EBERLEIN, S. A., METZGER, M. F., ARABI, Y. & STEFANOVIC, T. 2020. Electrospun, synthetic bone void filler promotes human MSC function and BMP-2 mediated spinal fusion. *Journal of Biomaterials Applications*, 0885328220937999.
- GLOWACKI, J. & MIZUNO, S. 2008. Collagen scaffolds for tissue engineering. *Biopolymers*, 89, 338-344.
- GO, E. J., KANG, E. Y., LEE, S. K., PARK, S., KIM, J. H., PARK, W., KIM, I. H., CHOI, B. & HAN, D. K. 2020. An osteoconductive PLGA scaffold with bioactive  $\beta$ -TCP and anti-inflammatory Mg (OH) 2 to improve in vivo bone regeneration. *Biomaterials Science*, 8, 937-948.
- GOIMIL, L., SANTOS-ROSALES, V., DELGADO, A., ÉVORA, C., REYES, R., LOZANO-PÉREZ, A. A., AZNAR-CERVANTES, S. D., CENIS, J. L., GÓMEZ-AMOZA, J. L., CONCEIRO, A., ALVAREZ-LORENZO, C. & GARCÍA-GONZÁLEZ, C. A. 2019. scCO<sub>2</sub>-foamed silk fibroin aerogel/poly( $\epsilon$ -caprolactone) scaffolds containing dexamethasone for bone regeneration. *Journal of CO<sub>2</sub> Utilization*, 31, 51-64.
- GOLAN, K., KOLLET, O. & LAPIDOT, T. 2013. Dynamic Cross Talk between S1P and CXCL12 Regulates Hematopoietic Stem Cells Migration, Development and Bone Remodeling. *Pharmaceuticals (Basel)*, 6, 1145-69.
- GOMEZ-BARRENA, E., ROSSET, P., LOZANO, D., STANOVICI, J., ERMTHALLER, C. & GERBHARD, F. 2015. Bone fracture healing: cell therapy in delayed unions and nonunions. *Bone*, 70, 93-101.
- GONZALEZ-CABRERA, P. J., JO, E., SANNA, M. G., BROWN, S., LEAF, N., MARSOLAIS, D., SCHAEFFER, M. T., CHAPMAN, J., CAMERON, M., GUERRERO, M., ROBERTS, E. & ROSEN, H. 2008. Full pharmacological efficacy of a novel S1P1 agonist that does not require S1P-like headgroup interactions. *Mol Pharmacol*, 74, 1308-18.
- GOULET, F., AUGER, F. A., CLOUTIER, R., LAMONTAGNE, J., SIMON, F., CHABAUD, S., GERMAIN, L. & HART, D. A. 2014. Chapter 59 - Tendons and Ligament Tissue Engineering. In: LANZA, R., LANGER, R. & VACANTI, J. (eds.) *Principles of Tissue Engineering (Fourth Edition)*. Boston: Academic Press.
- GOULET, J. A., SENUNAS, L. E., DESILVA, G. L. & GREENFIELD, M. L. 1997. Autogenous iliac crest bone graft. Complications and functional assessment. *Clin Orthop Relat Res*, 76-81.
- GRADINARU, S., POPESCU, V., LEASU, C., PRICOPIE, S., YASIN, S., CIULUVICA, R. & UNGUREANU, E. 2015. Hydroxyapatite ocular implant and non-integrated implants in eviscerated patients. *Journal of medicine and life*, 8, 90-93.
- GREENWALD, A. S., BODEN, S. D., GOLDBERG, V. M., KHAN, Y., LAURENCIN, C. T. & ROSIER, R. N. 2001. Bone-graft substitutes: facts, fictions, and applications. *JBJS*, 83, S98-103.
- GREY, A., CHEN, Q., CALLON, K., XU, X., REID, I. R. & CORNISH, J. 2002. The phospholipids sphingosine-1-phosphate and lysophosphatidic acid prevent apoptosis in osteoblastic cells via a signaling pathway involving G(i) proteins and phosphatidylinositol-3 kinase. *Endocrinology*, 143, 4755-4763.
- GREY, A., XU, X., HILL, B., WATSON, M., CALLON, K., REID, I. R. & CORNISH, J. 2004. Osteoblastic cells express phospholipid receptors and phosphatases and proliferate in response to sphingosine-1-phosphate. *Calcified Tissue International*, 74, 542-550.

- HAIDER, A., HAIDER, S. & KANG, I.-K. 2018. A comprehensive review summarizing the effect of electrospinning parameters and potential applications of nanofibers in biomedical and biotechnology. *Arabian Journal of Chemistry*, 11, 1165-1188.
- HAIDER, S., HAIDER, A., ALGHYAMAH, A. A., KHAN, R., ALMASRY, W. A. & KHAN, N. 2019. Electrohydrodynamic Processes and Their Affecting Parameters. *Electrospinning and Electrospaying-Techniques and Applications*. IntechOpen.
- HALEEM, A., JAVAID, M., KHAN, R. H. & SUMAN, R. 2020. 3D printing applications in bone tissue engineering. *Journal of Clinical Orthopaedics and Trauma*, 11, S118-S124.
- HALL BARRIENTOS, I. J., PALADINO, E., SZABO, P., BROZIO, S., HALL, P. J., OSEGHLE, C. I., PASSARELLI, M. K., MOUG, S. J., BLACK, R. A., WILSON, C. G., ZELKO, R. & LAMPROU, D. A. 2017. Electrospun collagen-based nanofibres: A sustainable material for improved antibiotic utilisation in tissue engineering applications. *Int J Pharm*, 531, 67-79.
- HANEL, P., ANDREANI, P. & GRALER, M. H. 2007. Erythrocytes store and release sphingosine 1-phosphate in blood. *FASEB J*, 21, 1202-9.
- HANKE, T., MERK, D., STEINHILBER, D., GEISSLINGER, G. & SCHUBERT-ZSILAVECZ, M. 2016. Small molecules with anti-inflammatory properties in clinical development. *Pharmacology & Therapeutics*, 157, 163-187.
- HANKENSON, K. D., GAGNE, K. & SHAUGHNESSY, M. 2015. Extracellular signaling molecules to promote fracture healing and bone regeneration. *Adv Drug Deliv Rev*, 94, 3-12.
- HARRIS, L. D., KIM, B. S. & MOONEY, D. J. 1998. Open pore biodegradable matrices formed with gas foaming. *J Biomed Mater Res*, 42, 396-402.
- HARRIS, S. A., ENGER, R. J., RIGGS, B. L. & SPELSBERG, T. C. 1995. Development and characterization of a conditionally immortalized human fetal osteoblastic cell line. *J Bone Miner Res*, 10, 178-86.
- HASHIMOTO, Y., KOBAYASHI, M., MATSUZAKI, E., HIGASHI, K., TAKAHASHI-YANAGA, F., TAKANO, A., HIRATA, M. & NISHIMURA, F. 2016. Sphingosine-1-phosphate-enhanced Wnt5a promotes osteogenic differentiation in C3H10T1/2 cells. *Cell Biology International*, 40, 1129-1136.
- HASHIMOTO, Y., MATSUZAKI, E., HIGASHI, K., TAKAHASHI-YANAGA, F., TAKANO, A., HIRATA, M. & NISHIMURA, F. 2015. Sphingosine-1-phosphate inhibits differentiation of C3H10T1/2 cells into adipocyte. *Mol Cell Biochem*, 401, 39-47.
- HAUGEN, H. J., LYGSTADAAS, S. P., ROSSI, F. & PERALE, G. 2019. Bone grafts: which is the ideal biomaterial? *Journal of Clinical Periodontology*, 46, 92-102.
- HE, S., LIN, K.-F., SUN, Z., SONG, Y., ZHAO, Y.-N., WANG, Z., BI, L. & LIU, J. 2016. Effects of Nano-hydroxyapatite/Poly(DL-lactic-co-glycolic acid) Microsphere-Based Composite Scaffolds on Repair of Bone Defects: Evaluating the Role of Nano-hydroxyapatite Content. *Artificial Organs*, 40, E128-E135.
- HEILMANN, A., SCHINKE, T., BINDL, R., WEHNER, T., RAPP, A., HAFFNER-LUNTZER, M., LIEDERT, A., AMLING, M. & IGNATIUS, A. 2013. Systemic treatment with the sphingosine-1-phosphate analog FTY720 does not improve fracture healing in mice. *J Orthop Res*, 31, 1845-50.
- HENCH, L. L. 2013. *An introduction to bioceramics*, World Scientific Publishing Company.
- HENCH, L. L., SPLINTER, R. J., ALLEN, W. & GREENLEE, T. 1971. Bonding mechanisms at the interface of ceramic prosthetic materials. *Journal of biomedical materials research*, 5, 117-141.
- HENCH, L. L., XYNOS, I. D. & POLAK, J. M. 2004. Bioactive glasses for in situ tissue regeneration. *Journal of Biomaterials Science, Polymer Edition*, 15, 543-562.

- HENDRIKSON, W. J., VAN BLITTERSWIJK, C. A., ROUWKEMA, J. & MORONI, L. 2017. The Use of Finite Element Analyses to Design and Fabricate Three-Dimensional Scaffolds for Skeletal Tissue Engineering. *Front Bioeng Biotechnol*, 5, 30.
- HENKEL, J., WOODRUFF, M. A., EPARI, D. R., STECK, R., GLATT, V., DICKINSON, I. C., CHOONG, P. F. M., SCHUETZ, M. A. & HUTMACHER, D. W. 2013. Bone Regeneration Based on Tissue Engineering Conceptions - A 21st Century Perspective. *Bone Research*, 1, 216-248.
- HIGASHI, K., MATSUZAKI, E., HASHIMOTO, Y., TAKAHASHI-YANAGA, F., TAKANO, A., ANAN, H., HIRATA, M. & NISHIMURA, F. 2016. Sphingosine-1-phosphate/S1PR2-mediated signaling triggers Smad1/5/8 phosphorylation and thereby induces Runx2 expression in osteoblasts. *Bone*, 93, 1-11.
- HINTON, P. V., RACKARD, S. M. & KENNEDY, O. D. 2018. In Vivo Osteocyte Mechanotransduction: Recent Developments and Future Directions. *Curr Osteoporos Rep*, 16, 746-753.
- HISANO, Y., NISHI, T. & KAWAHARA, A. 2012. The functional roles of S1P in immunity. *J Biochem*, 152, 305-11.
- HLA, T. 2004. Physiological and pathological actions of sphingosine 1-phosphate. *Semin Cell Dev Biol*, 15, 513-20.
- HLA, T. & BRINKMANN, V. 2011. Sphingosine 1-phosphate (S1P): Physiology and the effects of S1P receptor modulation. *Neurology*, 76, S3-S8.
- HO, I. A., CHAN, K. Y., NG, W. H., GUO, C. M., HUI, K. M., CHEANG, P. & LAM, P. Y. 2009. Matrix metalloproteinase 1 is necessary for the migration of human bone marrow-derived mesenchymal stem cells toward human glioma. *Stem Cells*, 27, 1366-75.
- HO, J. W., MAN, K., SUN, C. K., LEE, T. K., POON, R. T. & FAN, S. T. 2005. Effects of a novel immunomodulating agent, FTY720, on tumor growth and angiogenesis in hepatocellular carcinoma. *Mol Cancer Ther*, 4, 1430-8.
- HOFFMAN, T., KHADEMHOSEINI, A. & LANGER, R. 2019. Chasing the Paradigm: Clinical Translation of 25 Years of Tissue Engineering. *Tissue Eng Part A*, 25, 679-687.
- HOPPE, A., GÜLDAL, N. S. & BOCCACCINI, A. R. 2011. A review of the biological response to ionic dissolution products from bioactive glasses and glass-ceramics. *Biomaterials*, 32, 2757-2774.
- HOQUE, M. E., NUGE, T., YEOW, T. K., NORDIN, N. & PRASAD, R. 2015. Gelatin based scaffolds for tissue engineering-a review. *Polymers Research Journal*, 9, 15-32.
- HSU, L. C., REDDY, S. V., YILMAZ, O. & YU, H. 2019. Sphingosine-1-Phosphate Receptor 2 Controls Podosome Components Induced by RANKL Affecting Osteoclastogenesis and Bone Resorption. *Cells*, 8.
- HUANG, C., DAS, A., BARKER, D., THOLPADY, S., WANG, T., CUI, Q. J., OGLE, R. & BOTCHWEY, E. 2012. Local delivery of FTY720 accelerates cranial allograft incorporation and bone formation. *Cell and Tissue Research*, 347, 553-566.
- HUANG, C. Y. & OGAWA, R. 2010. Mechanotransduction in bone repair and regeneration. *Faseb Journal*, 24, 3625-3632.
- HULL, C. W. 1984. Apparatus for production of three-dimensional objects by stereolithography. *United States Patent, Appl., No. 638905, Filed*.
- HUNTER, N. L. & SHERMAN, R. E. 2017. Combination products: modernizing the regulatory paradigm. *Nature Reviews Drug Discovery*, 16, 513-514.
- HUTMACHER, D. W. 2000. Scaffolds in tissue engineering bone and cartilage. *Biomaterials*, 21, 2529-2543.

- IAQUINTA, M. R., MAZZONI, E., MANFRINI, M., D'AGOSTINO, A., TREVISIOL, L., NOCINI, R., TROMBELLI, L., BARBANTI-BRODANO, G., MARTINI, F. & TOGNON, M. 2019. Innovative Biomaterials for Bone Regrowth. *Int J Mol Sci*, 20.
- IGARASHI, J., ERWIN, P. A., DANTAS, A. P. V., CHEN, H. & MICHEL, T. 2003. VEGF induces S1P1 receptors in endothelial cells: Implications for cross-talk between sphingolipid and growth factor receptors. *Proceedings of the National Academy of Sciences*, 100, 10664-10669.
- IGARASHI, M., KAMIYA, N., HASEGAWA, M., KASUYA, T., TAKAHASHI, T. & TAKAGI, M. 2004. Inductive effects of dexamethasone on the gene expression of Cbfa1, Osterix and bone matrix proteins during differentiation of cultured primary rat osteoblasts. *J Mol Histol*, 35, 3-10.
- INAGAMI, T., NARUSE, M. & HOOVER, R. 1995. Endothelium as an endocrine organ. *Annu Rev Physiol*, 57, 171-89.
- ISHII, M., EGEN, J. G., KLAUSCHEN, F., MEIER-SCHELLERSHEIM, M., SAEKI, Y., VACHER, J., PROIA, R. L. & GERMAIN, R. N. 2009. Sphingosine-1-phosphate mobilizes osteoclast precursors and regulates bone homeostasis. *Nature*, 458, 524-8.
- ISHII, M., KIKUTA, J., SHIMAZU, Y., MEIER-SCHELLERSHEIM, M. & GERMAIN, R. N. 2010. Chemorepulsion by blood S1P regulates osteoclast precursor mobilization and bone remodeling in vivo. *J Exp Med*, 207, 2793-8.
- ISOGAI, Y., AKATSU, T., ISHIZUYA, T., YAMAGUCHI, A., HORI, M., TAKAHASHI, N. & SUDA, T. 1996. Parathyroid hormone regulates osteoblast differentiation positively or negatively depending on the differentiation stages. *J Bone Miner Res*, 11, 1384-93.
- ISOGLU, I. A., BOLGEN, N., KORKUSUZ, P., VARGEL, I., CELIK, H. H., KILIC, E., GUZEL, E., CAVUSOGLU, T., UCKAN, D. & PISKIN, E. 2019. Stem cells combined 3D electrospun nanofibrous and macrochannelled matrices: a preliminary approach in repair of rat cranial bones. *Artif Cells Nanomed Biotechnol*, 47, 1094-1100.
- JAIN, R. K., AU, P., TAM, J., DUDA, D. G. & FUKUMURA, D. 2005. Engineering vascularized tissue. *Nature biotechnology*, 23, 821-823.
- JANG, J. H., CASTANO, O. & KIM, H. W. 2009. Electrospun materials as potential platforms for bone tissue engineering. *Adv Drug Deliv Rev*, 61, 1065-83.
- JANG, J. H. & SHEA, L. D. 2003. Controllable delivery of non-viral DNA from porous scaffolds. *J Control Release*, 86, 157-68.
- JEONG, J., KIM, J. H., SHIM, J. H., HWANG, N. S. & HEO, C. Y. 2019. Bioactive calcium phosphate materials and applications in bone regeneration. *Biomaterials Research*, 23, 4.
- JEYHANI, M., MAK, S. Y., SAMMUT, S., SHUM, H. C., HWANG, D. K. & TSAI, S. S. H. 2017. Controlled Electrospray Generation of Nonspherical Alginate Microparticles. *Chemphyschem*.
- JIANG, T., CARBONE, E. J., LO, K. W. H. & LAURENCIN, C. T. 2015. Electrospinning of polymer nanofibers for tissue regeneration. *Progress in Polymer Science*, 46, 1-24.
- JIN, S., SUN, F. H., ZOU, Q., HUANG, J. H., ZUO, Y., LI, Y. B., WANG, S. P., CHENG, L., MAN, Y., YANG, F. & LI, J. D. 2019. Fish Collagen and Hydroxyapatite Reinforced Poly(lactide-co-glycolide) Fibrous Membrane for Guided Bone Regeneration. *Biomacromolecules*, 20, 2058-2067.
- JO, E., SANNA, M. G., GONZALEZ-CABRERA, P. J., THANGADA, S., TIGYI, G., OSBORNE, D. A., HLA, T., PARRILL, A. L. & ROSEN, H. 2005. S1P1-selective in vivo-active agonists from high-throughput screening: off-the-shelf chemical probes of receptor interactions, signaling, and fate. *Chem Biol*, 12, 703-15.

- JOHNSON, E. O., TROUPIS, T. & SOUCACOS, P. N. 2011. Tissue-engineered vascularized bone grafts: basic science and clinical relevance to trauma and reconstructive microsurgery. *Microsurgery*, 31, 176-82.
- JONGSMA, M., HENDRIKS-BALK, M. C., MICHEL, M. C., PETERS, S. L. & ALEWIJNSE, A. E. 2006. BML-241 fails to display selective antagonism at the sphingosine-1-phosphate receptor, S1P(3). *Br J Pharmacol*, 149, 277-82.
- JOSE, M. V., THOMAS, V., DEAN, D. R. & NYAIRO, E. 2009a. Fabrication and characterization of aligned nanofibrous PLGA/Collagen blends as bone tissue scaffolds. *Polymer*, 50, 3778-3785.
- JOSE, M. V., THOMAS, V., JOHNSON, K. T., DEAN, D. R. & NYALRO, E. 2009b. Aligned PLGA/HA nanofibrous nanocomposite scaffolds for bone tissue engineering. *Acta Biomaterialia*, 5, 305-315.
- JUNG, B., OBINATA, H., GALVANI, S., MENDELSON, K., DING, B. S., SKOURA, A., KINZEL, B., BRINKMANN, V., RAFII, S., EVANS, T. & HLA, T. 2012. Flow-regulated endothelial S1P receptor-1 signaling sustains vascular development. *Dev Cell*, 23, 600-10.
- KAČAREVIĆ, Ž. P., RIDER, P. M., ALKILDANI, S., RETNASINGH, S., SMEETS, R., JUNG, O., IVANIŠEVIĆ, Z. & BARBECK, M. 2018. An Introduction to 3D Bioprinting: Possibilities, Challenges and Future Aspects. *Materials (Basel, Switzerland)*, 11, 2199.
- KADOW, S., JUX, B., CHMILL, S. & ESSER, C. 2009. Small molecules as friends and foes of the immune system. *Future medicinal chemistry*, 1, 1583-1591.
- KAIGLER, D., WANG, Z., HORGER, K., MOONEY, D. J. & KREBSBACH, P. H. 2006. VEGF Scaffolds Enhance Angiogenesis and Bone Regeneration in Irradiated Osseous Defects. *Journal of Bone and Mineral Research*, 21, 735-744.
- KANAKARIS, N. K. & GIANNOUDIS, P. V. 2007. The health economics of the treatment of long-bone non-unions. *Injury*, 38 Suppl 2, S77-84.
- KARAPLIS, A. C. 2002. Embryonic Development of Bone and the Molecular Regulation of Intramembranous and Endochondral Bone Formation. In: BILEZIKIAN, J. P., RAISZ, L. G. & RODAN, G. A. (eds.) *Principles of Bone Biology*. San Diego, California 92101-4495, USA: ACADEMIC PRESS.
- KAZIMIERCZAK, P., BENKO, A., PALKA, K., CANAL, C., KOLODYNKA, D. & PRZEKORA, A. 2020. Novel synthesis method combining a foaming agent with freeze-drying to obtain hybrid highly macroporous bone scaffolds. *Journal of Materials Science & Technology*, 43, 52-63.
- KELLER, J., CATALA-LEHNEN, P., HUEBNER, A. K., JESCHKE, A., HECKT, T., LUETH, A., KRAUSE, M., KOEHNE, T., ALBERS, J., SCHULZE, J., SCHILLING, S., HABERLAND, M., DENNINGER, H., NEVEN, M., HERMANS-BORGMEYER, I., STREICHERT, T., BREER, S., BARVENCIK, F., LEVKAU, B., RATHKOLB, B., WOLF, E., CALZADA-WACK, J., NEFF, F., GAILUS-DURNER, V., FUCHS, H., DE ANGELIS, M. H., KLUTMANN, S., TSOURDI, E., HOFBAUER, L. C., KLEUSER, B., CHUN, J., SCHINKE, T. & AMLING, M. 2014. Calcitonin controls bone formation by inhibiting the release of sphingosine 1-phosphate from osteoclasts. *Nature Communications*, 5.
- KIKUTA, J., IWAI, K., SAEKI, Y. & ISHII, M. 2011. S1P-targeted therapy for elderly rheumatoid arthritis patients with osteoporosis. *Rheumatol Int*, 31, 967-9.
- KIKUTA, J., KAWAMURA, S., OKIJI, F., SHIRAZAKI, M., SAKAI, S., SAITO, H. & ISHII, M. 2013. Sphingosine-1-phosphate-mediated osteoclast precursor monocyte migration is a critical point of control in antibone-resorptive action of active vitamin D. *Proc Natl Acad Sci U S A*, 110, 7009-13.



- KIM, H. K., KIM, J. H., PARK, D. S., PARK, K. S., KANG, S. S., LEE, J. S., JEONG, M. H. & YOON, T. R. 2012. Osteogenesis induced by a bone forming peptide from the prodomain region of BMP-7. *Biomaterials*, 33, 7057-63.
- KIM, H. K., LEE, J. S., KIM, J. H., SEON, J. K., PARK, K. S., JEONG, M. H. & YOON, T. R. 2017. Bone-forming peptide-2 derived from BMP-7 enhances osteoblast differentiation from multipotent bone marrow stromal cells and bone formation. *Exp Mol Med*, 49, e328.
- KIM, J.-W., YANG, B.-E., HONG, S.-J., CHOI, H.-G., BYEON, S.-J., LIM, H.-K., CHUNG, S.-M., LEE, J.-H. & BYUN, S.-H. 2020. Bone Regeneration Capability of 3D Printed Ceramic Scaffolds. *International Journal of Molecular Sciences*, 21, 4837.
- KIM, S.-S., SUN PARK, M., JEON, O., YONG CHOI, C. & KIM, B.-S. 2006. Poly(lactide-co-glycolide)/hydroxyapatite composite scaffolds for bone tissue engineering. *Biomaterials*, 27, 1399-1409.
- KIM, S., KIM, S.-S., LEE, S.-H., EUN AHN, S., GWAK, S.-J., SONG, J.-H., KIM, B.-S. & CHUNG, H.-M. 2008. In vivo bone formation from human embryonic stem cell-derived osteogenic cells in poly(D,L-lactic-co-glycolic acid)/hydroxyapatite composite scaffolds. *Biomaterials*, 29, 1043-1053.
- KIM, S. S., CHRISTOPHER, L. & JOHN, D. B. 2019a. *Bancroft's Theory and Practice of Histological Techniques E-Book*, [Place of publication not identified], Elsevier.
- KIM, Y. H., FURUYA, H. & TABATA, Y. 2014. Enhancement of bone regeneration by dual release of a macrophage recruitment agent and platelet-rich plasma from gelatin hydrogels. *Biomaterials*, 35, 214-24.
- KIM, Y. H. & TABATA, Y. 2015. Dual-controlled release system of drugs for bone regeneration. *Adv Drug Deliv Rev*, 94, 28-40.
- KIM, Y. S., SMOAK, M. M., MELCHIORRI, A. J. & MIKOS, A. G. 2019b. An Overview of the Tissue Engineering Market in the United States from 2011 to 2018. *Tissue Eng Part A*, 25, 1-8.
- KIM, Y. W., KIM, S. H., XU, X., CHOI, C. H., PARK, C. B. & KIM, H. D. 2002. Fabrication of porous preceramic polymers using carbon dioxide. *Journal of Materials Science Letters*, 21, 1667-1669.
- KLONTZAS, M. E., KENANIDIS, E. I., MACFARLANE, R. J., MICHAIL, T., POTOUPNIS, M. E., HELIOTIS, M., MANTALARIS, A. & TSIRIDIS, E. 2016. Investigational drugs for fracture healing: preclinical & clinical data. *Expert Opin Investig Drugs*, 25, 585-96.
- KO, Y. G., PARK, J. H., LEE, J. B., OH, H. H., PARK, W. H., CHO, D. & KWON, O. H. 2016. Growth behavior of endothelial cells according to electrospun poly(D,L-lactic-co-glycolic acid) fiber diameter as a tissue engineering scaffold. *Tissue Engineering and Regenerative Medicine*, 13, 343-351.
- KOHANE, D. S. & LANGER, R. 2010. Biocompatibility and drug delivery systems. *Chemical Science*, 1, 441-446.
- KOKUBO, T. 1998. Apatite formation on surfaces of ceramics, metals and polymers in body environment. *Acta Materialia*, 46, 2519-2527.
- KOLAMBKAR, Y. M., BOERCKEL, J. D., DUPONT, K. M., BAJIN, M., HUEBSCH, N., MOONEY, D. J., HUTMACHER, D. W. & GULDBERG, R. E. 2011. Spatiotemporal delivery of bone morphogenetic protein enhances functional repair of segmental bone defects. *Bone*, 49, 485-92.
- KONG, Y., WANG, H., LIN, T. & WANG, S. 2014. Sphingosine-1-phosphate/S1P receptors signaling modulates cell migration in human bone marrow-derived mesenchymal stem cells. *Mediators Inflamm*, 2014, 565369.

- KONO, M., MI, Y. D., LIU, Y. J., SASAKI, T., ALLENDE, M. L., WU, Y. P., YAMASHITA, T. & PROIA, R. L. 2004. The sphingosine-1-phosphate receptors S1P1, S1P2, and S1P3 function coordinately during embryonic angiogenesis. *Journal of Biological Chemistry*, 279, 29367-29373.
- KOONS, G. L., DIBA, M. & MIKOS, A. G. 2020. Materials design for bone-tissue engineering. *Nature Reviews Materials*, 5, 584-603.
- KORYCKA, P., MIREK, A., KRAJEK-ROMANOWSKA, K., GRZECZKOWICZ, M. & LEWIŃSKA, D. 2018. Effect of electrospinning process variables on the size of polymer fibers and bead-on-string structures established with a 23 factorial design. *Beilstein Journal of Nanotechnology*, 9, 2466-2478.
- KOZAWA, O., KAWAMURA, H. & UEMATSU, T. 2000. Sphingosine 1-phosphate amplifies phosphoinositide hydrolysis stimulated by prostaglandin f2 alpha in osteoblasts: involvement of p38MAP kinase. *Prostaglandins Leukot Essent Fatty Acids*, 62, 355-9.
- KOZAWA, O., NIWA, M., MATSUNO, H., TOKUDA, H., MIWA, M., ITO, H., KATO, K. & UEMATSU, T. 1999. Sphingosine 1-phosphate induces heat shock protein 27 via p38 mitogen-activated protein kinase activation in osteoblasts. *Journal of Bone and Mineral Research*, 14, 1761-1767.
- KOZAWA, O., TOKUDA, H., MATSUNO, H. & UEMATSU, T. 1997. Activation of mitogen-activated protein kinase is involved in sphingosine 1-phosphate-stimulated interleukin-6 synthesis in osteoblasts. *Febs Letters*, 418, 149-151.
- KRETLOW, J. D. & MIKOS, A. G. 2007. Mineralization of synthetic polymer scaffolds for bone tissue engineering. *Tissue engineering*, 13, 927-938.
- KRETLOW, J. D., YOUNG, S., KLOUDA, L., WONG, M. & MIKOS, A. G. 2009. Injectable Biomaterials for Regenerating Complex Craniofacial Tissues. *Advanced Materials*, 21, 3368-3393.
- KRISHNAN, L., PRIDDY, L. B., ESANCY, C., KLOSTERHOFF, B. S., STEVENS, H. Y., TRAN, L. & GULDBERG, R. E. 2017. Delivery vehicle effects on bone regeneration and heterotopic ossification induced by high dose BMP-2. *Acta Biomater*, 49, 101-112.
- KUTTAPPAN, S., MATHEW, D., JO, J. I., TANAKA, R., MENON, D., ISHIMOTO, T., NAKANO, T., NAIR, S. V., NAIR, M. B. & TABATA, Y. 2018. Dual release of growth factor from nanocomposite fibrous scaffold promotes vascularisation and bone regeneration in rat critical sized calvarial defect. *Acta Biomater*, 78, 36-47.
- KWON, Y. G., MIN, J. K., KIM, K. M., LEE, D. J., BILLIAR, T. R. & KIM, Y. M. 2001. Sphingosine 1-phosphate protects human umbilical vein endothelial cells from serum-deprived apoptosis by nitric oxide production. *J Biol Chem*, 276, 10627-33.
- LAI, Y., LI, Y., CAO, H., LONG, J., WANG, X., LI, L., LI, C., JIA, Q., TENG, B., TANG, T., PENG, J., EGLIN, D., ALINI, M., GRIJPMAN, D. W., RICHARDS, G. & QIN, L. 2019. Osteogenic magnesium incorporated into PLGA/TCP porous scaffold by 3D printing for repairing challenging bone defect. *Biomaterials*, 197, 207-219.
- LAMONTAGNE, K., LITTLEWOOD-EVANS, A., SCHNELL, C., O'REILLY, T., WYDER, L., SANCHEZ, T., PROBST, B., BUTLER, J., WOOD, A., LIAU, G., BILLY, E., THEUER, A., HLA, T. & WOOD, J. 2006. Antagonism of sphingosine-1-phosphate receptors by FTY720 inhibits angiogenesis and tumor vascularization. *Cancer Res*, 66, 221-31.
- LAMPASSO, J. D., KAMER, A., MARGARONE, J. & DZIAK, R. 2001. Sphingosine-1-phosphate effects on PKC isoform expression in human osteoblastic cells. *Prostaglandins Leukotrienes and Essential Fatty Acids*, 65, 139-146.
- LAMPASSO, J. D., MARZEC, N., MARGARONE, J. & DZIAK, R. 2002. Role of protein kinase C alpha in primary human osteoblast proliferation. *Journal of Bone and Mineral Research*, 17, 1968-1976.

- LAURENCIN, C., KHAN, Y. & EL-AMIN, S. F. 2006. Bone graft substitutes. *Expert Rev Med Devices*, 3, 49-57.
- LAURENCIN, C. T., ASHE, K. M., HENRY, N., KAN, H. M. & LO, K. W. 2014. Delivery of small molecules for bone regenerative engineering: preclinical studies and potential clinical applications. *Drug Discov Today*, 19, 794-800.
- LEE, D. E., KIM, J. H., CHOI, S. H., CHA, J. H., BAK, E. J. & YOO, Y. J. 2017. The sphingosine-1-phosphate receptor 1 binding molecule FTY720 inhibits osteoclast formation in rats with ligature-induced periodontitis. *J Periodontal Res*, 52, 33-41.
- LEE, H., GOETZL, E. J. & AN, S. 2000. Lysophosphatidic acid and sphingosine 1-phosphate stimulate endothelial cell wound healing. *Am J Physiol Cell Physiol*, 278, C612-8.
- LEE, J. F., GORDON, S., ESTRADA, R., WANG, L., SIOW, D. L., WATTENBERG, B. W., LOMINADZE, D. & LEE, M. J. 2009. Balance of S1P1 and S1P2 signaling regulates peripheral microvascular permeability in rat cremaster muscle vasculature. *Am J Physiol Heart Circ Physiol*, 296, 33-42.
- LEE, M. J., THANGADA, S., CLAFFEY, K. P., ANCELLIN, N., LIU, C. H., KLUK, M., VOLPI, M., SHA'AFI, R. I. & HLA, T. 1999a. Vascular endothelial cell adherens junction assembly and morphogenesis induced by sphingosine-1-phosphate. *Cell*, 99, 301-12.
- LEE, O. H., KIM, Y. M., LEE, Y. M., MOON, E. J., LEE, D. J., KIM, J. H., KIM, K. W. & KWON, Y. G. 1999b. Sphingosine 1-phosphate induces angiogenesis: its angiogenic action and signaling mechanism in human umbilical vein endothelial cells. *Biochem Biophys Res Commun*, 264, 743-50.
- LEE, Y. J., LEE, J. H., CHO, H. J., KIM, H. K., YOON, T. R. & SHIN, H. 2013. Electrospun fibers immobilized with bone forming peptide-1 derived from BMP7 for guided bone regeneration. *Biomaterials*, 34, 5059-69.
- LEI, Y., XU, Z., KE, Q., YIN, W., CHEN, Y., ZHANG, C. & GUO, Y. 2017. Strontium hydroxyapatite/chitosan nanohybrid scaffolds with enhanced osteoinductivity for bone tissue engineering. *Materials Science and Engineering: C*, 72, 134-142.
- LEIJTEN, J., CHAI, Y. C., PAPANTONIOU, I., GERIS, L., SCHROOTEN, J. & LUYTEN, F. P. 2015. Cell based advanced therapeutic medicinal products for bone repair: Keep it simple? *Adv Drug Deliv Rev*, 84, 30-44.
- LEVI, B., HYUN, J. S., MONTORO, D. T., LO, D. D., CHAN, C. K., HU, S., SUN, N., LEE, M., GROVA, M. & CONNOLLY, A. J. 2012. In vivo directed differentiation of pluripotent stem cells for skeletal regeneration. *Proceedings of the National Academy of Sciences*, 109, 20379-20384.
- LI, L., LI, J., GUO, J., ZHANG, H., ZHANG, X., YIN, C., WANG, L., ZHU, Y. & YAO, Q. 2019a. 3D molecularly functionalized cell-free biomimetic scaffolds for osteochondral regeneration. *Advanced Functional Materials*, 29, 1807356.
- LI, S., SONG, C., YANG, S., YU, W., ZHANG, W., ZHANG, G., XI, Z. & LU, E. 2019b. Supercritical CO<sub>2</sub> foamed composite scaffolds incorporating bioactive lipids promote vascularized bone regeneration via Hif-1 $\alpha$  upregulation and enhanced type H vessel formation. *Acta Biomater*, 94, 253-267.
- LIM, H. & HOAG, S. W. 2013. Plasticizer effects on physical-mechanical properties of solvent cast Soluplus(R) films. *AAPS PharmSciTech*, 14, 903-10.
- LIU, C. H. & HLA, T. 1997. The mouse gene for the inducible G-protein-coupled receptor edg-1. *Genomics*, 43, 15-24.
- LIU, H., LIN, M., LIU, X., ZHANG, Y., LUO, Y., PANG, Y., CHEN, H., ZHU, D., ZHONG, X., MA, S., ZHAO, Y., YANG, Q. & ZHANG, X. 2020. Doping bioactive elements into a collagen scaffold based on synchronous self-assembly/mineralization for bone tissue engineering. *Bioactive Materials*, 5, 844-858.

- LIU, J., HSU, A., LEE, J. F., CRAMER, D. E. & LEE, M. J. 2011. To stay or to leave: Stem cells and progenitor cells navigating the S1P gradient. *World J Biol Chem*, 2, 1-13.
- LIU, R., FARACH-CARSON, M. C. & KARIN, N. J. 1995. Effects of sphingosine derivatives on MC3T3-E1 pre-osteoblasts: psychosine elicits release of calcium from intracellular stores. *Biochem Biophys Res Commun*, 214, 676-84.
- LIU, Y., PAPOUTSAKIS, D. & RODDY, E. 2012. Polymorphic form of 1-(4-{1-[(E)-4-cyclohexyl-3-trifluoromethyl-benzoyloxyimino]-ethyl}-2-ethyl-benzyl)-azetidine-3-carboxylic. Google Patents.
- LIU, Y., WADA, R., YAMASHITA, T., MI, Y., DENG, C. X., HOBSON, J. P., ROSENFELDT, H. M., NAVA, V. E., CHAE, S. S., LEE, M. J., LIU, C. H., HLA, T., SPIEGEL, S. & PROIA, R. L. 2000. Edg-1, the G protein-coupled receptor for sphingosine-1-phosphate, is essential for vascular maturation. *J Clin Invest*, 106, 951-61.
- LOI, F., CORDOVA, L. A., PAJARINEN, J., LIN, T. H., YAO, Z. & GOODMAN, S. B. 2016. Inflammation, fracture and bone repair. *Bone*, 86, 119-30.
- LONG, F. 2011. Building strong bones: molecular regulation of the osteoblast lineage. *Nat Rev Mol Cell Biol*, 13, 27-38.
- LOTINUN, S., KIVIRANTA, R., MATSUBARA, T., ALZATE, J. A., NEFF, L., LUTH, A., KOSKIVIRTA, I., KLEUSER, B., VACHER, J., VUORIO, E., HORNE, W. C. & BARON, R. 2013. Osteoclast-specific cathepsin K deletion stimulates S1P-dependent bone formation. *Journal of Clinical Investigation*, 123, 666-681.
- LOU, Y.-R., TOH, T. C., TEE, Y. H. & YU, H. 2017. 25-Hydroxyvitamin D(3) induces osteogenic differentiation of human mesenchymal stem cells. *Scientific reports*, 7, 42816-42816.
- LUCKE, S. & LEVKAU, B. 2010. Endothelial functions of sphingosine-1-phosphate. *Cell Physiol Biochem*, 26, 87-96.
- LUKAS, S., PATNAUDE, L., HAXHINASTO, S., SLAVIN, A., HILL-DRZEWI, M., HORAN, J. & MODIS, L. K. 2014. No Differences Observed among Multiple Clinical S1P(1) Receptor Agonists (Functional Antagonists) in S1P(1) Receptor Down-regulation and Degradation. *Journal of Biomolecular Screening*, 19, 407-416.
- LUPINO, L., PERRY, T., MARGIELEWSKA, S., HOLLOWES, R., IBRAHIM, M., CARE, M., ALLEGOOD, J., TOOZE, R., SABBADINI, R., REYNOLDS, G., BICKNELL, R., RUDZKI, Z., LIN HOCK, Y., ZANETTO, U., WEI, W., SIMMONS, W., SPIEGEL, S., WOODMAN, C. B. J., ROWE, M., VRZALIKOVA, K. & MURRAY, P. G. 2019. Sphingosine-1-phosphate signalling drives an angiogenic transcriptional programme in diffuse large B cell lymphoma. *Leukemia*.
- LYONS, J. M. & KARIN, N. J. 2001. A role for G protein-coupled lysophospholipid receptors in sphingolipid-induced Ca<sup>2+</sup> signaling in MC3T3-E1 osteoblastic cells. *J Bone Miner Res*, 16, 2035-42.
- MACEYKA, M., HARIKUMAR, K. B., MILSTIEN, S. & SPIEGEL, S. 2012. Sphingosine-1-phosphate signaling and its role in disease. *Trends Cell Biol*, 22, 50-60.
- MACEYKA, M. & SPIEGEL, S. 2014. Sphingolipid metabolites in inflammatory disease. *Nature*, 510, 58-67.
- MAKADIA, H. K. & SIEGEL, S. J. 2011. Poly Lactic-co-Glycolic Acid (PLGA) as Biodegradable Controlled Drug Delivery Carrier. *Polymers (Basel)*, 3, 1377-1397.
- MALLADI, L., MAHAPATRO, A. & GOMES, A. S. 2018. Fabrication of magnesium-based metallic scaffolds for bone tissue engineering. *Materials Technology*, 33, 173-182.
- MANGIAVINI, L., MERCERON, C., ARALDI, E., KHATRI, R., GERARD-O'RILEY, R., WILSON, T. L., SANDUSKY, G., ABADIE, J., LYONS, K. M., GIACCIA, A. J. & SCHIPANI, E. 2015. Fibrosis and hypoxia-inducible factor-1alpha-dependent tumors of the soft tissue on loss of von Hippel-Lindau in mesenchymal progenitors. *Am J Pathol*, 185, 3090-101.

- MARCINIAK, A., CAMP, S. M., GARCIA, J. G. N. & POLT, R. 2018. An update on sphingosine-1-phosphate receptor 1 modulators. *Bioorg Med Chem Lett*, 28, 3585-3591.
- MAREI, H. F., MAHMOOD, K. & ALMAS, K. 2018. Critical Size Defects for Bone Regeneration Experiments in the Dog Mandible: A Systematic Review. *Implant Dent*, 27, 135-141.
- MARSELL, R. & EINHORN, T. A. 2011. The biology of fracture healing. *Injury*, 42, 551-5.
- MARTIN, T. J. & SIMS, N. A. 2015. Calcitonin physiology, saved by a lysophospholipid. *J Bone Miner Res*, 30, 212-5.
- MARTINO, M. M., BRIQUEZ, P. S., MARUYAMA, K. & HUBBELL, J. A. 2015. Extracellular matrix-inspired growth factor delivery systems for bone regeneration. *Adv Drug Deliv Rev*, 94, 41-52.
- MARYCZ, K., KRZAK, J., MAREDZIAK, M., TOMASZEWSKI, K. A., SZCZUREK, A. & MOSZAK, K. 2016. The influence of metal-based biomaterials functionalized with sphingosine-1-phosphate on the cellular response and osteogenic differentiation potential of human adipose derived mesenchymal stem cells invitro. *Journal of Biomaterials Applications*, 30, 1517-1533.
- MASAEI, R., ZANDSALIMI, K., RASOULIANBOROUJENI, M. & TAYEBI, L. 2019. Challenges in Three-Dimensional Printing of Bone Substitutes. *Tissue Engineering Part B: Reviews*, 25, 387-397.
- MASUKO, K., MURATA, M., NAKAMURA, H., YUDOH, K., NISHIOKA, K. & KATO, T. 2007. Sphingosine-1-phosphate attenuates proteoglycan aggrecan expression via production of prostaglandin E2 from human articular chondrocytes. *BMC Musculoskelet Disord*, 8, 29.
- MATIC, I., MATTHEWS, B. G., WANG, X., DYMENT, N. A., WORTHLEY, D. L., ROWE, D. W., GRCEVIC, D. & KALAJZIC, I. 2016. Quiescent Bone Lining Cells Are a Major Source of Osteoblasts During Adulthood. *Stem Cells*, 34, 2930-2942.
- MATSUZAKI, E., HIRATSUKA, S., HAMACHI, T., TAKAHASHI-YANAGA, F., HASHIMOTO, Y., HIGASHI, K., KOBAYASHI, M., HIROFUJI, T., HIRATA, M. & MAEDA, K. 2013. Sphingosine-1-phosphate promotes the nuclear translocation of beta-catenin and thereby induces osteoprotegerin gene expression in osteoblast-like cell lines. *Bone*, 55, 315-324.
- MATUANA, L. M. 2008. Solid state microcellular foamed poly(lactic acid): morphology and property characterization. *Bioresour Technol*, 99, 3643-50.
- MEHTA, M., SCHMIDT-BLEEK, K., DUDA, G. N. & MOONEY, D. J. 2012. Biomaterial delivery of morphogens to mimic the natural healing cascade in bone. *Advanced Drug Delivery Reviews*, 64, 1257-1276.
- MEHTA, S., BLAGG, R., WILLCOCKSON, J., GOCIMAN, B., YAMASHIRO, D. & SIDDIQI, F. 2018. Cost-Effectiveness Analysis of Demineralized Bone Matrix and rhBMP-2 versus Autologous Iliac Crest Bone Grafting in Alveolar Cleft Patients. *Plast Reconstr Surg*, 142, 737-743.
- MERIANE, M., DUHAMEL, S., LEJEUNE, L., GALIPEAU, J. & ANNABI, B. 2006. Cooperation of matrix metalloproteinases with the RhoA/Rho kinase and mitogen-activated protein kinase kinase-1/extracellular signal-regulated kinase signaling pathways is required for the sphingosine-1-phosphate-induced mobilization of marrow-derived stromal cells. *Stem Cells*, 24, 2557-65.
- MESHCHERYAKOVA, A., MECHTCHERIAKOVA, D. & PIETSCHMANN, P. 2017. Sphingosine 1-phosphate signaling in bone remodeling: multifaceted roles and therapeutic potential. *Expert Opin Ther Targets*, 21, 725-737.
- MILLS, L. A. & SIMPSON, A. H. 2013. The relative incidence of fracture non-union in the Scottish population (5.17 million): a 5-year epidemiological study. *BMJ Open*, 3.

- MOGHADAM, M. Z., HASSANAJILI, S., ESMAEILZADEH, F., AYATOLLAHI, M. & AHMADI, M. 2017. Formation of porous HPCL/LPCL/HA scaffolds with supercritical CO<sub>2</sub> gas foaming method. *Journal of the Mechanical Behavior of Biomedical Materials*, 69, 115-127.
- MOHAMED, A. M. 2008. An overview of bone cells and their regulating factors of differentiation. *The Malaysian journal of medical sciences : MJMS*, 15, 4-12.
- MOHIUDDIN, O. A., CAMPBELL, B., POCHE, J. N., MA, M., ROGERS, E., GAUPP, D., HARRISON, M. A. A., BUNNELL, B. A., HAYES, D. J. & GIMBLE, J. M. 2019. Decellularized Adipose Tissue Hydrogel Promotes Bone Regeneration in Critical-Sized Mouse Femoral Defect Model. *Front Bioeng Biotechnol*, 7, 211.
- MONTORO, D. T., WAN, D. C. & LONGAKER, M. T. 2014. Chapter 60 - Skeletal Tissue Engineering. In: LANZA, R., LANGER, R. & VACANTI, J. (eds.) *Principles of Tissue Engineering (Fourth Edition)*. Boston: Academic Press.
- MOONEY, D. J., BALDWIN, D. F., SUH, N. P., VACANTI, J. P. & LANGER, R. 1996. Novel approach to fabricate porous sponges of poly(d,l-lactic-co-glycolic acid) without the use of organic solvents. *Biomaterials*, 17, 1417-1422.
- MOSTAFA, N. Z., FITZSIMMONS, R., MAJOR, P. W., ADESIDA, A., JOMHA, N., JIANG, H. & ULUDAĞ, H. 2012. Osteogenic differentiation of human mesenchymal stem cells cultured with dexamethasone, vitamin D<sub>3</sub>, basic fibroblast growth factor, and bone morphogenetic protein-2. *Connect Tissue Res*, 53, 117-31.
- MULLERSHAUSEN, F., ZECRI, F., CETIN, C., BILLICH, A., GUERINI, D. & SEUWEN, K. 2009. Persistent signaling induced by FTY720-phosphate is mediated by internalized S1P<sub>1</sub> receptors. *Nat Chem Biol*, 5, 428-34.
- MURAKAMI, M., SAITO, T. & TABATA, Y. 2014. Controlled release of sphingosine-1-phosphate agonist with gelatin hydrogels for macrophage recruitment. *Acta Biomater*, 10, 4723-9.
- MURPHY, C. M., HAUGH, M. G. & O'BRIEN, F. J. 2010. The effect of mean pore size on cell attachment, proliferation and migration in collagen-glycosaminoglycan scaffolds for bone tissue engineering. *Biomaterials*, 31, 461-6.
- MURPHY, S. V. & ATALA, A. 2014. 3D bioprinting of tissues and organs. *Nature Biotechnology*, 32, 773-785.
- NAKATANI, Y., TSUNOI, M., HAKEDA, Y., KURIHARA, N., FUJITA, K. & KUMEGAWA, M. 1984. Effects of parathyroid hormone on cAMP production and alkaline phosphatase activity in osteoblastic clone MC3T3-E1 cells. *Biochem Biophys Res Commun*, 123, 894-8.
- NASH, T. J., HOWLETT, C. R., MARTIN, C., STEELE, J., JOHNSON, K. A. & HICKLIN, D. J. 1994. Effect of platelet-derived growth factor on tibial osteotomies in rabbits. *Bone*, 15, 203-208.
- NEREM, R. M. & SCHUTTE, S. C. 2014. Chapter 2 - The Challenge of Imitating Nature. In: LANZA, R., LANGER, R. & VACANTI, J. (eds.) *Principles of Tissue Engineering (Fourth Edition)*. Boston: Academic Press.
- NGIAM, M., LIAO, S., PATIL, A. J., CHENG, Z., CHAN, C. K. & RAMAKRISHNA, S. 2009. The fabrication of nano-hydroxyapatite on PLGA and PLGA/collagen nanofibrous composite scaffolds and their effects in osteoblastic behavior for bone tissue engineering. *Bone*, 45, 4-16.
- NGUYEN, T. T. & JEONG, J. H. 2018. Development of a single-jet electrospray method for producing quercetin-loaded poly (lactic-co-glycolic acid) microspheres with prolonged-release patterns. *Journal of Drug Delivery Science and Technology*, 47, 268-274.

- NIESSEN, F., SCHAFFNER, F., FURLAN-FREGUIA, C., PAWLINSKI, R., BHATTACHARJEE, G., CHUN, J., DERIAN, C. K., ANDRADE-GORDON, P., ROSEN, H. & RUF, W. 2008. Dendritic cell PAR1-S1P3 signalling couples coagulation and inflammation. *Nature*, 452, 654-8.
- NIJSURE, M. P. & KISHORE, V. 2017. Collagen-Based Scaffolds for Bone Tissue Engineering Applications. In: LI, B. & WEBSTER, T. (eds.) *Orthopedic Biomaterials: Advances and Applications*. Cham: Springer International Publishing.
- NISHIHARA, S., IKEDA, M., OZAWA, H., AKIYAMA, M., YAMAGUCHI, S. & NAKAHAMA, K. I. 2018. Role of cAMP in phenotypic changes of osteoblasts. *Biochem Biophys Res Commun*, 495, 941-946.
- NOF, M. & SHEA, L. D. 2002. Drug-releasing scaffolds fabricated from drug-loaded microspheres. *Journal of Biomedical Materials Research*, 59, 349-356.
- O'SULLIVAN, C., SCHUBART, A., MIR, A. K. & DEV, K. K. 2016. The dual S1PR1/S1PR5 drug BAF312 (Siponimod) attenuates demyelination in organotypic slice cultures. *J Neuroinflammation*, 13, 31.
- OGLE, M. E., OLINGY, C. E., AWOJODU, A. O., DAS, A., ORTIZ, R. A., CHEUNG, H. Y. & BOTCHWEY, E. A. 2017. Sphingosine-1-Phosphate Receptor-3 Supports Hematopoietic Stem and Progenitor Cell Residence Within the Bone Marrow Niche. *Stem Cells*, 35, 1040-1052.
- OGLE, M. E., SEFCIK, L. S., AWOJODU, A. O., CHIAPPA, N. F., LYNCH, K., PEIRCE-COTTLER, S. & BOTCHWEY, E. A. 2014. Engineering in vivo gradients of sphingosine-1-phosphate receptor ligands for localized microvascular remodeling and inflammatory cell positioning. *Acta Biomater*, 10, 4704-14.
- OGLE, M. E., SEGAR, C. E., SRIDHAR, S. & BOTCHWEY, E. A. 2016. Monocytes and macrophages in tissue repair: Implications for immunoregenerative biomaterial design. *Exp Biol Med (Maywood)*, 241, 1084-97.
- OHMORI, T., YATOMI, Y., OKAMOTO, H., MIURA, Y., RILE, G., SATOH, K. & OZAKI, Y. 2001. G(i)-mediated Cas tyrosine phosphorylation in vascular endothelial cells stimulated with sphingosine 1-phosphate: possible involvement in cell motility enhancement in cooperation with Rho-mediated pathways. *J Biol Chem*, 276, 5274-80.
- OKUDA, T., TOMINAGA, K. & KIDOAKI, S. 2010. Time-programmed dual release formulation by multilayered drug-loaded nanofiber meshes. *J Control Release*, 143, 258-64.
- OLIVERA, A. & SPIEGEL, S. 1993. Sphingosine-1-phosphate as second messenger in cell proliferation induced by PDGF and FCS mitogens. *Nature*, 365, 557-60.
- ORYAN, A., BAGHABAN ESLAMINEJAD, M., KAMALI, A., HOSSEINI, S., MOSHIRI, A. & BAHARVAND, H. 2018. Mesenchymal stem cells seeded onto tissue-engineered osteoinductive scaffolds enhance the healing process of critical-sized radial bone defects in rat. *Cell and Tissue Research*, 374, 63-81.
- OSKERITZIAN, C. A., PRICE, M. M., HAIT, N. C., KAPITONOV, D., FALANGA, Y. T., MORALES, J. K., RYAN, J. J., MILSTIEN, S. & SPIEGEL, S. 2010. Essential roles of sphingosine-1-phosphate receptor 2 in human mast cell activation, anaphylaxis, and pulmonary edema. *J Exp Med*, 207, 465-74.
- OYAMA, O., SUGIMOTO, N., QI, X., TAKUWA, N., MIZUGISHI, K., KOIZUMI, J. & TAKUWA, Y. 2008. The lysophospholipid mediator sphingosine-1-phosphate promotes angiogenesis in vivo in ischaemic hindlimbs of mice. *Cardiovasc Res*, 78, 301-7.
- PANDOLFI, L., MINARDI, S., TARABALLI, F., LIU, X., FERRARI, M. & TASCOTTI, E. 2016. Composite microsphere-functionalized scaffold for the controlled release of small molecules in tissue engineering. *J Tissue Eng*, 7, 2041731415624668.

- PANETTI, T. S. 2002. Differential effects of sphingosine 1-phosphate and lysophosphatidic acid on endothelial cells. *Biochimica et Biophysica Acta (BBA)-Molecular and Cell Biology of Lipids*, 1582, 190-196.
- PARHIZKAR, M., REARDON, P. J. T., KNOWLES, J. C., BROWNING, R. J., STRIDE, E., PEDLEY, R. B., GREGO, T. & EDIRISINGHE, M. 2017. Performance of novel high throughput multi electrospray systems for forming of polymeric micro/nanoparticles. *Materials & Design*, 126, 73-84.
- PARK, P. I. P. & JONNALAGADDA, S. 2006. Predictors of glass transition in the biodegradable polylactide and poly-lactide-co-glycolide polymers. *Journal of Applied Polymer Science*, 100, 1983-1987.
- PATMANATHAN, S. N., WANG, W., YAP, L. F., HERR, D. R. & PATERSON, I. C. 2017. Mechanisms of sphingosine 1-phosphate receptor signalling in cancer. *Cellular signalling*, 34, 66-75.
- PEARSON, J. J., GERKEN, N., BAE, C., LEE, K.-B., SATSANGI, A., MCBRIDE, S., APPLEFORD, M. R., DEAN, D. D., HOLLINGER, J. O., ONG, J. L. & GUDA, T. 2020. In vivo hydroxyapatite scaffold performance in infected bone defects. *Journal of Biomedical Materials Research Part B: Applied Biomaterials*, 108, 1157-1166.
- PEDERSON, L., RUAN, M., WESTENDORF, J. J., KHOSLA, S. & OURSLER, M. J. 2008. Regulation of bone formation by osteoclasts involves Wnt/BMP signaling and the chemokine sphingosine-1-phosphate. *Proc Natl Acad Sci U S A*, 105, 20764-9.
- PEPPAS, N. A. 1983. A model of dissolution-controlled solute release from porous drug delivery polymeric systems. *J Biomed Mater Res*, 17, 1079-87.
- PEREZ, J. R., KOUROUPIS, D., LI, D. J., BEST, T. M., KAPLAN, L. & CORREA, D. 2018. Tissue Engineering and Cell-Based Therapies for Fractures and Bone Defects. *Frontiers in Bioengineering and Biotechnology*, 6.
- PETIT, C., BATOOL, F., STUTZ, C., ANTON, N., KLYMCHENKO, A., VANDAMME, T., BENKIRANE-JESSEL, N. & HUCK, O. 2020. Development of a thermosensitive statin loaded chitosan-based hydrogel promoting bone healing. *International Journal of Pharmaceutics*, 586, 119534.
- PETITE, H., VIATEAU, V., BENSALID, W., MEUNIER, A., DE POLLAK, C., BOURGUIGNON, M., OUDINA, K., SEDEL, L. & GUILLEMIN, G. 2000. Tissue-engineered bone regeneration. *Nat Biotechnol*, 18, 959-63.
- PETRIE ARONIN, C. E., SEFCIK, L. S., THOLPADY, S. S., THOLPADY, A., SADIK, K. W., MACDONALD, T. L., PEIRCE, S. M., WAMHOFF, B. R., LYNCH, K. R., OGLE, R. C. & BOTCHWEY, E. A. 2010a. FTY720 promotes local microvascular network formation and regeneration of cranial bone defects. *Tissue Eng Part A*, 16, 1801-9.
- PETRIE ARONIN, C. E., SHIN, S. J., NADEN, K. B., RIOS, P. D., JR., SEFCIK, L. S., ZAWODNY, S. R., BAGAYOKO, N. D., CUI, Q., KHAN, Y. & BOTCHWEY, E. A. 2010b. The enhancement of bone allograft incorporation by the local delivery of the sphingosine 1-phosphate receptor targeted drug FTY720. *Biomaterials*, 31, 6417-24.
- PHAM, Q. P., SHARMA, U. & MIKOS, A. G. 2006. Electrospinning of polymeric nanofibers for tissue engineering applications: a review. *Tissue Eng*, 12, 1197-211.
- PHIPPS, M. C., CLEM, W. C., GRUNDA, J. M., CLINES, G. A. & BELLIS, S. L. 2012a. Increasing the pore sizes of bone-mimetic electrospun scaffolds comprised of polycaprolactone, collagen I and hydroxyapatite to enhance cell infiltration. *Biomaterials*, 33, 524-534.
- PHIPPS, M. C., XU, Y. & BELLIS, S. L. 2012b. Delivery of Platelet-Derived Growth Factor as a Chemotactic Factor for Mesenchymal Stem Cells by Bone-Mimetic Electrospun Scaffolds. *PLOS ONE*, 7, e40831.



- POLO-CORRALES, L., LATORRE-ESTEVEZ, M. & RAMIREZ-VICK, J. E. 2014. Scaffold design for bone regeneration. *Journal of nanoscience and nanotechnology*, 14, 15-56.
- PRASAD, A., SANKAR, M. R. & KATIYAR, V. 2017. State of Art on Solvent Casting Particulate Leaching Method for Orthopedic Scaffolds Fabrication. *Materials Today: Proceedings*, 4, 898-907.
- PRICE, S. T., BECKHAM, T. H., CHENG, J. C., LU, P., LIU, X. & NORRIS, J. S. 2015. Sphingosine 1-Phosphate Receptor 2 Regulates the Migration, Proliferation, and Differentiation of Mesenchymal Stem Cells. *Int J Stem Cell Res Ther*, 2.
- QI, X., OKAMOTO, Y., MURAKAWA, T., WANG, F., OYAMA, O., OHKAWA, R., YOSHIOKA, K., DU, W., SUGIMOTO, N., YATOMI, Y., TAKUWA, N. & TAKUWA, Y. 2010. Sustained delivery of sphingosine-1-phosphate using poly(lactic-co-glycolic acid)-based microparticles stimulates Akt/ERK-eNOS mediated angiogenesis and vascular maturation restoring blood flow in ischemic limbs of mice. *Eur J Pharmacol*, 634, 121-31.
- QU, H., FU, H., HAN, Z. & SUN, Y. 2019. Biomaterials for bone tissue engineering scaffolds: a review. *RSC advances*, 9, 26252-26262.
- QUANCARD, J., BOLLBUCK, B., JANSER, P., ANGST, D., BERST, F., BUEHLMAYER, P., STREIFF, M., BEERLI, C., BRINKMANN, V., GUERINI, D., SMITH, P. A., SEABROOK, T. J., TRAEBERT, M., SEUWEN, K., HERSPERGER, R., BRUNS, C., BASSILANA, F. & BIGAUD, M. 2012. A Potent and Selective S1P(1) Antagonist with Efficacy in Experimental Autoimmune Encephalomyelitis. *Chemistry & Biology*, 19, 1142-1151.
- QUINT, P., RUAN, M., PEDERSON, L., KASSEM, M., WESTENDORF, J. J., KHOSLA, S. & OURSLER, M. J. 2013. Sphingosine 1-phosphate (S1P) receptors 1 and 2 coordinately induce mesenchymal cell migration through S1P activation of complementary kinase pathways. *J Biol Chem*, 288, 5398-406.
- RAGGATT, L. J. & PARTRIDGE, N. C. 2010. Cellular and molecular mechanisms of bone remodeling. *Journal of Biological Chemistry*, 285, 25103-25108.
- RAHAMAN, M. N., DAY, D. E., SONNY BAL, B., FU, Q., JUNG, S. B., BONEWALD, L. F. & TOMSIA, A. P. 2011. Bioactive glass in tissue engineering. *Acta Biomaterialia*, 7, 2355-2373.
- RAHMAN, C. V., BEN-DAVID, D., DHILLON, A., KUHN, G., GOULD, T. W. A., MÜLLER, R., ROSE, F. R. A. J., SHAKESHEFF, K. M. & LIVNE, E. 2014. Controlled release of BMP-2 from a sintered polymer scaffold enhances bone repair in a mouse calvarial defect model. *Journal of Tissue Engineering and Regenerative Medicine*, 8, 59-66.
- RAMESH, N., MORATTI, S. C. & DIAS, G. J. 2018. Hydroxyapatite-polymer biocomposites for bone regeneration: A review of current trends. *Journal of Biomedical Materials Research Part B: Applied Biomaterials*, 106, 2046-2057.
- RATAJCZAK, M. Z., SUSZYNSKA, M., BORKOWSKA, S., RATAJCZAK, J. & SCHNEIDER, G. 2014. The role of sphingosine-1 phosphate and ceramide-1 phosphate in trafficking of normal stem cells and cancer cells. *Expert Opinion on Therapeutic Targets*, 18, 95-107.
- REY-VINOLAS, S., ENGEL, E. & MATEOS-TIMONEDA, M. A. 2019. 7 - Polymers for bone repair. In: PAWELEC, K. M. & PLANELL, J. A. (eds.) *Bone Repair Biomaterials (Second Edition)*. Woodhead Publishing.
- REZWAN, K., CHEN, Q. Z., BLAKER, J. J. & BOCCACCINI, A. R. 2006. Biodegradable and bioactive porous polymer/inorganic composite scaffolds for bone tissue engineering. *Biomaterials*, 27, 3413-31.
- RHO, J.-Y., KUHN-SPEARING, L. & ZIOUPOS, P. 1998. Mechanical properties and the hierarchical structure of bone. *Medical Engineering & Physics*, 20, 92-102.

- RIKITAKE, Y., HIRATA, K., KAWASHIMA, S., OZAKI, M., TAKAHASHI, T., OGAWA, W., INOUE, N. & YOKOYAMA, M. 2002. Involvement of endothelial nitric oxide in sphingosine-1-phosphate-induced angiogenesis. *Arterioscler Thromb Vasc Biol*, 22, 108-14.
- RILEY, C. M., FUEGY, P. W., FIRPO, M. A., SHU, X. Z., PRESTWICH, G. D. & PEATTIE, R. A. 2006. Stimulation of in vivo angiogenesis using dual growth factor-loaded crosslinked glycosaminoglycan hydrogels. *Biomaterials*, 27, 5935-43.
- RODAN, G. A., BOURRET, L. A., HARVEY, A. & MENSİ, T. 1975. Cyclic AMP and cyclic GMP: mediators of the mechanical effects on bone remodeling. *Science*, 189, 467-9.
- ROELOFSEN, T., AKKERS, R., BEUMER, W., APOTHEKER, M., STEEGHS, I., VAN DE VEN, J., GELDERBLUM, C., GARRITSEN, A. & DECHERING, K. 2008. Sphingosine-1-Phosphate Acts as a Developmental Stage Specific Inhibitor of Platelet-Derived Growth Factor-induced Chemotaxis of Osteoblasts. *Journal of Cellular Biochemistry*, 105, 1128-1138.
- RØHL, L., LARSEN, E., LINDE, F., ODGAARD, A. & JØRGENSEN, J. 1991. Tensile and compressive properties of cancellous bone. *Journal of Biomechanics*, 24, 1143-1149.
- ROMANELLO, M., MORO, L., PIRULLI, D., CROVELLA, S. & D'ANDREA, P. 2001. Effects of cAMP on intercellular coupling and osteoblast differentiation. *Biochem Biophys Res Commun*, 282, 1138-44.
- ROSEN, H., GONZALEZ-CABRERA, P., MARSOLAIS, D., CAHALAN, S., DON, A. S. & SANNA, M. G. 2008. Modulating tone: the overture of S1P receptor immunotherapeutics. *Immunol Rev*, 223, 221-35.
- ROSEN, H., GONZALEZ-CABRERA, P. J., SANNA, M. G. & BROWN, S. 2009. Sphingosine 1-phosphate receptor signaling. *Annual review of biochemistry*, 78, 743-768.
- ROSETI, L., PARISI, V., PETRETTA, M., CAVALLO, C., DESANDO, G., BARTOLOTTI, I. & GRIGOLO, B. 2017. Scaffolds for Bone Tissue Engineering: State of the art and new perspectives. *Mater Sci Eng C Mater Biol Appl*, 78, 1246-1262.
- RUAN, F., ZHENG, Q. & WANG, J. 2012. Mechanisms of bone anabolism regulated by statins. *Bioscience reports*, 32, 511-519.
- RYU, J., KIM, H. J., CHANG, E. J., HUANG, H., BANNO, Y. & KIM, H. H. 2006. Sphingosine 1-phosphate as a regulator of osteoclast differentiation and osteoclast-osteoblast coupling. *Embo Journal*, 25, 5840-5851.
- RYU, Y., TAKUWA, N., SUGIMOTO, N., SAKURADA, S., USUI, S., OKAMOTO, H., MATSUI, O. & TAKUWA, Y. 2002. Sphingosine-1-phosphate, a platelet-derived lysophospholipid mediator, negatively regulates cellular Rac activity and cell migration in vascular smooth muscle cells. *Circ Res*, 90, 325-32.
- SABIR, M. I., XU, X. & LI, L. 2009. A review on biodegradable polymeric materials for bone tissue engineering applications. *Journal of Materials Science*, 44, 5713-5724.
- SALOMONE, S. & WAEBER, C. 2011. Selectivity and specificity of sphingosine-1-phosphate receptor ligands: caveats and critical thinking in characterizing receptor-mediated effects. *Front Pharmacol*, 2, 9.
- SAMSONRAJ, R. M., DUDAKOVIC, A., ZAN, P., PICHURIN, O., COOL, S. M. & VAN WIJNEN, A. J. 2017. A Versatile Protocol for Studying Calvarial Bone Defect Healing in a Mouse Model. *Tissue engineering. Part C, Methods*, 23, 686-693.
- SANCHEZ, T., ESTRADA-HERNANDEZ, T., PAIK, J. H., WU, M. T., VENKATARAMAN, K., BRINKMANN, V., CLAFFEY, K. & HLA, T. 2003. Phosphorylation and action of the immunomodulator FTY720 inhibits vascular endothelial cell growth factor-induced vascular permeability. *J Biol Chem*, 278, 47281-90.
- SANCHEZ, T., SKOURA, A., WU, M. T., CASSERLY, B., HARRINGTON, E. O. & HLA, T. 2007. Induction of vascular permeability by the sphingosine-1-phosphate receptor-2

- (S1P2R) and its downstream effectors ROCK and PTEN. *Arterioscler Thromb Vasc Biol*, 27, 1312-8.
- SANLLEHI, P., ABAD, J. L., CASAS, J. & DELGADO, A. 2016. Inhibitors of sphingosine-1-phosphate metabolism (sphingosine kinases and sphingosine-1-phosphate lyase). *Chem Phys Lipids*, 197, 69-81.
- SANNA, M. G., WANG, S. K., GONZALEZ-CABRERA, P. J., DON, A., MARSOLAIS, D., MATHEU, M. P., WEI, S. H., PARKER, I., JO, E., CHENG, W. C., CAHALAN, M. D., WONG, C. H. & ROSEN, H. 2006. Enhancement of capillary leakage and restoration of lymphocyte egress by a chiral S1P1 antagonist in vivo. *Nat Chem Biol*, 2, 434-41.
- SARTAWI, Z., RYAN, K. B. & WAEBER, C. 2020a. Bone regenerative potential of the selective sphingosine 1-phosphate receptor modulator siponimod: In vitro characterisation using osteoblast and endothelial cells. *Eur J Pharmacol*, 173262.
- SARTAWI, Z., SCHIPANI, E., RYAN, K. B. & WAEBER, C. 2017. Sphingosine 1-phosphate (S1P) signalling: Role in bone biology and potential therapeutic target for bone repair. *Pharmacol Res*, 125, 232-245.
- SARTAWI, Z., WAEBER, C., SCHIPANI, E. & RYAN, K. B. 2020b. Development of electrospun polymer scaffolds for the localized and controlled delivery of siponimod for the management of critical bone defects. *International Journal of Pharmaceutics*, 119956.
- SASSOLI, C., PIERUCCI, F., TANI, A., FRATI, A., CHELLINI, F., MATTEINI, F., VESTRI, A., ANDERLONI, G., NOSI, D., ZECCHI-ORLANDINI, S. & MEACCI, E. 2018. Sphingosine 1-Phosphate Receptor 1 Is Required for MMP-2 Function in Bone Marrow Mesenchymal Stromal Cells: Implications for Cytoskeleton Assembly and Proliferation. *Stem Cells Int*, 2018, 5034679.
- SATO, C., IWASAKI, T., KITANO, S., TSUNEMI, S. & SANO, H. 2012. Sphingosine 1-phosphate receptor activation enhances BMP-2-induced osteoblast differentiation. *Biochemical and Biophysical Research Communications*, 423, 200-205.
- SCHINDELER, A., MCDONALD, M. M., BOKKO, P. & LITTLE, D. G. 2008. Bone remodeling during fracture repair: The cellular picture. *Semin Cell Dev Biol*, 19, 459-66.
- SCHLICKWEI, C. W., KLEINERTZ, H., THIESEN, D. M., MADER, K., PRIEMEL, M., FROSCH, K. H. & KELLER, J. 2019. Current and Future Concepts for the Treatment of Impaired Fracture Healing. *Int J Mol Sci*, 20.
- SCHMID, G., GUBA, M., ISCHENKO, I., PAPYAN, A., JOKA, M., SCHREPFER, S., BRUNS, C. J., JAUCH, K. W., HEESCHEN, C. & GRAEB, C. 2007. The immunosuppressant FTY720 inhibits tumor angiogenesis via the sphingosine 1-phosphate receptor 1. *J Cell Biochem*, 101, 259-70.
- SCHMIDMAIER, G., HERRMANN, S., GREEN, J., WEBER, T., SCHARFENBERGER, A., HAAS, N. P. & WILDEMANN, B. 2006. Quantitative assessment of growth factors in reaming aspirate, iliac crest, and platelet preparation. *Bone*, 39, 1156-1163.
- SCHNEIDER, C. A., RASBAND, W. S. & ELICEIRI, K. W. 2012. NIH Image to ImageJ: 25 years of image analysis. *Nat Methods*, 9, 671-5.
- SCHNEIDER, O. D., MOHN, D., FUHRER, R., KLEIN, K., KÄMPF, K., NUSS, K. M., SIDLER, M., ZLINSZKY, K., VON RECHENBERG, B. & STARK, W. J. 2011. Biocompatibility and bone formation of flexible, cotton wool-like PLGA/calcium phosphate nanocomposites in sheep. *The Open Orthopaedics Journal*, 5, 63.
- SECRETO, F. J., HOEPPNER, L. H. & WESTENDORF, J. J. 2009. Wnt signaling during fracture repair. *Curr Osteoporos Rep*, 7, 64-9.
- SECUNDA, R., VENNILA, R., MOHANASHANKAR, A. M., RAJASUNDARI, M., JESWANTH, S. & SURENDRAN, R. 2015. Isolation, expansion and characterisation of mesenchymal

- stem cells from human bone marrow, adipose tissue, umbilical cord blood and matrix: a comparative study. *Cytotechnology*, 67, 793-807.
- SEFCIK, L. S., ARONIN, C. E. P., AWOJODU, A. O., SHIN, S. J., MAC GABHANN, F., MACDONALD, T. L., WAMHOFF, B. R., LYNCH, K. R., PEIRCE, S. M. & BOTCHWEY, E. A. 2011. Selective Activation of Sphingosine 1-Phosphate Receptors 1 and 3 Promotes Local Microvascular Network Growth. *Tissue Engineering Part A*, 17, 617-629.
- SEFCIK, L. S., PETRIE ARONIN, C. E., WIEGHAUS, K. A. & BOTCHWEY, E. A. 2008. Sustained release of sphingosine 1-phosphate for therapeutic arteriogenesis and bone tissue engineering. *Biomaterials*, 29, 2869-77.
- SEMENZA, G. L. 2007. Vasculogenesis, angiogenesis, and arteriogenesis: mechanisms of blood vessel formation and remodeling. *J Cell Biochem*, 102, 840-7.
- SHAH, A. A., GOURISHETTI, K. & NAYAK, Y. 2019. Osteogenic Activity of Resveratrol in Human Fetal Osteoblast Cells. *Pharmacognosy Magazine*, 15, 250-255.
- SHEKARAN, A. & GARCÍA, A. J. 2011. Extracellular matrix-mimetic adhesive biomaterials for bone repair. *Journal of biomedical materials research. Part A*, 96, 261-272.
- SHEN, Y., ZHAO, S., WANG, S., PAN, X., ZHANG, Y., XU, J., JIANG, Y., LI, H., ZHANG, Q., GAO, J., YANG, Q., ZHOU, Y., JIANG, S., YANG, H., ZHANG, Z., ZHANG, R., LI, J. & ZHOU, D. 2019. S1P/S1PR3 axis promotes aerobic glycolysis by YAP/c-MYC/PGAM1 axis in osteosarcoma. *EBioMedicine*, 40, 210-223.
- SHU, R., MCMULLEN, R., BAUMANN, M. & MCCABE, L. 2003. Hydroxyapatite accelerates differentiation and suppresses growth of MC3T3-E1 osteoblasts. *Journal of Biomedical Materials Research Part A: An Official Journal of The Society for Biomaterials, The Japanese Society for Biomaterials, and The Australian Society for Biomaterials and the Korean Society for Biomaterials*, 67, 1196-1204.
- SIKAVITSAS, V. I., VAN DEN DOLDER, J., BANCROFT, G. N., JANSEN, J. A. & MIKOS, A. G. 2003. Influence of the in vitro culture period on the in vivo performance of cell/titanium bone tissue-engineered constructs using a rat cranial critical size defect model. *Journal of Biomedical Materials Research Part A*, 67a, 944-951.
- SILVA, J. C., CARVALHO, M. S., UDANGAWA, R. N., MOURA, C. S., CABRAL, J. M. S., C, L. D. S., FERREIRA, F. C., VASHISHTH, D. & LINHARDT, R. J. 2020. Extracellular matrix decorated polycaprolactone scaffolds for improved mesenchymal stem/stromal cell osteogenesis towards a patient-tailored bone tissue engineering approach. *J Biomed Mater Res B Appl Biomater*, 108, 2153-2166.
- SINGH, M., SANDHU, B., SCURTO, A., BERKLAND, C. & DETAMORE, M. S. 2010. Microsphere-based scaffolds for cartilage tissue engineering: Using subcritical CO<sub>2</sub> as a sintering agent. *Acta Biomaterialia*, 6, 137-143.
- SINGLETON, P. A., CHATCHAVALVANICH, S., FU, P., XING, J., BIRUKOVA, A. A., FORTUNE, J. A., KLIVANOV, A. M., GARCIA, J. G. & BIRUKOV, K. G. 2009. Akt-mediated transactivation of the S1P1 receptor in caveolin-enriched microdomains regulates endothelial barrier enhancement by oxidized phospholipids. *Circ Res*, 104, 978-86.
- SINGLETON, P. A., DUDEK, S. M., CHIANG, E. T. & GARCIA, J. G. 2005. Regulation of sphingosine 1-phosphate-induced endothelial cytoskeletal rearrangement and barrier enhancement by S1P1 receptor, PI3 kinase, Tiam1/Rac1, and alpha-actinin. *FASEB J*, 19, 1646-56.
- SINGLETON, P. A., MORENO-VINASCO, L., SAMMANI, S., WANDERLING, S. L., MOSS, J. & GARCIA, J. G. 2007. Attenuation of vascular permeability by methylnaltrexone: role of mOP-R and S1P3 transactivation. *Am J Respir Cell Mol Biol*, 37, 222-31.

- SOARES, R. M. D., SIQUEIRA, N. M., PRABHAKARAM, M. P. & RAMAKRISHNA, S. 2018. Electrospinning and electrospray of bio-based and natural polymers for biomaterials development. *Materials Science and Engineering: C*, 92, 969-982.
- SOBEL, K., MONNIER, L., MENYHART, K., BOLINGER, M., STUDER, R., NAYLER, O. & GATFIELD, J. 2015. FTY720 Phosphate Activates Sphingosine-1-Phosphate Receptor 2 and Selectively Couples to G $\alpha$ 12/13/Rho/ROCK to Induce Myofibroblast Contraction. *Mol Pharmacol*, 87, 916-27.
- SOLA, A., BERTACCHINI, J., D'AVELLA, D., ANSELM, L., MARALDI, T., MARMIROLI, S. & MESSORI, M. 2019. Development of solvent-casting particulate leaching (SCPL) polymer scaffolds as improved three-dimensional supports to mimic the bone marrow niche. *Materials Science and Engineering: C*, 96, 153-165.
- SOLIMAN, S., SANT, S., NICHOL, J. W., KHABIRY, M., TRAVERSA, E. & KHADEMHOSEINI, A. 2011. Controlling the porosity of fibrous scaffolds by modulating the fiber diameter and packing density. *Journal of Biomedical Materials Research Part A*, 96, 566-574.
- SPICER, P. P., KRETLOW, J. D., YOUNG, S., JANSEN, J. A., KASPER, F. K. & MIKOS, A. G. 2012. Evaluation of bone regeneration using the rat critical size calvarial defect. *Nat Protoc*, 7, 1918-29.
- SPIEGEL, S. & MILSTIEN, S. 2000. Sphingosine-1-phosphate: signaling inside and out. *FEBS Lett*, 476, 55-7.
- SPIEGEL, S. & MILSTIEN, S. 2002. Sphingosine 1-phosphate, a key cell signaling molecule. *J Biol Chem*, 277, 25851-4.
- SPIEGEL, S. & MILSTIEN, S. 2003. Sphingosine-1-phosphate: an enigmatic signalling lipid. *Nat Rev Mol Cell Biol*, 4, 397-407.
- STEVENS, M. M. 2008. Biomaterials for bone tissue engineering. *Materials Today*, 11, 18-25.
- STRADNER, M. H., HERMANN, J., ANGERER, H., SETZNAGL, D., SUNK, I., WINDHAGER, R. & GRANINGER, W. B. 2008. Sphingosine-1-phosphate stimulates proliferation and counteracts interleukin-1 induced nitric oxide formation in articular chondrocytes. *Osteoarthritis Cartilage*, 16, 305-11.
- STREET, J., BAO, M., DEGUZMAN, L., BUNTING, S., PEALE, F. V., JR., FERRARA, N., STEINMETZ, H., HOFFEL, J., CLELAND, J. L., DAUGHERTY, A., VAN BRUGGEN, N., REDMOND, H. P., CARANO, R. A. & FILVAROFF, E. H. 2002. Vascular endothelial growth factor stimulates bone repair by promoting angiogenesis and bone turnover. *Proc Natl Acad Sci U S A*, 99, 9656-61.
- STUCKENSEN, K., SCHWAB, A., KNAUER, M., MUIÑOS-LÓPEZ, E., EHLCHE, F., REBOREDO, J., GRANERO-MOLTÓ, F., GBURECK, U., PRÓSPER, F., WALLIS, H. & GROLL, J. 2018. Tissue Mimicry in Morphology and Composition Promotes Hierarchical Matrix Remodeling of Invading Stem Cells in Osteochondral and Meniscus Scaffolds. *Advanced Materials*, 30, 1706754.
- SUI, G., YANG, X., MEI, F., HU, X., CHEN, G., DENG, X. & RYU, S. 2007. Poly-L-lactic acid/hydroxyapatite hybrid membrane for bone tissue regeneration. *Journal of Biomedical Materials Research Part A*, 82A, 445-454.
- SUN, Q., LI, Z., LIU, B., YUAN, X., GUO, S. & HELMS, J. A. 2019. Improving intraoperative storage conditions for autologous bone grafts: An experimental investigation in mice. *Journal of Tissue Engineering and Regenerative Medicine*, 13, 2169-2180.
- SUN, T., MORI, S., ROPER, J., BROWN, C., HOOSER, T. & BURR, D. 1992. Do different fluorochrome labels give equivalent histomorphometric information? *Bone*, 13, 443-446.
- SZIVEK, J. A., GONZALES, D. A., WOJTANOWSKI, A. M., MARTINEZ, M. A. & SMITH, J. L. 2019. Mesenchymal stem cell seeded, biomimetic 3D printed scaffolds induce complete

- bridging of femoral critical sized defects. *J Biomed Mater Res B Appl Biomater*, 107, 242-252.
- TAKAHASHI, K. & YAMANAKA, S. 2006. Induction of pluripotent stem cells from mouse embryonic and adult fibroblast cultures by defined factors. *cell*, 126, 663-676.
- TAKEDA, H., OZAKI, K., YASUDA, H., ISHIDA, M., KITANO, S. & HANAZAWA, S. 1998. Sphingomyelinase and ceramide inhibit formation of F-actin ring in and bone resorption by rabbit mature osteoclasts. *FEBS Lett*, 422, 255-8.
- TAKUWA, Y. 2002. Subtype-specific differential regulation of Rho family G proteins and cell migration by the Edg family sphingosine-1-phosphate receptors. *Biochim Biophys Acta*, 1582, 112-20.
- TAKUWA, Y., DU, W., QI, X., OKAMOTO, Y., TAKUWA, N. & YOSHIOKA, K. 2010. Roles of sphingosine-1-phosphate signaling in angiogenesis. *World J Biol Chem*, 1, 298-306.
- TAKUWA, Y., OKAMOTO, Y., YOSHIOKA, K. & TAKUWA, N. 2008. Sphingosine-1-phosphate signaling and biological activities in the cardiovascular system. *Biochim Biophys Acta*, 1781, 483-8.
- TAKUWA, Y., OKAMOTO, Y., YOSHIOKA, K. & TAKUWA, N. 2012. Sphingosine-1-phosphate signaling in physiology and diseases. *Biofactors*, 38, 329-337.
- TAN, L., YU, X., WAN, P. & YANG, K. 2013. Biodegradable materials for bone repairs: a review. *Journal of Materials Science & Technology*, 29, 503-513.
- TANAKA, K., HASHIZUME, M., MIHARA, M., YOSHIDA, H., SUZUKI, M. & MATSUMOTO, Y. 2014. Anti-interleukin-6 receptor antibody prevents systemic bone mass loss via reducing the number of osteoclast precursors in bone marrow in a collagen-induced arthritis model. *Clinical and Experimental Immunology*, 175, 172-180.
- TANAKA, Y., OKABE, S., TAUCHI, T., ITO, Y., UMEZU, T., OHYASHIKI, J. H. & OHYASHIKI, K. 2013. Therapeutic Potential Of Targeting Sphingosine-1-Phosphate and Sphingosine Kinases In Multiple Myeloma. *Blood*, 122.
- TANNOURY, C. A. & AN, H. S. 2014. Complications with the use of bone morphogenetic protein 2 (BMP-2) in spine surgery. *Spine Journal*, 14, 552-559.
- TANTIKANLAYAPORN, D., TOURKOVA, I. L., LARROUTURE, Q., LUO, J., PIYACHATURAWAT, P., WITT, M. R., BLAIR, H. C. & ROBINSON, L. J. 2018. Sphingosine-1-Phosphate Modulates the Effect of Estrogen in Human Osteoblasts. *JBMR Plus*, 2, 217-226.
- TARRASON, G., AULI, M., MUSTAFA, S., DOLGACHEV, V., DOMENECH, M. T., PRATS, N., DOMINGUEZ, M., LOPEZ, R., AGUILAR, N., CALBET, M., PONT, M., MILLIGAN, G., KUNKEL, S. L. & GODESSART, N. 2011. The sphingosine-1-phosphate receptor-1 antagonist, W146, causes early and short-lasting peripheral blood lymphopenia in mice. *Int Immunopharmacol*, 11, 1773-9.
- TATANGELO, G., WATTS, J., LIM, K., CONNAUGHTON, C., ABIMANYI-OCHOM, J., BORGSTROM, F., NICHOLSON, G. C., SHORE-LORENTI, C., STUART, A. L., IULIANO-BURNS, S., SEEMAN, E., PRINCE, R., MARCH, L., CROSS, M., WINZENBERG, T., LASLETT, L. L., DUQUE, G., EBELING, P. R. & SANDERS, K. M. 2019. The Cost of Osteoporosis, Osteopenia, and Associated Fractures in Australia in 2017. *J Bone Miner Res*, 34, 616-625.
- TEITELBAUM, S. L. 2007. Osteoclasts: What Do They Do and How Do They Do It? *The American Journal of Pathology*, 170, 427-435.
- TENGOOD, J. E., KOVACH, K. M., VESCOVI, P. E., RUSSELL, A. J. & LITTLE, S. R. 2010. Sequential delivery of vascular endothelial growth factor and sphingosine 1-phosphate for angiogenesis. *Biomaterials*, 31, 7805-12.

- TENGOOD, J. E., RIDENOUR, R., BRODSKY, R., RUSSELL, A. J. & LITTLE, S. R. 2011. Sequential delivery of basic fibroblast growth factor and platelet-derived growth factor for angiogenesis. *Tissue Eng Part A*, 17, 1181-9.
- TETI, A. 2013. Mechanisms of osteoclast-dependent bone formation. *Bonekey Rep*, 2, 449.
- THOMSON, J. A., ITSKOVITZ-ELDOR, J., SHAPIRO, S. S., WAKNITZ, M. A., SWIERGIEL, J. J., MARSHALL, V. S. & JONES, J. M. 1998. Embryonic stem cell lines derived from human blastocysts. *science*, 282, 1145-1147.
- THURSTON, G., SURI, C., SMITH, K., MCCLAIN, J., SATO, T. N., YANCOPOULOS, G. D. & MCDONALD, D. M. 1999. Leakage-resistant blood vessels in mice transgenically overexpressing angiopoietin-1. *Science*, 286, 2511-4.
- THUY, A. V., REIMANN, C. M., HEMDAN, N. Y. & GRALER, M. H. 2014. Sphingosine 1-phosphate in blood: function, metabolism, and fate. *Cell Physiol Biochem*, 34, 158-71.
- TOKUHARA, Y., WAKITANI, S., IMAI, Y., NOMURA, C., HOSHINO, M., YANO, K., TAGUCHI, S., KIM, M., KADOYA, Y. & TAKAOKA, K. 2010. Local delivery of rolipram, a phosphodiesterase-4-specific inhibitor, augments bone morphogenetic protein-induced bone formation. *Journal of bone and mineral metabolism*, 28, 17.
- TOMLINSON, R. E. & SILVA, M. J. 2013. Skeletal Blood Flow in Bone Repair and Maintenance. *Bone Res*, 1, 311-22.
- TONDEVOLD, E. & ELIASSEN, P. 1982. Blood flow rates in canine cortical and cancellous bone measured with 99Tcm-labelled human albumin microspheres. *Acta Orthop Scand*, 53, 7-11.
- TURAN, A., KOSTAKOGLU, N., TUNCEL, U., GOKCE, E. & MARKOC, F. 2016. Scapular Bone Grafts: Good Options for Craniofacial Defects? *Ann Plast Surg*, 76, 509-16.
- TÜRER, A., TÜRER, Ç. C., BALLI, U., DURMUSLAR, M. C., ÖNGER, M. E. & ÇELİK, H. H. 2016. Effect of local rosuvastatin administration on calvarial bone defects. *Journal of Craniofacial Surgery*, 27, 2036-2040.
- TURNBULL, G., CLARKE, J., PICARD, F., RICHES, P., JIA, L., HAN, F., LI, B. & SHU, W. 2018. 3D bioactive composite scaffolds for bone tissue engineering. *Bioact Mater*, 3, 278-314.
- URIST, M. R. 1965. Bone: formation by autoinduction. *Science*, 150, 893-899.
- VACANTI, J. P. & VACANTI, C. A. 2014. Chapter 1 - The History and Scope of Tissue Engineering. In: LANZA, R., LANGER, R. & VACANTI, J. (eds.) *Principles of Tissue Engineering (Fourth Edition)*. Boston: Academic Press.
- VACCARO, A. R., PATEL, T., FISCHGRUND, J., ANDERSON, D. G., TRUUMES, E., HERKOWITZ, H., PHILLIPS, F., HILIBRAND, A. & ALBERT, T. J. 2003. A pilot safety and efficacy study of OP-1 putty (rhBMP-7) as an adjunct to iliac crest autograft in posterolateral lumbar fusions. *European Spine Journal*, 12, 495-500.
- VALLET-REGÍ, M. & RUIZ-HERNÁNDEZ, E. 2011. Bioceramics: From Bone Regeneration to Cancer Nanomedicine. *Advanced Materials*, 23, 5177-5218.
- VAN DE WATERING, F. C. J., VAN DEN BEUCKEN, J., WALBOOMERS, X. F. & JANSEN, J. A. 2012. Calcium phosphate/poly(D,L-lactic-co-glycolic acid) composite bone substitute materials: evaluation of temporal degradation and bone ingrowth in a rat critical-sized cranial defect. *Clin Oral Implants Res*, 23, 151-159.
- WAEBER, C. 2013a. Sphingosine 1-Phosphate (S1P) Signaling and the Vasculature. In: CHUN, J., HLA, T., SPIEGEL, S. & MOOLENAAR, W. (eds.) *Lysophospholipid Receptors: Signaling and Biochemistry*. Hoboken, NJ: John Wiley & Sons, Inc.
- WAEBER, C. 2013b. Sphingosine 1-Phosphate (S1P) Signaling and the Vasculature. In: CHUN, J., HLA, T., SPIEGEL, S. & MOOLENAAR, W. (eds.) *Lysophospholipid Receptors: Signaling and Biochemistry*. Hoboken, NJ: John Wiley & Sons Ltd.

- WAEBER, C., BLONDEAU, N. & SALOMONE, S. 2004. Vascular sphingosine-1-phosphate S1P1 and S1P3 receptors. *Drug News Perspect*, 17, 365-82.
- WAEBER, C. & MOSKOWITZ, M. A. 1995. [3H]sumatriptan labels both 5-HT<sub>1D</sub> and 5-HT<sub>1F</sub> receptor binding sites in the guinea pig brain: an autoradiographic study. *Naunyn Schmiedebergs Arch Pharmacol*, 352, 263-75.
- WAEBER, C. & WALTHER, T. 2014. Sphingosine-1-phosphate as a potential target for the treatment of myocardial infarction. *Circ J*, 78, 795-802.
- WAGONER JOHNSON, A. J. & HERSCHLER, B. A. 2011. A review of the mechanical behavior of CaP and CaP/polymer composites for applications in bone replacement and repair. *Acta Biomaterialia*, 7, 16-30.
- WALL, J. C., CHATTERJI, S. K. & JEFFERY, J. W. 1979. Age-related changes in the density and tensile strength of human femoral cortical bone. *Calcif Tissue Int*, 27, 105-8.
- WALSH, J. S. 2015. Normal bone physiology, remodelling and its hormonal regulation. *Surgery (Oxford)*, 33, 1-6.
- WALSH, W. R., PELLETIER, M. H., WANG, T., LOVRIC, V., MORBERG, P. & MOBBS, R. J. 2019. Does implantation site influence bone ingrowth into 3D-printed porous implants? *Spine J*, 19, 1885-1898.
- WANG, C., CAO, X. & ZHANG, Y. 2017. A novel bioactive osteogenesis scaffold delivers ascorbic acid,  $\beta$ -glycerophosphate, and dexamethasone in vivo to promote bone regeneration. *Oncotarget*, 8, 31612-31625.
- WANG, F., VAN BROCKLYN, J. R., HOBSON, J. P., MOVAFAGH, S., ZUKOWSKA-GROJEC, Z., MILSTIEN, S. & SPIEGEL, S. 1999. Sphingosine 1-phosphate stimulates cell migration through a G(i)-coupled cell surface receptor. Potential involvement in angiogenesis. *J Biol Chem*, 274, 35343-50.
- WANG, J., CUI, X., ZHOU, Y. & XIANG, Q. 2014. Core-shell PLGA/collagen nanofibers loaded with recombinant FN/CDHs as bone tissue engineering scaffolds. *Connect Tissue Res*, 55, 292-8.
- WANG, S.-J., JIANG, D., ZHANG, Z.-Z., CHEN, Y.-R., YANG, Z.-D., ZHANG, J.-Y., SHI, J., WANG, X. & YU, J.-K. 2019. Biomimetic Nanosilica–Collagen Scaffolds for In Situ Bone Regeneration: Toward a Cell-Free, One-Step Surgery. *Advanced Materials*, 31, 1904341.
- WANG, T., KRIEGER, J., HUANG, C., DAS, A., FRANCIS, M. P., OGLE, R. & BOTCHWEY, E. 2016a. Enhanced osseous integration of human trabecular allografts following surface modification with bioactive lipids. *Drug Deliv Transl Res*, 6, 96-104.
- WANG, X., XU, S., ZHOU, S., XU, W., LEARY, M., CHOONG, P., QIAN, M., BRANDT, M. & XIE, Y. M. 2016b. Topological design and additive manufacturing of porous metals for bone scaffolds and orthopaedic implants: A review. *Biomaterials*, 83, 127-41.
- WEI, K., LI, Y., MUGISHIMA, H., TERAMOTO, A. & ABE, K. 2012. Fabrication of core-sheath structured fibers for model drug release and tissue engineering by emulsion electrospinning. *Biotechnol J*, 7, 677-85.
- WIMMER, C., KRISMER, M., GLUCH, H., OGON, M. & STÖCKL, B. 1999. Autogenic Versus Allogenic Bone Grafts in Anterior Lumbar Interbody Fusion. *Clinical Orthopaedics and Related Research (1976-2007)*, 360.
- WONG, S. C., BAJI, A. & LENG, S. W. 2008. Effect of fiber diameter on tensile properties of electrospun poly(epsilon-caprolactone). *Polymer*, 49, 4713-4722.
- WU, C., FAN, W., ZHU, Y., GELINSKY, M., CHANG, J., CUNIBERTI, G., ALBRECHT, V., FRIIS, T. & XIAO, Y. 2011. Multifunctional magnetic mesoporous bioactive glass scaffolds with a hierarchical pore structure. *Acta Biomaterialia*, 7, 3563-3572.



- WU, J. & HONG, Y. 2016. Enhancing cell infiltration of electrospun fibrous scaffolds in tissue regeneration. *Bioactive Materials*, 1, 56-64.
- WU, J., ZHANG, Z., GU, J., ZHOU, W., LIANG, X., ZHOU, G., HAN, C. C., XU, S. & LIU, Y. 2020. Mechanism of a long-term controlled drug release system based on simple blended electrospun fibers. *J Control Release*, 320, 337-346.
- XIA, H., HASHIMOTO, Y., MORITA, T. & HIRAI, T. 2014. Formation of polyketone particle structure by hexafluoroisopropanol solvent evaporation and effects of plasticizer addition. *Journal of Polymer Science Part B: Polymer Physics*, 52, 887-892.
- XU, C., SU, P., CHEN, X., MENG, Y., YU, W., XIANG, A. P. & WANG, Y. 2011. Biocompatibility and osteogenesis of biomimetic Bioglass-Collagen-Phosphatidylserine composite scaffolds for bone tissue engineering. *Biomaterials*, 32, 1051-1058.
- XU, F., REN, H., ZHENG, M., SHAO, X., DAI, T., WU, Y., TIAN, L., LIU, Y., LIU, B., GUNSTER, J., LIU, Y. & LIU, Y. 2020. Development of biodegradable bioactive glass ceramics by DLP printed containing EPCs/BMSCs for bone tissue engineering of rabbit mandible defects. *Journal of the Mechanical Behavior of Biomedical Materials*, 103, 103532.
- XU, Y., PENG, J., RICHARDS, G., LU, S. & EGLIN, D. 2019. Optimization of electrospray fabrication of stem cell-embedded alginate-gelatin microspheres and their assembly in 3D-printed poly( $\epsilon$ -caprolactone) scaffold for cartilage tissue engineering. *Journal of Orthopaedic Translation*, 18, 128-141.
- XUE, J., WU, T., DAI, Y. & XIA, Y. 2019a. Electrospinning and Electrospun Nanofibers: Methods, Materials, and Applications. *Chem Rev*, 119, 5298-5415.
- XUE, Y., WU, M., LIU, Z., SONG, J., LUO, S., LI, H., LI, Y., JIN, L., GUAN, B., LIN, M., CHEN, F., JIN, C., LIU, D., LI, Y. & ZHANG, X. 2019b. In vitro and in vivo evaluation of chitosan scaffolds combined with simvastatin-loaded nanoparticles for guided bone regeneration. *Journal of Materials Science: Materials in Medicine*, 30, 47.
- YAMAMOTO, M., TAKAHASHI, Y. & TABATA, Y. 2003. Controlled release by biodegradable hydrogels enhances the ectopic bone formation of bone morphogenetic protein. *Biomaterials*, 24, 4375-83.
- YAN, Y., CHEN, H., ZHANG, H., GUO, C., YANG, K., CHEN, K., CHENG, R., QIAN, N., SANDLER, N. & ZHANG, Y. S. 2019. Vascularized 3D printed scaffolds for promoting bone regeneration. *Biomaterials*, 190, 97-110.
- YANCOPOULOS, G. D., DAVIS, S., GALE, N. W., RUDGE, J. S., WIEGAND, S. J. & HOLASH, J. 2000. Vascular-specific growth factors and blood vessel formation. *Nature*, 407, 242-8.
- YANG, L., FITIE, C. F., VAN DER WERF, K. O., BENNINK, M. L., DIJKSTRA, P. J. & FEIJEN, J. 2008. Mechanical properties of single electrospun collagen type I fibers. *Biomaterials*, 29, 955-62.
- YANG, S., LEONG, K. F., DU, Z. & CHUA, C. K. 2001. The design of scaffolds for use in tissue engineering. Part I. Traditional factors. *Tissue Eng*, 7, 679-89.
- YANG, X., LI, Y., HE, W., HUANG, Q., ZHANG, R. & FENG, Q. 2018. Hydroxyapatite/collagen coating on PLGA electrospun fibers for osteogenic differentiation of bone marrow mesenchymal stem cells. *J Biomed Mater Res A*, 106, 2863-2870.
- YAO, J., KUANG LIM, L., XIE, J., HUA, J. & WANG, C.-H. 2008. Characterization of electrospraying process for polymeric particle fabrication. *Journal of Aerosol Science*, 39, 987-1002.
- YE, C.-S., LIN, C. & FANG, X.-L. 2009. Experimental measurements and correlations of vapor-liquid equilibrium data for the binary system of chloroform+N,N-dimethylformamide at 101.3kPa. *Fluid Phase Equilibria*, 278, 85-89.

- YOON, S. J., PARK, K. S., KIM, M. S., RHEE, J. M., KHANG, G. & LEE, H. B. 2007. Repair of diaphyseal bone defects with calcitriol-loaded PLGA scaffolds and marrow stromal cells. *Tissue engineering*, 13, 1125-1133.
- YU, H., HERBERT, B. A., VALERIO, M., YARBOROUGH, L., HSU, L. C. & ARGRAVES, K. M. 2015. FTY720 inhibited proinflammatory cytokine release and osteoclastogenesis induced by *Aggregatibacter actinomycetemcomitans*. *Lipids Health Dis*, 14, 66.
- YUAN, X., ZHANG, M., WANG, Y., ZHAO, H. & SUN, D. 2019. Using co-axial electrospray deposition to eliminate burst release of simvastatin from microparticles and to enhance induced osteogenesis. *Journal of Biomaterials Science, Polymer Edition*, 30, 355-375.
- ZENG, Y., ZHOU, M., MOU, S., YANG, J., YUAN, Q., GUO, L., ZHONG, A., WANG, J., SUN, J. & WANG, Z. 2020. Sustained delivery of alendronate by engineered collagen scaffold for the repair of osteoporotic bone defects and resistance to bone loss. *J Biomed Mater Res A*, 108, 2460-2472.
- ZEUGOLIS, D. I., KHEW, S. T., YEW, E. S., EKAPUTRA, A. K., TONG, Y. W., YUNG, L. Y., HUTMACHER, D. W., SHEPPARD, C. & RAGHUNATH, M. 2008. Electro-spinning of pure collagen nano-fibres - just an expensive way to make gelatin? *Biomaterials*, 29, 2293-305.
- ZHAI, X., RUAN, C., MA, Y., CHENG, D., WU, M., LIU, W., ZHAO, X., PAN, H. & LU, W. W. 2018. 3D-Bioprinted Osteoblast-Laden Nanocomposite Hydrogel Constructs with Induced Microenvironments Promote Cell Viability, Differentiation, and Osteogenesis both In Vitro and In Vivo. *Advanced Science*, 5, 1700550.
- ZHANG, H., DESAI, N. N., OLIVERA, A., SEKI, T., BROOKER, G. & SPIEGEL, S. 1991. Sphingosine-1-phosphate, a novel lipid, involved in cellular proliferation. *J Cell Biol*, 114, 155-67.
- ZHANG, J. & SONG, J. 2014. Amphiphilic degradable polymers for immobilization and sustained delivery of sphingosine 1-phosphate. *Acta Biomater*, 10, 3079-90.
- ZHANG, J. N., ZHAO, Y., LIU, C., HAN, E. S., YU, X., LIDINGTON, D., BOLZ, S. S. & YOU, L. 2015. The role of the sphingosine-1-phosphate signaling pathway in osteocyte mechanotransduction. *Bone*, 79, 71-8.
- ZHANG, K., FAN, Y., DUNNE, N. & LI, X. 2018. Effect of microporosity on scaffolds for bone tissue engineering. *Regen Biomater*, 5, 115-124.
- ZHANG, Q., LI, Y., LIN, Z. Y., WONG, K. K. Y., LIN, M., YILDIRIMER, L. & ZHAO, X. 2017. Electrospun polymeric micro/nanofibrous scaffolds for long-term drug release and their biomedical applications. *Drug Discovery Today*, 22, 1351-1366.
- ZHANG, R., LI, X., LIU, Y., GAO, X., ZHU, T. & LU, L. 2019a. Acceleration of bone regeneration in critical-size defect using BMP-9-loaded nHA/Coll/MWCNTs scaffolds seeded with bone marrow mesenchymal stem cells. *BioMed research international*, 2019.
- ZHANG, X., WANG, C., LIAO, M., DAI, L., TANG, Y., ZHANG, H., COATES, P., SEFAT, F., ZHENG, L., SONG, J., ZHENG, Z., ZHAO, D., YANG, M., ZHANG, W. & JI, P. 2019b. Aligned electrospun cellulose scaffolds coated with rhBMP-2 for both in vitro and in vivo bone tissue engineering. *Carbohydr Polym*, 213, 27-38.
- ZHAO, Y., WANG, Z., JIANG, Y., LIU, H., SONG, S., WANG, C., LI, Z., YANG, Z., LIU, H., WANG, J., YANG, B. & LIN, Q. 2019. Biomimetic Composite Scaffolds to Manipulate Stem Cells for Aiding Rheumatoid Arthritis Management. *Advanced Functional Materials*, 29, 1807860.
- ZHU, N. & CHEN, X. 2013. Biofabrication of Tissue Scaffolds. *Advances in Biomaterials Science and Biomedical Applications*. IntechOpen.
- ZHU, R., SNYDER, A. H., KHAREL, Y., SCHAFFTER, L., SUN, Q., KENNEDY, P. C., LYNCH, K. R. & MACDONALD, T. L. 2007. Asymmetric synthesis of conformationally constrained

- fingolimod analogues--discovery of an orally active sphingosine 1-phosphate receptor type-1 agonist and receptor type-3 antagonist. *J Med Chem*, 50, 6428-35.
- ZONG, C., XUE, D., YUAN, W., WANG, W., SHEN, D., TONG, X., SHI, D., LIU, L., ZHENG, Q., GAO, C. & WANG, J. 2010. Reconstruction of rat calvarial defects with human mesenchymal stem cells and osteoblast-like cells in poly-lactic-co-glycolic acid scaffolds. *Eur Cell Mater*, 20, 109-20.
- ZONG, X. H., KIM, K., FANG, D. F., RAN, S. F., HSIAO, B. S. & CHU, B. 2002. Structure and process relationship of electrospun bioabsorbable nanofiber membranes. *Polymer*, 43, 4403-4412.

# Appendix A

## Supplementary material to Chapter 3

*Unpublished data*

## 7.1 Introduction

S1P receptor induced proliferation has previously been shown for both rat and human osteoblasts (Carpio et al., 1999, Lampasso et al., 2001, Dziak et al., 2003). And while osteoblasts are known to express S1P<sub>1</sub>, S1P<sub>2</sub> and S1P<sub>3</sub> receptors (Grey et al., 2004, Ryu et al., 2006, Keller et al., 2014), the response appears to be S1P<sub>1</sub>-mediated (Lampasso et al., 2001, Grey et al., 2004). Therefore **Chapter 3** explored the effects of the S1P<sub>1</sub> receptor agonist siponimod on the proliferation effects of osteoblasts, alongside determining its effects on osteoblast differentiation and migration.

The following supplementary data describes viability and proliferation experiments conducted on additional osteoblastic cell models, MC3T3-E1 and Saos-2.

## 7.2 Materials and methods

### 7.2.1 Materials

The cell lines Saos-2 (ATCC<sup>®</sup> HTB-85<sup>™</sup>), and MC3T3-E1 Subclone 4 (ATCC<sup>®</sup> CRL-2593<sup>™</sup>) were acquired from ATCC. The alamarBlue<sup>™</sup> Cell Viability Reagent was acquired from Thermo Fisher Scientific, USA. All other materials were identical to those listed in **Chapter 3** materials section.

### 7.2.2 Cell culture materials

MC3T3-E1 cells were maintained in  $\alpha$ -MEM supplemented with FBS (10 %), L-glutamine (1 %), and penicillin-streptomycin (1 %). Saos-2 cells were maintained in McCoy's 5 $\alpha$  supplemented with FBS (15 %), L-glutamine (1 %), and penicillin-streptomycin (1 %). For both cell types incubation was at 37 °C and 5 % CO<sub>2</sub>.

### 7.2.3 Viability and proliferation of MC3T3-E1 and Saos-2

Initial investigations using the osteoblast cell lines MC3T3-E1 and Saos-2 were performed to explore the effect of siponimod on cell metabolic activity and proliferation, and to a lesser extent evaluate the impact of reduced serum concentration (1 % FBS) that was necessary to limit the effect of serum lipids.

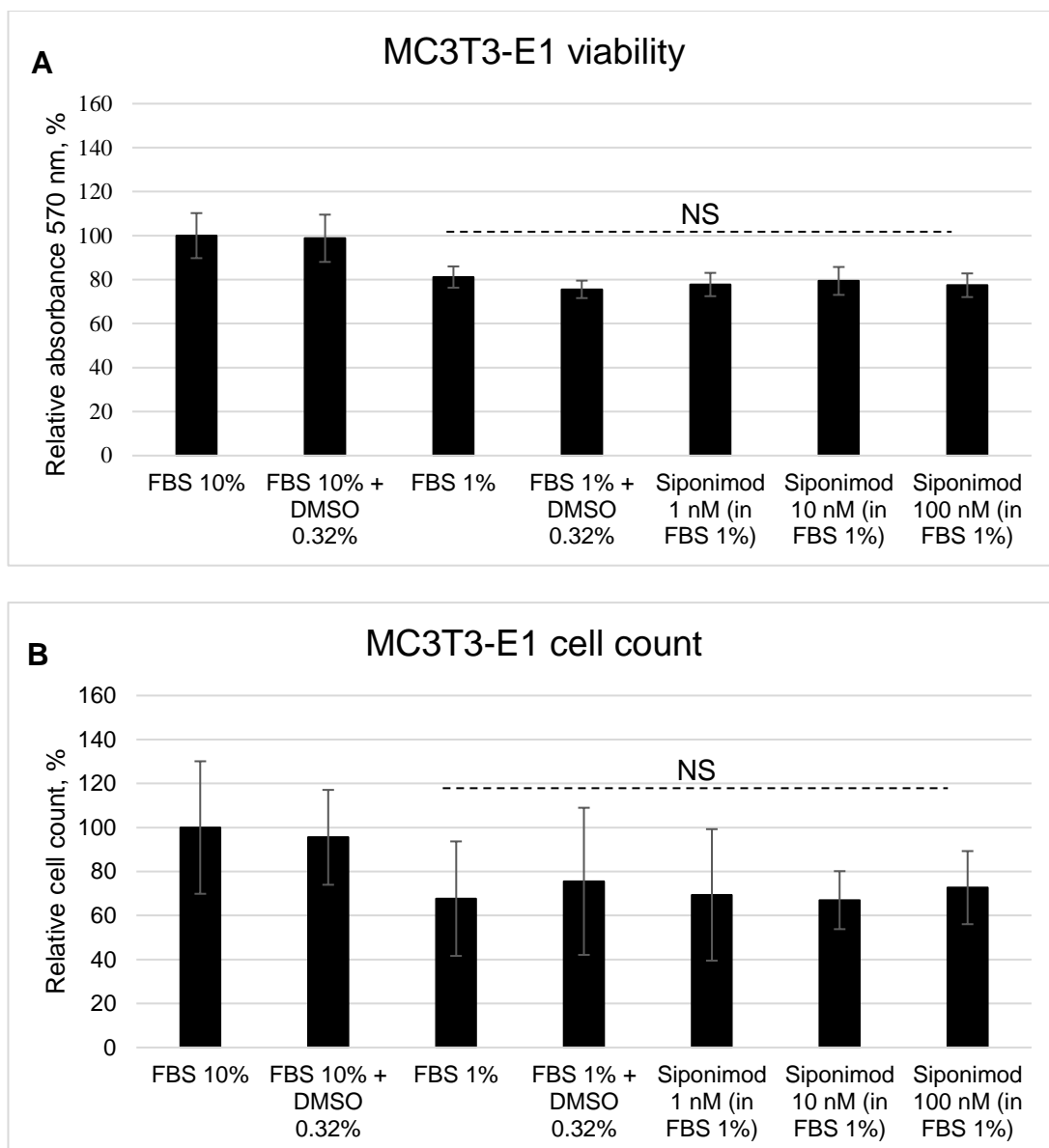
MC3T3-E1 and Saos-2 were seeded at a density of  $5 \times 10^3$  cells per well in 96-well plates. Cells were then incubated for 24 hrs in medium with reduced serum (1 % FBS) to induce quiescence. Thereafter, MC3T3-E1 and Saos-2 cell were treated for 2 and 3 days respectively with three concentrations of siponimod (1, 10, and 100 nM). Following incubation, 10  $\mu$ l of alamarBlue™ was added for 4 hrs. Thereafter, absorbance was acquired at 570 and at 595 nm to correct for overlap between oxidised and reduced forms of alamarBlue™ according to manufacturer's protocol.

## 7.3 Results

The results of alamarBlue™ and cell count assays are shown in Figure 7.1, and are presented as a percentage of the positive control. Incubating MC3T3-E1 cells with three concentrations of siponimod showed no statistically significant difference compared to controls ( $77.7 \pm 5.3$  % for 1 nM,  $79.4 \pm 6.3$  % for 10 nM, and  $77.4 \pm 5.4$  % for 100 nM compared to  $75.6 \pm 4.0$  % for the control). Results of cell counting were in agreement, with no statistically significant change in cell counts with the addition of siponimod ( $69.4 \pm 29.9$  % for 1 nM,  $67.0 \pm 13.2$  % for 10 nM, and  $72.7 \pm 16.6$  % for 100 nM compared to  $75.5 \pm 33.4$  % for the control). For the Saos-2 cells there was no significant change in alamarBlue™ absorbance values with the addition of

siponimod ( $76.8 \pm 3.7$  % for 1 nM,  $76.0 \pm 5.3$  % for 10 nM, and  $72.6 \pm 5.5$  % compared to  $75.5 \pm 4.0$  % for the control). Again, cell counting data was in agreement with the alamarBlue™ assay with no statistically significant effects following incubation with siponimod ( $71.3 \pm 20.2$  % for 1 nM,  $71.2 \pm 23.4$  % for 10 nM, and  $61.7 \pm 11.5$  % for 100 nM compared to  $74.5 \pm 28.2$  % for the control).

There was no significant change in metabolic activity for the addition of high (10 or 15 %) and low (1 %) serum conditions across both cell lines.





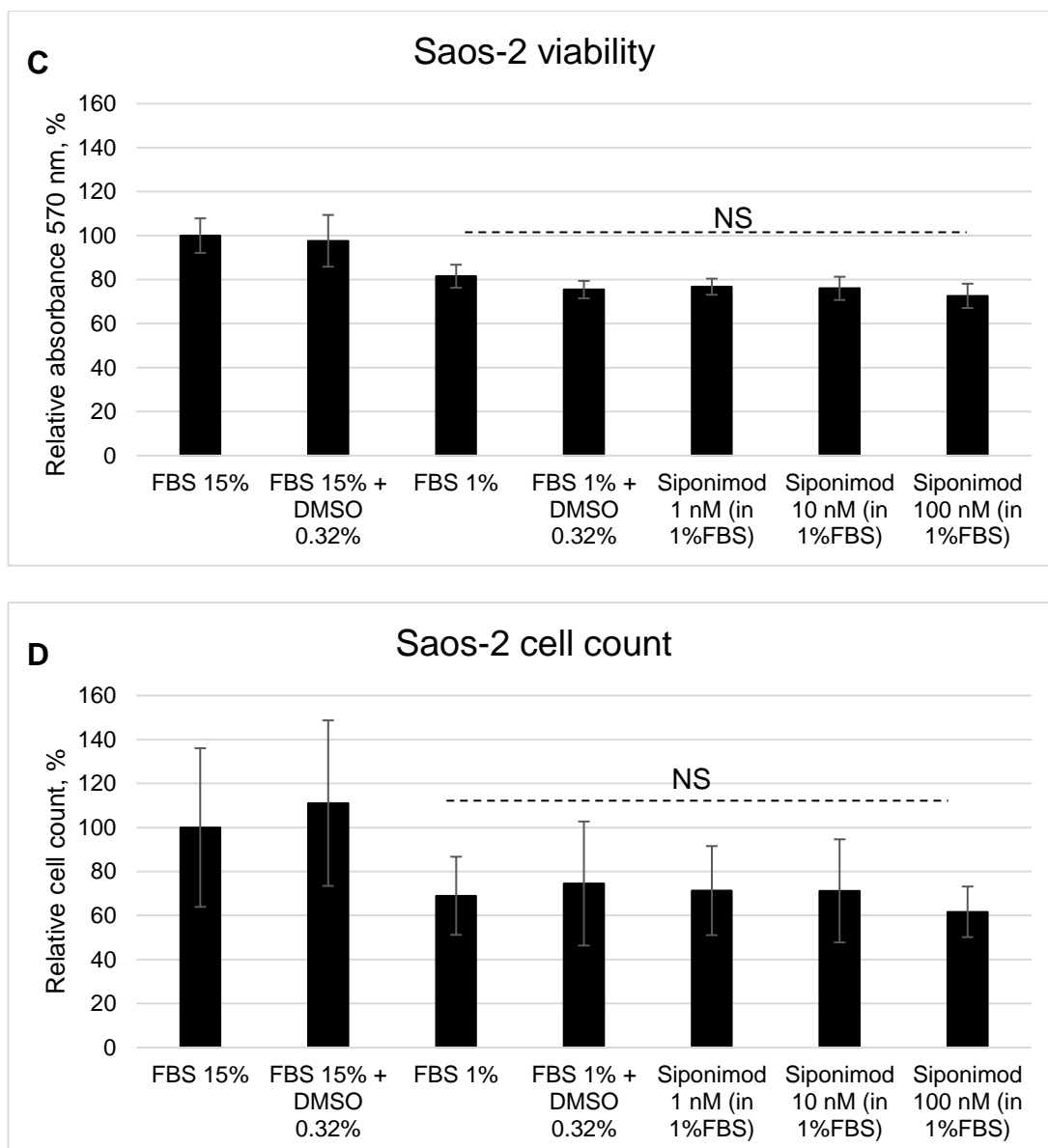


**Figure 7.1** Viability and proliferation assays for MC3T3-E1 and Saos-2 cells. (A & B) MC3T3-E1 alamarBlue™ assay and cell count after 48 hrs,  $n=3$  (5 technical replicates) (C & D) Saos-2 alamarBlue™ assay and cell count after 72 hrs,  $n=3$  (5 technical replicates). For A-D, data is expressed as a percentage (positive control set to 100 %). For both cell types, siponimod was added to cell culture medium containing 1 % FBS serum supplement, with standard growth medium acting as positive control (a-MEM + 10 % FBS for MC3T3-E1, and McCoy's 5a + 15 % FBS for Saos-2). “ $n=$ ”

represents the number of independently repeated experiments. Data is presented as mean  $\pm$  SD, statistical analysis by one-way ANOVA. NS: No statistical significance.

## 7.4 Discussion

As was the case in **Chapter 3**, there was no significant effect on the viability and proliferation of MC3T3-E1 and Saos-2 cells. This data provides some additional evidence that there is no short term impact from siponimod on the viability and proliferation of osteoblasts as expressed in the literature (Carpio et al., 1999, Lampasso et al., 2001, Dziak et al., 2003). Rather it appears that siponimod stimulates osteoblast differentiation (Sartawi et al., 2020a).

# Appendix B

## Supplementary material to Chapter 4

*Unpublished data*

## 8.1 Introduction

Despite bone having excellent regenerative properties in most cases, in severely injurious situations the size of a defect can limit recovery. These are termed critical bone defects, which are defects that do not naturally recover over time. As described in earlier chapters, normal bone repair requires a combination of early immunogenic response followed by intramembranous or endochondral ossification with associated development of new vasculature. In critical defects, each of these aspects of repair represent possible targets when developing new treatment methodologies to compete with the current gold standard, autologous bone grafts.

An ideal material to replace the inherently limited supply of autograft would aim to be highly conducive to new bone formation by mimicking the natural inorganic-organic split in bone composition (Kuttappan et al., 2018). Replicating the osteogenic nature of bone in an implantable material is even more difficult than replicating osteoconductivity, and has so far has most promisingly been achieved through the combination of biocompatible materials with mesenchymal stem cells prior to implantation within defects (Szivek et al., 2019).

There are a number of well-developed models available to investigate critical bone defects which include femoral (Mohiuddin et al., 2019), mandibular (Marei et al., 2018), and cranial defects (Das et al., 2014b). Although the latter two models do not take into account the effect of weight bearing and mechanotransduction on bone repair (Huang and Ogawa, 2010), this also means that there is no requirement for defect stabilisation (Samsonraj et al., 2017). Therefore, these models are powerful tools in

clearly identifying bone regeneration induced by added growth factors or small molecules therapeutics.

Recently, various electrospun materials have been investigated as replacement implant materials, and as vectors for the delivery of medicinal cargoes in critical cranial defects. For example, electrospun polycaprolactone terminally enriched with bone marrow stromal cells (Isoglu et al., 2019), and polycaprolactone and poly vinyl alcohol coaxially spun with platelet-rich plasma (Cheng et al., 2018), and PLGA, which has been electrospun and coated with BMP fragments for use in a cranial defect (Lee et al., 2013). Our own data in **Chapter 4** showed that siponimod could easily and efficiently be incorporated into an electrospun delivery system that produced a controlled release of functionally active siponimod. However, scaffolds ultimately did not result in significant enhanced bone regeneration in rat critical cranial defects.

The following supplementary data shows additional *in vitro* and qualitative *in vivo* results from using the aforementioned electrospun scaffolds design in the critical cranial defect described in **Chapter 4**. Specifically, the *in vitro* data is included to confirm the cytocompatibility of the same batch of electrospun scaffolds that was soon after used in the cranial defect study. While the qualitative *in vivo* H & E staining contributes to our understanding of the state of the defect after the 12-week experimental timeframe.

## 8.2 Materials and methods

### 8.2.1 Materials

Hematoxylin, Eosin Y, and HistoChoice® Clearing Agent were all acquired from Sigma-Aldrich. Permount™ Mounting Medium was acquired from Thermo Fisher Scientific. All other materials were identical to those listed in **Chapter 4** materials section.

### 8.2.2 Electrospun sample preparation

Sample preparation is identical to that described in **Chapter 4** electrospinning procedure section.

### 8.2.3 Cell culture

Human foetal osteoblasts (hFOB) were cultured in DMEM/F12 supplemented with FBS (10 %), L-glutamine (1 %), and penicillin-streptomycin (1 %). Incubation was at 34 °C and 5 % CO<sub>2</sub>.

Electrospun samples (8 mm diameter) were incubated with pre-seeded hFOB ( $5 \times 10^4$  cells/well) for 5 days in 24 well plates. Thereafter, viability of cells was determined by 2 h incubation with MTT solution (5 mg/ml stock) directly added to wells.

To determine scaffold surface compatibility with cell growth, hFOB ( $5 \times 10^4$  cells/well) were seeded directly onto the surface of scaffolds that had been shaped to the bottom of 96-well plates. Incubation was continued for 5 days, at which time metabolic activity was determined by 2 hrs incubation with MTT solution (5 mg/ml stock) directly added to wells.

#### 8.2.4 Procedure for H&E staining of cranial bone tissue

Following extraction of cranial bones, 6 samples per group were set aside for undecalcified sectioning (results shown in **Chapter 4**) and 4 samples per group were assigned to undergo decalcified sectioning (results included in this supplement). H&E staining was used to observe defect healing, cellular infiltration into the scaffolds, and the integration of scaffolds with the surrounding tissue.

Samples were decalcified using a 10 % EDTA solution for 5 days prior to embedding in Shandon™ M-1 Embedding Matrix (Thermo Fisher Scientific, USA), 20 µm sections were cut using a cryostat microtome set at -20 °C and collected on poly lysine coated glass slides.

Light microscope images were acquired using a BX51 microscope, with images used qualitatively to inspect the defect region and scaffold remains at the end of the 12-week experimental timeframe.

##### 8.2.4.1 Haematoxylin and eosin staining reagents

- Mayer's haematoxylin: 5 % Ammonium aluminium sulfate (ammonium alum), 0.1 % haematoxylin, 0.02 % sodium iodate, 2 % (v/v) acetic acid in deionised water.
- Eosin Y stock solution: 1 % eosin Y in 5:1 mixture of 95 % ethanol and deionised water
- Eosin Y working solution: 0.25 % eosin Y stock solution, 0.5 % acetic acid in 80 % ethanol.

##### 8.2.4.2 Haematoxylin and eosin staining procedure

- 1 min in 95 % ethanol, 1 min in 70 % ethanol, 1 min deionised water.

- 8 min in Mayer's haematoxylin.
- 2 min wash in deionised water.
- 1 min Eosin Y working solution.
- 1 min in 70 % ethanol, 1 min in 95 % ethanol, 1 min 100 % ethanol.
- 1 min clearing agent.
- Mount

Interpretation:

- Nuclei: blue/black
- Cytoplasm: various shades of pink
- Muscle/fibrin: deep pink

## 8.3 Results

### 8.3.1 Cell culture

Results from incubating hFOB with electrospun samples are shown in Figure 8.1A. There were no significant differences in cell metabolic activity between any of the experimental conditions after 5 days incubation, as determined by MTT. Additionally, there was no significant difference in metabolic activity between cells incubated alone, and cells incubated with any of the experimental conditions.

Figure 8.1B shows the metabolic activity of hFOB seeded directly on the scaffolds surface and incubated for a period of 5 days. For PLGA and for Si 0.5:100, there were statistically significant increases in metabolic activity compared to the other scaffolds. For the PLGA control scaffolds, its absorbance value after 5 days ( $0.28 \pm 0.03$ ) was



higher than those of Si 2:100 ( $0.14 \pm 0.07$ ) ( $p < 0.01$ ) and Fi 0.5:100 ( $0.10 \pm 0.02$ ) ( $p < 0.001$ ). The Si 0.5:100 scaffold ( $0.34 \pm 0.01$ ) showed a significant increase compared to each of Si 2:100 ( $0.14 \pm 0.07$ ) ( $p < 0.001$ ), SiCol ( $0.21 \pm 0.02$ ) ( $p < 0.05$ ), and Fi 0.5:100 ( $0.10 \pm 0.02$ ) ( $p < 0.001$ ). However, there was no significant difference between PLGA control and Si 0.5:100 scaffolds.

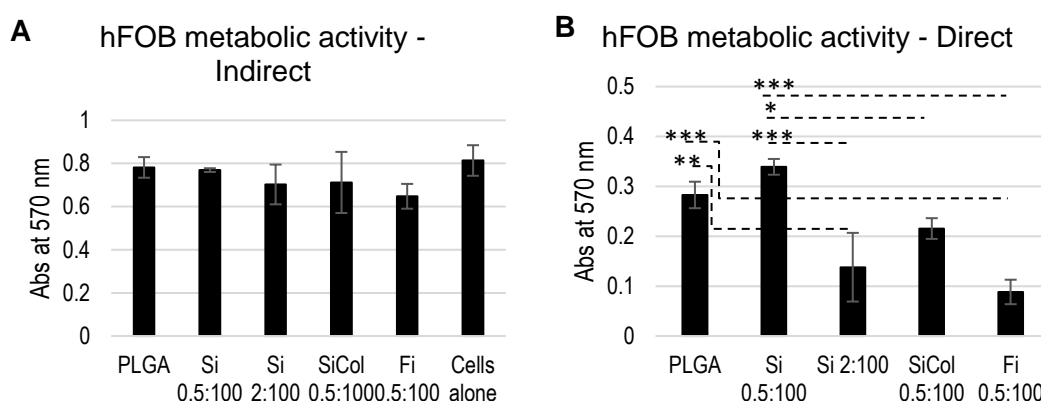


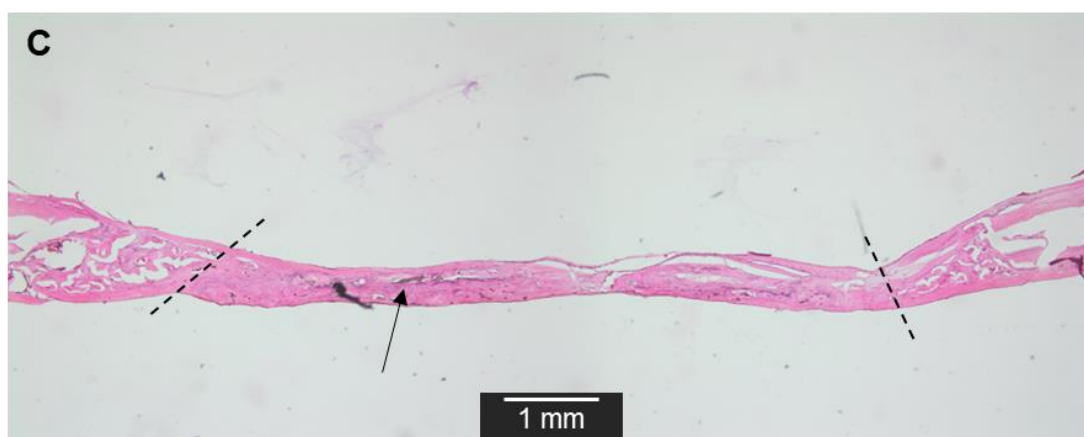
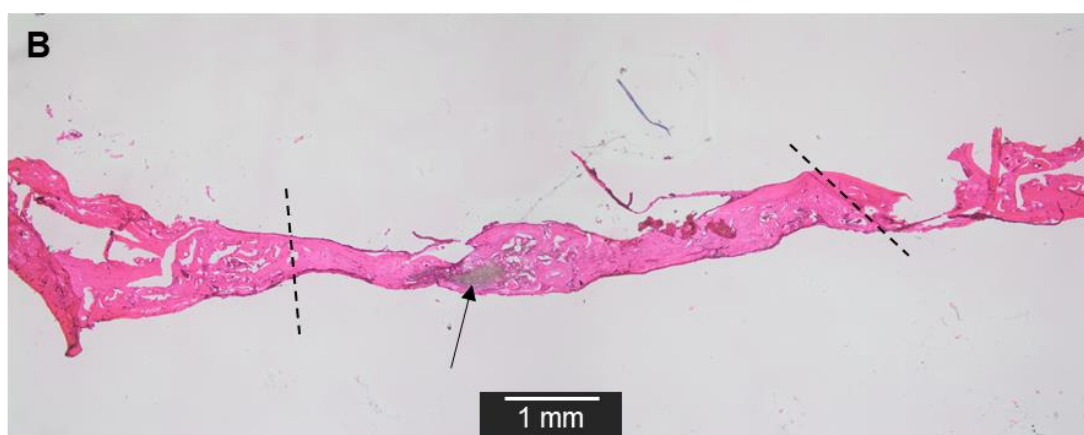
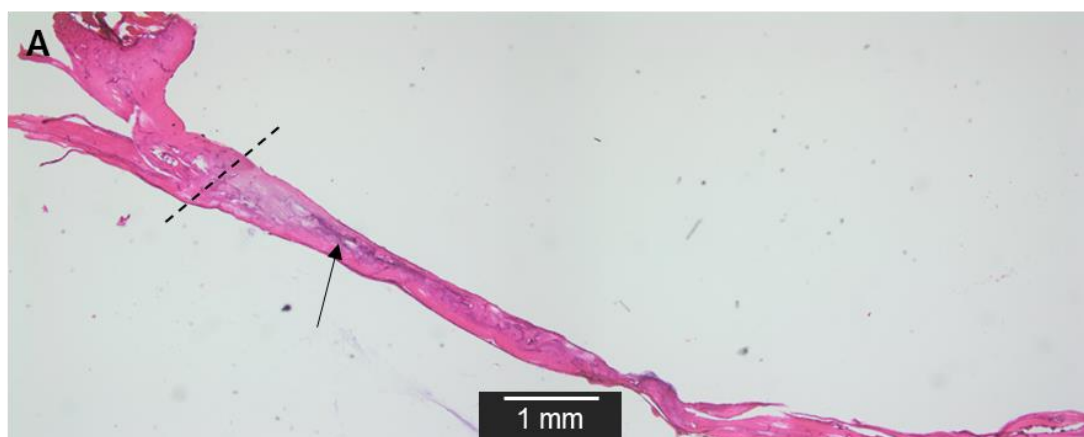
**Figure 8.1** Indirect and direct metabolic activity of hFOB incubated with electrospun scaffolds. (A) hFOB Indirect metabolic activity and (B) hFOB direct metabolic activity was determined using MTT assay after a 5 day exposure of cells to the various samples, for both A & B  $n=3$  independently repeated experiments with 3 technical replicates. Data represents the average absorbance values at 570 nm. Data is presented as mean  $\pm$  SD. For A & B, statistical analysis was by one-way ANOVA. \*:  $p < 0.05$ , \*\*:  $p < 0.01$ , \*\*\*:  $p < 0.001$ .

### 8.3.2 Haematoxylin and Eosin staining of decalcified cranial defect samples

Four samples were decalcified over 5 days using EDTA and processed to produce coronal plane sections of cranial bone samples encompassing the defect. These

samples were used, qualitatively, to investigate the interaction between the implanted material and the regenerating tissue (Figure 8.2).

Results indicated a small difference between the experimental groups PLGA, Si 0.5:100, Si 2:100, and Fi 0.5:100 (Figure 8.2A-C & E) which appeared to integrate well with surrounding tissue, and the SiCol 0.5:100 group (Figure 8.2D) which showed signs of poor degradation of the polymer material and little to no cellular infiltration. Furthermore, although the samples were decalcified, there is a clear delineation in stain intensity between the original bone tissue and the new tissue in the centre of the defect; the difference is more easily seen when juxtaposed with the image of an H&E stained decalcified control without a defect (Figure 8.2F).



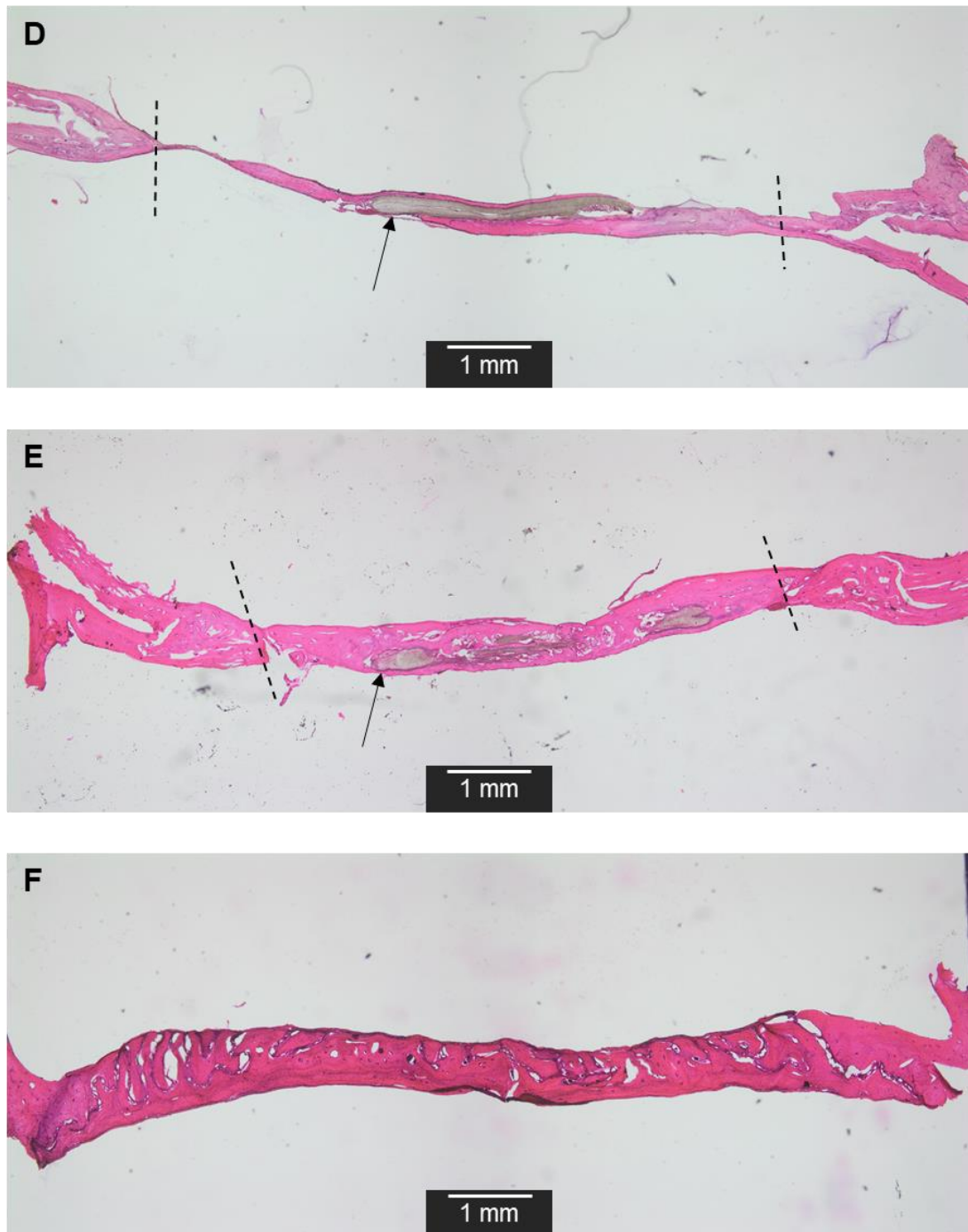


**Figure 8.2** H&E staining of representative decalcified samples. (A) PLGA (B) Si 0.5:100 (C) Si 2:100 (D) SiCol 0.5:100 (E) Fi 0.5:100 (F) control with no defect. Black arrows indicate the scaffold remains (stained blue), while dotted lines indicate the edges of the cranial defect.

## 8.4 Discussion

The work described in **Chapter 4** showed that all the developed electrospun scaffolds produced some mineralisation within the critical cranial defects, albeit with no significant differences between the experimental groups. Here, supplementary data was presented that sheds additional light on the behaviour of the scaffolds immediately following the 12-week cranial defect study.

Cell-based metabolic activity studies were conducted before commencing the *in vivo* study and showed that none of the electrospun scaffolds altered hFOB metabolic activity after 5 days indirect incubation. Interestingly however, the direct metabolic activity study showed that the PLGA and Si 0.5:100 provided a significantly better surface for the growth and viability of osteoblasts than Si 2:100, SiCol 0.5:100, and Fi 0.5:100. This was somewhat similar to the results seen in the main body of **Chapter 4**, which hinted that Si 0.5:100 showed superior metabolic activity and cell infiltration, despite not being statistically significant. All in all, the potentially superior growth and metabolic activity data for the PLGA and Si 0.5:100 scaffolds did not translate to significant mineralisation of the defect, but all available evidence pointed to these two samples being the most likely to induce significant results and should therefore be investigated further to confirm these effects.

The results of H&E staining of decalcified samples were used qualitatively, and so cannot be used to make definitive statements. However, the trend in the available data indicated that the scaffolds PLGA, Si 0.5:100, Si 2:100, and Fi 0.5:100 all underwent substantial degradation and were replaced with regenerating tissue. The remaining scaffold SiCol 0.5:100 showed the least evidence of biodegradation, indeed even after

12 weeks there appeared to be no cellular infiltration within the fibre matrix with the scaffold surrounded by only a thin layer of tissue. The result seen with SiCol 0.5:100 was likely due to the density of fibres observed in collagen containing samples described in **Chapter 4** (Sartawi et al., 2020b). Overall, this supplementary data contributed to our understanding that increased cellular infiltration within the scaffolds may be necessary to achieve better results with future scaffold designs, by reducing the density of packed fibres, especially in scaffolds containing collagen.